

Micro-Mechanical Simulation of Composite Materials Using the Serial/Parallel Mixing Theory

Xavier Martínez

Advisor: S. Oller

~ PhD Thesis ~



UNIVERSITAT POLITÈCNICA DE CATALUNYA
ESCOLA TÈCNICA SUPERIOR D'ENGINYERS
DE CAMINS, CANALS I PORTS



DEPARTAMENT DE RESISTÈNCIA DE MATERIALS
I ESTRUCTURES A L'ENGINYERIA

Micro Mechanical Simulation of Composite Materials Using the Serial/Parallel Mixing Theory

Doctoral Thesis

Xavier Martínez

Advisor:

Dr. SERGIO OLLER

Barcelona, June 2008

ACKNOWLEDGMENTS

I would like to express my grateful acknowledgment to my supervisor, Sergio Oller, who gave me the opportunity and the trust to start this project. Without his help and knowledge on the topics discussed in this document, and on many others, this work would never have been possible.

I also want to give thanks to CIMNE, specially to Eugenio Oñate, for its financial support and for giving me the opportunity to collaborate in some of the research projects that have helped to create this document¹. My most sincere gratitude to all the people of CIMNE, the RMEE department of the UPC, and the MAE department of WVU, among them Alex Barbat and Ever Barbero, for their interaction during the development of this project. No research is possible without interacting with other people; thanks for your ideas, comments, suggestions and knowledge.

Thanks to all my friends, for all the conversations in which the finite elements and the composite materials where not the main topic. Thanks to my family, specially my parents, for the education received, for teaching me how to enjoy learning. And thanks Iria. This work is as much mine as yours.

¹Most of the developments included in this work are consequence of several research projects. The institutions and companies responsible of these projects are gratefully acknowledged. These are, CEE-FP6 (LESSLOSS project, ref. FP6-50544(GOCE)); the Spanish Government through the Ministerio de Ciencia y Tecnología (RECOMP project, ref. BIA2005-06952 and DECOMAR project, ref. MAT2003-08700-C03-02) and the Ministerio de Fomento (project “Retrofitting and reinforcement of reinforced concrete structures with composite materials. Numerical and experimental developments applied to joint of bars and composites anchorage proposal”); AIRBUS through the project FEMCOM and ACCIONA Infraestructuras through the project SPHERA

ABSTRACT

In last decades, advanced composites have become a revolution in structural engineering. Their high strength/weight and stiffness/weight ratios, together with the possibility to tailor made the material for the specific loading environment in which it is used, make these new materials optimal for many structural applications, specially in the aeronautical and nautical fields. However, despite all existing information and actual knowledge about these materials, their complex behavior, highly non-linear, anisotropic and with different failure causes not found in traditional materials, requires a greater effort in their study in order to improve their performance and take advantage of all possibilities offered by them.

Among all possible numerical procedures and formulation available to predict the mechanical performance of fiber reinforced composites, this work uses the serial/parallel mixing theory. This theory obtains the mechanical performance of the composite by coupling the constitutive performance of its constituents, fiber and matrix. This is done taking into account the directional behavior of fibers, which contribution to the strength and stiffness of the composite is found, mainly, in their longitudinal direction.

However, although it is necessary to consider material non-linearities for a correct characterization of fiber reinforced composites, it is not sufficient. The most common failure modes of advance composites, like delamination or fiber buckling, are produced by the interaction between the composite components, and not as a result of a material failure. Therefore, an accurate simulation of composites must take into account the micro-mechanical interaction between its components, in order to be able to characterize their failure modes.

This work studies and proposes different formulations and numerical procedures to simulate the micro-mechanical phenomenons that take place in composites, using the serial/parallel mixing theory. Two different failure modes are discussed: delamination and compression failure due to fiber buckling.

Delamination consists in the lost of adherence between the different layers of the composite, which leads to a reduction of the section strength and stiffness, that can finish in a structural failure. This failure mode is simulated straightforward with the serial/parallel mixing theory, if the appropriate constitutive equations are chosen to predict the mechanical performance of the composite constituents.

The compression strength of composite materials is defined by the fiber micro-buckling phenomenon. This failure mode depends as much on fiber material (stiffness and initial misalignments), as it depends on the confinement made by matrix over fibers. To predict this failure mode a new methodology has been developed, consisting in the introduction of the micro-structural interaction between fibers and matrix into the serial/parallel mixing theory. This is done using an homogenization procedure, that modifies the constitutive performance of fiber and matrix, taking into account their micro-mechanical interaction. The methodology proposed not only solves the fiber buckling problem, but it can also be used to characterize other micro-structural effects, such as the interaction between fibers in woven composites.

All formulations and procedures included in this work provide a new numerical approach to characterize composite materials, capable of considering both, the material non-linearities and the micro-mechanical phenomenons that take place in them. Simulations performed with this new formulation can contribute to increase the actual knowledge of advanced composites, improving their reliability and opening new application fields.

Table of Contents

1	Introduction	1
1.1	Motivation and background	3
1.2	Objectives of this work	12
1.3	Outline	14
	References	19
2	Simulation of the mechanical performance of composite materials	23
2.1	Introduction	25
2.2	Mechanical performance of composite materials. Numerical procedures and formulations	27
2.2.1	Numerical procedures used to simulate composites	27
2.2.2	Stiffness of composite materials	31
2.2.3	Failure criteria of composite materials	32
2.2.4	Homogenization theory	33
2.2.5	Other numerical formulations for composite materials	36
2.3	Mixing theory	37
2.3.1	Classical mixing theory	38
2.3.2	Mixing theory as a constitutive equation manager	40
2.3.3	Serial/parallel mixing theory	42
2.3.4	Enriched serial/parallel mixing theory	46
2.3.5	Tangent constitutive tensor	48
2.3.6	Laminates using the serial/parallel mixing theory	50
2.4	Reinforcement and retrofitting of RC structures with FRP	53
2.4.1	Introduction	53
2.4.2	Retrofitted structures. Construction stages algorithm	55
2.4.3	Validation of the formulation: Beam reinforcement	58
2.4.4	Beam Retrofitting	64
2.4.5	FRP Reinforcement of a RC framed structure	65
2.5	Conclusions	70
	References	73

3	Delamination in composites	79
3.1	Introduction	81
3.2	Delamination in composite materials	82
3.2.1	Description of the delamination problem	83
3.2.2	Experimental simulation of delamination	84
3.2.3	Numerical procedures to simulate delamination	86
3.2.4	Delamination using the serial/parallel mixing theory	90
3.3	Damage formulation	92
3.3.1	Damage constitutive law	92
3.3.2	Friction damage constitutive law	99
3.4	Numerical Example: End Notch Flexure (ENF) test	102
3.4.1	Experimental test description	102
3.4.2	Numerical model description	103
3.4.3	Comparison between the numerical and the experimental results	104
3.4.4	Detailed study of the numerical results	105
3.5	Numerical Example: Ply drop-off test	108
3.5.1	New procedure to take into account delamination in large scale simulations of laminated composites	109
3.5.2	Description of the ply drop-off test	113
3.5.3	Numerical models developed	114
3.5.4	Results obtained	119
3.6	Conclusions and further work	132
3.6.1	Conclusions	132
3.6.2	Further work	134
	References	135
4	Compression Strength of Composite Materials	139
4.1	Introduction	141
4.2	Compression strength of composite materials	144
4.2.1	Rosen model	144
4.2.2	Fiber initial misalignments	147
4.2.3	Barbero and Tomblin model	147
4.2.4	Balacó de Morais model	148
4.2.5	Drapier model	149
4.2.6	Other authors dealing with the problem. Structural models	149
4.2.7	Puig and Oller model	150
4.3	Homogenized constitutive equations. CuBER problem	151
4.3.1	Representative Volume Element to solve the fibre buckling problem	151
4.3.2	CuBER equations	152
4.3.3	Boundary conditions and solution of the CuBER problem	156
4.3.4	Definition of the CuBER problem using the composite properties	157

4.3.5	Fibre homogenized constitutive equation	159
4.3.6	Matrix homogenized constitutive equation	163
4.4	Validation of the homogenization method	168
4.4.1	Models description	168
4.4.2	Results to be studied in the code validation	172
4.4.3	Detailed comparison of the results obtained with the micro-Bmod and RoM-Bmod simulations	173
4.4.4	Comparison of the results obtained with the micro and RoM models for the different RVE considered	180
4.5	Numerical procedure to obtain the compression strength of composites	184
4.5.1	General description of the numerical procedure developed	184
4.5.2	Compression strength in fibres without initial misalignments	185
4.5.3	Compression strength in fibres with initial misalignments	194
4.5.4	Parameters defining the fibre buckling problem	199
4.5.5	Implementation of the numerical procedure proposed in a finite element code	200
4.5.6	Numerical performance of the procedure developed to obtain the com- pression strength of composite materials. Numerical examples	203
4.6	Validation of the formulation proposed and numerical example	214
4.6.1	Validation of the formulation developed to obtain the compression strength of composite materials	215
4.6.2	Numerical simulation of a cantilever beam	221
4.7	Conclusions and further work	226
4.7.1	Conclusions	226
4.7.2	Further work	228
	References	231
5	Final Remarks	235
5.1	Conclusions	237
5.2	Further work	242
5.2.1	Improvements of the formulation developed	242
5.2.2	New research lines	243
5.3	Original contributions of this work	244
	List of Figures	247
	List of Tables	255

Chapter 1
Introduction

1.1 Motivation and background

Composites can be defined as those materials composed by two or more components with different properties and distinct boundaries between the components (Vasiliev and Morozov, 2001). A large number of materials are included under this definition, some of them naturally occurring such as wood, made of cellulose fibers in a lignin matrix or the human bone, made of fiberlike osteons embedded in an interstitial bone matrix (Barbero, 1999). Of all existing materials that can be defined as composites, this work is focussed in the study of the fiber reinforced composites (FRC) usually referred as *advanced composites*. These composites can be defined as a man-made blend of two or more components, one of which is made up of stiff, long fibers, and the other, a binder of matrix which holds the fibers in place (Peters, 1998). In these composites, fiber reinforcements are long, with length to diameter ratios over 100; and their strength is, at least, 25 to 50 times larger than the strength of matrix material (Oller, 2003).

The use of man-made fiber reinforced composites (FRC) dates back to ancient times, as when the addition of straw to reinforce clay bricks was used. In the nineteenth century, iron rods were used to reinforce masonry; this same concept was used afterwards to reinforce concrete with steel bars. However, although FRC already existed, it is not until the middle of the twentieth century that advance composites make their apparition in structural engineering, with the development of industrial processes capable to manufacture fibrous materials with diameters in the order of micro-meters (commercial glass fibers were created in 1939 by Owens-Corning; Peters 1998). This first development lead to the apparition of new materials and applications in the following years. According to Daniel and Ishai (1994), the first fiberglass boat was made in 1942. At the same time, reinforced plastics were used in aeronautical and electrical applications. Filament winding was invented in 1946 and applied to missiles in the 1950s. The first boron and high strength carbon fibers were introduced in the early 1960s and applied to aircraft components. Kevlar was developed in 1973. And the list can continue until nowadays, in which nano-technology has begun to create a new generation of fiber materials, and the use of composite materials has been extended to the point in which the new Airbus A380 contains more than 25% of its weight of composite materials and the new Boeing 787 increases the amount of composites to 50% of its body weight.

With the development of new advance composites and the number of applications in which they are used, has also increased the knowledge of these new materials. This is proved by the number of books and publications that have appeared in recent years related to composite applications, manufacturing processes, properties and mechanical characterization. According to the list of books on composites presented by Herakovich in *Mechanics of fibrous composites*, in 1995 there were 35 books published in this field (Vasiliev and Morozov, 2001). Nowadays, Amazon's web page references a total of 632 different books with the words "composite materials" in their title, restricting the search to the technical engineering domain. Also, more than 21 journals are specifically dedicated to composite materials.

However, despite all existing information and actual knowledge about these materials, their complex behavior, highly non-linear, anisotropic and with different failure causes not found in traditional materials, requires a greater effort in their study in order to improve their performance and take advantage of all possibilities offered by this new generation of materials. Up to this point, advance composites are used, and many times though of, as if they were traditional materials. New ways of using and applying composites are required to get the most of them. If this is achieved, composite materials can become one of the most relevant improvements in the XXI century structural engineering field.

Advanced composite materials

The classification of advanced fiber reinforced composites is made following two different criteria: their constituent materials and the length and distribution of fibre reinforcements. According to the definition used to characterize advanced composites, these are obtained combining several components, however advanced composites are usually found as the combination of only two components: a fiber reinforcement in an homogeneous substrate referred to as matrix. Fibers are added to the matrix material following different patterns.

The number of composites that can be obtained by the addition of a fibrous material into a matrix can be extremely large. However, not all combinations provide a resultant material with improved properties. Therefore, some fiber-matrix combinations are the most common, as these combinations take the most of both component materials. Following this idea, Daniel and Ishai (1994) provide the classification of composite materials displayed in table 1.1, according to the type of matrix used in the composite.

Matrix type	Fiber	Matrix
Polymer	E-glass	Epoxy
	S-glass	Polyimide
	Carbon (graphite)	Polyester
	Aramid (Kevlar)	Thermoplastics
	Boron	PEEK, polysulfone, etc.
Metal	Boron	Aluminum
	Borsic	Magnesium
	Carbon (graphite)	Titanium
	Silicon carbide	Copper
Ceramic	Silicon carbide	Silicon carbide
	Alumina	Alumina
	Silicon nitride	Glass-ceramic
Carbon	Carbon	Carbon

Table 1.1: Types of composite materials (Daniel and Ishai, 1994)

Because this work is mainly focused in the simulation of fiber reinforced polymers (FRP), it is worth to provide a more detailed description of the mechanical properties of the components related to these composites. Table 1.2 provides a description of the main mechanical properties of fiber materials and in table 1.3 are described the mechanical properties of the most common matrix materials used in FRP. The parameters included in these two tables have been obtained from Gay et al. (2003) and Barbero (1999). The table that describes fiber characteristics also includes the properties of steel for comparison.

Fiber	Diameter [μm]	Density [kg/m^3]	Young M. [GPa]	Poisson	Tens. Strength [MPa]
E-Glass	16	2600	74	0.25	2500
S-Glass	10	2500	86	0.20	3200
Carbon T300	7	1750	230	0.20	3530
Kevlar 49	12	1450	130	0.40	2900
Boron	100	2600	400	0.20	3400
Steel		7800	205	0.30	400–1600

Table 1.2: Mechanical properties of fiber materials

A more detailed characterization of the materials described in tables 1.2 and 1.3, as well as

Matrix	Density [kg/m ³]	Young M. [GPa]	Poisson	Tens. Strength [MPa]
Epoxy	1200	4.5	0.40	130
Polyimide	1400	4.0–19.0	0.35	70
Polyester	1200	4.0	0.40	80
PEEK	1320	3.2	0.40	100
Polysulfone	1350	3.0		85

Table 1.3: Mechanical properties of polymer matrix materials

a detailed description of other materials used in advanced composites can be found in Peters (1998), Barbero (1999), Car (2000) and Oller (2003), among others.

The second criterion commonly used to classify composites is based on the reinforcement topology inside the composite. This is, the fiber length and its distribution. Figure 1.1 provides a possible fiber reinforced composites classification according to fiber topology.

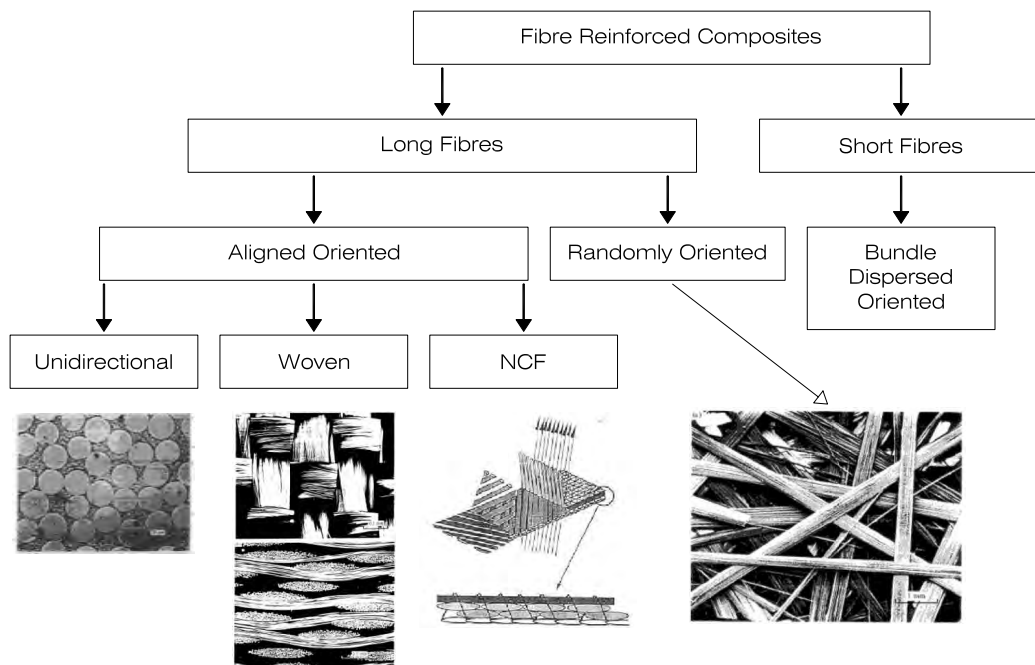


Figure 1.1: Classification of FRP composites according to their fibre distribution

This figure shows that the first distinction made is according to fiber length. The properties of composites with short fibers are lower than those of continuous (or long) fiber composites because the transmission of efforts, from matrix to fiber, is ineffective due to the fiber short length. An study of this phenomenon, as well as a numerical formulation to characterize it using the mixing theory, is described in Oller and Car (2002).

In case of having long fibers, these can be oriented or randomly distributed. Random fibers have the advantage of providing a composite material with similar properties in all its directions, as fiber contribution to the composite strength and stiffness is the same in all composite directions. However, the strength of this composite configuration is smaller than the strength obtained in composites with aligned fibers. Therefore, the most commonly advance composites used in engineering applications are those with oriented fibers. Different layers are stacked with different fiber orientations in order to obtain a material with different strength direc-

tions. The material obtained from this assembly is known as a composite laminate. This procedure provides tailored composite materials, in which their directions of strength and stiffness can be defined to match that of the loading environment (Peters, 1998).

Composite laminates can be obtained using different layers of unidirectional fiber composites, in which fibers with different orientations are independent, or can be obtained with woven composites, in which fibers with different orientations are coupled together. Non-Crimp Fabric (NCF) composites are those in which the different layers of the laminate are stitched together, as it is shown in figure 1.1. This process improves the laminate performance for different failure modes such as delamination.

Two of the main advantages provided by advance composites, when compared to traditional materials, have been already shown when describing their classification criterions: the relation strength/weight and stiffness/weight and the possibility of tailor made the composite for the specific application in which it is used. These two characteristics, among others, explain the spectacular increase, observed in last decades, of the engineering structural applications in which these new materials are used.

Table 1.2 shows that fibers double the strength of the strongest steel, having less than a third of its weight. This weight is not increased by matrix material, which density is half of fibers density. This improvement in the strength/weight ratio makes advance composites optimal for nautical and aeronautical applications; in fact, these two engineering fields have been the precursors in the use of these materials. The strength/weight ratio is also improved with the possibility of reinforcing only the required directions, in the places where the reinforcement is needed, avoiding the presence of redundant material in the structure.

There are other advantages of these new materials that makes them the most adequate for certain applications, such as the improved corrosion properties. However, advance composites have also some disadvantages, such as the difficulty to join different structural parts or matrix environmental degradation. Table 1.4 summarizes the main advantages and disadvantages of advanced composites defined by Peters (1998).

Advantages	Disadvantages
Weight reduction High strength or stiffness to weight ratio	Cost of raw materials and fabrication
Tailorable properties Strength and stiffness oriented in load direction	Transverse properties may be weak
Redundant load paths (fiber to fiber)	Matrix is weak, low toughness
Long life (no corrosion)	Reuse and disposal may be difficult
Lower manufacturing costs because less part count	Difficult to attach
Inherent damping	Analysis is difficult
Increased (or decreased) thermal or electrical conductivity	Matrix subject to environmental degradation

Table 1.4: Advantages and disadvantages of advanced composites (Peters, 1998)

Applications of composite materials

Besides the disadvantages shown in table 1.4, the use of fiber reinforced composites in structural applications has increased enormously in recent years. An example of this growth is provided by the world prediction of the required production capacity of carbon fibers: in 2006 the production of PAN-based carbon fiber exceeded 27.000 tonnes, this production is expected to increase at least 15% each year to reach 76.000 tonnes by 2010 (CompositesWorld, 2008).

The aeronautical field is the main responsible for this increase. The ratios strength/weight and stiffness/weight of advance composites makes them ideal for aircraft applications. This is proved with the amount of composite materials included in the two new airplanes developed by Airbus and Boeing: the amount of composites included in the Airbus A380 represent the 25% of its weight and in the Boeing 787 Dreamliner this value reaches the 50%. Also in the aeronautical field it is worth to mention the SpaceShip One, the first spacecraft that completed a privately funded human spaceflight (June 21, 2004). This spacecraft is completely made with composite materials by Scaled Composites.

But the responsible of the increase in the use of advanced composites is not only the aerospace industry. Nowadays, these new materials are being used in nearly all engineering fields and the number of applications in which they are used keeps increasing. In the following are described the main structural applications of composite materials:

Aeronautical applications: As has been already said, advanced composites are widely used in the aeronautical field. These are used in nearly all types of aircrafts, from rockets to helicopters. The composites used in this field are mainly laminates made with fiber reinforced polymers, although this industry also uses other composites such as metal and ceramic reinforced composites. In example, in the airplane engines, the regions with high temperatures use metal matrix reinforced composites and, when this temperatures are extremely high, the materials used are ceramic matrix composites (Car, 2000).

Nautical applications: Composites have also found numerous applications in the nautical engineering field, as their relation stiffness/weight and strength/weight makes them more attractive than conventional materials. However, there are more advantages that make composites the most suitable material for nautical applications, like their resistance to corrosion and their low magnetic conductivity. This last property has made composites the best material to be used to construct anti-mine ships (Oller, 2003). Composites are found in nautical applications as solid stiff materials (laminates or a single thick layer with randomly oriented fibers) or as textile materials. The last is the case of fabric materials, that are used to construct inflatable structures such as hovercrafts, boats, liferafts, etc.

Automotive applications: The use of composite materials in the automotive industry can be divided in two different sectors: commercial and high-performance automobiles. Commercial vehicles have begun introducing composites in some of their components such as bumpers, however their use has not been extended significantly yet. On the other hand, in high-performance automobiles, such the ones developed for F1, composites are used to manufacture nearly all components, from the chassis to the gearbox (Savage et al., 2004).

Civil engineering applications: The use of composites in civil engineering is still in its first stages. These materials are used in some specific applications, such as cables (Car,

2000) or for reinforcement and retrofitting of existing structures (Meier, 1995; Pulido and Sobrino, 1998). In this last case, layers of fiber reinforced polymers are bonded to the existing structure to increase its structural capacity in front of bending, shear or compression forces. However, the use of composites in civil engineering has not been widely extended yet, mainly because the difficulty to join the different structure components. New applications for composites in civil engineering, nowadays under study and with some examples already constructed, are the use of fiber reinforced bars to reinforce concrete structures (Nanni, 2003) or the construction of bridges using pultrusion beams (Pulido and Sobrino, 2002).

Energy applications: One of the main applications of advanced composites in the energy field is in the construction of wind turbine blades. The loud demands for environmental protection have increased the wind energy sector, which is developing larger rotor blades, reaching 60 m long, to fulfill energy requirements. The construction of these blades will not be possible without the use of composites (Reichl, 2007).

Other applications: Besides the different applications described, composites are used in many other fields, most of them described in (Gay et al., 2003). Some random applications in which fiber reinforced composites can be found are, among others, antennas, tanks for corrosive products, tennis rackets or skis.

As has been shown, the list of applications in which advance composites are used is long and its growth has been fast (the first boat made of glass fibers was manufactured just 50 years ago). However, in order to keep increasing the number of applications is necessary to solve some of the drawbacks of these new materials, among them the join of different composite structural elements and the calculation techniques, which must take into account the specific failure causes of these materials.

Structural analysis of composites

One of the main drawbacks found when using advance composites in structural applications is the difficulty of obtaining a reliable design, as the structural analysis processes used to simulate the mechanical behavior of composite structures are not yet developed enough to take into account the specific performance of these materials (Oller, 2003).

According to the review made by Orifici et al. (2008), a complete and validated methodology for predicting the behavior of composite structures including the effects of damage has not yet been fully achieved. This is largely due to the complex nature of composites, which performance and development of damage is dependent on a wide range of parameters including the geometry, material, loading conditions, load history and failure modes. Therefore, traditionally, numerical simulations of composites have been performed using orthotropic materials with average properties from their constituents. With this approach, no model has been found that is able to function beyond the elastic limit state of its constituents.

Since composite structures are commonly calculated considering the composite an elastic material, in most cases the calculation of this structures is performed using strength of materials formulations (Timoshenko, 1940). However, when the structural application requires taking into account the complex mechanical performance of the composites, i.e. its high anisotropy, the calculation must be performed using numerical techniques. Among them, the most relevant is the finite element method (Zienkiewicz and Taylor, 1991; Oñate, 1995). In most cases, the finite element method is coupled with the classical lamination theory (Jones, 1999;

Reddy, 2003), as most composite structures are made with laminates and this theory provides the mechanical performance of the composite taking into account its lamination configuration (stacking sequence, fiber orientation, etc.)

Either if the structural performance is obtained using strength of materials or a finite element formulation, the failure load of the the structure is obtained comparing the elastic stresses in the composite with a limit value, obtained from experimental tests. In order to improve the failure simulation of composites, numerous studies have been developed around the world to define fracture criterions, most of them based in fracture mechanics or damage mechanics. Proposed theories are mostly based in the characterization of a specific failure mode and are applied to a ply (layer) level.

Among all theories and formulations proposed to characterize the composite performance and their fracture criterions, two different theories outstand from the rest as they propose to deal with composite materials following a completely different approach. Instead of trying to characterize the composite performance, considering the composite a single material with properties inherited from its constituents, these theories center their effort in modeling the constituents performance and, more important, on how the results obtained from the constituents can be used and extrapolated to predict the global behavior of the composite. These two theories are: homogenization and the rule of mixtures (or mixing theory).

Homogenization theory: This method deals with the global composite structure problem in a two-scale context. On the macroscopic scale the composite materials determine the global response of the structure. Composites are considered to be homogeneous materials in this scale. The microscopic scale represents an elemental characteristic volume in which the microscopic fields inside the composite are obtained. This scale deals with the component materials of the composite, each one with its own constitutive equation. Homogenization theory relates these two scales by assuming a periodic configuration of the composite material (Sánchez-Palencia, 1987; Oller et al., 2005).

Mixing theory: The first formulation of the mixing theory was developed by Trusdell and Toupin (1960) and it is based on two main hypotheses: 1. All composite constituents are subject to same strains. 2. Each constituent contributes to the composite behavior according to its volumetric participation. The main drawback of the mixing theory is the iso-strain condition which enforces a parallel distribution of the constituents in the composite. This problem has been solved by Rastellini (2006), with the development of the serial/parallel mixing theory. This new formulation replaces the iso-strain hypothesis for an iso-strain condition in fiber direction and an iso-stress condition in the rest of the composite directions.

Of these two theories, the homogenization theory is the one capable to take into account with more accuracy all micro-mechanical phenomenons that take place in the composite (from material degradation to specific failure modes). However, this theory has a computational cost unbearable by nowadays personal computers: each element in which the structure is discretized requires a finite element simulation (that can contain hundreds or thousands of elements) to obtain its mechanical performance.

On the other hand, the mixing theory and its improved version, the serial/parallel mixing theory (Rastellini et al., 2007), is capable to obtain the constitutive performance of the composite, from the mechanical behavior of its constituents, with an affordable computational cost. However, one of the main disadvantages of this theory, compared to homogenization, is

that the mechanical performance of the composite is obtained only using constitutive formulations, disregarding failure causes produced by micro-structural phenomena as, for example, fiber buckling or delamination. In order to improve the accuracy of composite simulations, using the serial/parallel mixing theory, the micro-structural failure causes should be included in the formulation.

Micro-mechanics of composites

There is a wide variety of failure mechanisms in composites, dependent on the loads applied, manufacturing process and type of composite, among them: fiber failure, matrix cracking, buckling, fibre-matrix debonding and delamination. In most of these cases, the failure of the composite is produced by the interaction between its components and not as the result of a material failure, as occurs with traditional materials (such as metals or frictional materials). Based on this failure mechanisms, it can be more appropriate to consider composites as a structure rather than as a material (Orifici et al., 2008). Thus, it can be concluded that composites are a new material which failure criterions have to be redefined and new formulations must be proposed to characterize their failure modes.

Among all failure causes of composites, the most common failure mechanisms, consequence of the micro-structural interaction between the composite components, are fiber buckling and delamination. Both of them are hereafter described.

Delamination: Delamination is a failure mechanism found in laminated composites. The lost of adherence between the different layers of the composite leads to a reduction of the section strength and stiffness that can finish in a structural failure.

The importance of this phenomenon is demonstrated by the amount of authors that have developed theories and formulations to deal with it. All authors that have studied the problem agree that the delamination process is characterized by two main phenomena, the crack initiation and its propagation along the composite. Crack initiation can be obtained by comparing the strain-stress state of the material, in the region where delamination takes place, with a critical one (Jansson and Larsson, 2001; Camanho and Dávila, 2002; Turon et al., 2006; Balzani and Wagner, 2007) or in terms of the traction versus relative displacement (Borg et al., 2002, 2004; Pinho et al., 2006). And the delamination propagation is usually treated opening the mesh to simulate the crack effect where it takes place. To open the mesh different procedures are proposed. One of them is the virtual crack closure technique (VCCT) Krueger (2004), based on the assumption that when a crack is extended, the energy required to open the crack is the same required to close it. Another procedure, each time more used, is the use of a cohesive zone model (Camanho and Dávila, 2002). The cohesion elements are placed in the interface of the layers that can suffer delamination and its propagation is obtained with damage or plastic formulations applied to those elements.

All known formulations, developed to characterize the delamination phenomenon, have two main drawbacks. The first one is that there are many formulations in which the two surfaces found at each side of the fracture become completely independent, being necessary to use remeshing techniques and contact formulations to obtain the delamination propagation. The second drawback affects all known formulations, and is the necessity to define a special element in which delamination occurs. This situation forces to predefine the delamination path where place these special elements. And, if the exact place where the delamination takes place is unknown, these elements must be included

between all layers, which makes the calculation unbearable due to its computational cost.

Fiber Buckling: One of the main failure causes of compressed fiber reinforced polymers (FRP) is the fibre buckling phenomenon. Fibres are very slender elements and their second order effects are avoided by the matrix elastic restraint. However, as damage in matrix evolves, fiber restraint becomes weaker and fibre buckling occurs.

First studies about fibre buckling correspond to Rosen (1965), who defined two different buckling modes: extensional and shear buckling. He also defined the compression stress at which fiber buckling occurs. This stress value is defined by the matrix shear strength and by the amount of fibres found in the composite. From this initial approximation, different authors have developed new models in order to obtain a better prediction of composite compression strength due to fibre buckling. Among different existing studies, it is worth to mention the works by Barbero and Tomblin (1996), Balacó de Moraes and Torres Marques (1997) and Drapier et al. (1999). All these authors consider composites as a single orthotropic material. Using energetic equilibriums, they develop micro-mechanical models from which the final compression stress in the composite is obtained.

The expressions found in all different models agree in the dependence of the critical compression stress on three main parameters: (a) Matrix shear strength, (b) fibre initial misalignment and (c) proportion between fibre and matrix in the composite. Hence, the limit compression stress of these new formulations depends on the same parameters pointed out by Rosen and on a new one: fibre initial misalignments. According to Jochum and Grandidier (2004), fibre misalignments are produced in the composite manufacturing process, during the matrix curing. These misalignments are regular along the whole fibre and can be represented by a sinusoidal shape.

A problem found in most of the formulations existing in literature to simulate the fiber buckling phenomenon is that these only provide a stress value for which fiber buckling occurs. Only the formulation developed by Barbero and Tomblin provides the post-critical strength of the composite, obtained after fiber buckling. Also, all formulations treat the composite as a single material, with average properties from its constituents. This scope forces to pre-define the constitutive performance of the composite constituents, i.e. fibers are elastic, reducing the application range of the formulation, which cannot be applied if the component properties are different to the ones considered when developing the formulation.

These two failure modes, fiber buckling and delamination, illustrate the importance of micro-mechanical effects in composite failure. And, despite the amount of formulations found in literature that try to characterize them, a complete and validated formulation capable to predict these failures has yet not been achieved. Also, all formulations known are based in the characterization of a single failure mechanism, but they are not capable to relate all of them, taking into account the complex micro-mechanical performance of fiber reinforced composites.

Therefore, besides the amount of applications in which these materials are used, more research is still needed in order to obtain reliable theories and formulations capable to obtain the mechanical performance of advance composites, taking into account their complex micro-structural configuration and their specific failure modes.

1.2 Objectives of this work

Previous section has shown that advance composite materials have become, besides their recent apparition in the middle of twentieth century, one of the most suitable materials to be used in many structural applications. Their high strength/weight and stiffness/weight ratios, together with the possibility to tailor made the material for the specific application in which it is used, are the two main advantages responsible of the increase experienced in the use of these new materials.

However, as composites can be considered more as a micro-structural system than as a material, new formulations and theories are required to predict their mechanical performance accurately. Most of the formulations used nowadays to simulate composites treat them as a single material, with properties inherited from its constituents. This has proven to be inaccurate, as most of the failure mechanisms of composites are because of the micro-structural interaction between its components, interaction that cannot be simulated if the composite is treated as a single material.

Two different formulations are known that do not treat the composite as a single material: the homogenization theory and the mixing theory. These two theories obtain the composite mechanical performance from the constitutive behavior of their constituents. To simulate large structures made with composite materials, the homogenization theory has to be disregarded, as it requires a computational effort that cannot be provided by nowadays personal computers. Therefore, the formulation that remains left, to perform large simulations of composite structures, taking into account the constitutive performance of the composite constituents, is the serial/parallel mixing theory, developed by Rastellini (2006).

When describing the serial/parallel mixing theory (SP RoM) it has been said that this theory does not take into account micro-structural effects. This work will show that this assumption is not correct, as it proves that some micro-structural phenomena, such as delamination, can be captured by the SP RoM if the appropriate constitutive laws are used to characterize the composite components. This work will also demonstrate, and this is probably the most important result of this work, that the micro-structural interaction between the composite components can be included in the mixing theory by modifying their constitutive performance.

Therefore, the main objective of this work can be summarized as the improvement of the serial/parallel mixing theory, by using the appropriate constitutive equations and by developing new numerical procedures, to take into account the micro-structural phenomena that lead to the composite failure.

To fulfill the main objective of this work, three different objectives have to be achieved. First it is required to assess the capability of the SP RoM to perform large scale simulations of composite structures. After proving this capability, new formulations and numerical procedures will be developed to take into account the micro-mechanical performance and failure of composites. The micro-mechanical failure modes that will be solved are: delamination and fiber buckling. Figure 1.2 shows a schematic representation of the main objective of this work and the three different objectives that have to be achieved to reach the final goal.

It is important to remark that the main goal of this work is to develop methodologies and numerical procedures to include the micro-mechanical performance of the composite into the serial/parallel mixing theory. Although this work is focused in the solution of the delamination and the fiber buckling problem, the methodology developed can be extrapolated afterwards to other failure mechanisms. If this objective is achieved, it will be proved that the

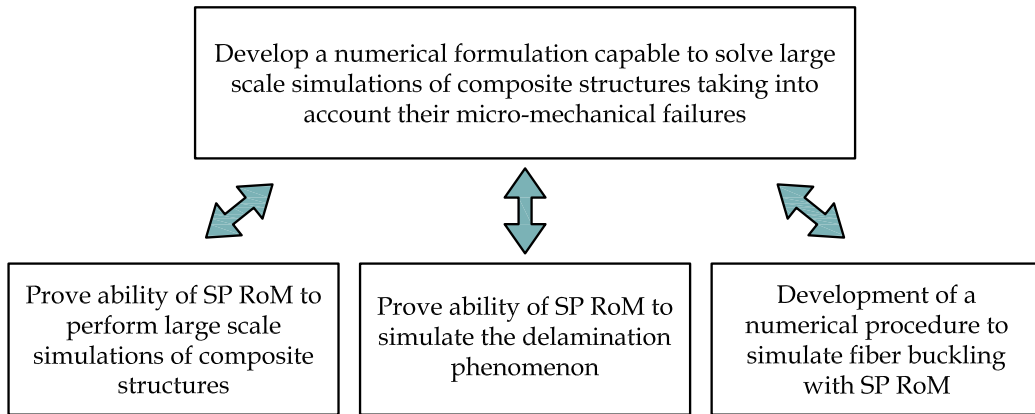


Figure 1.2: Main objectives of this work

serial/parallel mixing theory is capable not only to obtain the composite performance from its components materials, but also to include in its formulation the interaction between these components. The resultant formulation will become a powerful tool to perform numerical simulations of large structures made with composite materials.

In the following is included a detailed description of the objectives sought when solving each one of the problems required to obtain the numerical tool sought.

Numerical simulation of composites using the SP RoM

1. Solve the problem of reinforcement and retrofitting of reinforced concrete structures with FRP using the SP RoM. The solution of this problem will prove the capacity of the SP RoM to perform large scale simulations of composite structures.
2. Verify the ability of FRP to improve the mechanical performance of reinforced concrete structures. Compare the improvement obtained when the structure is reinforced or retrofitted.
3. Improve the SP RoM formulation so it can perform simulations of structures with a previous level of damage when the FRP reinforcement is applied.
4. Improve the SP RoM algorithm with a formulation capable to obtain the tangent constitutive tensor for any possible yield law. To fulfill this objective, a numerical derivation of the constitutive law is performed.

Simulation of delamination with the SP RoM

5. Asses the ability of the serial/parallel mixing theory to simulate accurately the delamination phenomenon. This objective will be achieved using the appropriate constitutive equations and yield laws to simulate the component materials.
6. Include the effect of friction in the delamination crack propagation and study how the friction between the fractured layers affects the delamination process.

7. Develop a numerical procedure to perform large scale numerical simulations of laminated structures, using the classical lamination theory and the serial/parallel mixing theory, and taking into account the delamination failure mode.

Simulation of fiber buckling with the SP RoM

8. Develop a new methodology to include the micro-structural performance of composite materials in the serial/parallel mixing theory. This methodology is applied to characterize the fiber micro-buckling phenomenon.
9. Develop a formulation and numerical procedure capable to obtain the compression strength of composite materials, due to fiber buckling, in large scale simulations of composites. The new formulation developed must be computationally efficient and must be able to obtain the post-critical compression strength of the composite, as the failure of one region of the structure does not imply the global failure of the structure, and the code must be capable to continue the calculation process.
10. Prove the ability of the numerical procedure developed to obtain the compression strength for different fiber reinforced composites.

The objective of this work is not only to develop formulations to simulate composite structures, taking into account their micro-mechanical failure modes, but to be able to use these developments to perform numerical simulations of real structures. With this aim, most of the formulations and numerical procedures developed have been implemented in PLCd code (CIMNE, 2008), an implicit finite element code developed by several researchers, professors and PhD candidates at CIMNE (International Center for Numerical Methods in Engineering) and RMEE (Department of Structures and Strength of Materials, UPC). Also, in the frame of the FEMCOM project (CIMNE-AIRBUS), the new procedure to simulate delamination, in composite structures using the lamination theory, has been implemented in ComPack-Aero (CIMNE and Quantech, 2008).

Besides the specific objectives previously enumerated, this work has also contributed to the development of several research projects, for governmental administrations and for private companies. It has been also sought the dissemination of the results, with the participation in international congresses and with the publication of the results in scientific journals.

1.3 Outline

In the description, in previous section, of the main objective of this work, it has been shown that its achievement requires to fulfill three different objectives: (1) Prove that the serial/parallel mixing theory is capable to perform large scale simulations of composite structures, this is done using it to solve the problem of FRP reinforcement and retrofitting of reinforced concrete structures. (2) Prove that delamination can be simulated with the SP RoM and develop a numerical procedure to take into account delamination failure in laminated structures simulated with the classical lamination theory. And (3), develop a methodology to take into account micro-structural effects in composites using the SP RoM. This methodology is applied to the characterization of the compression strength of fiber reinforced composites due to the fibre buckling phenomenon.

Because each one of these three objectives has enough entity by itself, as proves the amount of existing literature dealing with them, it has been thought convenient to divide this document in three different chapters completely independent between them. Each chapter has been written to be self-contained, providing enough information to define in detail the problem to be solved, the solution proposed to solve the problem and, finally, the conclusions obtained from the work performed. Therefore, those readers interested in just one of the topics contained in this document will be capable to follow it without needing to read the complete work.

However, this document can also be read as a whole. In this case, the reader will obtain a global comprehension of the procedure that is proposed to perform numerical simulations of composite structures, how the composite is treated and how its micro-mechanical effects can be considered. All numerical procedures and formulations described in the three chapters in which this work is divided are expected to become, together, the numerical tool sought. A numerical tool capable to predict the mechanical performance of large composite structures, taking into account their micro-mechanical effects and failure modes.

In the following are described the contents of each one of the chapters mentioned. This document ends with the conclusions obtained from the work performed, and with the proposal of further research lines.

Chapter 2: Numerical formulation of composite materials

This chapter describes, in section 2.2, the formulations and numerical procedures used nowadays to obtain the mechanical performance of composite materials. This section also includes a description of the homogenization theory and of other existing numerical formulations that can be used in the simulation of composite structures.

Once knowing the formulations that are more commonly used to simulate composite structures, in section 2.3 is described in detail the mixing theory and its improved version, the serial/parallel mixing theory. This section also describes how the tangent constitutive tensor can be obtained performing a numerical derivation. Finally, it is explained how the SP RoM can be applied to laminated structures: either using solid elements or either coupling it with the classical lamination theory.

At the end, in section 2.4, the potentiality of the serial/parallel mixing theory is proved using it to solve the problem of reinforcement and retrofitting of reinforced concrete structures using FRP. To solve this problem a new construction stages algorithm has been developed that allows introducing the reinforcement in the structure when it has reached a certain level of damage. The ability of the SP RoM to solve this problem is proved with three different numerical examples. The first one is used to validate the formulation, comparing numerical with experimental results, the second one compares the structural performance obtained in case of reinforcement and retrofitting and, the third case, solves a large structure with different FRP reinforcements to obtain the reinforcement configuration that provides a better performance.

Some of the results included in this section have been already published in Martínez et al. (2006, 2007a,d, 2008b)

Chapter 3: Delamination in composites

Once having described the formulation used to simulate composite materials, the serial/parallel mixing theory, this chapter shows how this formulation can solve the micro-mechanical problem of delamination.

In section 3.2 it is described the delamination problem and the different formulations existing in literature to solve it. Afterwards is shown how this failure cause can be solved using the serial/parallel mixing theory. Because the solution of the delamination problem using the SP RoM depends on the constitutive equations used to simulate the composite constituents, section 3.3 describes in detail the damage formulation used to characterize them.

The ability of the procedure proposed is proved, in section 3.4, comparing the numerical with the experimental results obtained for the End Notch Flexure test (ENF), which obtains the delamination toughness of a composite laminate with a three point bending test.

Section 3.5 includes another delamination simulation, the Ply Drop-Off test. This simulation consist in applying a tensile stress to a laminate with a thickness variation in its mid-span. This numerical example is also used to present a new procedure to take into account the delamination phenomenon in large scale structural simulations of laminated composites using the classical lamination theory. The results obtained with this simulation prove the ability of the developed procedure to take into account delamination failure when the composite performance is obtained using the serial/parallel mixing theory and the classical lamination theory.

Results shown in this section have been already published in Martínez et al. (2007c, 2008a); Oller et al. (2008)

Chapter 4: Compression strength of composite materials

The last micro-mechanical failure included in this work is the compression failure of composites due to fibre micro-buckling. This failure mode is used to describe the new methodology proposed to take into account micro-mechanical effects in the serial/parallel mixing theory.

This chapter contains a first section (section 4.2) in which are described the different numerical formulations proposed in literature to obtain the compression strength of long fiber reinforced composites.

Afterwards, in section 4.3 is described the procedure proposed to include the fiber buckling effect in the SP RoM. This procedure is based in an homogenization of the constitutive equations used to characterize fiber and matrix materials, to take into account their micro-structural interaction. The validation of the homogenization procedure proposed is described in section 4.4, comparing the results obtained with the new formulation with the results provided by a finite element micro-model.

Having validated the homogenization method used to consider the interaction between the composite constituents in the SP RoM, this method is used to develop a numerical procedure capable to obtain the compression strength of composite structures. The procedure proposed is described in section 4.5. This procedure takes into account the different loading cases that can be found in the composite as well as the level of fiber misalignment.

The validation of the compression strength formulation developed is described in section 4.6, comparing some experimental results obtained from literature with the numerical results

provided by the developed formulation. This section also includes a numerical example which provides a better comprehension of the numerical procedure proposed to obtain the compression strength of fiber reinforced composites.

A first formulation of the theory described in this section, as well as some preliminary results obtained with it, have been already published in Martínez et al. (2007b)

References

- Balacó de Morais, A. and Torres Marques, A. (1997). A micromechanical model for the prediction of the lamina longitudinal compression strength of composite laminates. *Journal of Composite Materials*, 31(14):1397–1412.
- Balzani, C. and Wagner, W. (2007). An interface element for the simulation of delamination in unidirectional fiber-reinforced composite laminates. *Engineering Fracture Mechanics*, doi:10.1016/j.engfracmech.2007.03.013.
- Barbero, E. J. (1999). *Introduction to composite materials design*. Taylor & Francis, Philadelphia, USA.
- Barbero, E. J. and Tomblin, J. S. (1996). A damage mechanics model for compression strength of composites. *International Journal of Solids and Structures*, 33(29):4379–4393.
- Borg, R., Nilsson, L., and Simonsson, K. (2002). Modeling of delamination using a discretized cohesive zone and damage formulation. *Composites and Science Technology*, 62(10–11):1299–1314.
- Borg, R., Nilsson, L., and Simonsson, K. (2004). Simulating DCB, ENF and MMB experiments using shell elements and cohesive zone model. *Composites and Science Technology*, 64(2):269–278.
- Camanho, P. P. and Dávila, C. G. (2002). Mixed-mode decohesion finite elements for the simulation of delamination in composite materials. Technical Report TM-2002-211737, NASA.
- Car, E. (2000). *Modelo constitutivo continuo para el estudio del comportamiento mecánico de los materiales compuestos*. PhD thesis, Departament de Resistència de Materials i Estructures a l'Enginyeria (RMEE) – UPC. Directors: Sergio Oller and Eugenio Oñate.
- CIMNE (1991-2008). *PLCd Manual. Non-linear thermomechanic finite element code oriented to PhD student education*. Finite element code developed at CIMNE.
- CIMNE and Quantech (2008). *ComPack-Aero. Innovative finite element methods for non linear analysis of composite structures*. Explicit finite element code developed by CIMNE & Quantech ATZ. www.cimne.com; www.quantech.es/QuantechATZ/Stampack.html.
- CompositesWorld (2008). Sourcebook 2008. Article: Fiber demand and supply. www.compositesworld.com/sb.
- Daniel, I. M. and Ishai, O. (1994). *Engineering mechanics of composite materials*. Oxford Univeristy Press, New York, USA.
- Drapier, S., Grandidier, J. C., and Potier-Ferry, M. (1999). Towards a numerical model of the compressive strength for long fibre composites. *European Journal of Mechanics A/Solids*, 18(1):69–92.
- Gay, D., Hoa, S. H., and Tsai, S. T. (2003). *Composite materials. Design and applications*. CRC Press LLC, Boca Raton, Florida, USA.
- Jansson, N. E. and Larsson, R. (2001). A damage model for simulation of mixed-mode delamination growth. *Composite Structures*, 53(4):409–417.

- Jochum, C. and Grandidier, J.-C. (2004). Microbuckling elastic modelling approach of a single carbon fibre embedded in an epoxy matrix. *Composites and Science Technology*, 64(16):2441–2449.
- Jones, R. M. (1999). *Mechanics of composite materials*. Taylor & Francis, Philadelphia, USA, 2nd edition.
- Krueger, R. (2004). Virtual crack closure technique: history, approach and applications. *Applied Mechanics Reviews*, 57(2):109–143.
- Martínez, X., Oller, S., and Barbat, A. (2006). Numerical tool to study structural reinforcement of steel reinforced concrete (RC) structures under seismic loads using fibre reinforced polymers (FRP). In *ECEES – First European Conference on Earthquake Engineering and Seismology*, September, Geneva, Switzerland.
- Martínez, X., Oller, S., and Barbat, A. (2007a). Herramienta numérica para el estudio de refuerzos de estructuras de hormigón mediante polímeros reforzados con fibras. In *AEIS-3. 3er Congreso Nacional de Ingeniería sísmica*, May, Girona, Spain.
- Martínez, X., Oller, S., Barbat, A., and Rastellini, F. (2007b). New procedure to calculate compression strength of FRP using the serial/parallel mixing theory. In *FRPRCS-8 – 8th International Symposium on Fiber Reinforced Polymer Reinforcement for Concrete Structures*, July, Patras, Greece.
- Martínez, X., Oller, S., and Barbero, E. (2007c). Study of delamination in composites by using the serial/parallel mixing theory and a damage formulation. In *Composites 2007 – ECCOMAS thematic conference on mechanical response of composites*, September, Porto, Portugal.
- Martínez, X., Oller, S., and Barbero, E. (2008a). *Mechanical response of composites*, chapter Study of delamination in composites by using the Serial/Parallel mixing theory and a damage formulation. Springer, ECCOMAS series edition.
- Martínez, X., Oller, S., Rastellini, F., and Barbat, A. (2007d). Numerical procedure for the computation of RC structures reinforced with FRP using the serial/parallel mixing theory. In *9th USNCCM – US National Congress on Computational Mechanics*, July, Berkeley, San Francisco, USA.
- Martínez, X., Oller, S., Rastellini, F., and Barbat, A. (2008b). A numerical procedure simulating RC structures reinforced with FRP using the serial/parallel mixing theory. *Computers and Structures*, doi:10.1016/j.compstruc.2008.01.007.
- Meier, U. (1995). Strengthening of structures using carbon fibre/epoxy composites. *Construction and Building Materials*, 9(6):341–351.
- Nanni, A. (2003). North american design guidelines for concrete reinforcement and strengthening using FRP: principles, applications and unresolved issues. *Construction and Building Materials*, 17(6-7):439–446.
- Oller, S. (2003). *Simulación numérica del comportamiento mecánico de los materiales compuestos*. CIMNE (Centro Internacional de Métodos Numéricos en Ingeniería), Barcelona, Spain.
- Oller, S. and Car, E. (2002). *Análisis y cálculo de estructuras de materiales compuestos*, chapter Teoría de mezclas para el estudio de los materiales compuestos: Matriz reforzada con fibras largas y cortas, pages 145–186. CIMNE (Centro Internacional de Métodos Numéricos en Ingeniería), Barcelona, Spain.

- Oller, S., Martínez, X., Barbat, A., and Rastellini, F. (2008). Advance composite materials. In Martins, R., Branco, C. M., Teixeira, J., and Fernandes, F., editors, *11th Portuguese conference on fracture*, pages 3–22, February, Lisbon, Portugal
- Oller, S., Miquel, J., and Zalamea, F. (2005). Composite material behaviour using a homogenization double scale method. *Journal of Engineering Mechanics*, 131(1):65–79.
- Oñate, E. (1995). *Cálculo de estructuras por el método de elementos finitos. Análisis estático lineal*. CIMNE (Centro Internacional de Métodos Numéricos en Ingeniería), Barcelona, Spain, 2nd edition.
- Orifici, A. C., Herszberg, I., and Thomson, R. S. (2008). Review of methodologies for composite material modelling incorporating failure. *Composite Structures*, 10.1016/j.compstruct.2008.03.007.
- Peters, S. T. (1998). *Handbook of composites*. Chapman & Hall, London, UK, 2nd edition.
- Pinho, S. T., Iannucci, L., and Robinson, P. (2006). Formulation and implementation of decohesion elements in an explicit finite element code. *Composites Part A: Applied science and manufacturing*, 37(5):778–789.
- Pulido, M. D. G. and Sobrino, J. A. (1998). Los materiales compuestos en el refuerzo de puentes. *Revista Internacional de Ingeniería y Estructuras*, 3(1):75–95.
- Pulido, M. D. G. and Sobrino, J. A. (2002). *Análisis y cálculo de estructuras de materiales compuestos*, chapter Hacia la aplicación de los materiales compuestos en el diseño de pasarelas, pages 295–320. CIMNE (Centro Internacional de Métodos Numéricos en Ingeniería), Barcelona, Spain.
- Rastellini, F. (2006). *Modelización numérica de la no-linealidad constitutiva de laminados compuestos*. PhD thesis, Departament de Resistència de Materials i Estructures a l'Enginyeria (RMEE) – UPC. Directors: Sergio Oller and Eugenio Oñate.
- Rastellini, F., Oller, S., Salomon, O., and Oñate, E. (2007). Composite materials non-linear modelling for long fibre reinforced laminates: Continuum basis, computational aspects and validations. *Computers and Structures*, doi:10.1016/j.compstruc.2007.04.009.
- Reddy, J. N. (2003). *Mechanics of laminated composite plate and shells: theory and analysis*. CRC Press, Boca Raton, Florida, USA, 2nd edition.
- Reichl, M. (2007). Composites turn the blades. *Reinforced Plastics*, 51(4):18–19, 21.
- Rosen, B. (1965). *Fibre composite materials*, pages 37–45. ASM Metals Park, Ohio, USA.
- Sánchez-Palencia, E. (1987). *Homogenization techniques for composite media*, chapter Boundary layers and edge effects in composites, pages 121–192. Springer-Verlag, Berlin, Germany.
- Savage, G., Bomphray, I., and Oxley, M. (2004). Exploiting the fracture properties of carbon fibre composites to design lightweight energy absorbing structures. *Engineering Failure Analysis*, 11(5):677–694.
- Timoshenko, S. P. (1940). *Strength of materials. Part I. Elementary theory and problems*. D. Van Nostrand Company, New York, USA.
- Trusdell, C. and Toupin, R. (1960). *The Classical Field Theories*. Springer Verlag, Berlin, Germany, handbuch der physik iii/i edition.

- Turon, A., Camanho, P. P., Costa, J., and Dávila, C. G. (2006). A damage model for the simulation of delamination in advanced composites under variable-mode loading. *Mechanics of Materials*, 38(11):1072–1089.
- Vasiliev, V. V. and Morozov, E. V. (2001). *Mechanics and analysis of composite materials*. Elsevier, Oxford, UK.
- Zienkiewicz, O. C. and Taylor, L. R. (1991). *The finite element method*. McGraw–Hill Book Company, London, UK.

Chapter 2

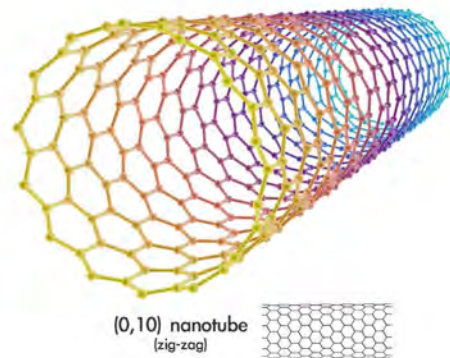
Simulation of the mechanical performance of composite materials

2.1 Introduction

Composites materials can be defined as those materials formed by combining two or more constituents with the intention of obtaining a new material with some improved properties, compared to the ones provided by the constituents on their own. Usually, to consider that a material is a composite, it is required to be able to differentiate its constituents (under this scope, metallic alloys are not considered composites). This sort of materials have been used since ancient times. Probably one of the oldest composite materials known, still being used, is the adobe (figure 2.1a). This is a mixture of clay and straw which main application is found in building constructions. The clay gives consistency to the resultant material, allowing to define a “shape”, while the straw provides the strength. From this ancient composite, the technology of composite materials has suffered enormous improvements, leading to a new generation of composites which properties were unthinkable some years ago. These improvements have appeared in all fields related to the composites, from their manufacturing process to the properties and composition of their constituents. Figure 2.1b shows the structure of a single walled carbon nano-tube, which can provide plastic elongations of 280% before its failure (Huang et al., 2006).



(a) Adobe bricks



(b) Single-walled carbon nanotube

Figure 2.1: Evolution of composite materials, from adobe to nano-technology

As composite materials have become more technological, improving their properties and performance, the calculation tools have also improved. New theories and formulations have appeared in recent decades with the objective of predict the mechanical performance of composite materials. These formulations take into account the anisotropic properties of composites, their structural configuration (pultruded elements, laminates, etc.) and their failure modes. However, despite all improvements, the existing calculation methods are still some steps behind the manufacturing technologies: composites performance increase without having formulations capable to predict it. This makes the design of composite structures to be based, in many occasions, in experimental simulations.

Most of the existing formulations, developed to obtain the mechanical performance of composites, consider the composite a single material, which mechanical properties are inherited from its constituents. This approach provides formulations that are valid for an specific composite but that cannot be used if the constituent materials present a different mechanical performance to the one considered when developing the formulation. In example, many of these formulations treat long fiber reinforced composites assuming a linear elastic behavior of fiber material, therefore, the formulation loses its applicability when fibers become non-linear. Thus, it can be concluded that nowadays formulations and theories to calculate composite structures, most of them based in analytical techniques, are unable to obtain an accurate

prediction of the composite performance when non-linear effects must be considered (Oller, 2003).

To solve this drawback, two different theories are being developed in recent years which deal with composite materials with a completely different approach. Instead of developing a formulation that provides the performance of the composite, what these theories propose is to obtain the composite performance from the result provided by a model that deals with the composite constituents. These new approaches center their effort in modeling the constituents performance and, more important, on how the results obtained from the constituents can be used and extrapolated to predict the global behavior of the composite. These two theories are: homogenization and the rule of mixtures.

The homogenization theory deals with composite structures using a two-scale approach. On the macroscopic scale the composite materials determine the global response of the structure. Composites are considered to be homogeneous materials in this scale. The microscopic scale represents an elemental representative volume (RVE) in which the microscopic fields inside the composite are obtained. This scale deals with the component materials of the composite, each one with its own constitutive equation. Homogenization theory relates these two scales by assuming a periodic configuration of the composite material (Sánchez-Palencia, 1987; Oller et al., 2005).

The main problem of the homogenization method is its computational cost. It can be used in small simulations but the simulation of a real structure with it becomes unaffordable with nowadays computational means. Therefore, main studies on homogenization are focused on the study of the structural performance of the RVE (González and Llorca, 2007a) or on how the information can be trespassed from the micro-scale to the macro-scale (Zalamea, 2001; Car et al., 2002).

The other theory, in development, to obtain the performance of the composite from the performance of its constituents is the rule of mixtures or mixing theory. The first formulation of the mixing theory was developed by Trusdell and Toupin (1960) and it is based on two main hypotheses: 1. All composite constituents are subject to same strains. 2. Each constituent contributes to the composite behavior according to its volumetric participation. This first theory has been coupled with the finite element method by Car (2000), whom transformed it into a constitutive equation manager. Any amount of components can be included in the composite, each one with its own constitutive equation, and the mixing theory will obtain the constitutive performance of the composite by coupling the different constituents behaviors. The work made by Car has been improved by Rastellini (2006) with his formulation of the serial/parallel mixing theory. This new formulation replaces the iso-strain hypothesis by an iso-strain hypothesis in fiber direction and a iso-stress hypothesis on the remaining directions.

The main advantage of the mixing theory over the homogenization theory is that it is a procedure that can be used with nowadays computational means to simulate structural elements. Although it cannot reproduce as many micro-structural effects as an homogenization method, it is a powerful numerical procedure that allows simulate composite structures taking into account the non-linear constitutive performance of the composite components. Also, in this work (chapters 3 and 4) it will be shown that some micro-structural phenomenons can be included in the formulation improving the capabilities of the mixing theory.

This chapter contains a first section (section 2.2) that describes the most important theories and formulations developed to obtain the mechanical performance of composite materials. This description goes from the numerical procedures used to simulate composites to the existing failure criterions of the composite. This section also includes a description of the

homogenization theory and presents other formulations, related to the finite element method, that can be used to obtain a better simulation of composites.

Once having reviewed the different available formulations to compute composite materials, section 2.3 describes the mixing theory. The theory is described from its beginnings to the formulation that is used in the present work, the serial/parallel mixing theory. This section also proposes a perturbation method to obtain the tangent constitutive tensor of the composite constituents, and describes how the mixing theory deals with laminated composites.

Finally, section 2.4 shows the potentiality of the serial/parallel mixing theory by solving the problem of reinforced concrete structures reinforced and/or retrofitted with fiber reinforced polymers (FRP). To solve this problem a new construction stages algorithm has been developed and implemented in order to simulate FRP retrofitting in already damaged structures. After describing this new algorithm, a first numerical simulation is performed to validate the code. Afterwards, two different numerical simulations are included to show how the serial/parallel mixing theory deals with large scale problems, such the FRP reinforcement and retrofitting of concrete structures.

2.2 Mechanical performance of composite materials. Numerical procedures and formulations

2.2.1 Numerical procedures used to simulate composites

There are two main numerical procedures that are used to simulate composite materials: Lamination theory and solid finite elements. While solid finite elements, two-dimensional and three-dimensional, can be used to simulate any type of composite structures, lamination theory is a procedure developed for the simulation of laminated composites (shell or membrane elements in which the composite consist of different layers with a different fibers orientation). These two procedures are described in the following.

Finite element method

The finite element method is a numerical approximation technique that provides solution to the differential equations that define the behavior of a continuum domain by discretizing the domain in small regions and providing a solution to the discrete system generated. In structural mechanics, the finite element method is often based on an energy principle such as the virtual work principle or the total potential energy principle. A full description of this method and its numerical implementation can be found in Zienkiewicz and Taylor (1991), Oñate (1995), Bathe (1996) and Belytschko et al. (2000).

The principle of virtual work states that the equilibrium of a body requires that for any compatible small virtual displacement imposed on the body in its state of equilibrium, the total internal virtual work is equal to the total external virtual work:

$$\int_V \delta \varepsilon^T \sigma \, dV = \int_V \delta u \, b \, dV = \int_A \delta u \, t \, dA + \sum \delta u_i \, q_i \quad (2.1)$$

where V and A are the volume and the area of the body where the body forces b , surface forces t and concentrated forces q are applied; δu are the virtual displacements and $\delta \varepsilon$ the

virtual strains.

The discretization of the body into small regions transforms the continuum displacement field u into a discrete one. This discretization is made using the shape functions, N . These functions relate the displacement of the nodes that define the discretization region of the solid (see figure 2.2), with the displacement field of the points found inside the finite element:

$$u = \begin{Bmatrix} u \\ v \\ w \end{Bmatrix} = \sum_{i=1}^K N_i a_i \quad (2.2)$$

Where K is the number of nodes contained in the finite element. In the case shown in figure 2.2, $K = 4$.

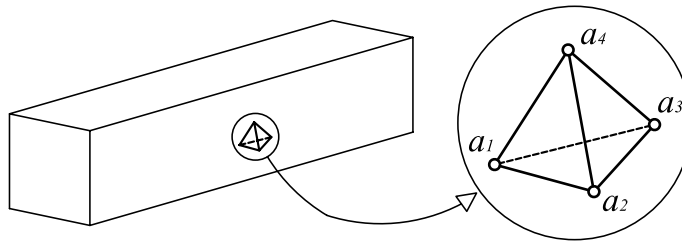


Figure 2.2: Discretization of a beam structure in tetrahedral elements

Using the classical elasticity theory the displacement field is related to the strain field and the forces acting on the body are related to the stresses found in each node used to discretize the structure. Applying these relations, the principle of virtual work is transformed into a linear system of equations that will solve the structural problem. This system provides the displacements of each node of the structure according to the forces applied to it:

$$KU = R \quad (2.3)$$

In equation 2.3, K is the structure stiffness matrix, U the nodal displacement vector and R the nodal force vector. The stiffness matrix is obtained using the deformation matrix, B , that contains the derivatives of the shape functions, and the constitutive stiffness matrix of the material. This matrix provides the mechanical performance of the material relating its stress and strains fields:

$$\sigma = \mathbb{C} : \varepsilon \quad (2.4)$$

The finite element method can be used to solve any kind of structures, having different formulations depending on the typology of the structure: two dimensional or three dimensional solid elements, beam elements, shells, membranes, etc. However, unless providing the finite element method with more tools to deal with composite materials, such as the lamination theory, the homogenization theory or the mixing theory, only a single material can be defined for each element in which the structure is discretized. Figure 2.3 shows two different finite element simulations of composite materials. The simulation shown in figure 2.3a is represented the plastic strains of a compressed fiber reinforced composite in which fibers and matrix are discretized independently (González and Llorca, 2007a). Figure 2.3b shows the

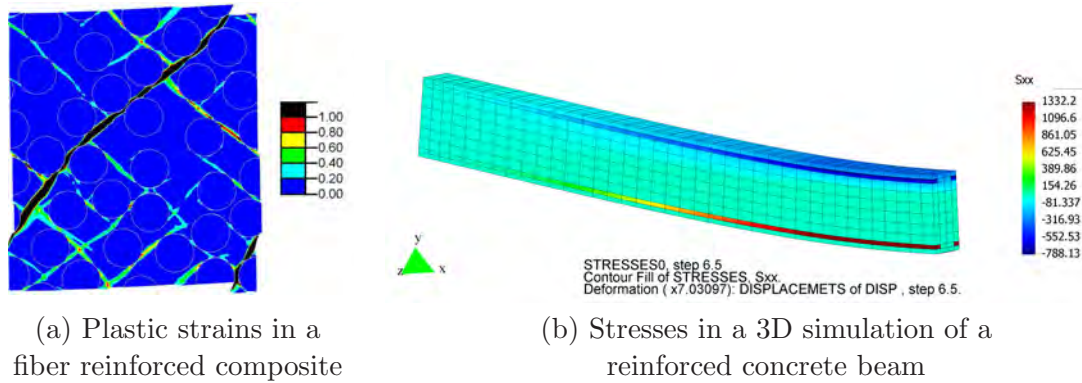


Figure 2.3: 2D and 3D finite element simulations of composite structures

stresses obtained in a reinforced concrete beam; the elements with larger stresses correspond to a composite made of concrete with steel reinforcement (Martínez et al., 2008).

In the two finite element simulations shown in figure 2.3 each finite element contains the information of a material, either a simple material or a composite material. Therefore, to perform these numerical simulations is required the constitutive stiffness matrix of each material defined in the model. In case of composites there are several theories and formulations that provide the elastic parameters required to compute the stiffness matrix. These formulations are described in following sections.

Lamination theory

Composite materials are usually used in structural engineering applications as plates or shells. This structural typology is characterized for having one of its dimensions orders of magnitude smaller than the other two. The composites used in this sort of structures are laminates, which are obtained by stacking different layers made of fibers embedded in a matrix. Being the fibers the material that provide stiffness and strength to each layer (in their longitudinal direction), the layer orientation is characterized by fiber direction. Figure 2.4 shows a laminate made of four layers with orientations $+0/+45/-45/+0$.

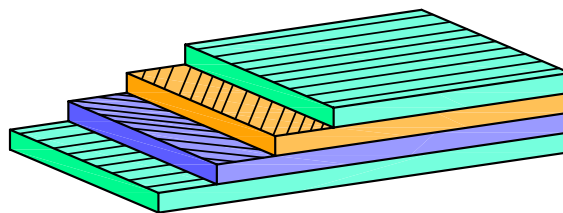


Figure 2.4: Laminated composite with layer orientation $+0/+45/-45/+0$

The success of laminates in structural applications is found because they offer the possibility to be manufactured for the specific application in which they are used (Barbero, 1999). Layer orientation is chosen to provide the adequate stiffness and strength in the direction of the applied loads, being possible to have different strengths in different directions if loads are different in those directions. Therefore, in order to simulate structures made with laminated composites, it is necessary to have a formulation able to provide the composite stiffness and strength, taking into account the layers orientations and their stacking sequence. This formulation is the classical lamination theory. A detailed description of the lamination theory

can be found in many sources such as Ochoa and Reddy (1992), Jones (1999), Barbero (1999) or Reddy (2003). Hereafter is exposed briefly how the composite plate stiffness is obtained with this theory. The outline followed in this description is the one used by Barbero (1999).

Classical lamination theory is based in the hypothesis that a line originally straight and perpendicular to the middle surface remains straight and perpendicular to the middle surface after deformation and that there are no variations in the thickness of the laminate. With these two assumptions, the displacement of each material point of the lamina can be obtained, after deformation, as:

$$\begin{aligned} u(x, y, z) &= u_0(x, y) - z\phi_x(x, y) \\ v(x, y, z) &= v_0(x, y) - z\phi_y(x, y) \\ w(x, y, z) &= w_0(x, y) \end{aligned} \quad (2.5)$$

Being u_0 , v_0 and w_0 the displacements before deformation, u , v and w the displacements after deformation, ϕ_x and ϕ_y the curvature angles in x and y direction and z the position of the point in the laminate thickness. The strain field of the lamina is obtained as a function of the displacements. Using the displacement definition shown in equation 2.5, the strain field can be written as,

$$\begin{Bmatrix} \varepsilon_x \\ \varepsilon_y \\ \gamma_{xy} \end{Bmatrix} = \begin{Bmatrix} \varepsilon_x^0 \\ \varepsilon_y^0 \\ \gamma_{xy}^0 \end{Bmatrix} + z \begin{Bmatrix} \kappa_x \\ \kappa_y \\ \kappa_{xy}^0 \end{Bmatrix} \quad (2.6)$$

where κ is the curvature of the laminate.

The forces applied to the lamina can be obtained integrating, along the thickness, the stress field of each layer, which provides the following set of equations (neglecting the transverse shear deformations),

$$\begin{Bmatrix} N_x \\ N_y \\ N_{xy} \end{Bmatrix} = \sum_{k=1}^N \int_{z_{k-1}}^{z_k} \begin{Bmatrix} \sigma_x \\ \sigma_y \\ \sigma_{xy} \end{Bmatrix}^k dz \quad (2.7)$$

$$\begin{Bmatrix} M_x \\ M_y \\ M_{xy} \end{Bmatrix} = \sum_{k=1}^N \int_{z_{k-1}}^{z_k} \begin{Bmatrix} \sigma_x \\ \sigma_y \\ \sigma_{xy} \end{Bmatrix}^k z dz$$

being N the number of layers in the laminate and z_k the coordinate of the top surface of the k th layer.

At this point, the constitutive relation between strains, defined by the stiffness matrix of the material, \mathbb{C} , is used to replace the stress field of equation 2.7 by the strain field defined in 2.6. This leads to the laminate stiffness matrix that can be written as:

$$\begin{pmatrix} N_x \\ N_y \\ N_{xy} \\ M_x \\ M_y \\ M_{xy} \end{pmatrix} = \begin{bmatrix} A & B \\ B & C \end{bmatrix} \begin{pmatrix} \varepsilon_x \\ \varepsilon_y \\ \gamma_{xy} \\ \kappa_x \\ \kappa_y \\ \kappa_{xy} \end{pmatrix} \quad (2.8)$$

with,

$$A = \sum_{k=1}^N \mathbb{C}_k t_k \quad B = \frac{1}{2} \sum_{k=1}^N \mathbb{C}_k t_k \bar{z}_k \quad D = \frac{1}{3} \sum_{k=1}^N \mathbb{C}_k \left(t_k \bar{z}_k^2 + \frac{t_k^3}{12} \right) \quad (2.9)$$

In equation 2.9, t is the thickness of the layer and \bar{z}_k the z position of its medium plane. Matrix A is called inplane stiffness matrix, as it relates the inplane strains with the inplane forces. Matrix D is the bending stiffness matrix, which relates curvatures with bending moments. And, matrix B relates inplane strains to bending moments and curvatures to inplane forces. This matrix becomes zero in homogeneous plates or symmetric laminates.

Equation 2.9 shows the dependence of the laminate stiffness matrix in the composite constitutive matrix, \mathbb{C} . As has been shown when describing the finite element method, this matrix must contain the information of the composite, taking into account the contribution of fibers and matrix. In the following are exposed the most common formulations used to obtain this tensor.

2.2.2 Stiffness of composite materials

As has been shown when defining the numerical procedures most commonly used to obtain the mechanical performance of composite structures both, the lamination theory and the finite element method, require the stiffness tensor of the composite. This tensor is usually obtained from the elastic properties of the composite that are obtained combining the elastic properties of the composite components. There are different models in literature that provide expressions to obtain the elastic parameters of the composite from its constituents, some of them are described in Jones (1999); Barbero (1999); Vasiliev and Morozov (2001).

The elastic parameters required to obtain the constitutive stiffness tensor of a composite material are, in a two-dimensional case (chosen for the sake of simplicity), the in plane elastic modulus or longitudinal modulus E_1 , the transversal modulus E_2 , the poisson's ratio ν and the shear modulus G_{12} . With these parameters, the stiffness tensor is obtained as:

$$\mathbb{C}_{2D} = \frac{1}{1 - 2\nu} \begin{bmatrix} E_1 & \nu E_1 & 0 \\ \nu E_2 & E_2 & 0 \\ 0 & 0 & (1 - 2\nu)G_{12} \end{bmatrix} \quad (2.10)$$

Probably one of the formulations most commonly used to obtain the elastic parameters of the composite, because of its simplicity, is the rule of mixtures (RoM) and the inverse rule of mixtures (inverse RoM) (Trusdell and Toupin, 1960). These formulations consider that the contribution of the composite components to the composite stiffness is proportional to their volumetric participation in the composite. The rule of mixtures considers an iso-strain condition and is applied to the properties in the fiber direction:

$$\begin{aligned} E_1 &= {}^f k^f E_1 + {}^m k^m E_1 \\ \nu &= {}^f k^f \nu + {}^m k^m \nu \end{aligned} \quad (2.11)$$

Being ${}^f k$ and ${}^m k$ the volumetric participation of fiber and matrix in the composite, respectively. The rest of elastic parameters are calculated using the inverse RoM, which considers an iso-stress condition to obtain the composite properties. Therefore,

$$\begin{aligned} \frac{1}{E_2} &= \frac{{}^f k}{{}^f E_2} + \frac{{}^m k}{{}^m E_2} \\ \frac{1}{G_{12}} &= \frac{{}^f k}{{}^f G_{12}} + \frac{{}^m k}{{}^m G_{12}} \end{aligned} \quad (2.12)$$

From this first approximation, defined by equations 2.11 and 2.12, different authors have tried to improve the formulation to predict the elastic parameters of the composite. Paul (1960) bounded the values of the elastic parameters. The lower bound was obtained with the principle of minimum complementary energy while the upper bound was obtained with the principle of minimum of potential energy. These boundaries were attempted to be tightened by Hashin, Hashin and Shtrikman, and Hashin and Rosen (Jones, 1999).

Another approach to improve the prediction of the elastic parameters of the composite is found with the introduction of semi-empirical parameters in the formulation. Tsai (1964) proposed a formulation in which a new variable C is included in equations 2.11 and 2.12. C represents the degree of contiguity in the fibers, being $C = 0$ the case of isolated fibers and $C = 1$ the case of having all fibers in contact. Tsai formulation provides improved expressions for E_2 , ν and G_{12} . Halpin and Tsai (1969) introduce an empirical parameter ξ in the formulation. This parameter depends on the fiber geometry, packing geometry and loading conditions. These authors include this parameter in the calculation of E_2 and G_{12} . Actually, these equations seem to be a commonly accepted approach to obtain the elastic parameters of the composite (Jones, 1999).

2.2.3 Failure criteria of composite materials

As well as with the stiffness prediction of composite materials, there are also different models that propose expressions to obtain the maximum stresses that can be applied to the composite before its failure. There are several reviews of the different methods available in literature, among them it is worth to mention the ones by Sun et al. (1996), Barbero (1999) and Mayugo (2003).

According to Sun et al. (1996), the most commonly used methods to predict the failure of the composite are, from the most used to the less used, the maximum strain criterion, the maximum stress criterion, the Tsai-Hill criterion and the Tsai-Wu criterion. The first two criteria predicts the material failure when at least one of the strains or stresses (respectively) of the composite reach the maximum allowed value. The maximum strain or stress values are obtained for each direction independently, using experimental simulations or micro-mechanical approaches.

The main problem of this approach is that it does not consider any interaction between the different strain/stress components. In example, if σ_1 and σ_2 are very close to their limit stress

value but does not reach it, the material does not fail. Experimental data has proven that these two approaches are too conservative. The Tsai-Hill and Tsai-Wu criteria are developed to address this shortcoming (Barbero, 1999).

These two methods relate the different stresses found in the composite, defining an equation that provides the maximum combination of stresses that can be found in the composite before its failure (a constitutive law). The Tsai-Hill criterion states that the composite fails when the following equation is fulfilled:

$$\frac{(\sigma_1)^2}{(F_1)^2} - \frac{(\sigma_1\sigma_2)}{(F_1)^2} + \frac{(\tau_{12})^2}{(F_{12})^2} = 1 \quad (2.13)$$

Being σ_1 , σ_2 and τ_{12} the stress components in the composite (considering a two dimensional formulation) and F_1 , F_2 and F_{12} the maximum stresses that can be applied to the composite in each direction.

The Tsai-Wu criterion uses a complete quadratic expression and takes into account the different strength values obtained in the composite for tensile and compressive states. According to this criterion, failure in the composite will occur when:

$$f_1(\sigma_1) + f_2(\sigma_2) + f_{11}(\sigma_1)^2 + f_{22}(\sigma_2)^2 + 2f_{12}(\sigma_1\sigma_2) + f_3(\tau_{12})^2 = 1 \quad (2.14)$$

With,

$$\begin{aligned} f_1 &= \frac{1}{F_{1t}} - \frac{1}{F_{1c}} & f_2 &= \frac{2}{F_{2t}} - \frac{2}{F_{2c}} \\ f_{11} &= \frac{1}{F_{1t}F_{1c}} & f_{22} &= \frac{1}{F_{2t}F_{2c}} \\ f_{12} &= -\frac{1}{2F_{1t}^2} & f_3 &= \frac{1}{F_{12}^2} \end{aligned} \quad (2.15)$$

Besides the models described, exist other quadratic failure criterions such the ones defined by Azzi-Tsai, Hoffman or Chamis, whose models vary the parameters F_i and F_{ij} of the failure mode proposed by Tsai-Wu (Rastellini, 2006). Another approach is the one proposed by Hasin and Hasin-Rotem in which the failure of the composite is divided by failure modes: fiber failure and matrix failure (Sun et al., 1996). Hasin model has been improved recently by Dávila et al. (2005), with a phenomenological formulation that takes into account local effects that can lead to the composite failure.

2.2.4 Homogenization theory

All formulations and numerical procedures described so far are based on a linear elastic behavior of the composite components. Composite failure is determined using experimental data or micro-mechanical formulations that, again, consider a linear elastic performance of the composite constituents. The validity of the results obtained, together with the simplicity of the formulations, make this approach the most commonly used in industry to calculate composite structures. Besides, when designing composite structures, usually the materials are kept in their elastic range for safety purposes. However, these formulations cannot be used to obtain failure modes of the composite or to perform simulations in which the composite

components are loaded beyond its elastic range. With the aim of solving this drawback, two different formulations can be considered, in the frame of numerical simulations of composite materials, the homogenization theory and the mixing theory. In this section, the homogenization theory is briefly described.

An homogenization method deals with the global problem of composite material in a two-scale context. The first scale, named macroscopic or global scale, uses the composite materials to obtain the global response of the structure; composites are treated as homogeneous materials. The second scale, named microscopic or local scale, characterizes an elemental characteristic volume in which the microscopic fields inside the composite are obtained; this scale deals with the component materials.

An schematic representation of an homogenization method is shown in figure 2.5. This figure shows that the macro-scale solves the global structural problem dividing the structure in different Representative Volume Elements (RVE). The mechanical performance of each RVE is obtained with a micro-model of the composite. Once having the mechanical performance of the micro-model, the results can be trespassed to the macro-scale to obtain the global structural response to the loads applied. With this approach, complex finite element models can be used to simulate the composite in its micro-scale, taking into account micro-structural phenomenons such as fiber-matrix debonding, fiber buckling, fiber kink-band, matrix degradation, thermal effects, performance of woven-type composites, etc.

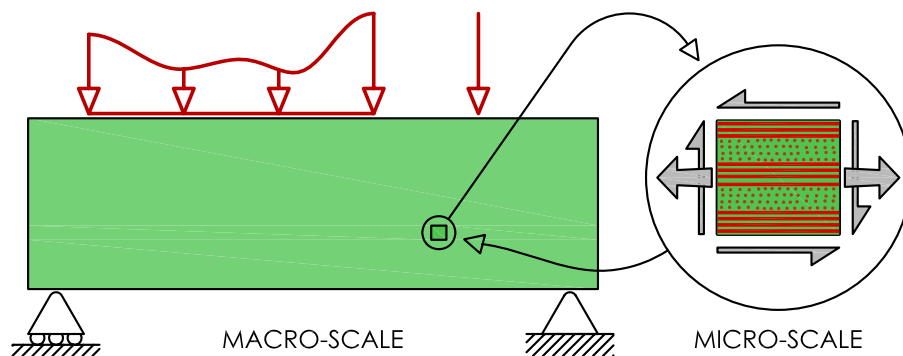


Figure 2.5: Homogenization method applied to a composite beam

The main problem of homogenization theory is its computational cost. An example the computational effort required to solve a composite structure with an homogenization method is provided by Zalamea (2001) in his PhD dissertation. Zalamea solved the problem of a fiber reinforced thick cylinder with an internal compression. The macro-model of the cylinder was simulated with 60 finite elements while the representative volume element micro-model contained 108 elements. The problem was solved using a parallel process with 4 processors. The time required to solve the problem was 1 hour and 15 minutes. Figure 2.6 shows solutions obtained for the macro and the micro-model.

Due to the difficulty of developing large scale simulations with complex micro-structures using the homogenization method with nowadays computer capabilities, main efforts are focussed in the development of reliable micro-models to simulate the RVE and on the development of processes to trespass the information obtained from the micro-model to the macro-model.

Many authors have developed models, usually using the finite element method, to study the mechanical behavior of composite RVE's. Different models are proposed according to the effect that wants to be studied. To name a few, González and Llorca have developed models to study the effect of transversal compression in unidirectional fiber reinforced composites

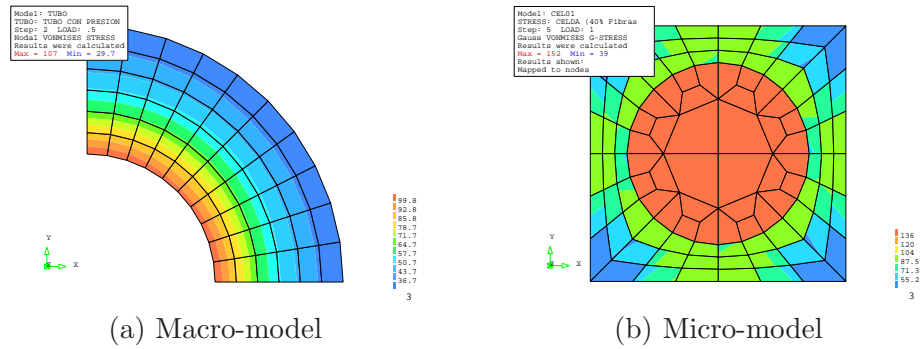


Figure 2.6: Finite Element simulation of a thick composite cylinder with an internal compression using an homogenization method (Zalamea, 2001)

(González and Llorca, 2007a) and the effects of an initial notch in a unidirectional fiber reinforced composite under bending loads (González and Llorca, 2007b). Bahei-El-Din et al. (2004) propose a RVE model to study the micro-mechanical performance of woven composites. Oller et al. (2002) propose a model to simulate masonry structures; and Ravi Annapragada et al. (2007) have developed a model to predict the thermo-mechanical properties of particulate composites.

Regarding the methods to trespass the information obtained from the micro-model to the macro-model, homogenization theory assumes a periodical configuration of the composite material to relate these two scales. Assuming this periodicity, the effective value of stresses, strains and internal variables in the macroscopic scale becomes associated to an average of these fields in the microscopic scale. Several techniques have been developed to relate these both scales, among them, four should be remarked:

Auto-consistent method: All phases of the material are included in an equivalent medium, which properties are the ones to be determined. Once these properties are obtained, the composite material will be computed with them. This method is based in the work of Eshelby (1957), in which the inclusion of an ellipsoid in an elastic medium was studied.

Variational contours method: This method consist on defining an upper and a lower limit values to the stiffness of the system. This first idea was proposed by Hill (1963) defining the limits obtained imposing the iso-strain and iso-stress states. This method has been improved, reducing the limit range, by several authors.

Average method: This method is based in the definition of a characteristic volume in the composite used to obtain its average properties. This procedure was improved by Suquet (1982) with its extension to periodical mediums.

Asymptotic homogenization method: This methodology proposes solving the problem in two different scales: a macroscopic scale for the composite and a microscopic scale for its constituents. The relation between these two scales is defined with a parameter that takes into account the magnitude difference between them. The methodology proposal and its major development corresponds to Sánchez-Palencia (1987). An improvement of the theory, in the context of continuum mechanics, and formulated using the Finite Element Method is proposed by Zalamea (2001). This last formulation has been improved by Oller et al. (2005).

2.2.5 Other numerical formulations for composite materials

In this work, the mechanical performance of composite materials is obtained using a finite element formulation that deals with composite materials using the serial/parallel mixing theory. The serial/parallel mixing theory is described in detailed in the following section (section 2.3), from the first model developed by Trusdell and Toupin (1960) to the final formulation proposed by Rastellini (2006). However, before moving to the mixing theory formulation, it is worth to describe other numerical formulations and procedures that can be used to perform finite element simulations of composite materials. Some of these formulations are used in this work.

Anisotropy using a mapping space theory

This theory is based on the transport of all the constitutive parameters and the stress and strain states of the structure, from a real anisotropic space, to a fictitious isotropic space. Once all variables are in the fictitious isotropic space, an isotropic constitutive model can be used to obtain the new structure configuration. This theory allows considering materials with high anisotropy, such as composite materials, using all the techniques and procedures already developed for isotropic materials.

All the anisotropy information is contained in two fourth order tensors. One of them, A_{ijkl}^σ , relates the stresses in the fictitious isotropic space ($\bar{\sigma}_{ij}$) with the stresses in the real anisotropic space (σ_{ij}) and the other one, A_{ijkl}^ε , does the same with the strains. The relation of both spaces for the strains and the stresses is exposed in the following equation:

$$\begin{aligned}\bar{\sigma}_{ij} &= A_{ijkl}^\sigma : \sigma_{ij} \\ \bar{\varepsilon}_{ij} &= A_{ijkl}^\varepsilon : \varepsilon_{ij}\end{aligned}\tag{2.16}$$

A representation of these transformations is displayed in figure 2.7. A more detailed description of this methodology, the extension to large strains and its numerical implementation can be obtained in (Car et al., 2000, 2001).

Fiber-matrix debonding

The apparition of matrix cracks in a composite material is usually followed by a relative movement between the fibers and the matrix. This lost of adherence implies a stiffness reduction in the composite material. This phenomenon is introduced in the elastic limit of the material as a modification of its yield surface criterion. The new fibre elastic limit becomes:

$$(F^R)_f = \min \{ (F^N)_f; (F^N)_m; [2(F^N)_{fm}/r_f] \}\tag{2.17}$$

Where $(F^R)_f$ is the new fiber strength, $(F^N)_f$ is the nominal fiber strength, $(F^N)_m$ is the matrix nominal strength, $(F^N)_{f-m}$ is the fiber-matrix interface nominal strength and r_f is the fiber diameter. Equation 2.17 shows that the debonding process takes place when one of the composite constituents reaches its nominal strength (considering the fiber-matrix interface a constituent). The nominal strength values are obtained from the material properties. The numerical implementation of this phenomenon is described in Car (2000) and Oller (2002).

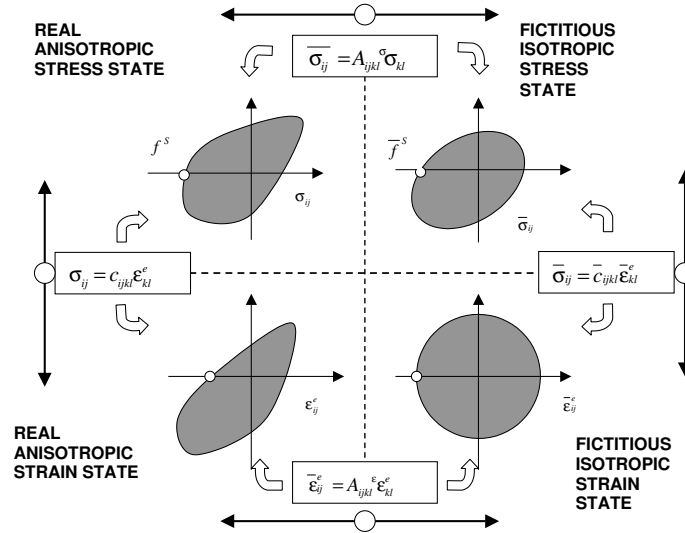


Figure 2.7: Anisotropy using a mapping space theory. Space transformations. Real and fictitious stress and strain spaces. (Car, 2000)

Constitutive equations and yield laws

The serial/parallel mixing theory obtains the performance of the composite material from the constitutive performance of its components. This constitutive performance is obtained using the constitutive equations and yield laws defined in continuum mechanics.

Among all constitutive theories existing in literature, this work uses mainly three of them: elasticity (Timoshenko, 1940; Marsden and Huges, 1983), plasticity (Malvern, 1968; Lubliner, 1990; Simo and Huges, 1998) and damage (Kachanov, 1986). The damage formulation used in this work is an improvement of Kachanov's damage theory, proposed by Oliver et al. (1990), which distinguish between tensile and compressive stresses and provides a different damage evolution in each case. Regarding constitutive equations, it is also worth to mention the plastic-damage formulation described by Oller (2001), as many epoxy resins used in composite materials follow the strength evolution defined by this formulation.

Plastic and damage formulations consider that the material has an elastic behavior until it reaches a stress state in which the elastic performance is lost, leading to a reduction or an increment of the material strength. The maximum stress state obtained before the variation of the mechanical performance of the material is defined by the yield law. Different yield laws have been defined and proposed for different materials in order to characterize its particular fracture mode, in example, steel is usually simulated with a Von-Mises criterion while concrete performance is better represented by a Mohr-Coulomb law. Several of these constitutive laws are described in Oller (2002).

2.3 Mixing theory

The classical rule of mixtures, or mixing theory, deals with composite materials using a macro-scale approach based on the mechanics of continuous mediums. The composite mechanical behavior is obtained from the constitutive performance of its component materials, being possible to include the constituents material non-linearities into the composite mechanical

performance. This approach represents a substantial improvement compared to other existing formulations developed to deal with composite materials, as these only provide an accurate prediction of the composite mechanical performance when its constituents are in their elastic range. Another advantage of the mixing theory is that it can use all existing numerical procedures and formulations already developed to simulate continuum materials to obtain the performance of the composite constituents.

Although the mixing theory does not take into account the micro-structural interaction among the composite components, as does the homogenization theory, it provides an accurate prediction of the composite mechanical performance, taking into account material non-linearities, with an affordable computational cost, which allows to perform large numerical simulations of composite structures.

This section describes the mixing theory following its development process. It starts with the first formulation proposed by Trusdell and Toupin (1960) and ends with the enhanced serial/parallel mixing theory formulated by Rastellini (2006). At the end of the section it is also described how the tangent stiffness tensor of the composite components can be obtained, for any yield function, using a perturbation method and, finally, how the mixing theory can be used to simulate laminated composites.

2.3.1 Classical mixing theory

The first formulation of the rule of mixtures corresponds to Trusdell and Toupin (1960). This first work became the base of future studies developed by Ortiz and Popov (1957, 1982) and Green and Naghdi (1965). The classical rule of mixtures define the way in which all substances composing a material interact to provide the material performance. This interaction is defined with the following hypothesis:

- i. Each infinitesimal volume of the composite contains a finite number of material components.
- ii. Each component contribution to the global behavior of the composite is proportional to its volumetric participation.
- iii. All components suffer the same strains (closing equation), iso-strain assumption.
- iv. The volume of each component is significantly smaller than the composite volume.

The closing equation, defined in condition (iii), defines an iso-strain field for all composite components. This can be written as:

$$c_\varepsilon = {}^1\varepsilon = {}^2\varepsilon = \dots = {}^n\varepsilon \quad (2.18)$$

Being c_ε the composite strain, ${}^s\varepsilon$ the strain in the composite component s and n the total number of components in the composite.

The stress field of the composite is obtained using the second hypothesis of the mixing theory:

$$c_\sigma = \sum_{s=0}^n {}^s k {}^s \sigma \quad (2.19)$$

Where ${}^s k$ is the volumetric participation of component s in the composite, which is defined by the relation between the volume of the component, V_s , and the total volume of the composite, V :

$${}^s k = \frac{V_s}{V} \quad \text{with} \quad \sum_{s=1}^n {}^s k = 1 \quad (2.20)$$

The relation between the strain and the stress fields is defined with the material constitutive tensor, \mathbb{C} (equation 2.4). Thus, the stress in the composite can be obtained from its strain field using equations 2.18 and 2.19:

$${}^c \sigma = \sum_{s=0}^n {}^s k {}^s \sigma = \sum_{s=1}^n {}^s k ({}^s \mathbb{C} : {}^s \varepsilon) = \sum_{s=1}^n {}^s k ({}^s \mathbb{C} : {}^c \varepsilon) = \left(\sum_{s=1}^n {}^s k {}^s \mathbb{C} \right) : {}^c \varepsilon \quad (2.21)$$

This last equation provides the expression of the composite constitutive tensor, which is defined as:

$${}^c \mathbb{C} = \sum_{s=1}^n {}^s k {}^s \mathbb{C} \quad (2.22)$$

The iso-strain hypothesis defined in the mixing theory implies a parallel distribution of the components in the composite. Depending on the direction in which the loads are applied to it, there are some situations in which the composite performance is better represented by an iso-stress relation between its components. This case is solved with the inverse mixing theory.

Inverse mixing theory

The inverse mixing theory replaces the iso-strain assumption by an iso-stress assumption, therefore:

$${}^c \sigma = {}^1 \sigma = {}^2 \sigma = \dots = {}^n \sigma \quad (2.23)$$

And, the strains in the composite are obtained according to the volumetric participation of each component material:

$${}^c \varepsilon = \sum_{s=0}^n {}^s k {}^s \varepsilon \quad (2.24)$$

Making use of the relation between strains and stresses, provided by the stiffness tensor, it can be obtained the relation between the stress and the strain field in the composite as:

$${}^c \varepsilon = \sum_{s=1}^n {}^s k ([{}^s \mathbb{C}]^{-1} : {}^s \sigma) = \left(\sum_{s=1}^n {}^s k [{}^s \mathbb{C}]^{-1} \right) : {}^c \sigma \quad (2.25)$$

which leads to the expression of the composite stiffness tensor:

$$[{}^c\mathbb{C}]^{-1} = \sum_{s=1}^n {}^s k [{}^s\mathbb{C}]^{-1} \quad (2.26)$$

These both formulations, the mixing theory and the inverse mixing theory, are widely used in the numerical simulation of composite materials; usually to obtain the elastic parameters of the composite from its constituents. However, the hypothesis defined by the mixing theory can be pushed forward, making the theory capable to provide the composite mechanical performance beyond its constituents elastic limit. This is explained in the following section.

2.3.2 Mixing theory as a constitutive equation manager

Oller et al. (1996) and Car (2000) coupled the mixing theory hypothesis with a thermodynamical description of the composite components. This provides a formulation for composite materials that obtains the relation between components, even when they have reached their elastic limit.

This new approach defines the Helmutz free energy of the composite, ${}^c\Psi$, as the sum of the free energies of each composite component, proportional to their volumetric participation. This is:

$${}^c\Psi({}^c\varepsilon^e, \theta, {}^c\alpha^m) = {}^c\Psi(\varepsilon, \theta, \underbrace{{}^c\varepsilon^p, {}^c\alpha^m}_{{}^c p_s}) = \sum_{s=1}^n {}^s k {}^s\Psi(\varepsilon, \theta, {}^s p_s) \quad (2.27)$$

Being ε , ε^e and ε^p the total, elastic and plastic strains (the total strain is the same for the composite and its constituents, according to the mixing theory hypothesis), θ the temperature and α^m , p_s sets of internal variables.

Once having defined the free energy of the composite in function of the free energies of its constituents, the procedure described in Malvern (1968), Lubliner (1990) and Oller (2002) to obtain the stress of single-phase materials from the free energy can be applied to both sides of equation 2.27, obtaining:

$${}^c\sigma = \sum_{s=1}^n {}^s k {}^s\sigma \quad (2.28)$$

It is worth to remark that although equations 2.28 and 2.19 are exactly the same, their meaning is not. Equation 2.28 is obtained following a thermodynamic procedure, which means that the stress values can be obtained using any constitutive law based on thermodynamic principles, such as plasticity or damage. Therefore, the mixing theory has been transformed in a constitutive equations manager, as it obtains the performance of the composite coupling the constitutive performance of its constituents.

The implementation of the mixing theory, as a constitutive equation manager, into a finite element code has been done by Oller et al. (1996) and afterwards improved by Car (2000) in his PhD dissertation, including in it the large deformation theory. The implementation algorithm developed by Car is shown in figure 2.8.

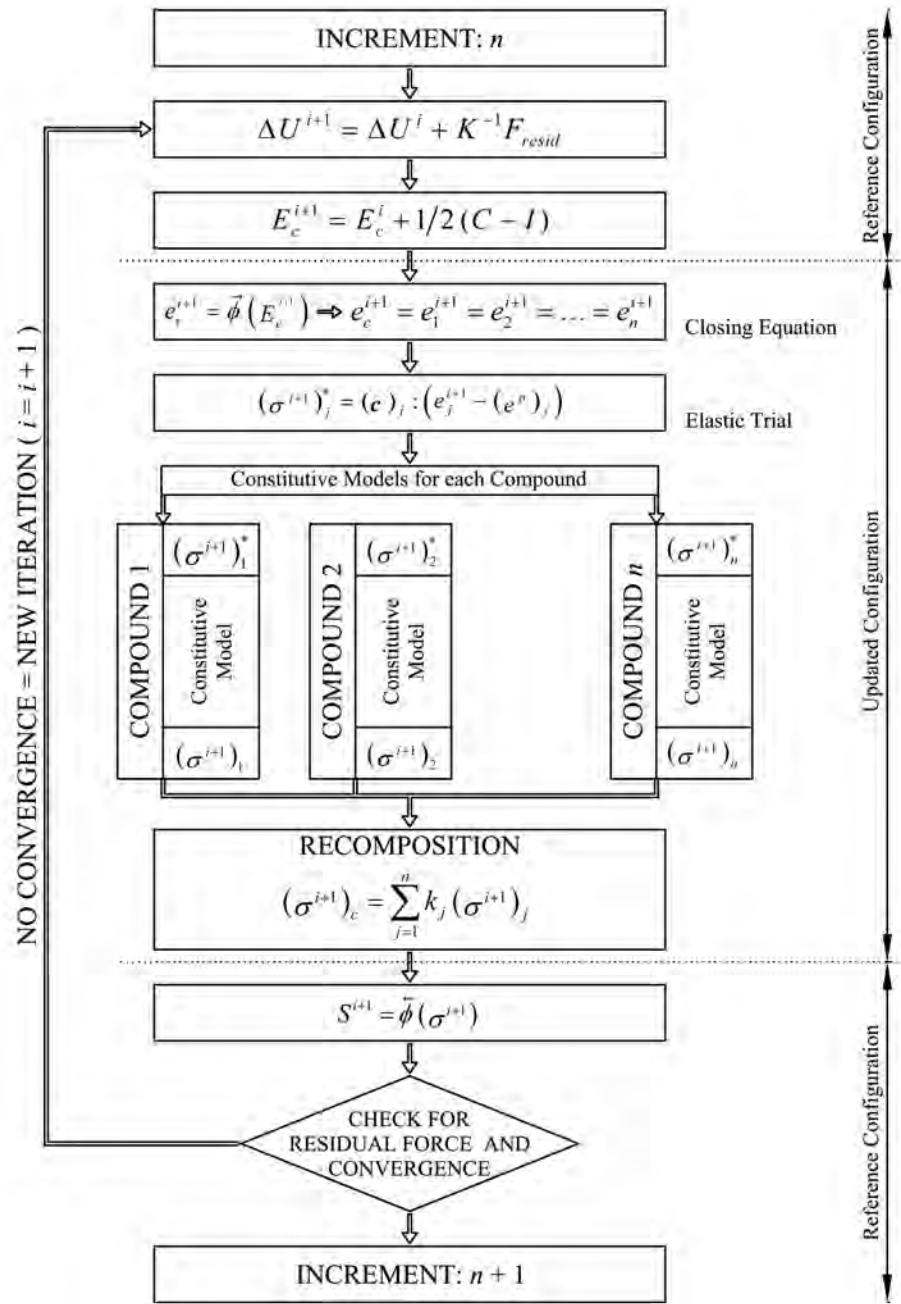


Figure 2.8: Implementation of the mixing theory in a finite element code (Car, 2000)

The validity of the new procedure developed to obtain the mechanical performance of composite materials, even when the composite constituents have reached its elastic yield stress, is proved in the numerical simulations described in Car (2000), Car et al. (2000, 2001) and Oller and Car (2002).

However, this new procedure has the problem already pointed out when describing the classical mixing theory developed by Trusdell and Toupin (1960), the closing equation assumes an iso-strain performance of the composite and its constituents, which forces a parallel behavior of the composite components (figure 2.9a). Although in most cases this assumption can be valid, usually composites are designed to work in fiber direction, depending on the direction of the loads applied other behaviors can be developed: a serial behavior (figure 2.9b) or, most

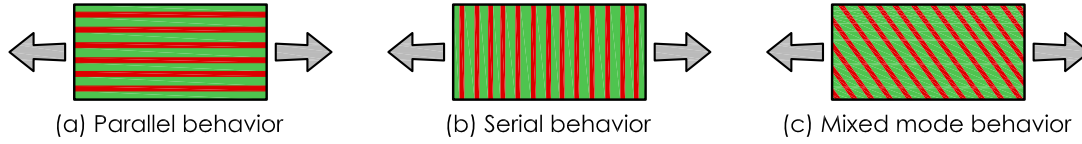


Figure 2.9: Serial-Parallel distribution of the components in a composite material

commonly, a mixed mode behavior (figure 2.9c).

Oller et al. (1995), Neamtu et al. (1997) and Car (2000) made a first attempt to develop a formulation of the mixing theory capable to take into account all possible behaviors of the composite: parallel, serial and mixed. This formulation defines the composite strains as a proportional sum of the serial and parallel strains found in it:

$${}^c\varepsilon_{ij} = (1 - \aleph) {}^c\varepsilon_{ij}^{par} + \aleph {}^c\varepsilon_{ij}^{ser} \quad (2.29)$$

Where ε_{ij}^{par} and ε_{ij}^{ser} stand for the parallel and serial strains, respectively, and \aleph is the proportionality parameter, that depends on the fibre orientation. This parameter has to be obtained from experimental data. The serial and parallel strains of the composite are obtained as a function of the strains of the constituent materials as follows,

$$\varepsilon_{ij}^{par} = \frac{1}{n} \sum_{s=1}^n {}^s\varepsilon_{ij} \quad \text{and} \quad \varepsilon_{ij}^{ser} = \sum_{s=1}^n {}^s\varepsilon_{ij} \quad (2.30)$$

One of the main drawbacks of this formulation is its dependence on experimental data, required to define the value of \aleph . Recently, Rastellini et al. (2003a,b) and Salomon et al. (2005) have developed a more general formulation of the mixing theory capable to take into account the serial and parallel performance of the composite automatically, without the need of experimental or calibration parameters. This theory has been improved with the enriched serial/parallel mixing theory (Rastellini, 2006; Rastellini et al., 2007). Both formulations are described in the following sections.

2.3.3 Serial/parallel mixing theory

The serial/parallel rule of mixtures is an improvement of the classical mixing theory, in which the iso-strain hypothesis is replaced by an iso-strain condition in the fiber direction and an iso-stress condition in the transversal directions. This theory has been developed by Rastellini (2006).

Definition of the serial and parallel components of the strain and stress tensors

The serial/parallel (SP) model considers that the constituent materials of the composite act in parallel in a certain direction and in serial in the remaining directions. Consequently, it is necessary to define and separate the serial and parallel components of the strain and stress tensors.

Defining e_1 as the director vector that determines the parallel behavior (fiber direction), the parallel projector tensor N_P can be defined as follows:

$$N_P = e_1 \otimes e_1 \quad (2.31)$$

From N_P , the 4th-order parallel projector tensor, P_P , is defined as:

$$P_P = N_P \otimes N_P \quad (2.32)$$

The serial projector tensor P_S is evaluated as its complement:

$$P_S = I - N_P \quad (2.33)$$

Both tensors can be used to find the parallel part of the strain tensor ε_P and its serial part ε_S :

$$\varepsilon_P = P_P : \varepsilon \quad \text{and} \quad \varepsilon_S = P_S : \varepsilon \quad (2.34)$$

Hence, the strain state is separated into its parallel and serial part:

$$\varepsilon = \varepsilon_P + \varepsilon_S \quad (2.35)$$

The stress state can be separated analogously, finding its parallel and serial parts using the 4th-order tensors P_P and P_S as:

$$\sigma = \sigma_P + \sigma_S \quad (2.36)$$

where

$$\sigma_P = P_P : \sigma \quad \text{and} \quad \sigma_S = P_S : \sigma \quad (2.37)$$

Numerical modeling hypotheses

The numerical model developed to obtain the strain-stress state in the composite is based on the following hypotheses:

- i. The constituent materials of the composite are subjected to the same strain in the parallel (fiber) direction.
- ii. The constituent materials are subjected to the same stress in the serial direction.
- iii. The response of the composite material is directly related to the volume fractions of its constituent materials.
- iv. The phases in the composite are considered to be homogeneously distributed.
- v. The constituent materials are considered to be perfectly bonded.

Although these hypotheses, as well as the serial/parallel mixing theory, can be applied to composites with any number of components, the developed formulation is restricted to only two of them. Therefore, for the sake of consistency, only two composite components will be included in the theory description: fiber and matrix.

Constitutive equations of compounding materials

When applying the serial/parallel mixing theory, it is possible to use any constitutive equation to describe the structural performance of the composite compounding materials. The constitutive equations used can be different for each component (i.e. an elastic law to describe the fiber behavior and a damage formulation to describe the matrix behavior). Considering that additive plasticity is used to formulate the constitutive equations of the materials, the stresses in the matrix and the fibre are obtained as:

$$\begin{aligned} m_{\sigma} &= m\mathbb{C} : (m_{\varepsilon} - m_{\varepsilon}^p) \\ f_{\sigma} &= f\mathbb{C} : (f_{\varepsilon} - f_{\varepsilon}^p) \end{aligned} \quad (2.38)$$

where m_{ε}^p and f_{ε}^p are the matrix and fiber plastic-strain tensors, respectively, and $m\mathbb{C}$ and $f\mathbb{C}$ are the matrix and fiber constitutive tensors.

These equations can be rewritten to consider the serial and parallel separation of the strain and stress tensors (equations 2.35 and 2.36)

$$\begin{bmatrix} i_{\sigma_P} \\ i_{\sigma_S} \end{bmatrix} = \begin{bmatrix} i\mathbb{C}_{PP} & i\mathbb{C}_{PS} \\ i\mathbb{C}_{SP} & i\mathbb{C}_{SS} \end{bmatrix} : \begin{bmatrix} i_{\varepsilon_P} - i_{\varepsilon_P}^p \\ i_{\varepsilon_S} - i_{\varepsilon_S}^p \end{bmatrix} \quad (2.39)$$

where

$$\begin{cases} i\mathbb{C}_{PP} = P_P : i\mathbb{C} : P_P \\ i\mathbb{C}_{PS} = P_P : i\mathbb{C} : P_S \\ i\mathbb{C}_{SP} = P_S : i\mathbb{C} : P_P \\ i\mathbb{C}_{SS} = P_S : i\mathbb{C} : P_S \end{cases} \quad \text{with} \quad i = m, f \quad (2.40)$$

Equilibrium and compatibility equations

The equations that define the stress equilibrium and establish the strain compatibility between the individual components follow the hypotheses previously described.

$$\begin{aligned} \text{Parallel behavior :} \quad c_{\varepsilon_P} &= m_{\varepsilon_P} = f_{\varepsilon_P} \\ c_{\sigma_P} &= m k^m \sigma_P + f k^f \sigma_P \end{aligned} \quad (2.41)$$

$$\begin{aligned} \text{Serial behavior :} \quad c_{\varepsilon_S} &= m k^m \varepsilon_S + f k^f \varepsilon_S \\ c_{\sigma_S} &= m \sigma_S = f \sigma_S \end{aligned} \quad (2.42)$$

where the superscripts c , m and f stand for composite, matrix and fiber, respectively and $i k$ is the volume-fraction coefficient of each constituent in the composite.

Serial/parallel rule of mixtures algorithm

The strain state of the composite material, ${}^c\varepsilon$, at time $t + \Delta t$ is the known variable entered into the algorithm. Using this variable, the serial/parallel rule of mixtures algorithm has to determine the strain and stress states of each component that fulfils the equilibrium, the compatibility and the constitutive equations and the evolution of the internal variables.

The first step of the algorithm is to separate the strain tensor into its parallel and its serial components in order to compute the strain state in the matrix and the fiber. According to equation 2.41, the parallel strain component is the same for both materials and for the composite. However, to determine the serial strains, it is necessary to predict the expected strains in one of the composite compounding materials. If this prediction is made for the matrix, the algorithm computes its serial strain increment as:

$$[{}^m\Delta\varepsilon_S]^0 = \mathbb{A} : \begin{bmatrix} {}^f\mathbb{C}_{SS} : {}^c\Delta\varepsilon_S + \\ {}^fk({}^f\mathbb{C}_{SP} - {}^m\mathbb{C}_{SP}) : {}^c\Delta\varepsilon_P \end{bmatrix} \quad (2.43)$$

where $\mathbb{A} = ({}^mk{}^f\mathbb{C}_{SS} + {}^fk{}^m\mathbb{C}_{SS})^{-1}$ and ${}^m\Delta\varepsilon_S = {}^{t+\Delta t}[\varepsilon_S] - {}^t[\varepsilon_S]$

The initial prediction of matrix serial strains, according to the method proposed by Rastellini et al. (2007) and shown in equation 2.43, is obtained considering that the parallel and serial components of the total strain are distributed according to the composite stiffness obtained in the previous time step. In the iteration step n , the predicted matrix serial strains are used to compute the fiber serial strains by using equation 2.42. Their expression is:

$${}^{t+\Delta t} [{}^f\Delta\varepsilon_S]^n = \frac{1}{{}^fk} {}^{t+\Delta t} [{}^c\varepsilon_S] - \frac{{}^mk}{{}^fk} {}^{t+\Delta t} [{}^m\varepsilon_S]^n \quad (2.44)$$

where ${}^{t+\Delta t} [{}^m\varepsilon_S]^n = {}^t [{}^m\varepsilon_S] + [{}^m\Delta\varepsilon_S]^n$

The next step is to recombine the serial and parallel components of the strain tensor (equation 2.35). The constitutive equations are then applied to the predicted strains to obtain the stress tensor and the updated internal variables for both materials. The fiber and matrix materials are modeled according to their own constitutive laws. In the case of an additive plasticity law, equation 2.38 is used to obtain the stress tensor for each one of them. The stresses obtained for fiber and matrix from their constitutive law must fulfill the following equation:

$$[\Delta\sigma_S]^n = {}^{t+\Delta t} [{}^m\sigma_S]^n - {}^{t+\Delta t} [{}^f\sigma_S]^n \leq \text{tolerance} \quad (2.45)$$

If the residual stress is smaller than the tolerance, the computed strains and stresses are considered correct and the structural calculation can continue. However, if equation 2.45 is not fulfilled, the initial prediction of the matrix strain tensor has to be corrected. This correction is performed using a Newton-Raphson scheme, which is updated using the Jacobian of the residual forces. The Jacobian is obtained deriving the residue function with respect to the unknown. According to Rastellini (2006), the expression for the Jacobian is given as follows:

$$\mathbb{J} = \left. \frac{\partial \Delta\sigma_S}{\partial {}^m\varepsilon_S} \right|_{{}^m\varepsilon_S = {}^{t+\Delta t} [{}^m\varepsilon_S]^n} = [{}^m\mathbb{C}_{SS}]^n + \frac{{}^mk}{{}^fk} [{}^f\mathbb{C}_{SS}]^n \quad (2.46)$$

and, the expression for correcting the matrix serial strains becomes:

$${}^{t+\Delta t} [{}^m \varepsilon_S]^{n+1} = {}^{t+\Delta t} [{}^m \varepsilon_S]^n - \mathbb{J}^{-1} : [\Delta \sigma_S]^n \quad (2.47)$$

The Jacobian must be obtained using the tangent constitutive tensor for the fibers and the matrix in order to reach quadratic convergence in the serial/parallel mixing theory. However, depending on the constitutive equation defined for each material, it is not always possible to obtain an analytical expression for this tensor. In order to obtain a reliable algorithm, the tangent constitutive tensor is computed with a numerical derivation, using a perturbation method.

Implementation in a finite element code

The serial/parallel mixing theory is implemented in PLCd (CIMNE, 2008) finite element code. This code works with two and three-dimensional solid geometries and with beam elements. It can deal with kinematic and material nonlinearities. It uses various constitutive laws to predict the material behavior (Elastic, visco-elastic, damage, damage-plasticity, etc. (Oller et al., 1990)) and uses different yield surfaces to control their evolution (Von-Mises, Mohr-Coulomb, improved Mohr-Coulomb, Drucker-Prager, etc. (Malvern, 1968; Lubliner et al., 1989)). The Newmark method (Barbat et al., 1997) is used to perform dynamic analysis. A more detailed description of the code can be obtained from Mata et al. (2007, 2008).

The serial/parallel mixing theory is implemented in PLCd code at the constitutive level, adding the iterative procedure described previously. This implementation is described in the flow chart shown in figure 2.10.

2.3.4 Enriched serial/parallel mixing theory

The validation of the serial/parallel mixing theory shows that the hypothesis of iso-stress in the transversal direction of the composite provides a lower bound of the composite transversal stiffness (Rastellini et al., 2007). In order to improve this performance, Rastellini has proposed an enrichment of the serial/parallel mixing theory formulation.

This enrichment consist in increasing the transversal stiffness of the weakest component of the composite, in the case considered the matrix material, with a parameter ${}^m \gamma$ that can be obtained through experimental calibration or through analytical analysis. In order to maintain the solution algorithm proposed by the serial/parallel mixing theory, Rastellini proposes to use the ${}^m \gamma$ parameter to enrich the strains, stresses and the stiffness tensor of matrix material, obtaining $({}^m \varepsilon)^*$, $({}^m \sigma)^*$ and $({}^m \mathbb{C})^*$. This new tensors are used in the serial/parallel rule of mixtures algorithm described in figure 2.10.

The new enriched values of the matrix strain, stress and stiffness tensor are obtained with the following expressions:

$$\begin{aligned} ({}^m \varepsilon)^* &= [\mathbb{K}]^{-1} : {}^m \varepsilon \\ ({}^m \sigma)^* &= \mathbb{K} : {}^m \sigma \\ ({}^m \mathbb{C})^* &= \mathbb{K} : {}^m \mathbb{C} : \mathbb{K} \end{aligned} \quad (2.48)$$

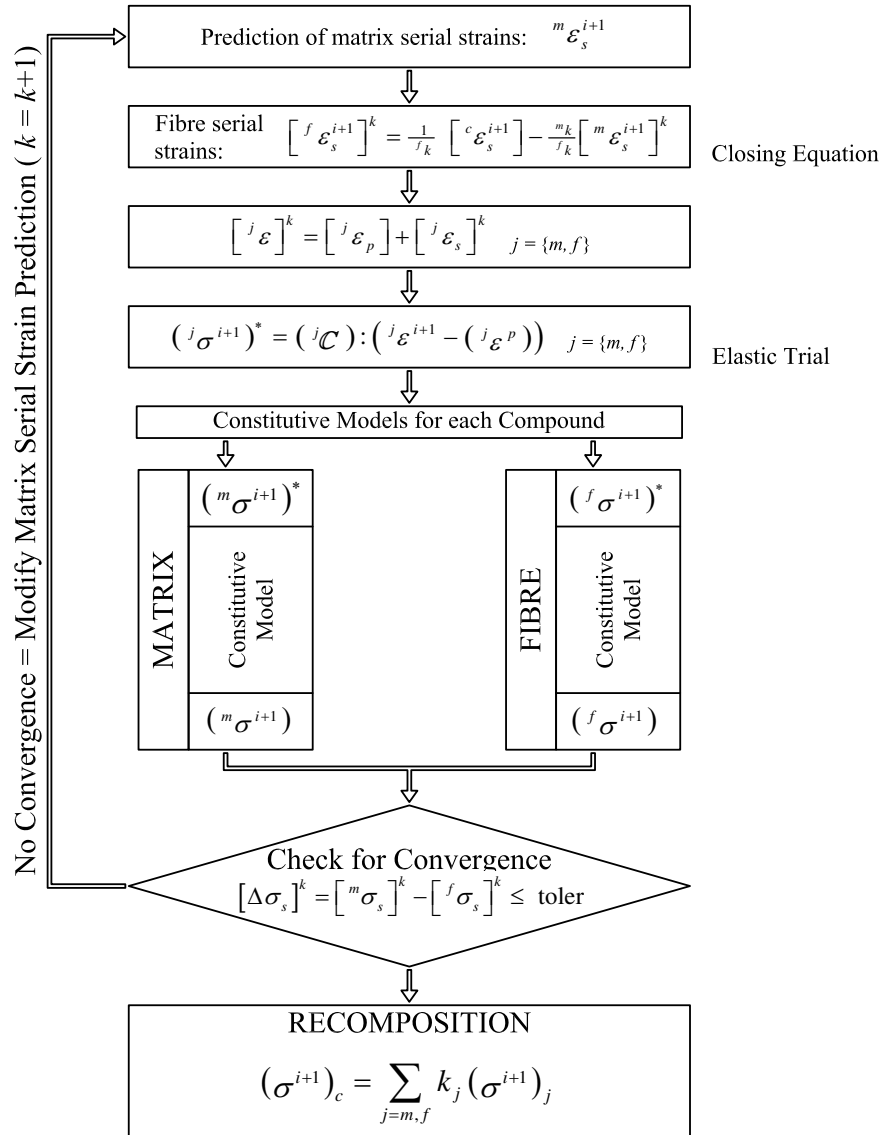


Figure 2.10: Flow chart of the serial/parallel rule of mixtures algorithm

with,

$$\mathbb{K} = P_P : I : P_P + {}^m \gamma P_S : I : P_S \quad (2.49)$$

And the expression of the ${}^m \gamma$ parameter, proposed by Rastellini et al. (2007) after performing some analytical analysis, is:

$${}^m \gamma = \frac{\sqrt{\eta + \omega^2(1 - \eta)}}{\eta + \omega(1 - \eta)} \quad \text{with} \quad \omega = 1 + (R - 1)\sqrt{f k} \quad (2.50)$$

$$\eta = \frac{\sqrt{f k}}{1 + f k}$$

$$R = \frac{f E}{m E}$$

The gain obtained with the new enriched formulation is shown in figure 2.11, in which the relative transversal stiffness of a carbon/epoxy laminate is computed with different composite formulations. This figure shows that the results obtained with the enriched model are as good as the results obtained with the Halpin-Tsai formulation, with the advantage that the enriched serial/parallel mixing theory can be used also when the composite components have reached their yield stress.

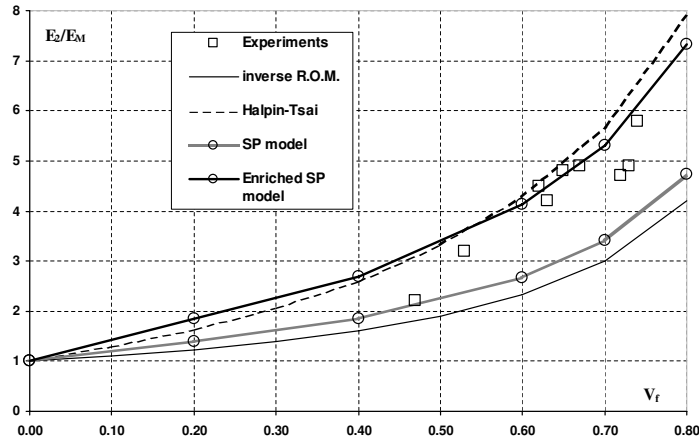


Figure 2.11: Relative transversal stiffness of a carbon/epoxy composite. Comparison of different formulations with experimental results (Rastellini, 2006)

2.3.5 Tangent constitutive tensor

In a non-linear analysis, the tangent stiffness tensor takes over the role of the stiffness matrix in a linear analysis, providing the relation between an increment of stresses and an increment of strains. The most accurate the determination of this tensor, the better will be the convergence of the non-linear problem.

The tangent constitutive tensor depends on the yield surface used to model each material. A general expression of this tensor is provided by Crisfield (1991). Crisfield's expression depends on the second derivative of the yield function, which makes very difficult, and in some cases impossible, to obtain an analytical expression to compute it. Oller (2002) proposes some analytical approximations of the tangent constitutive tensor for some yield laws. However, due to the complexity to obtain an analytical solution for the tangent constitutive tensor and in order to take advantage of the full potential of the serial/parallel mixing theory, it is necessary to develop a numerical procedure to obtain the tangent constitutive tensor for any yield function used to simulate the composite constituents.

With this aim, in the following is proposed a numerical procedure to obtain the tangent constitutive tensor that can be used for any constitutive law. This procedure is based on performing a numerical derivation using a perturbation method. A similar approach to the one described has been already used by Car et al. (1997) with promising results.

Perturbation method to obtain the tangent constitutive tensor

A perturbation method is used to obtain the tangent constitutive tensor, \mathbb{C}^t , numerically for each constituent material of the composite. The tangent constitutive tensor is defined as follows:

$$\dot{\sigma} = \mathbb{C}^t : \dot{\varepsilon} \quad (2.51)$$

This tensor can be written for isotropic and orthotropic materials, by reducing the tensors to their matrix description:

$$\begin{bmatrix} \dot{\sigma}_1 \\ \vdots \\ \dot{\sigma}_n \end{bmatrix} = \begin{bmatrix} c_{11}^t & \dots & c_{1n}^t \\ \vdots & \ddots & \vdots \\ c_{n1}^t & \dots & c_{nn}^t \end{bmatrix} \begin{bmatrix} \dot{\varepsilon}_1 \\ \vdots \\ \dot{\varepsilon}_n \end{bmatrix} \quad (2.52)$$

The stress vector rate of equation 2.52 can be obtained as the sum of n stress vectors ($^j\dot{\sigma}$), which are the product of the j component of the strain vector rate and the j column of the tangent stiffness tensor. This is:

$$\dot{\sigma} \equiv \sum_{j=1}^n {}^j\dot{\sigma} = \sum_{j=1}^n \mathbf{c}_j^t \cdot \dot{\varepsilon}_j \quad (2.53)$$

with

$$\mathbf{c}_j^t = [c_{1j}^t \ c_{2j}^t \ \dots \ c_{nj}^t]^T \quad (2.54)$$

Equation 2.53 can be used to obtain the j column of the tangent stiffness tensor, which is unknown:

$$\mathbf{c}_j^t = \frac{{}^j\dot{\sigma}}{\dot{\varepsilon}_j} \equiv \frac{\delta^j \sigma}{\delta \varepsilon_j} \quad (2.55)$$

The perturbation method consists in defining n small variations, or perturbations, of the strain vector $\delta \varepsilon_j$, to obtain n stress vectors $\delta^j \sigma$ that will be used in equation 2.55 to obtain the numerical expression of the tangent constitutive tensor.

Numerical implementation of the tangent constitutive tensor

In a finite element code the material constitutive law provides the stress tensor σ and the internal variables q associated with a given strain tensor ε . With the strain and stress vectors resulting from the constitutive equation, a small perturbation is applied to the j component of the strain tensor to obtain its associated stress tensor. The obtained stresses and the defined perturbation are then used to compute the j column of the tangent constitutive matrix as shown in equation 2.55. Figure 2.12 shows the flow chart of the algorithm implemented in PLCd code.

In the procedure proposed, the smaller the perturbation value the better the approximation of the tangent constitutive tensor. With this consideration in mind, the perturbation value defined for each component of the strain tensor is obtained by applying the following procedure:

$$\begin{aligned} \text{if } \varepsilon_j \neq 0 & \rightarrow \delta \varepsilon_j = \varepsilon_j \cdot 10^{-5} \\ \text{if } \varepsilon_j = 0 & \rightarrow \delta \varepsilon_j = \min \{ \varepsilon_k \} \cdot 10^{-5} \quad \forall k = 1, n \end{aligned} \quad (2.56)$$

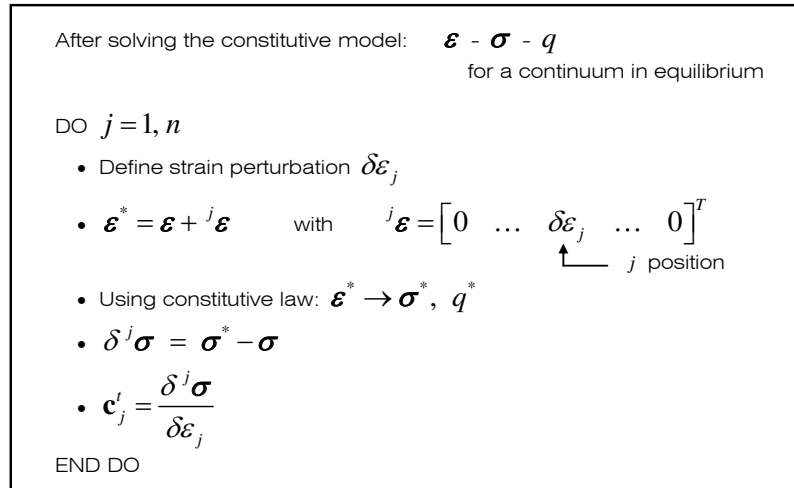


Figure 2.12: Flow chart of the perturbation method algorithm for obtaining the tangent constitutive tensor

Selecting the perturbation value by using this method, the strain increment will always be small enough to ensure that the stress variation is close to the computed value. However, this procedure can provide perturbation values close to zero (i.e. when one of the strain values is almost zero). This case will lead to an indetermination in equation 2.55. To prevent this problem from arising, the following condition is imposed to ensure that the perturbation value is sufficiently high.

$$\delta\varepsilon_j > \max\{\varepsilon_k\} \cdot 10^{-10} \quad \forall k = 1, n \quad (2.57)$$

This procedure provides an accurate approximation of the tangent constitutive tensor for any constitutive law used and any yield surface; and ensures that the numerical process converges satisfactorily.

2.3.6 Laminates using the serial/parallel mixing theory

Because most of the composites employed in structural applications are laminates, it is worth to provide a detailed description of some procedures that can be used to simulate laminate composites with the serial/parallel mixing theory. In this work, all simulations are performed using a finite element method and laminates are treated either with solid elements or with the lamination theory. The procedures used to couple the serial/parallel mixing theory with these two finite element formulations are described in the following.

Simulation of laminates using solid elements

Before describing how laminates can be simulated using solid elements and the serial/parallel mixing theory, it has to be said that the best way to simulate laminate composites, besides performing a micro-model in which all layers are simulated with solid elements, is using a lamination theory. This theory collapses all layers in a single gauss point taking into account the fiber orientation and the layers staking sequence. However, there are some simulations in which a lamination theory cannot be used, such the ones that will be shown in section

2.4 and are also described in Martínez et al. (2006, 2008). In these examples a reinforced concrete structure is strengthened with different layers of carbon fiber reinforced polymers. It will be shown that, although the composite reinforcement could be better simulated using a lamination theory, the reinforced concrete structure must be simulated with three dimensional solid elements to obtain a good representation of the mechanical phenomenons that take place. Another reason for simulating laminates with solid elements is that, with solid elements, all components of the strain and stress tensors are included in the formulation, which allows to take into account effects like the composite failure due to interlaminar shear stresses (these stresses are not always represented with the lamination theory).

Having explained the necessity to develop a procedure to simulate laminate structures with solid elements, to develop this procedure the strains that are found in a three dimensional solid element are analyzed. Figure 2.13 shows the strains found in a 3-D finite element with three layers oriented at $+0/+90/+0$.

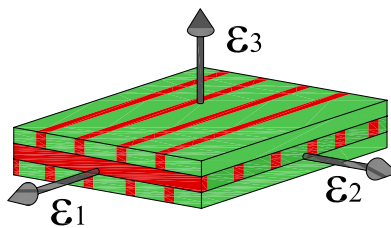


Figure 2.13: Strains in a 3D finite element representing a laminate

Because a solid finite element does not contain bending efforts, in-plane strains (ε_1 and ε_2) must be equal for all layers contained in laminate depicted in figure 2.13; these layers present a parallel behavior and the mixing theory can be applied to them. On the other hand, in the out-of-plane direction (ε_3), layers present a serial distribution and the performance of the composite should be obtained using an inverse mixing theory. However, in a laminate structure, out-of-plane strains are very small compared with the in-plane strains (in fact, lamination theory considers them zero). With this assumption it can be concluded that the error obtained in the simulation, if all layers are defined with the same strain value in ε_3 direction, will be negligible.

Once defined an iso-strain behavior for all layers existing in the finite element, and assuming that the error obtained with this approximation is negligible, the mixing theory can be applied to the finite element to obtain its stresses, considering each layer a constituent material. The stresses in each layer are computed using the serial/parallel mixing theory in order to take into account the unidirectional behavior of fiber material in the layer.

The procedure proposed is summarized in the following algorithm:

1. For a given strain of the composite, the strain of each composite layer is obtained applying the mixing theory.

$$c_{\varepsilon} = L_1 \varepsilon = L_2 \varepsilon = \dots = L_n \varepsilon$$

2. The stress field in each layer is obtained using, either the serial/parallel mixing theory, in case of layers with oriented fibres, either the classical mixing theory, in case of having a layer with an homogeneous material. The classical mixing theory can be also applied to layers with randomly oriented fibers, in which the stiffness provided by fibers is the same in all directions.

$${}^{L_k} \varepsilon \rightarrow {}^{L_k} \sigma \quad \text{using C RoM or SP RoM}$$

3. The stresses of the composite are obtained composing the stresses obtained in each composite layer, according to the mixing theory:

$${}^c \sigma = \sum_{j=1}^n {}^{L_j} k {}^{L_j} \sigma$$

With the procedure described, it has to be noticed that to consider the bending effects in laminate composites, it is necessary to simulate the laminate with more than one finite element in its thickness. However, this problem is found always that a laminate structure is simulated with solid elements, either if the material is a laminated composite or if it is a single homogeneous material. The advantage of the formulation proposed is that laminates with large number of layers, like the ones used in aeronautical applications, can be simulated with solid elements grouping layers in stacks, which can reduce significantly the computational time required to perform the simulation.

Coupling of a laminate formulation and the serial/parallel mixing theory

Because many of the structures made of composite materials are laminates, one of the most used formulations to solve those is the classical lamination theory (Barbero, 1999; Reddy, 2003). This formulation defines the mechanical properties of each layer averaging the stiffness of its constituents (fiber and matrix) and obtains the composite response integrating each layer performance through the laminate thickness, taking into account the fiber orientation and the stacking sequence of the layers in the laminate. On the other hand, when the material non-linear response wants to be taken into account, the best results are obtained using formulations that obtain the composite performance from its constituent materials. Among them, the serial/parallel mixing theory must be remarked. Therefore, a procedure that couples both formulations will be able to take into account the laminate structural configuration and also the material non-linear performance. In this section this procedure is described.

The lamination theory obtains the deformation of each layer from the deformation of the laminate middle surface and its curvature. This can be written as,

$${}^{L_i} [\varepsilon_x \ \varepsilon_y \ \gamma_{xy}]^T = {}^0 [\varepsilon_x \ \varepsilon_y \ \gamma_{xy}]^T + {}^{L_i} \bar{z} {}^0 [\kappa_x \ \kappa_y \ \kappa_{xy}]^T \quad (2.58)$$

with ${}^{L_i} \bar{z}$ the position in the laminate of the middle surface of layer L_i and ${}^0[\cdot]$ the values of strains and curvatures of the middle surface.

Once knowing the strains in each layer, the lamination theory uses the constitutive equation defined for the material to obtain the stresses in the layer. As the serial/parallel mixing theory is implemented as a constitutive equation (that calls the constitutive equations of the component materials to obtain the composite performance), no modifications are required to the code except the implementation of the serial/parallel mixing theory as another constitutive equation available. Therefore, the stresses in the layer are obtained using the serial/parallel mixing theory:

$${}^{L_i} [\varepsilon_x \ \varepsilon_y \ \tau_{xy}]^T \rightarrow \text{Serial/parallel mixing theory} \rightarrow {}^{L_i} [\sigma_x \ \sigma_y \ \tau_{xy}]^T \quad (2.59)$$

The stresses obtained for each layer are integrated along the thickness of the laminate to obtain the laminate efforts. The serial/parallel mixing theory not only provides the stresses for each layer of the laminate but also provides their constitutive tangent tensors. These tensors are used to compute the laminae stiffness matrix, defined by matrices A, B and D; which, according to Barbero (1999), can be obtained as,

$$A = \sum_{k=1}^N {}^{L_i} \mathbb{C}_k^T t_k \quad B = \frac{1}{2} \sum_{k=1}^N {}^{L_i} \mathbb{C}_k^T t_k \bar{z}_k \quad D = \frac{1}{3} \sum_{k=1}^N {}^{L_i} \mathbb{C}_k^T \left(t_k \bar{z}_k^2 + \frac{t_k^3}{12} \right) \quad (2.60)$$

being ${}^{L_i} \mathbb{C}^T$ the tangent stiffness tensor of layer L_i .

With this procedure, the composite laminate can be modeled taking advantage of both formulations. The serial/parallel mixing theory provides the laminate non-linear performance from the stress-strain relation of its constituents, while the classic lamination theory provides the composite response taking into account the laminate structural configuration.

The coupling of the serial/parallel mixing theory with the classical lamination theory has been already performed in the finite element code ComPack-Aero (CIMNE and Quantech, 2008), in the frame of the FEMCOM project (Oñate et al., 2007). This implementation has been made together with Fernando Rastellini and Fernando Flores. An example of a numerical simulation performed with the developed procedure is included in this work, in section 3.5.

2.4 Application of the formulation proposed: Reinforcement and retrofitting of RC structures with FRP

2.4.1 Introduction

In this chapter have been presented the most significant numerical procedures used nowadays to perform numerical simulations of composite structures. Among them, the one used in this work is the serial/parallel mixing theory. This formulation can take into account the composite non-linearities, produced by the material non-linear behavior of its components, without increasing substantially the computational cost required to perform the simulation. These two features converts the serial/parallel mixing theory into the most appropriate formulation to perform large simulations of composite structures.

In order to show the potentiality and performance of the serial/parallel mixing theory, this section contains three different finite element simulations of composite structures in which the composite mechanical behavior is obtained with the serial/parallel mixing theory. The simulations included are found in the civil engineering field and they solve the problem of reinforcement and/or retrofitting of reinforced concrete (RC) structures using fiber reinforced polymers (FRP). The results of the simulations have been already presented in the First European Conference on Earthquake Engineering and Seismology (Martínez et al., 2006) and are also described in Martínez et al. (2008). The problem has been solved in the framework of the research projects: CEE-FP6 (LESSLOSSS Project, Ref. FP6-50544 (GOCE)) and “Metodología para la simulación numérica del comportamiento de estructuras de hormigón

armado reparadas y/o reforzadas con materiales compuestos” (Ministerio de Fomento 2003-2005).

Description of the problem solved

The reinforcement of reinforced concrete structures using fiber reinforced polymers consist in attaching one or several layers of fiber reinforced polymers (usually carbon fibers) to the structure to be reinforced. The reinforcement increases the strength of the structure in the fiber direction of the region where it is attached. Figure 2.14 shows (a) the attachment of the FRP and (b) the final FRP disposition, in the reinforcement of a bridge to increase its bending strength.



a) Attachment of FRP to the structure b) Final disposition of the FRP

Figure 2.14: Bending FRP reinforcement of the Pont del Dragó (Pedelta, 1996)

First known application of fibre reinforced polymers to retrofit a reinforced concrete structure corresponds to Meier (1995) in the retrofit of the Ibach bridge, in 1991, Lucern, Switzerland. In Spain, this technology was first used in 1996, in the retrofit of the *Pont del Dragó* bridge, Barcelona, by Pulido and Sobrino (1998). FRP where used, in both cases, because the structural retrofitting had to be fast and could not stop the traffic underneath the damaged bridge. The good results provided by the first applications of this new technology have lead to an exponential increase of the reinforcements and retrofitting made with FRP, as well as an increase in the number of applications in which FRP are used, such as columns reinforcements or shear reinforcements.

The main advantages of using fibre reinforced polymers to retrofit RC structures instead of traditional materials, such as steel, are:

1. FRP are lighter and their apply is easier than with traditional materials. These two aspects simplifies the retrofitting process reducing its cost.
2. As the reinforcement does not require large machinery, it can be done without affecting significantly the structure serviceability.
3. The reinforcement does not affect the structure capacity, as the FRP lightness does not overload the existing structure.
4. FRP does not have the corrosion and damage problems usually found in steel material, having improved mechanical characteristics.
5. FRP have better fatigue behavior compared to traditional materials.
6. This sort of reinforcements are more adaptable to different shapes, being able to apply them to, for example, circular columns.

The calculation of FRP reinforcements is based in considering the composite a single orthotropic material, which mechanical characteristics are obtained experimentally. With this assumption, its calculation is done using simple formulations based on the elasticity theory. These formulations can be found in the manufacturers manuals (Sika, 2008; Bettor, 2008).

All existing knowledge about structural reinforcement and/or retrofitting of RC structures with FRP is based in experimental simulations. These simulations deal with different sort of reinforcement applications as can be bending reinforcement (Spadea et al., 1998), shear reinforcement (Khalifa and Nanni, 2002; Li et al., 2001), columns wrapping (Li et al., 2006), anchorage of the reinforcement to the existing structure (Khalifa et al., 1999), etc.

Under this scope, a special mention must be done about the EMPA (Swiss Federal Laboratories for Materials Testing and Research), where most of the initial experimental work was performed (Oller, 2005). It also has to be mentioned the work developed at the *Universitat Politècnica de Catalunya* (UPC), *Departament d'Enginyeria de la Construcció*, where three different PhD thesis have been written dealing with the structural reinforcement of concrete structures using CFRP: Avilés (2000), Alarcón (2002) and Oller (2005). These three works deal with the problem, also, using an experimental point of view.

In despite of all existing research made about FRP reinforcements, few of it is found in which the problem is treated using a non-experimental approach. And, the non-experimental studies found, are based on analytical formulations focused in an specific problem of FRP reinforcements. This is the case of the paper by Rabinovitch (2004), in which an analytical formulation, solved using numerical techniques, is developed to obtain the compression strength of the reinforcement. Thus, in the scope of numerical simulation of FRP reinforcements, no information is found in literature.

Therefore, the simulations included in this section not only will show the potentiality of the serial/parallel mixing theory to perform numerical simulations of large structural composite problems; but they also will provide a new approach to solve the problem of reinforcement and retrofitting of RC structures with FRP. Once having proved the validity of this approach, it can be used to perform numerical simulations of different FRP reinforcement configurations to obtain the better retrofitting solution for a concrete case under study.

Contents of this section

Before describing the simulations performed, in next section is described a new algorithm that has been developed to perform numerical simulations of structural retrofitting. In structural retrofitting, the FRP is applied to the structure when this last one has reached a certain level of damage. Afterwards it will be shown the simulation of a RC beam reinforced with FRP to increase its bending strength. This simulation has been used to validate the formulation proposed. The same beam used to validate the formulation is used to show the performance of the construction stages algorithm developed to perform retrofitting simulations. Finally, the full potentiality of the formulation is shown with the simulation of a framed structure in which different FRP reinforcements are applied to the beam, column and beam-column connecting joint.

2.4.2 Retrofitted structures. Construction stages algorithm

There are many situations in which an existing structure can be damaged and can require to be retrofitted. The damage in the structure can be caused by several reasons, such as a

collision (Pulido and Sobrino, 1998) or after an earthquake (Gómez Soberón et al., 2002). Therefore, structural retrofitting is probably one of the main applications of CFRP in civil engineering structures.

In order to simulate a structural retrofitting, it is necessary to add the CFRP reinforcement once the structure is already damaged. With this aim, a construction-stages algorithm is implemented in the PLCd code (CIMNE, 2008), so that it is possible to add or remove structural elements during the calculation process.

This algorithm enables the code to run the numerical simulation for the desired load cases, with only some structural elements active in the structure. Being possible to add new elements at a given load case, without interrupting the calculation process. These elements must be free from strains and stresses when they are activated.

Figure 2.15 shows how this solution scheme is used when simulating a retrofit process. The example shown corresponds to a beam to which a bending moment is applied. The beam is reinforced with CFRP when the first tensile cracks appear on the bottom edge.

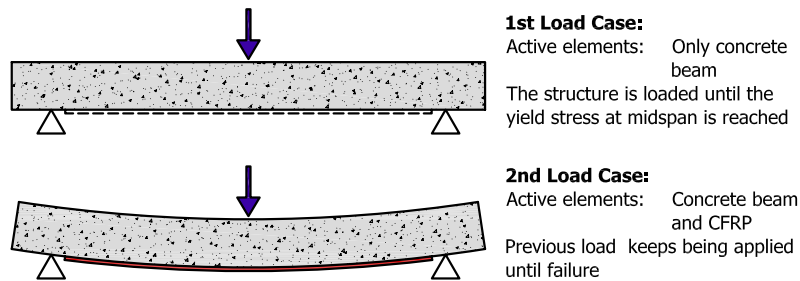


Figure 2.15: Retrofit process of a beam with a bending moment

The finite element method is based on the numerical integration of the virtual work equation; this integration implies to solve the problem:

$$K X = R \quad (2.61)$$

where K is the global stiffness matrix, X is the vector of nodal displacements and R is the vector of external forces applied to the structure. Once the nodal displacements have been found, the strains in each element, ε^e , are computed using the following equation:

$$\varepsilon^e = B^e X^e \quad (2.62)$$

where B^e is the element deformation matrix.

Finally, once the element strains have been obtained, the following equation is used to compute the stresses in each element:

$$\sigma^e = \mathbb{C}^e \varepsilon^e \quad (2.63)$$

where \mathbb{C}^e is the element constitutive matrix.

The stress tensor in equation 2.63 corresponds to the elastic stresses. This expression is modified in a material non-linear analysis. However, for the sake of simplicity, the explanation of the procedure is limited to the linear case.

Considering that there are n load cases in the calculation process, equations 2.62 and 2.63 can be re-written as:

$$\begin{aligned}\varepsilon^e &= \varepsilon_1^e + \varepsilon_2^e + \dots + \varepsilon_n^e = B^e X^e \\ \sigma^e &= \sigma_1^e + \sigma_1^e + \dots + \sigma_n^e = \mathbb{C}^e \varepsilon^e\end{aligned}\tag{2.64}$$

If new elements are introduced into the structural mesh during finite element analysis (i.e. in the second load case), they will take values of $\varepsilon_1^e = 0$ and $\sigma_1^e = 0$; and the strains in the element will correspond only to the second load case:

$$\varepsilon^e = \varepsilon_2^e = B^e X^e\tag{2.65}$$

However, the element displacement introduced in equation 2.65 corresponds to the total displacement of the structure. This means that the strains in the new element correspond to the displacements of the structure during the first and the second construction stages. The same applies to the stress tensor. Consequently, the new elements try to adapt to the global deformation of the structure by adopting strains that are greater than the ones that correspond to the new load increase.

By considering all of the structural elements during all construction stages, it is possible to prevent this situation. Then, it is necessary to separate the strain tensor into two components, one active (ε_A) and one non-active (ε_{NA}), that is:

$$\varepsilon^e = \varepsilon_A^e + \varepsilon_{NA}^e\tag{2.66}$$

When the element is not present in the structure, all strains are included in the non-active tensor:

$$\varepsilon^e = \varepsilon_{NA}^e = B^e X^e \quad \text{and} \quad \varepsilon_A^e = 0\tag{2.67}$$

and, if the element is active, equation 2.66 is used to calculate the active strain tensor:

$$\varepsilon_A^e = \varepsilon^e - \varepsilon_{NA}^e = B^e X^e - \varepsilon_{NA}^e\tag{2.68}$$

With this procedure, only the strains that correspond to the construction stage in which the element is active are considered; as these are obtained removing the strains of the previous construction stage (non active strains) from the total strains.

Element stresses are computed by considering only the active strains:

$$\sigma^e = \mathbb{C}^e \varepsilon_A^e\tag{2.69}$$

Thus, no stresses are obtained if the element is non-active.

The algorithm must take into account that the elemental stiffness matrices (K^e) of any non-active elements present in the structure are included in the global stiffness matrix K . As a result, these elements contribute to the global stiffness of the structure. The elemental

stiffness matrices of the non-active elements should therefore be nullified at the beginning of the construction stage to prevent this contribution from affecting the results.

Figure 2.16 shows a flow chart of the construction-stages algorithm implemented in the PLCd code.

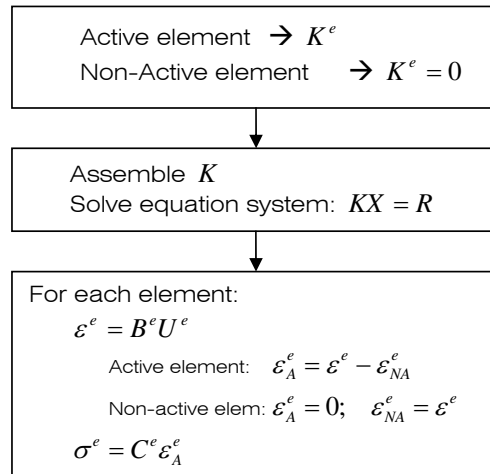


Figure 2.16: Flow chart of the construction stages algorithm

This procedure has been implemented in the PLCd code and it provides correct results, as will be shown in the retrofitting beam simulation included in this section.

2.4.3 Validation of the formulation: Beam reinforcement

To validate the ability of the proposed formulation to perform large simulations of composite materials, a numerical model of a RC beam reinforced with FRP has been developed. The beam considered is the same as the one defined by Spadea et al. (1998). The numerical results obtained with PLCd are compared with the experimental results given in Spadea et al. (1998).

Beam and model description

The structure used to validate the formulation is a simply supported beam with two equidistant vertical loads that produce a constant bending moment between them. Figure 2.17 shows the beam geometry and the reinforcement added to it.

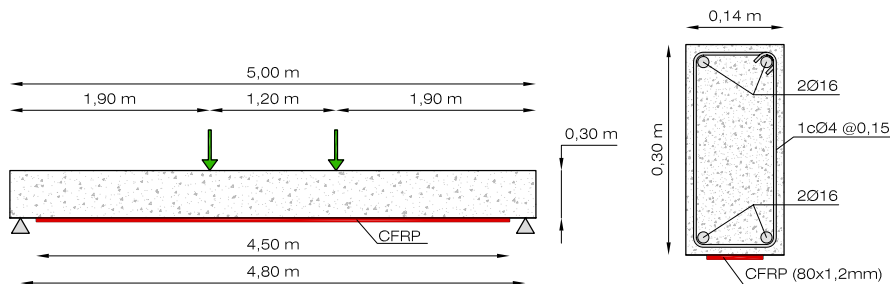


Figure 2.17: Geometric definition of the studied beam

The experimental simulations reported in Spadea et al. (1998) consist in using a displacement-control mechanism to apply a load until the beam fails. Different CFRP reinforcement configurations are applied to the beam to obtain the force-displacement response for each one. Two of these results are used to validate the proposed numerical model: the first is for the non-reinforced beam and the second is for the beam with the CFRP reinforcement displayed in figure 2.17. The reinforcement applied is 1.2 mm thick and composed of 66% of carbon fibers, oriented along the longitudinal axis of the beam, and 34% of polymeric matrix. The experimental results are compared with the numerical results for the developed models. These are:

Sp3D-R0: Beam without CFRP reinforcement

Sp3D-R1: Beam with bending CFRP reinforcement

The constitutive performance of each composite material used to simulate the beam is determined by combining the constitutive behaviors of their constituent materials. Table 2.1 shows the simple materials considered in the models and their mechanical characteristics. In this table, E stands for the Young modulus, ν for the Poisson modulus, σ_C and σ_T for the yielding compression and tension stresses, respectively, and G_C and C_T for the energy release rates per unit area in compression and tension.

Material	Yielding criterion	E [MPa]	ν	σ_C [MPa]	σ_T [MPa]	G_C [kJ/m ²]	G_T [kJ/m ²]
Concrete	Mohr-Coulomb	$2.5 \cdot 10^4$	0.2	30.0	3.0	5.0	0.5
Steel	Von-Mises	$1.0 \cdot 10^5$	0.0	270	270	2000	2000
Polymeric matrix	Mohr-Coulomb	$1.2 \cdot 10^4$	0.2	87.5	25.0	10.5	3.0
Carbon fibers	Von-Mises	$1.5 \cdot 10^5$	0.0	2300	2300	2000	2000

Table 2.1: Mechanical characteristics of the constituent materials defined in the beam models

Concrete and matrix are simulated by a damage formulation. Steel and carbon fibers are simulated by a plastic law. Young modulus of steel has been reduced to take into account the effect of fiber debonding (Car et al., 2002). Steel plastic evolution is defined by an initial hardening law until it reaches a peak of 435 MPa, at which point the hardening law is replaced by a softening law. Figure 2.18 shows the one-dimensional strain-stress evolution of each material considered in the simulation in the case of tensile stresses.

The numerical models developed are based on hexahedral elements. Six different composite materials are defined by a combination of six different constituents: concrete, matrix, fibers and three steel materials. Different steel materials are defined according to their orientation because the direction of the fibrous material is required as a material property in the serial/parallel mixing theory. Transversal and vertical steel refer to the steel stirrups and longitudinal steel refers to the bending steel reinforcement.

Table 2.2 contains the definitions of each composite material according to the volumetric participation of their constituents. Figure 2.19 shows the distribution of these materials in the beam model and the mesh defined for the simulation. Only half of the beam has been modeled because of the symmetry at midspan.

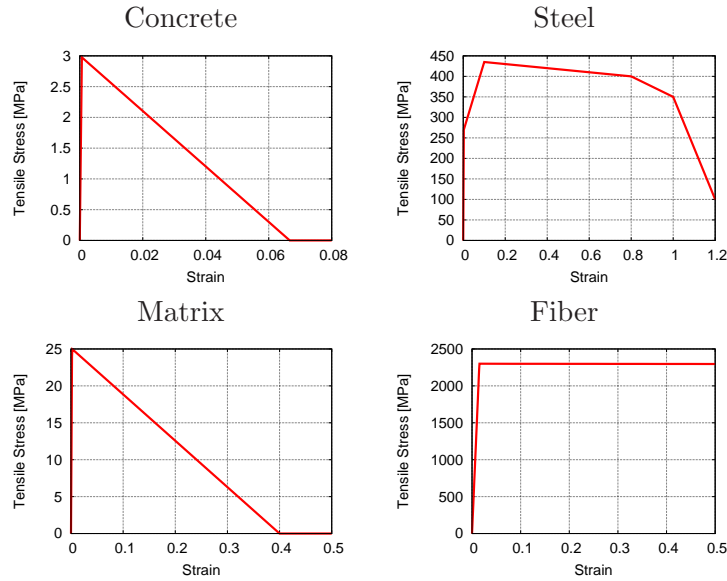


Figure 2.18: Strain-stress evolution of each constituent material considered in the analysis

Constituent materials	Composite materials					
	Mat-01	Mat-02	Mat-03	Mat-04	Mat-05	Mat-06
Concrete	1.00	0.57	0.99	0.98	0.99	
Longitudinal steel		0.42				
Transversal steel				0.01	0.01	
Vertical steel		0.01	0.01	0.01		
Polymeric matrix						0.34
Long. carbon fibers						0.66

Table 2.2: Definition of composite materials. Volumetric participation of each constituent material in the composite

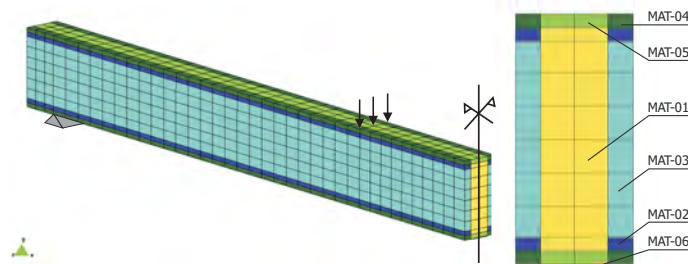


Figure 2.19: Definition of the mesh and composite materials of the simulated beam. The model assumes symmetry at mid-span

Figure 2.19 also shows the potentiality of the serial/parallel mixing theory, together with a finite element formulation, to simulate composite structures: Complex material distributions in the cross-section of the beam are taken into account without having to model each single element independently, reducing the computational cost of the simulation without losing its accuracy.

Comparison between the numerical and experimental results

The force-displacement curves (capacity curves) obtained in each case (figure 2.20) are used to compare the numerical and experimental models. The displacement corresponds to the point at which the load is applied. The agreement between the results is good enough to indicate that the formulation is capable to deal with this sort of composite simulations.

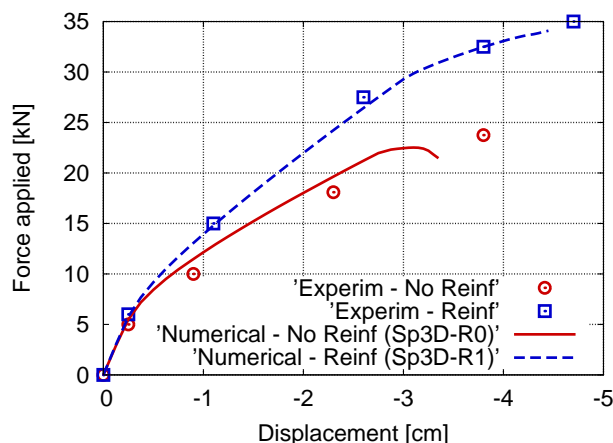


Figure 2.20: Comparison between numerical and experimental capacity curves

The agreement between the experimental and numerical results can be observed not only in the structural response of the beam but also in its failure mode. The failure modes reported by Spadea *et al.* are:

No reinforced beam: Tension steel yielding and concrete crushing.

Reinforced beam: Sudden and total loss of load capacity; explosive debonding of CFRP plate.

The failure mode in the non-reinforced beam model (Sp3D-R0) is the same as the one obtained in the experimental test. This can be seen in figures 2.21 and 2.22, which show the damage to the concrete and the plastic damage to the steel reinforcement for the final calculation step and for the most severely damaged beam section. These figures show that the steel has started to yield and that the compressed concrete has also reached its limit stress (onset of concrete crushing). Under these conditions the transversal section cannot develop more stresses and the code cannot determine a valid solution for the current load step. This situation can be interpreted as beam failure.

The failure mode of the CFRP reinforced beam model (Sp3D-R1) is similar to that of the non-reinforced beam model (Sp3D-R0). In the most severely damaged section the entire concrete reaches its elastic limit stress and the steel yields (figure 2.23). The developed model assumes a perfect bond between the concrete and the reinforcement. Under this assumption, it is impossible to simulate the explosive debonding of the CFRP plate observed in the experimental test. However, if debonding occurred, the beam would suddenly lose load capacity and the results would be identical to the experimental ones.

CFRP reinforcement increases the tensile strength of the beam and reduces the crack opening, which increases the load capacity of the beam. Crack opening increases exponentially in the most severely damaged section of the non-reinforced beam model (Sp3D-R0) when steel

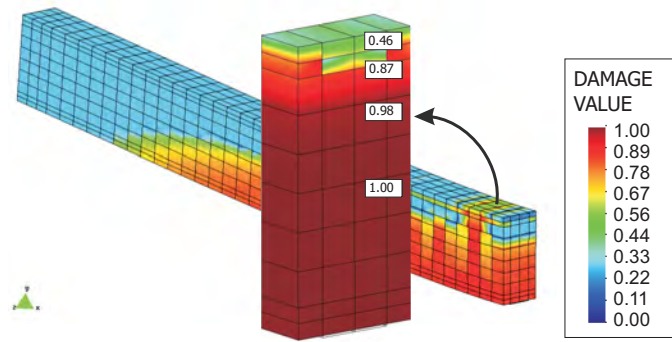


Figure 2.21: Damage to the concrete at beam failure and detail of the most severely damaged cross-section. The numbers shown correspond to the damage parameter in each finite element. Sp3D-R0 model

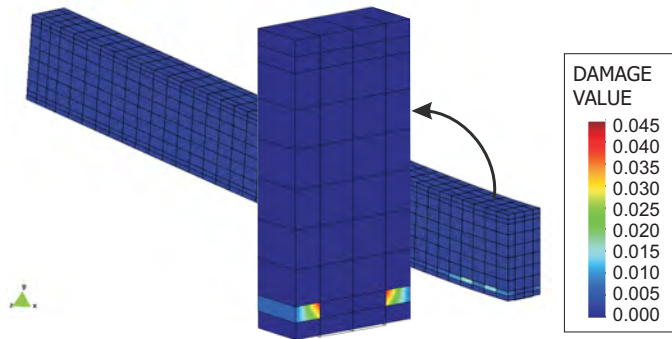


Figure 2.22: Plastic damage to the steel at beam failure and detail of the most severely damaged cross-section. Sp3D-R0 model

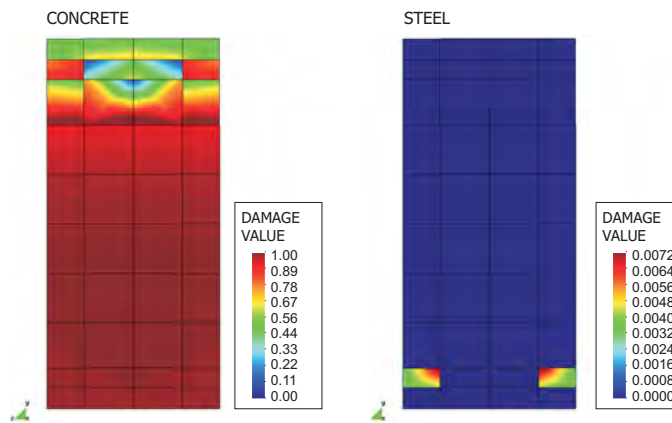


Figure 2.23: Damage at the cross-section supporting heavier loads at beam failure. Sp3D-R1 model

yielding begins. This increase is not observed when the beam is reinforced with CFRP. This can be seen in figure 2.24 which shows the relative displacement between the nodes found on either side of the most severely damaged section in both models. The strength is increased and crack opening is reduced because the carbon fibers are still under elastic conditions; in fact, they are at less than 30% of their elastic capacity, although damage has already started to appear in the polymeric matrix (figure 2.25).

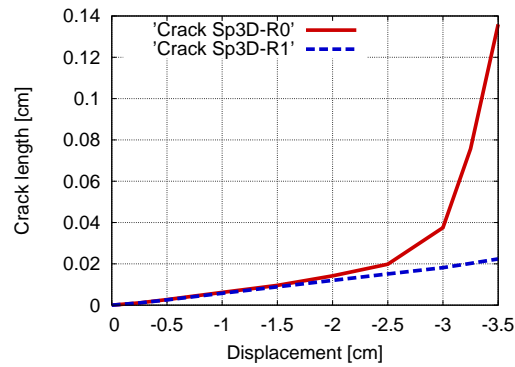
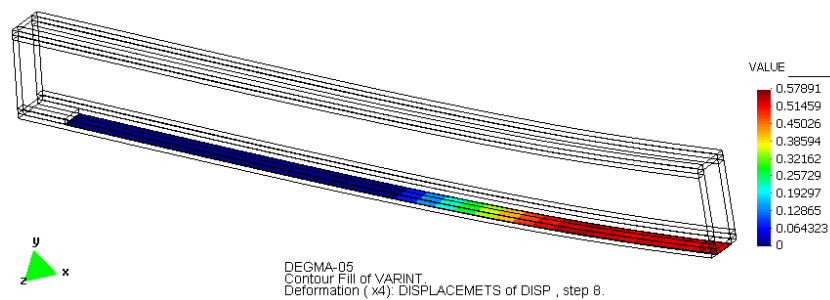


Figure 2.24: Crack opening in the most severely damaged section

Damage parameter in matrix material



Stresses in carbon fibers



Figure 2.25: Stress state in CFRP reinforcement. Sp3D-R1 model

S/P mixing theory performance

The models developed for validating the code are also used to study the performance of the serial/parallel mixing theory. Fibrous materials work in their longitudinal direction, consequently the stresses should be greater in this direction. The serial/parallel mixing theory should simulate this behavior. To verify this, the performance of steel stirrups is studied herein. Beam strains in transversal direction tend to increase in the upper bound of the cross-section and to decrease in its lower bound due to Poisson effects. Concrete confinement reduces this effect by means of steel stirrups. Figure 2.26 shows the transverse stresses in the stirrups, which correspond to stresses in the longitudinal direction of the stirrups. This demonstrates that the model is capable of simulating the confinement of the concrete.

The serial/parallel rule of mixtures is providing correct results if the global longitudinal stresses in the stirrups (transverse stresses according to their orientation) are the same as in the concrete. This situation is achieved, as shown in figure 2.27. Moreover, steel stresses in the longitudinal direction of the beam are lower than the stresses found in the transverse

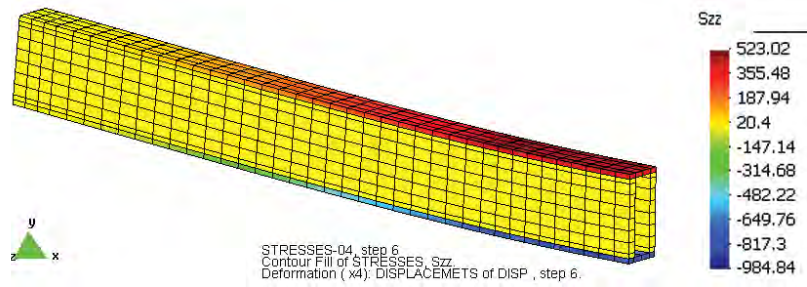
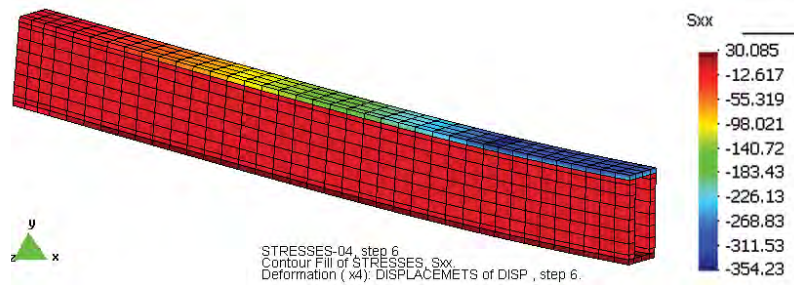


Figure 2.26: Transverse stresses in transverse steel stirrups. Sp3D-R0 model

direction (which corresponds to the orientation of the studied stirrups).

Longitudinal stresses in stirrups



Longitudinal stresses in concrete

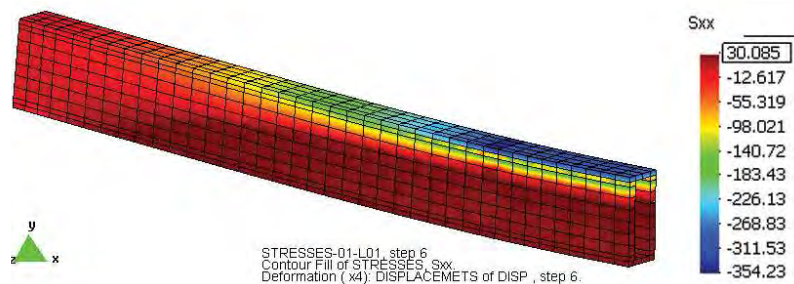


Figure 2.27: Longitudinal stresses in concrete and in steel stirrups. Sp3D-R0 model

2.4.4 Beam Retrofitting

Two different numerical models have been developed to study the effect of retrofitting a structure, depending on the existing level of damage in the beam when the CFRP reinforcement is applied. The beam retrofitted is the same that has been used in previous section. The models developed are:

Sp3D-Rt2: The CFRP reinforcement is applied when the damage appears in the concrete material.

Sp3D-Rt3: CFRP reinforcement is applied when the steel starts to yield

Results obtained with these two models are compared with those obtained when the beam is not reinforced (Sp3D-R0 model) and when the beam is reinforced from the beginning of the loading process (Sp3D-R1 model). Figure 2.28 shows the capacity curves for each model.

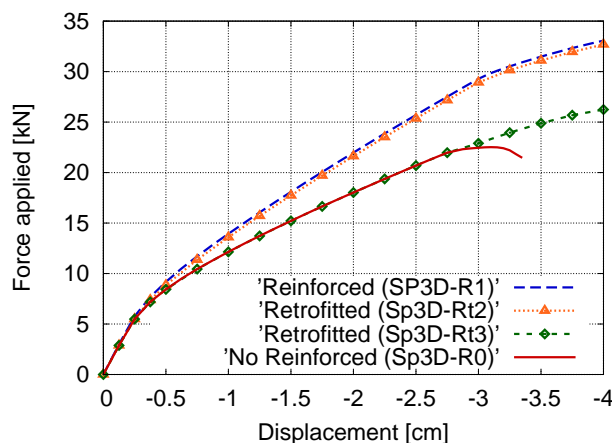


Figure 2.28: Comparison of CFRP reinforcements and retrofitting using capacity curves

These results show that the structural stiffness does not depend on the point at which the reinforcement is applied to the structure. The structural stiffness obtained when the CFRP reinforcement is applied after the steel has begun to yield (Sp3D-Rt3) does not differ significantly from the structural stiffness obtained after steel yielding in the reinforced model (Sp3D-R1). However, figure 2.28 also shows that retrofitted structures suffer greater deformation and damage than structures that are reinforced during the original construction. The resulting damage reduces the load capacity of the beam and the deformation can lead to a loss of serviceability (i.e. when a load of 25 kN is applied to the structure, the beam deformations are 45% greater in the retrofit model Sp3D-Rt3, than in the reinforced model Sp3D-R1).

This simulation shows how important is to reinforce the structure when a low level of damage is observed. Even if the structure stiffness does not vary if FRP is applied for reinforcement or retrofitting, the structural deformations and the stresses are greater if FRP is applied when the structure is already damaged. The simulation has also proved the good performance of the construction stages algorithm, developed to take into account pre-existing damage in the RC structure before applying the FRP reinforcement.

2.4.5 FRP Reinforcement of a RC framed structure

The main aim of this simulation is to apply the formulation developed to verify the ability of CFRP reinforcements to increase the strength of concrete frame structures. The connecting joints between the beams and columns can be often subject to greater stress than other zones of concrete frame structures and in most cases these joints are the cause of structural weakness. The frame joint is reinforced in the models developed for this study with two different CFRP configurations to analyze the strength mechanisms developed by the reinforcement to increase the frame strength and to determine which type of reinforcement configuration yields better results.

Model description

The concrete frame to be studied is designed to reflect the most common geometry and steel reinforcements used in this type of construction. Figure 2.29 shows the geometry considered and figure 2.30 shows the steel reinforcement and the CFRP reinforcement that will be applied to the frame joint. The dimensions of the cross-section of the beam and the steel

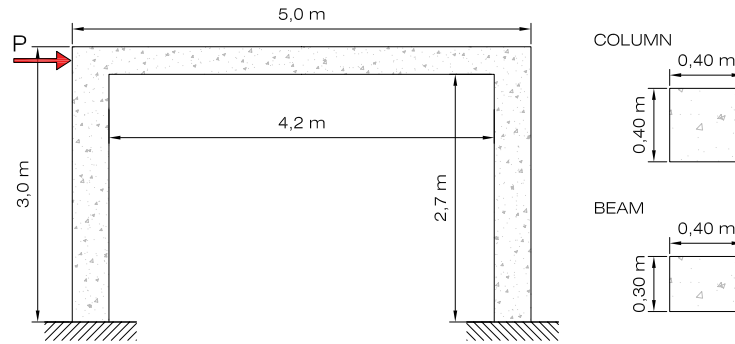


Figure 2.29: Geometric definition of the frame

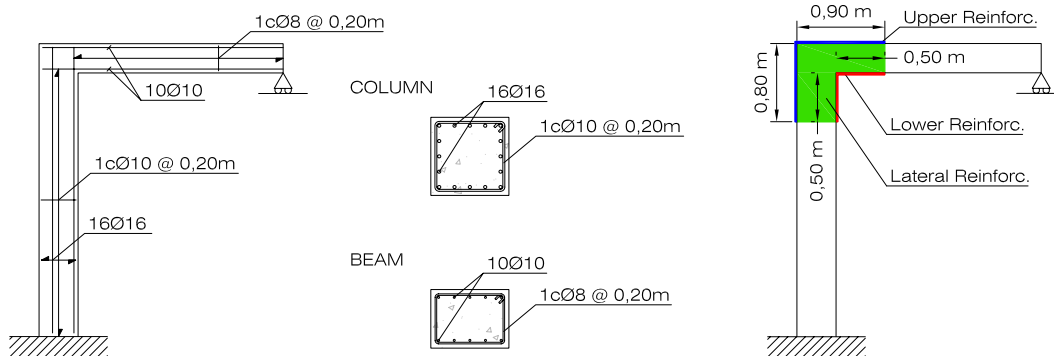


Figure 2.30: Reinforcements of the concrete frame

reinforcement are intended to ensure structural failure close to the joint. The height of the beam is smaller than the width and less steel reinforcement is used for the beam than for the column. This will increase the effect of the CFRP on in the frame joint. The structure is loaded by a horizontal force P applied in the middle of the frame joint (see Figure 2.29).

Two dimensional and three dimensional models have been developed for the concrete frame. The 2D models have been used to calibrate the mesh, as they require less computational effort than the 3D models. Results obtained with the 2D models are compared with those of the 3D models to asses the accuracy of each type of simulation. Three different structure models have been developed to study the effect of CFRP reinforcements on the frame joint:

2DF-noR and 3DF-noR models: Two and three dimensional models of the concrete frame without CFRP reinforcement

2DF-R and 3DF-R models: Two and three dimensional models of the concrete frame with upper and lower CFRP reinforcements

2DF-LR and 3DF-LR models: Two and three dimensional models of the concrete frame with upper, lower and lateral CFRP reinforcements.

The constituent materials of the different composites in each model are the same as those defined for the beam simulation (table 2.1). The CFRP reinforcement is 1.2mm thick and is composed of 66% of carbon fibers and 34% of polymeric matrix. The fibers in the upper and lower reinforcements are aligned with the longitudinal axis of the structure. Two layers are applied to the frame to provide lateral reinforcement, in which the fibres are oriented at $+0^\circ$ and $+90^\circ$ with respect to the horizontal.

2D results

The capacity curves obtained for each model (figure 2.31) are used to analyze the structural behavior of the frame joint with the different types of reinforcement. The x axis shows the horizontal displacement of the point to which the load is applied and the y axis shows the load applied. The displacement depends on the column, the beam and the joint stiffness. Any increase in the structure stiffness shown by the force-displacement graph will reflect an increase of the joint stiffness as a result of the CFRP reinforcement because the column and the beam are not modified in the different models.

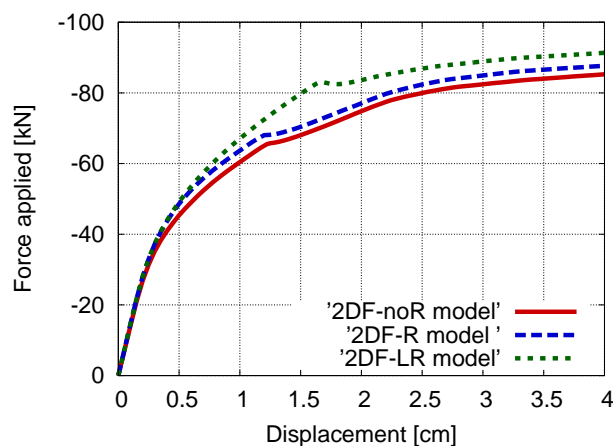


Figure 2.31: Capacity curves obtained with the 2D models

Figure 2.31 shows that the upper and lower CFRP reinforcements (2DF-R model) do not significantly improve the frame behavior. A substantially improvement is only found when the lateral reinforcement is applied to the concrete frame. All three curves contain a region in which the load is reduced, after which it begins to increase again. These points reflect the point at which a plastic hinge develops in the structure. The structure adopts a new strength mechanism at this load step, which increases its load capacity. If the load applied to the structure when the plastic hinge is developed is considered, results show that the lateral reinforcement (2DF-LR model) increases the structural load capacity by 25%, when compared with the non-reinforced model (2DF-noR). This increase is reduced to 4% if the structure is only reinforced with upper and lower CFRP.

The effects of each type of reinforcement can be better understood by studying the points at which the plastic hinges are formed. Figure 2.32 shows the longitudinal strains for each model at the last computed step. The cross-sections in which the plastic hinges are formed are subjected to the greatest strain.

Figure 2.32 shows the plastic hinge moves from the beam to the inner part of the joint, where no reinforcement is applied if only the upper and lower CFRP reinforcements are included into the structure. Therefore, the upper and lower CFRP reinforcement does not change the beam behavior substantially; once the hinge has been formed, both structures behave similarly (figure 2.31). On the other hand, when the lateral reinforcement is applied to the structure, it limits damage in the frame joint and causes the plastic hinge to move to the cross-section at which no CFRP reinforcement is applied. This increases the load capacity and the stiffness of the structure.

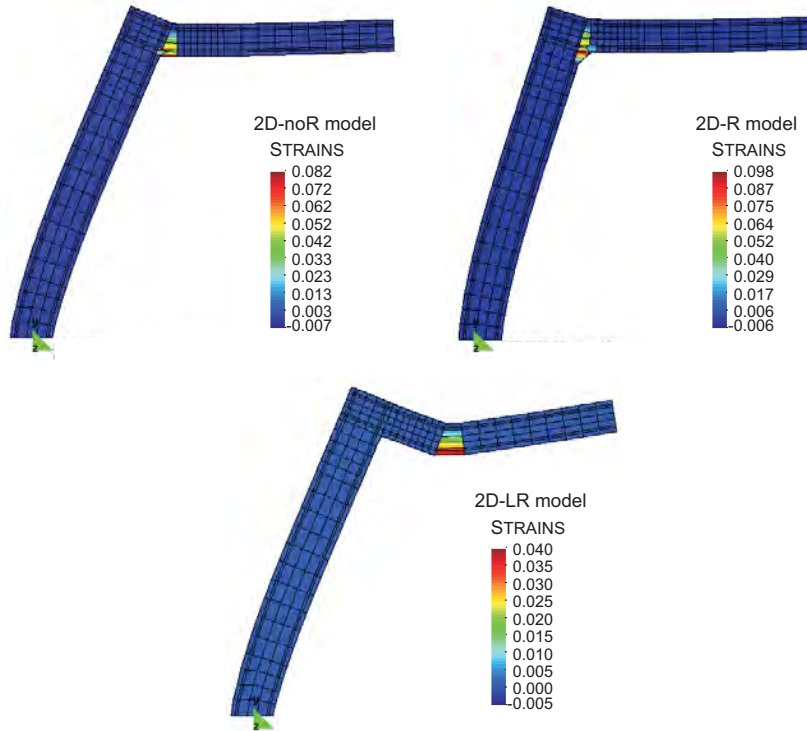


Figure 2.32: Plastic hinges in the concrete frame. 2D models

3D results

The capacity curves are also used to analyze the results obtained with the 3D models (figure 2.33). The main difference between the 3D and the 2D results is that the 3D models are stiffer and can support greater maximum loads than the 2D models. This is due to the fact that the concrete confinement is reproduced more accurately by the 3D models because the steel stirrups are modeled taking into account their 3D distribution rather than only one of their dimensions. This confinement enables the concrete to support greater longitudinal stresses and slows the spread of damage. Both of these improvements increase the strength and stiffness of the structure.

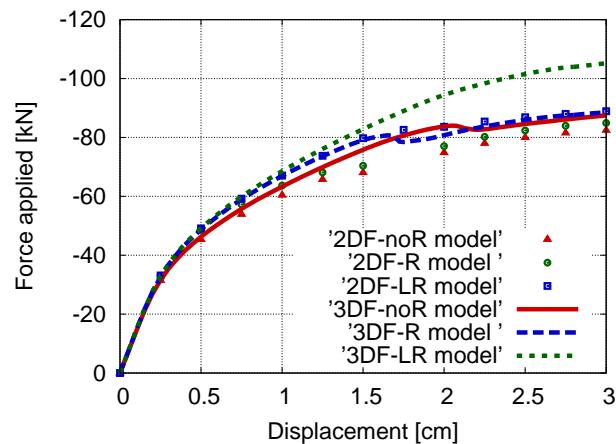


Figure 2.33: Capacity curves obtained with the 3D models

Figure 2.33 shows that the plastic hinges appear at the same load and displacement in the 3D

non-reinforced model (3DF-noR) and in the upper and lower reinforced model (3DF-R) as in the 2D lateral reinforced model (2DF-LR), due to the increased strength of the concrete. However the plastic hinges appear earlier in the reinforced model than in the non-reinforced one in the three dimensional simulation. This effect is illustrated by figure 2.34, which shows the maximum strains in the non-reinforced beam model (3DF-noR) before and after the formation of the plastic hinge, and figure 2.35, which shows the same results for the upper and lower reinforced model (3DF-R).

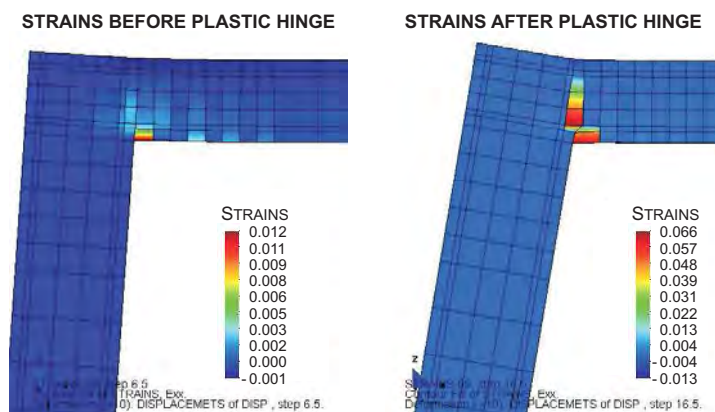


Figure 2.34: Crack evolution in the 3DF-noR model

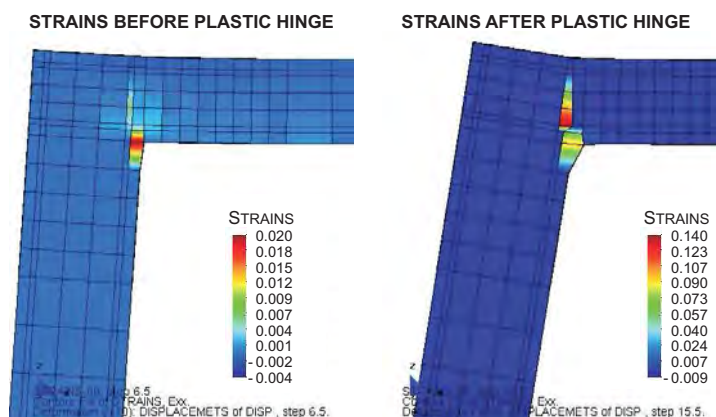


Figure 2.35: Crack evolution in the 3DF-R model

These figures show that the plastic hinge develops in almost the same cross-section in both models. However, since this cross-section is closer to the initial point of damage in the upper and lower reinforced model than in the non-reinforced model, the code finds faster the crack path in the reinforced case. Therefore, although CFRP reinforcement increases the joint stiffness, in this case the load that causes the plastic hinge to appear is lower when the joint is reinforced than when no reinforcement is applied.

More differences are found when the three dimensional model is compared with the two dimensional model for the case in which lateral CFRP reinforcement is applied to the frame joint (3DF-LR model). The first difference is that the capacity curve does not show the formation of a plastic hinge. This is because no section is completely damaged when the code no longer converges.

However, the main difference can be observed in the most severely damaged section. The

strains in the lateral sections of the frame joint (figure 2.36a) are similar to the ones seen in the 2D case: they are greater in the cross-section where the CFRP reinforcement ends than in the frame joint. But, when the strains in a longitudinal section of the structure are analyzed (figure 2.36b), it can be seen that the plastic hinge is developed in the frame joint. Two dimensional models assume that the CFRP reinforcement is applied through the entire cross-section whereas it is only applied to the lateral surfaces. Consequently, the reinforcement can prevent structural cracks from appearing on the surface of the frame joint but cannot protect the inside of the joint. This effect can be seen more clearly in figure 2.37, which shows a top view of the strains in the column section just below the frame joint.

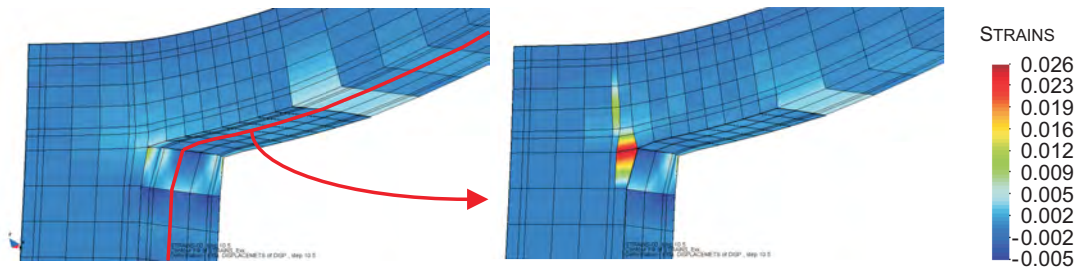


Figure 2.36: Plastic hinge in 3DF-LR model. Lateral view

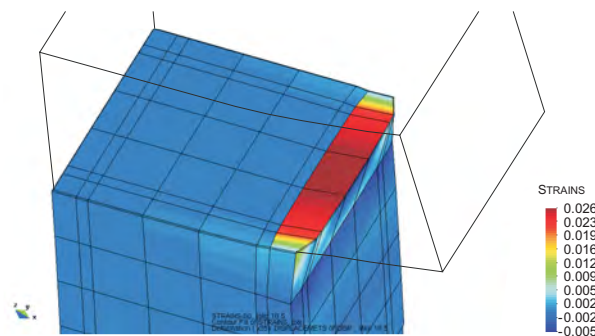


Figure 2.37: Elements with larger deformations in 3DF-LR model. Top view

These last two figures show that same structural failure occurs regardless of the CFRP reinforcement configuration applied. Therefore, it can be concluded that lateral CFRP reinforcement does not prevent the appearance of cracks in the joint and the subsequent formation of a plastic hinge, but it can delay the load step during which the first cracks appear and reduce the speed with which they propagate. These both effects increase the load of the frame by 20% when the horizontal displacement is 3.0 cm, which makes this type of reinforcement the optimum for strengthening the column-beam joint of concrete frame structures.

2.5 Conclusions

This chapter has shown the most common numerical procedures used to simulate composite structures. Most of them obtain the mechanical properties of the composite material from the elastic characteristics of its constituents, usually fiber and matrix. The composite failure can be determined by different discontinuity thresholds such as Tsai-Hill or Tsai-Wo. Although these procedures provide accurate results in the elastic range, they fail when the composite constituents reach their elastic limit strength. To solve this problem, two different methods have been presented, the homogenization theory and the mixing theory (and its most

recent version, the serial/parallel mixing theory). These two theories obtain the composite mechanical performance from the mechanical performance of its constituent materials, being possible to obtain the material non-linear performance of the composite once its components have reached their yield stress.

Due to the high computational effort demanded by the homogenization theory, in order to perform large simulations of composite structures, it has been concluded that the best method available, capable to take into account the composite material non-linearities, is the serial/parallel mixing theory. It has been shown that this theory, that can be understood as a constitutive equation manager, can be implemented in a finite element code and can be also coupled with the classical lamination theory. Both implementations have been performed in PLCd and ComPack-Aero codes, respectively.

The serial/parallel mixing theory is an improved formulation, based on the first mixing theory developed by Trusdell and Toupin, in which the unidirectional performance of fiber material is taken into account defining an iso-strain condition in fiber direction (parallel direction) and an iso-stress condition in the remaining directions (serial directions). It has also been described an enrichment of this theory that improves the performance of the composite in its serial directions. The serial/parallel mixing theory has been also improved with the implementation of a perturbation method to perform a numerical derivation to obtain the tangent constitutive tensor of the composite constituents. This method provides a good approximation to the tangent constitutive tensor, independently of the constitutive law used to simulate the composite constituents.

Finally, three different numerical simulations have been performed to prove the potentiality of the numerical procedure proposed to solve composite structures, taking into account their material non-linearities. This is, the use of the serial/parallel mixing theory together with the finite element method. The simulations have been used to solve the problem of reinforcement and retrofitting of reinforced concrete (RC) structures using fibre reinforced polymers (FRP). Hereafter are described some conclusions obtained from the solution of this problem.

- The results of the simulations developed show that the numerical procedure proposed to simulate FRP reinforcements of RC structures performs well. The results are in good agreement with existing experimental results. The code used (PLCd) is prepared to compute real structures that are reinforced or retrofitted with CFRP. Last simulation presented has shown that different numerical simulations with different FRP reinforcements can be performed with PLCd in order to obtain the most suitable reinforcement configuration for the problem under study.
- It has been developed a construction stages algorithm in order to be able to simulate the effect of the FRP reinforcement in already damaged RC structures. This algorithm has shown how important is to reinforce the structure when a low level of damage is observed. Even if the structure stiffness does not vary if FRP is applied for reinforcement or retrofitting, the structural deformations and the stresses are greater if FRP is applied when the structure is already damaged.
- The frame simulations have shown that it is necessary to use three dimensional elements to correctly simulate the behavior of the structure. Using two dimensional elements implies assuming that the materials are evenly distributed through the cross-section. However, this assumption can cause overestimation of the structural performance if the structural components are not evenly distributed, as is the case with the lateral reinforcements in the 2D frame structure simulation. Nevertheless, if the condition of an

evenly distribution of the elements through the cross-section can be assumed, 2D simulations provide almost the same results as 3D simulations and reduce the computational cost substantially.

- Finally, all of the simulations have demonstrated that the performance of the structure improves when it is reinforced or retrofitted with fiber reinforced polymers. The degree of improvement depends on the type and configuration of the reinforcement used and on the existing level of damage in the structure when it is applied. In the particular case of the RC frame structure, the best CFRP joint reinforcement configuration is to wrap the entire joint by applying the upper, lower and lateral CFRP reinforcements.

References

- Alarcón, A. (2002). *Estudio teórico-experimental sobre la reparación y refuerzo de puentes de dovelas con fibras de carbono*. PhD thesis, Departament d'Enginyeria de la Construcció – UPC. Directors: Gonzalo Ramos and Juan Ramón Casas.
- Avilés, G. L. (2000). *Estudio experimental sobre el refuerzo a cortante de estructuras de hormigón mediante compuestos*. PhD thesis, Departament d'Enginyeria de la Construcció – UPC. Directors: Gonzalo Ramos and Juan Ramón Casas.
- Bahei-El-Din, Y. A., Rajendran, A. M., and Zikry, M. A. (2004). A micromechanical model for damage progression in woven composite systems. *International Journal of Solids and Structures*, 41(9-10):2307–2330.
- Barbat, A. H., Oller, S., Oñate, E., and Hanganu, A. (1997). Viscous damage model for timoshenko beam structures. *International Journal of Solids and Structures*, 34(30):3953–3976.
- Barbero, E. J. (1999). *Introduction to composite materials design*. Taylor & Francis, Philadelphia, USA.
- Bathe, K. J. (1996). *Finite Element Procedures*. Prentice–Hall, New–Jersey, USA.
- Belytschko, T., Liu, W. K., and Moran, B. (2000). *Nonlinear finite elements for continua and structures*. John Wiley & Sons, Chichester, UK.
- Bettor (2008). *Bettor MBrace design guideline*.
- Car, E. (2000). *Modelo constitutivo continuo para el estudio del comportamiento mecánico de los materiales compuestos*. PhD thesis, Departament de Resistència de Materials i Estructures a l'Enginyeria (RMEE) – UPC. Directors: Sergio Oller and Eugenio Oñate.
- Car, E., Oller, S., and Oñate, E. (1997). Matrices tangentes algorítmicas en el problema elastoplástico. In *CILAMCE XVIII Congreso Ibero Latino Americano de Métodos Computacionales en Ingeniería*, pages 2039–2051, October, Brasilia, Brasil.
- Car, E., Oller, S., and Oñate, E. (2000). An anisotropic elasto plastic constitutive model for large strain analysis of fiber reinforced composite materials. *Computer Methods in Applied Mechanics and Engineering*, 185(2–4):245–277.
- Car, E., Oller, S., and Oñate, E. (2001). A large strain plasticity model for anisotropic materials – composite material application. *International Journal of Plasticity*, 17(11):1437–1463.
- Car, E., Zalamea, F., Oller, S., Miquel, J., and Oñate, E. (2002). Numerical simulation of fiber reinforced composites - two procedures. *International Journal of Solids and Structures*, 39(7):1967–1986.
- CIMNE (1991-2008). *PLCd Manual. Non-linear thermomechanic finite element code oriented to PhD student education*. Finite element code developed at CIMNE.
- CIMNE and Quantech (2008). *ComPack-Aero. Innovative finite element methods for non linear analysis of composite structures*. Explicit finite element code developed by CIMNE & Quantech ATZ. www.cimne.com; www.quantech.es/QuantechATZ/Stampack.html.
- Crisfield, M. A. (1991). *Non-linear finite element analysis of solids and structures. Volume 1. Essentials*. John Wiley & Sons, West Sussex, UK.

- Dávila, C. G., Camanho, P. P., and Rose, C. A. (2005). Failure criteria for FRP laminates. *Journal of Composite Materials*, 39(4):323–345.
- Eshelby, J. D. (1957). The determination of the elastic field of an ellipsoidal inclusion and related problems. *Proceedings of Royal Society of London, Series A*, 241:376–396.
- Gómez Soberón, G., Oller, S., and Barbat, A. (2002). Evaluación del daño sísmico en puentes de hormigón armado. *Revista Internacional de Métodos Numéricos para el Cálculo y Diseño en Ingeniería*, 18(2):309–329.
- González, C. and Llorca, J. (2007a). Mechanical behavior of unidirectional fiber-reinforced polymers under transverse compression: Microscopic mechanisms and modeling. *Composites and Science Technology*, 67(5):2795–2806.
- González, C. and Llorca, J. (2007b). Virtual fracture testing of composites: A computational micromechanics approach. *Engineering Fracture Mechanics*, 74(7):1126–1138.
- Green, A. and Naghdi, P. (1965). A dynamical theory of interacting continua. *Journal of Engineering Science*, 3:231–241.
- Halpin, J. and Tsai, S. W. (1969). Effects of environmental factors on composite materials. Technical Report 67-426, Air force materials lab. Department of Defense, USA.
- Hill, R. (1963). Elastic properties of reinforced solids: some theoretical principles. *Journal of the Mechanics and Physics of Solids*, 11(5):357–372.
- Huang, J. Y., Chen, S., Wang, Z. Q., Kempa, K., Wang, Y. M., Jo, S. H., Chen, G., Dresselhauss, M., and Ren, Z. (2006). Superplastic carbon nanotubes. *Nature*, 439:281.
- Jones, R. M. (1999). *Mechanics of composite materials*. Taylor & Francis, Philadelphia, USA, 2nd edition.
- Kachanov, L. M. (1986). *Introduction to continuum damage mechanics*. Mechanics of elastic stability. Martinus Nijhoff, Dordrecht, Netherlands.
- Khalifa, A., Alkhrdaji, T., Nanni, A., and Lansburg, S. (1999). Anchorage of surface mounted FRP reinforcement. *Concrete International: Design and Construction*, 21(10):49–54.
- Khalifa, A. and Nanni, A. (2002). Rehabilitation of rectangular simply supported RC beams with shear deficiencies using CFRP composites. *Construction and Building Materials*, 16(3):135–146.
- Li, A., Assih, J., and Delmas, Y. (2001). Shear strengthening of rc beams with externally bonded CFRP sheets. *Journal of Structural Engineering*, 127(4):374–380.
- Li, G., Maricherla, D., Singh, K., Pang, S.-S., and John, M. (2006). Effect of fiber orientation on the structural behavior of FRP wrapped concrete cylinders. *Composite Structures*, 74(4):475–483.
- Lubliner, J. (1990). *Plasticity theory*. MacMillan Publishing Company, New York, USA.
- Lubliner, J., Oliver, J., Oller, S., and Oñate, E. (1989). A plastic–damage model for concrete. *International Journal of Solids and Structures*, 25(3):299–326.
- Malvern, L. E. (1968). *Introduction to the mechanics of a continuous medium*. Prentice-Hall, Englewood Cliffs, NJ, USA.

- Marsden, J. E. and Huges, T. J. R. (1983). *Mathematical foundations of elasticity*. Dover Publications, New York, USA.
- Martínez, X., Oller, S., and Barbat, A. (2006). Numerical tool to study structural reinforcement of steel reinforced concrete (RC) structures under seismic loads using fibre reinforced polymers (FRP). In *ECEES – First European Conference on Earthquake Engineering and Seismology*, September, Geneva, Switzerland.
- Martínez, X., Oller, S., Rastellini, F., and Barbat, A. (2008). A numerical procedure simulating RC structures reinforced with FRP using the serial/parallel mixing theory. *Computers and Structures*, doi:10.1016/j.compstruc.2008.01.007.
- Mata, P., Oller, S., and Barbat, A. H. (2007). Static analysis of beam structures under nonlinear geometric and constitutive behaviour. *Computer Methods in Applied Mechanics and Engineering*, 196(45-48):4458–4478.
- Mata, P., Oller, S., and Barbat, A. H. (2008). Dynamic analysis of beam structures considering geometric and constitutive nonlinearity. *Computer Methods in Applied Mechanics and Engineering*, 197(6-8):857–878.
- Mayugo, J. A. (2003). *Estudio comparativo de compuestos laminados sometidos a cargas cíclicas*. PhD thesis, Departament de Resistència de Materials i Estructures a l'Enginyeria (RMEE) – UPC. Directors: Sergio Oller and Josep Costa.
- Meier, U. (1995). Strengthening of structures using carbon fibre/epoxi composites. *Construction and Building Materials*, 9(6):341–351.
- Neamtu, L., Oller, S., and Oñate, E. (1997). A generalized mixing theory elasto-damage-plastic model for finite element analysis of composites. In Owen, D., Oñate, E., and Hinton, E., editors, *Complas V – Computational Plasticity*, pages 1–5, March, Barcelona, Spain.
- Ochoa, O. O. and Reddy, J. N. (1992). *Finite element analysis of composite laminates*. Kluwer Academic Publishers, Dordrecht, Netherlands.
- Oliver, J., Cervera, M., Oller, S., and Lubliner, J. (1990). Isotropic damage models and smeared crack analysis of concrete. In Mang, H. and Bicanić, N., editors, *Second International Conference on Computer Aided Analysis and Design of Concrete Structures*, pages 945–958, April, Zell am See, Austria.
- Oller, E. (2005). *Peeling failure in beams by plate bonding: A design proposal*. PhD thesis, Departament d'Enginyeria de la Construcció – UPC. Directors: Diego Cobo.
- Oller, S. (2001). *Fractura mecánica. Un enfoque global*. CIMNE (Centro Internacional de Métodos Numéricos en Ingeniería), Barcelona, Spain.
- Oller, S. (2002). *Dinámica no-lineal*. CIMNE (Centro Internacional de Métodos Numéricos en Ingeniería), Barcelona, Spain.
- Oller, S. (2003). *Simulación numérica del comportamiento mecánico de los materiales compuestos*. CIMNE (Centro Internacional de Métodos Numéricos en Ingeniería), Barcelona, Spain.
- Oller, S. and Car, E. (2002). *Análisis y cálculo de estructuras de materiales compuestos*, chapter Teoría de mezclas para el estudio de los materiales compuestos: Matriz reforzada con fibras largas y cortas, pages 145–186. CIMNE (Centro Internacional de Métodos Numéricos en Ingeniería), Barcelona, Spain.

- Oller, S., Lubliner, J., and Lopez, J. (2002). *Análisis y cálculo de estructuras de materiales compuestos*, chapter La mampostería – Tratamiento como compuesto homogeneizado, pages 379–410. CIMNE (Centro Internacional de Métodos Numéricos en Ingeniería), Barcelona, Spain.
- Oller, S., Miquel, J., and Zalamea, F. (2005). Composite material behaviour using a homogenization double scale method. *Journal of Engineering Mechanics*, 131(1):65–79.
- Oller, S., Neamtu, L., and Oñate, E. (1995). Una generalización de la teoría de mezclas clásica para el tratamiento de compuestos en serie/paralelo. In París, F. and Cañas, J., editors, *MATCOMP 95*, pages 433–438, November, Sevilla, Spain.
- Oller, S., Oñate, E., Miquel, J., and Botello, S. (1996). A plastic damage constitutive model for composite materials. *International Journal of Solids and Structures*, 33(17):2501–2518.
- Oller, S., Oñate, E., Oliver, J., and Lubliner, J. (1990). Finite element non-linear analysis of concrete structures using a plastic-damage model. *Engineering Fracture Mechanics*, 35(1–3):219–231.
- Oñate, E. (1995). *Cálculo de estructuras por el método de elementos finitos. Análisis estático lineal*. CIMNE (Centro Internacional de Métodos Numéricos en Ingeniería), Barcelona, Spain, 2nd edition.
- Oñate, E., Oller, S., Flores, F., Rastellini, F., and Martinez, X. (2007). Femcom: An innovative finite element method for non linear analysis of composite structures. first annual report project. Technical report, CIMNE.
- Ortiz, M. and Popov, E. (1957). A physical model for the inelasticity of concrete. Proceedings of Royal Society of London, Series A, 383:101–125.
- Ortiz, M. and Popov, E. (1982). Plain concrete as a composite material. *Mechanics of Materials*, 1:139–150.
- Paul, B. (1960). Prediction of elastic constants of multiphase materials. In *Transactions of the metallurgical society of AIME*, pages 36–41.
- Pedelta (1996). *Structural engineering company*. www.pedelta.com.
- Pulido, M. D. G. and Sobrino, J. A. (1998). Los materiales compuestos en el refuerzo de puentes. *Revista Internacional de Ingeniería y Estructuras*, 3(1):75–95.
- Rabinovitch, O. (2004). Nonlinear (buckling) effects in rc beams strengthened with composite materials subjected to compression. *International Journal of Solids and Structures*, 41(20):5677–5695.
- Rastellini, F. (2006). *Modelización numérica de la no-linealidad constitutiva de laminados compuestos*. PhD thesis, Departament de Resistència de Materials i Estructures a l'Enginyeria (RMEE) – UPC. Directors: Sergio Oller and Eugenio Oñate.
- Rastellini, F., Oller, S., Salomon, O., and Oñate, E. (2003a). Advanced serial-parallel mixing theory for composite materials analysis. continuum basis and finite element applications. In Oñate, E. and Owen, D., editors, *COMPLAS 2003–Proceeding CD of the VII International Conference on Computational Plasticity*, April, Barcelona, Spain.
- Rastellini, F., Oller, S., Salomon, O., and Oñate, E. (2003b). Teoría de mezclas serie-paralelo avanzada para el análisis de materiales compuestos. In Miravete, A. and Cuartero, J., editors, *Composites 2003. V Congreso de la asociación española de materiales compuestos*, July, Zaragoza, Spain.

- Rastellini, F., Oller, S., Salomon, O., and Oñate, E. (2007). Composite materials non-linear modelling for long fibre reinforced laminates: Continuum basis, computational aspects and validations. *Computers and Structures*, doi:10.1016/j.compstruc.2007.04.009.
- Ravi Annapragada, S., Sun, D., and Garimella, S. V. (2007). Prediction of effective thermo-mechanical properties of particulate composites. *Computational Materials Science*, 40(2):255–266.
- Reddy, J. N. (2003). *Mechanics of laminated composite plate and shells: theory and analysis*. CRC Press, Boca Raton, Florida, USA, 2nd edition.
- Salomon, O., Rastellini, F., Oller, S., and Oñate, E. (2005). Fatigue prediction for composite materials and structures. In Research, N. and technology Organisation (RTO), editors, *Air Vehicle Technology: AVT-121. Symposium on the evaluation, control and prevention of high cycle fatigue*, October, Granada, Spain.
- Sánchez-Palencia, E. (1987). *Homogenization techniques for composite media*, chapter Boundary layers and edge effects in composites, pages 121–192. Springer-Verlag, Berlin, Germany.
- Sika (2008). *Sika CarboDur design guideline*. Sika Corp.
- Simo, J. C. and Hughes, T. J. R. (1998). *Computational inelasticity*. Springer Verlag, New York, USA.
- Spadea, G., Benicardino, F., and Swamy, R. N. (1998). Structural behaviour of composite RC beams with externally bonded CFRP. *Journal of Composites for Construction*, 2(3):132–137.
- Sun, C. T., Quinn, B. J., Tao, J., and Oplinger, D. W. (1996). Comparative evaluation of failure analysis methods for composite laminates. Technical Report DOT/FAA/AR-95/109, U.S. Department of transportation. Federal aviation administration.
- Suquet, P. (1982). *Plasticité et homogénéisation*. PhD thesis, Université Paris 6.
- Timoshenko, S. P. (1940). *Theory of Elasticity*. McGraw-Hill Book Company, New York, USA, 2nd edition.
- Trusdell, C. and Toupin, R. (1960). *The Classical Field Theories*. Springer Verlag, Berlin, Germany, Handbuch Der Physik III/I edition.
- Tsai, S. W. (1964). Structural behavior of composite materials. Technical Report CR-71, NASA.
- Vasiliev, V. V. and Morozov, E. V. (2001). *Mechanics and analysis of composite materials*. Elsevier, Oxford, UK.
- Zalamea, F. (2001). *Tratamiento numérico de materiales compuestos mediante la teoría de homogeneización*. PhD thesis, Departament de Resistència de Materials i Estructures a l'Enginyeria (RMEE) – UPC. Directors: Juan Miquel Canet and Sergio Oller.
- Zienkiewicz, O. C. and Taylor, L. R. (1991). *The finite element method*. McGraw-Hill Book Company, London, UK.

Chapter 3

Delamination in composites

3.1 Introduction

The use of new materials in structural applications implies dealing with new failure processes, not existing in traditional materials. One of these is the delamination phenomenon found in laminated composites. The lost of adherence between the different layers of the composite leads to a reduction of the section strength and stiffness that can finish in a structural failure. Figure 3.1 shows the delamination found in a carbon/epoxy composite under compression efforts.



Figure 3.1: Delamination due to compression in a carbon/epoxy composite (Paiva et al., 2005)

The importance of the delamination phenomenon is demonstrated by the amount of authors that have developed theories and formulations to deal with it. All authors that have studied the problem agree in characterizing the delamination process by two main phenomenons, the crack initiation and its propagation along the composite. Crack initiation can be obtained by comparing the strain–stress state of the material, in the region where delamination takes place, with a critical one (Jansson and Larsson, 2001; Camanho and Dávila, 2002; Turon et al., 2006; Balzani and Wagner, 2007) or in terms of the traction versus relative displacement (Borg et al., 2002, 2004; Pinho et al., 2006). And the delamination propagation is usually treated opening the mesh to simulate the crack effect where it takes place. To open the mesh different procedures are proposed. One of them is the virtual crack closure technique (VCCT) (Krueger, 2004), based on the assumption that when a crack is extended, the energy required to open the crack is the same required to close it. Another procedure, each time more used, is the use of a cohesive zone model (Camanho and Dávila, 2002). The cohesion elements are placed in the interface of the layers that can suffer delamination and its propagation is obtained using a damage mechanics formulation.

Besides the differences among the existing formulations found in literature to simulate the delamination phenomenon, all of them agree in defining a special formulation where the delamination takes place, with interface elements (Balzani and Wagner, 2007), cohesive zones (Camanho and Dávila, 2002) or coincident nodes (Borg et al., 2002). This approach predefines the path that will follow the delamination fracture or, if this path is unknown, forces to place these elements between all laminate layers, which becomes computationally very expensive.

In contrast to the scope used in known literature to solve the delamination problem, this work uses the continuum mechanics to simulate the delamination initiation and propagation, without making any distinction of the elements in which delamination takes place. The serial/parallel mixing theory (SP RoM) developed by Rastellini et al. (2007) is used to obtain the composite performance and to simulate the delamination process. This theory is based on the definition of some compatibility equations between the strain–stress states of the composite constituent materials. In the case of a composite made of fibre and matrix, what

the serial/parallel mixing theory does is to impose an iso-strain condition on the parallel direction, usually the fibre direction, and a iso-stress condition on the serial direction, usually the remaining directions of the stress and strain tensors. With this scope, if the matrix structural capacity is lost, the SP RoM reduces the structural capacity of fibre material in the serial directions due to the iso-stress condition. Thus, it is not possible for the composite layer to develop shear or transversal stresses, less to transmit them to the surroundings elements. The structural performance of a material in which serial stresses are zero corresponds to the performance of a delaminated material.

To obtain this structural behavior, the matrix material has to loose its strength for a certain stress state. This lost of strength must be permanent in order to simulate the real crack produced by delamination in the material. This is achieved with a damage formulation controlled by the fracture energy of the material.

With the proposed procedure, delamination is simulated straightforward, without needing to develop special elements neither to define where the delamination will take place. Although this methodology provides its best when it is applied to finite element simulations that use solid elements, a new procedure is described capable to characterize the delamination onset in simulations that use a lamination theory. This is an important achievement because most of the composites that fail due to delamination are laminates and the most efficient procedure to simulate them is with a lamination theory, specially if large structural problems are solved. The procedure proposed is capable to localize delamination failures in these sort of simulations, without increasing substantially the computational cost required.

This chapter contains a first section (section 3.2) that describes the delamination problem and the different experimental and numerical procedures used nowadays to characterize it. In this same section is also included a detailed description of the procedure proposed to solve the delamination problem, using the serial/parallel mixing theory developed by Rastellini et al. (2007). Afterwards, in section 3.3, is described the damage formulation used to characterize the delamination onset and propagation. This formulation has been improved with the addition of a friction parameter that takes into account the residual strength provided by the friction between the surfaces found at each side of the delamination fracture.

Finally, the validity of the approach proposed is proved with two different numerical simulations. The first simulation compares the results obtained from the experimental test made to obtain the mode II fracture energy of a composite with the results obtained from a numerical simulation of the same model. The experimental test is the End Notch Flexure (ENF) test. The results of this simulation have been already presented by Martínez et al. (2007) in the ECCOMAS thematic conference on mechanical response of composites (Composites 2007).

The second simulation corresponds to a ply drop-off test. This simulation is also used to present the new methodology proposed to take into account the delamination failure in large scale simulations of composite laminated structures using the lamination theory. The new procedure presented has been developed for the FEMCOM project (An innovative finite element method for non linear analysis of composite structures – CIMNE–AIRBUS) and is included in the technical report Martínez et al. (2007).

3.2 Delamination in composite materials

According to Bolotin (1996), the first study of the delamination phenomenon was made by Obreimoff (1930) who asses the surface energy in splitting mica (an anisotropic natural

laminate similar to modern composites). From this first study several authors treated with the problem but it was not until late 1960s that serious studies of delamination phenomena in composites began (Pagano and Schoeppner, 2000). Since then, a large amount of research has been made on the delamination problem, experimental and numerical, dealing with the delamination characterization, initiation and stability. A detailed survey of the historical treatment of the delamination problem and of the procedures used nowadays to deal with it can be found in Pagano and Schoeppner (2000), Blanco (2004) and Turon (2006).

This section provides a brief description of the delamination problem and of the experimental and numerical methods existing nowadays to treat it. The purpose sought is to give some hints about the actual knowledge without describing deeply any procedure, as these can be found in the fonts previously cited. Afterwards is described the new approach proposed in this work to characterize and simulate delamination. It will be shown that, although this new approach uses some of the formulation considered by other authors to simulate the delamination phenomenon, such as a continuum mechanics damage formulation, the procedure proposed is completely different. The delamination phenomenon is simulated straightforward with the developed formulation to characterize composite materials, the serial/parallel mixing theory, without the need of developing special elements or adding numerical procedures to the simulation, such as contact or remeshing techniques.

3.2.1 Description of the delamination problem

Delamination is a critical failure mode in composites, not because it causes the structure to break, but because it divides the composite in different layers not connected between them, which modifies the structural performance of the composite leading to its failure because of other mechanical phenomenons such as buckling, excessive vibration or loss of fatigue life (Pagano and Schoeppner, 2000). With this scope, Bolotin (1996) defines two kinds of delaminations: internal and near the surface. While the first ones affect the whole composite performance, the second ones only affect the external layers of the composite and lead, usually, to a local buckling.

The delamination phenomenon is characterized by two different processes: delamination onset and crack propagation. Delamination onset is defined by the damage resistance of the composite, the capability of the material to resist the initial occurrence of damage. The second process is delamination propagation, which is driven by the damage tolerance of the material. This damage tolerance can be defined as the capability of a damaged material to sustain a load, maintaining its structural performance. All formulations developed to simulate the delamination phenomenon focus their effort in characterize these two processes.

Delamination can be initiated by several factors, however there are some that are more common. In the manufacture stage delamination can occur due to the shrinkage of the matrix during curing (Blanco, 2004). Once the composite is in use, a common source of delamination is low velocity impacts, transversal to the laminate (Iannucci and Willows, 2006, 2007). There are also some design configurations that can lead to a potential delamination failure such as curved sections or tapers and transitions (Kedward, 2002). All these factors lead to the apparition of interlaminar normal stresses larger than the ones that can be taken by the composite, which produce the crack between layers or delamination.

Once delamination has occurred, the phenomenon is controlled by the toughness of the material to restrain its propagation along the composite. Three different delamination modes can be defined, according to the growth propagation of the interlaminar crack: mode I or opening mode, mode II or shearing mode and mode III or tearing mode. These modes are

displayed in figure 3.2. In practice, the most common fracture modes of delamination are mode I, mode II or a mixed mode I/II.

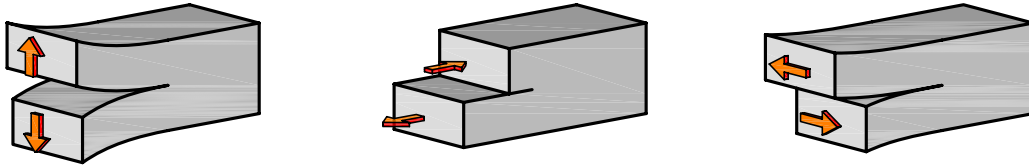


Figure 3.2: Crack modes defining the delamination growth

The composite toughness is usually characterized by the fracture energy, G , that can be defined as the energy released by the system due to the crack propagation (Oller, 2001). The fracture energy is associated to the fracture area. Therefore it can be obtained as the total work required to fracture an area A :

$$G = \frac{W^0}{A} + \frac{W^P}{A} \quad (3.1)$$

Being W^0 the kinetic work required to fracture the material and W^P the plastic work. This last work is zero in case of brittle materials, in which plastic deformations are zero. Three different fracture energies are usually defined, each one corresponding to a fracture mode: G_I , G_{II} and G_{III} . The fracture energy is commonly obtained for different materials experimentally, using equation 3.1. Most of the existing formulations developed to simulate delamination in composites use the fracture energy to characterize delamination onset and crack propagation.

Before describing some of the most common experimental tests used to characterize the delamination performance of composites, its worth to mention the relation between delamination and fatigue. Most of the in service failures of composites are produced by fatigue. On the other hand, delamination is considered the most important damage mechanism in composite laminates. Hence, the combination of both factors is critical for the composite integrity, being one of the most common failure causes of composite laminates. The importance of this relation is proven by the large number of studies on the subject, among them two PhD dissertations: Blanco (2004), who studies the problem using a numerical and an experimental approach; and Turon (2006), who extends the formulation of his zero thickness decohesion element to take into account fatigue loading conditions.

3.2.2 Experimental simulation of delamination

The experimental simulation of delamination in composites not only is used to improve the knowledge of the mechanical phenomenons that lead to the onset and propagation of delamination but also is used to obtain the fracture energy of the composite, parameter required by most of the formulations existing in literature to deal with the problem. The fracture energy of the composite is obtained with equation 3.1, using the delaminated area in the composite as the fracture area and calculating the work done using analytical formulations.

Most of the experimental tests are made on beam type composite specimens like the one shown in figure 3.3. The composite has an initial delamination in its mid-plane which is created adding a thin non-stick film between its layers when it is manufactured. In order to

add this film in the composite, the laminate is made with an even number of layers. Most of the tests are performed in unidirectional laminate composites. The results obtained from the tests are usually the force applied to the composite and its relative displacement. These values are used to obtain the work required to propagate the initial crack.

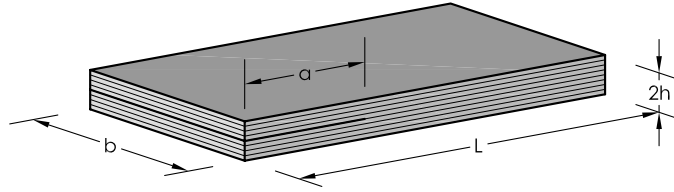


Figure 3.3: Most common tests used to obtain the delamination toughness of composites

As well as there is different crack modes and fracture energies related to these crack modes, also exist different tests that are developed to obtain the fracture energy for each particular crack mode. A survey of some of these tests can be found in Davies et al. (1998) and Brunner et al. (2007). Due to the relevance of the delamination failure in composite structures and also due to the necessity to have a reliable procedure to obtain the fracture energy of the composite, some of these tests have been standardized. All standards provide a detailed description of the sample to be used to perform the test, the loading procedure, the results that have to be obtained and the formulation to be used to calculate the fracture energy from the values obtained from the test.

The most common delamination modes in laminated composites are mode I, mode II and the mixed mode I/II. Each one of these fracture modes have a standardized test, which is described in the following. The tests configurations are displayed in figure 3.4.

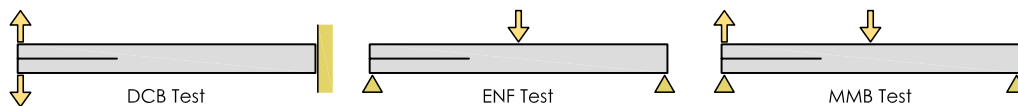


Figure 3.4: Most common tests used to obtain the delamination toughness of composites

DCB Test: *Double Cantilever Beam Test*. This test obtains the delamination toughness in fracture mode I. The initial delamination is forced to grow by applying a force in each side of the initial crack, of opposite direction and transversal to the crack surface. A detailed description of this test can be found in the standards ASTM D-5528 and JIS K-7086.

ENF Test: *End Notched Flexure Test*. This test obtains the delamination toughness in fracture mode II. This test applies a three point flexure load to the composite sample to increase the delamination in mode II. The main problem of this test is the propagation instability of the delamination (Davies et al., 1998). To solve this drawback, a four point flexure test (4ENF) is under study. A detailed description of the ENF test can be found in JIS K-7086.

MMB Test: *Mixed Mode Bending Test*. This test obtains the delamination toughness in mixed mode fracture I/II. This test is considered nowadays the best method for evaluating the fracture toughness as it loads the specimen with more realistic loads (Balacó de Morais and Pereira, 2006a). Figure 3.4 shows that this test is a combination of the

DCB and the ENF tests. The MMB test is described in standard ASTM D-6671. An analysis of the test, with proposals to reduce the non-linearities associated to it can be found in Reeder and Crews (1991)

3.2.3 Numerical procedures to simulate delamination

Most of the numerical procedures and formulations developed to characterize the delamination phenomenon are closely related to continuum mechanics, as they use fracture or damage mechanics to predict the delamination onset and propagation. With this relation in mind, Turon (2006) classifies the existing procedures for numerical simulation of delamination in two groups, one contains all formulations that apply fracture mechanics and the other the formulations that use damage mechanics. This criterion is also used in this work.

Continuum mechanics is used to obtain the delamination onset and propagation in the simulation. The formulation is applied to special elements or “delamination elements” that are developed to simulate the delamination process. Different authors propose different elements where to apply the continuum mechanics formulation, such as zero thickness decohesion elements (Jansson and Larsson, 2001; Camanho and Dávila, 2002), coincident nodes (Borg et al., 2001, 2002) or coincident surfaces (Pinho et al., 2006).

Therefore, delamination is simulated applying a continuum mechanics formulation to some special elements or “delamination elements”. When delamination occurs in these elements, the mesh is divided. Coincident nodes and coincident surfaces are already divided, having their nodes attached before delamination and released when delamination has occurred. Zero thickness decohesion elements can be opened to allow free displacement between the surfaces found at each side of the crack (Turon et al., 2006). These procedures have two main drawbacks, one technological because in some cases it is necessary to develop a contact formulation to avoid the interpenetration of one surface over the other if the loads applied to the composite are modified, and the other, probably more important, is that it is required to add these elements in all regions in which delamination is supposed to take place.

The mechanical properties required to characterize the “delamination elements” are those required by the continuum mechanics formulation used to simulate the delamination. These properties are usually assigned to matrix material although they can be also related to the adhesive used to attach the laminate layers or can be properties of a generic material which parameters are obtained from a delamination experimental test. In the following are described the most common continuum mechanics formulations used to characterize these elements.

Fracture mechanics

Delamination can be treated using linear elastic fracture mechanics. This theory provides the way in which delamination propagates and is usually complemented by a stress analysis that predicts the delamination onset (Turon, 2006). There are several fracture mechanics formulations that are used in the delamination problem, among them: the virtual crack closure technique (VCCT) (Krueger, 2004), the J-integral method (Rice, 1968; Oller, 2001), the virtual crack extension and the stiffness derivative. Among all these methods, probably the most widely used to solve the delamination problem is the virtual crack closure technique.

Virtual crack closure technique (VCCT)

The virtual crack closure technique is a two step method based on the assumption that the

energy ΔE released when the crack is extended a small amount is the same as the work required to close the crack. With this assumption, the fracture energy required to open the crack can be obtained as a function of the forces at the crack tip and the nodal displacements (Krueger, 2004). In a two dimensional case,

$$\begin{aligned} G_I &= \frac{1}{2\Delta a} Z \Delta w \\ G_{II} &= \frac{1}{2\Delta a} X \Delta u \end{aligned} \quad (3.2)$$

Being Δa the crack length, X , Z the horizontal and vertical forces in the crack tip, respectively, and Δu , Δw the horizontal and vertical displacements.

The fracture energies calculated in equation 3.2 are added to obtain the total energy release rate:

$$G_T = G_I + G_{II} \quad (3.3)$$

The VCCT states that the crack propagates when the total energy release rate is equal to the fracture toughness of the material, G_c (Turon, 2006):

$$G_T = G_c \quad (3.4)$$

This method has been used to predict the delamination performance of composites by Krueger (2002) and Balacó de Moraes and Pereira (2006a,b), among others.

Damage mechanics

A damage mechanics formulation is based on the analysis of the strain-stress state of the material, which provides the total energy that is released by the material per unit area (Oller, 2001). In figure 3.5 is displayed a possible strain-stress relation. The fracture energy per unit area corresponds to the area below the $\sigma - \varepsilon$ curve. The use of this formulation has the main advantage, compared to fracture mechanics, that the fracture onset and its propagation are unified in the formulation Turon (2006). When the energy used by the system is equal to the fracture toughness, stresses in the material become zero and the crack surfaces are formed.

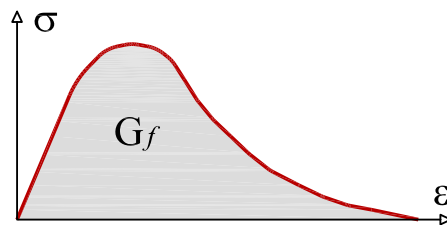


Figure 3.5: Fracture energy of the material

The use of damage mechanics to simulate delamination is used by many authors with different strategies. In example, Borg et al. (2001, 2002, 2004) apply it to define a penalty interface

in which coincident nodes are tied with three orthogonal springs, each one representing a different fracture mode. The mechanical behavior of these springs is defined using a damage mechanics formulation. However, the most common procedure used to simulate delamination is with the definition of an interface element in which its mechanical performance is defined by damage mechanics. Some examples of interface elements are the ones defined by Allix and Ladev  ze (1995), de Moura et al. (2000), Camanho et al. (2003), Turon et al. (2006) and Balzani and Wagner (2007).

Of all these elements, the zero thickness decohesion element defined by Turon (2006) in his PhD dissertation is described in this section, in order to provide an example of how the damage mechanics formulation is included in interface elements. This model is an improvement of the interface element defined in Camanho et al. (2003) and its detailed description can be found in Turon et al. (2004), Turon (2006) and Turon et al. (2006). Recently improvements of the model, in which the computational cost of the simulation is reduced, are described in Turon et al. (2007).

Zero thickness decohesion element

The zero thickness decohesion element proposed by Turon uses a cohesive zone model formulation. This formulation assumes that a cohesive zone develops near the crack tip. With this assumption, surface traction is related to displacement jumps at the interface where the crack may occur. The displacement jump is written as:

$$\|u\| = u^+ - u^- \quad (3.5)$$

Where u_i^+ corresponds to the displacement of the surface above the decohesion element and u_i^- corresponds to the surface under the element (see figure 3.6). The displacement jump is transformed to the local coordinate system using a rotation tensor Θ :

$$\Delta = \Theta \|u\| \quad (3.6)$$

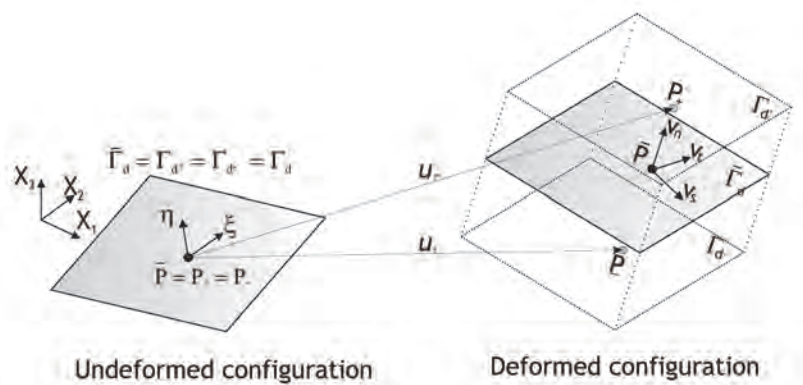


Figure 3.6: Displacements in the zero thickness decohesion element (Turon, 2006).

Once having defined the element displacements, these are related to the cohesion traction of the element (τ) using a constitutive law. This law is obtained following the thermodynamical principles defined in continuum mechanics (Oller, 2003) and using a damage mechanics model. The constitutive law proposed by Turon (2006) can be written as:

$$\tau = \tau(\Delta) = (1 - d)K\Delta - dK(\delta_{3j} \langle -\Delta_3 \rangle) \quad (3.7)$$

Being d the damage parameter, K a scalar value that represents the penalty stiffness of the element, δ the Kronecker delta and $\langle \cdot \rangle$ the MacAuley function, which is defined as: $\langle x \rangle = \frac{1}{2}(x + \|x\|)$. The use of the MacAuley function provides a different mechanical performance for tensile and compressive displacements. Only the tensile displacements are taken into account to predict delamination.

Delamination onset takes place when the interlaminar traction exceeds the maximum interfacial strength. In order to take into account the different fracture modes in the element, a quadratic criterion is chosen:

$$\left(\frac{\tau_1}{\tau_1^0}\right)^2 + \left(\frac{\tau_2}{\tau_2^0}\right)^2 + \left(\frac{\langle \tau_3 \rangle}{\tau_3^0}\right)^2 = 1 \quad (3.8)$$

with, $\tau = (\tau_1, \tau_2, \tau_3)$ the interlaminar traction in the element and $\tau^0 = (\tau_1^0, \tau_2^0, \tau_3^0)$ the maximum interfacial strength. When delamination onset occurs, the damage parameter becomes different of zero and the interface degradation starts. The evolution of the damage parameter is defined by the fracture energy of the element (delamination toughness), reaching a value of 1 when the system has released all its energy. At this point, the traction forces in the interface become zero and the two surfaces previously attached can move freely.

The calculation of the total energy released by the system, G_c , is made with the expression proposed by Benzeggagh and Kenane (1996), which also takes into account the three different fracture modes. Its expression is:

$$G_c = G_{Ic} + (G_{IIc} - G_{Ic}) \left(\frac{G_{shear}}{G_T}\right)^\eta \quad (3.9)$$

The quotient $\frac{G_{shear}}{G_T}$ is defined as the mixed mode ratio, being G_T the total energy of the system and $G_{shear} = G_{II} + G_{III}$.

An example of the results that are obtained with this formulation is shown in figure 3.7. This figure, obtained from Turon (2006), shows the debonding of a skin-stiffener resulting from applying a tensile load to the base laminate.

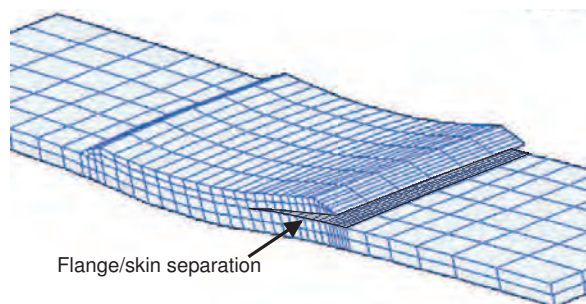


Figure 3.7: Simulation of a Skin-stiffener debonding (Turon, 2006).

3.2.4 Delamination using the serial/parallel mixing theory

Up to this point it has been shown that most of the procedures found in literature to simulate the delamination phenomenon in laminated composites are based on the definition of an interface element which is characterized by the interface toughness. When the criterion used to simulate the interlaminar strength is accomplished, either if it is based in fracture mechanics or if it is based in damage mechanics, the interface element loses its capacity to maintain attached the composite layers at each side of the fractured surface and delamination occurs.

As has been already stated, these procedures have two main drawbacks. The first one is that there are many formulations in which the two surfaces found at each side of the fracture become completely independent, being necessary to use remeshing techniques and contact formulations to obtain the delamination propagation. The second drawback affects all known formulations, and is the necessity to define an special element in which delamination will occur. This situation predefines the delamination path to the region where these elements are placed. And, if the exact place where the delamination takes place is unknown, these elements must be included between all layers, which makes the calculation unbearable due to its computational cost.

The procedure proposed here to simulate delamination solves these two drawbacks. It will be shown that using the serial/parallel mixing theory developed by Rastellini (2006) and described in chapter 2, section 2.3, the delamination phenomenon can be simulated straightforward, without the need of any additional element or formulation.

Delamination consist in the lost of adherence between the different layers existing in a laminate. This lost of adherence makes impossible the transmission of stresses between the different layers, reducing the composite strength and stiffness. The stress transmission between the layers of a composite is made by the stresses normal to the fractured area (mode I) or by shear stresses (modes II and III). If the problem is solved using a continuum mechanics formulation, the delamination effect can be represented by the impossibility of a layer to develop normal or shear stresses. This layer will represent a delaminated layer and it will not allow the transmission of stresses between the layers allocated above and below it.

Following this interpretation of the delamination phenomenon, the serial/parallel mixing theory can deal with the delamination problem. This theory is based on the definition of some compatibility equations between the strain-stress states of the composite constituent materials. In the case of a composite made of fibre and matrix, what the serial/parallel mixing theory does is to impose an iso-strain condition on the parallel direction (fibre direction) and an iso-stress condition on the serial directions (normal and shear directions).

The form in which the serial/parallel mixing theory solves the delamination process is shown with the help of figure 3.8, in which the stresses found in fiber and matrix material are depicted in a two dimensional delamination simulation.

If matrix material is completely damaged, its ability to sustain stresses is lost and, therefore, its stress tensor becomes zero:

$${}^m\sigma = [{}^m\sigma_1 \quad {}^m\sigma_2 \quad {}^m\sigma_{12}] = [0.0 \quad 0.0 \quad 0.0] \quad (3.10)$$

According to the serial/parallel mixing theory, the serial stresses in the composite are the same than the serial stresses of its components:

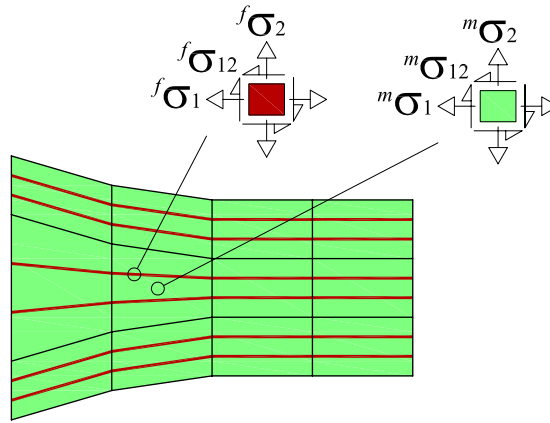


Figure 3.8: Stress state of composite constituents with the serial/parallel mixing theory

$${}^c\sigma_S = {}^m\sigma_S = {}^f\sigma_S \quad (3.11)$$

Hence,

$${}^f\sigma_S = 0.0 \quad \rightarrow \quad {}^f\sigma_2 = 0.0 ; \quad {}^f\sigma_{12} = 0.0 \quad (3.12)$$

And the final stress in the composite becomes:

$${}^c\sigma = {}^m k^m \sigma + {}^f k^f \sigma = \begin{bmatrix} {}^f k^f \sigma_1 & 0.0 & 0.0 \end{bmatrix} \quad (3.13)$$

So, with this scope, if matrix structural capacity is lost, it becomes impossible for the composite layer to develop any serial stress, neither to transmit them to the surroundings elements. This effect, can be understood as delamination. It is important to remark that the composite is unable to develop stresses only in its serial directions. Even if matrix is completely damaged, an iso-strain condition defines the performance of fiber and matrix in fiber direction, which provides a nearly undamaged mechanical performance of the composite in this direction.

With this approach, now the delamination phenomenon lays in the simulation of matrix material, that can be modeled with any constitutive law (Rastellini et al., 2007). Thus, it is possible to use any of the damage mechanics formulations referred by the different authors that have studied the delamination phenomenon to simulate the matrix performance and, consequently, the delamination onset and propagation. The formulation used in this chapter to obtain the mechanical performance of matrix material and, at the same time, the delamination phenomenon is the damage formulation developed by Oliver et al. (1990). This formulation is an evolution of the isotropic damage law originally defined by Kachanov (1986), and is explained in detail in next section.

The validity of the methodology proposed to solve delamination problems has been proved with the simulation of the ENF test (Martínez et al., 2007, 2008) and with the simulation of a ply drop-off test (Martínez et al., 2007). This last case also shows how the procedure proposed can be implemented in a lamination formulation. Both examples are included in this chapter, in sections 3.4 and 3.5, respectively.

As a final remark to the procedure proposed, it has to be said that the simulation of the delamination phenomenon lays in matrix material because the implementation made of the serial/parallel mixing theory limits the number of component materials of a laminate layer to two: fiber and matrix. However, the serial/parallel mixing theory can be extended to more than two components. In doing so, a third material with the mechanical characteristics of the layer interface can be defined. Delamination will take place when the interface material reaches its threshold strength. Although this procedure is less expensive than introducing new elements in the simulation, its computational cost is considered to be larger than the benefits obtained, as matrix material is capable to assume the delamination role providing accurate results.

3.3 Damage formulation

3.3.1 Damage constitutive law

The material degradation in a continuum solid, due to a fracture process, can be simulated with a damage formulation. This formulation takes into account the reduction of the effective area of the material by a reduction of its stiffness properties. The procedure proposed to simulate the delamination process uses a damage constitutive law to predict the matrix mechanical performance. This formulation is exposed in this section. The damage model considered is the isotropic continuum damage formulation developed by Oliver et al. (1990) and described in Oller (2001). This formulation is based on the theory of continuum damage developed by Kachanov (1986).

Isotropic damage model

A damage process can be simulated, in the context of continuum mechanics, by the introduction of a internal variable, \mathbf{M} , that represents the degree of damage existing in the material. This variable transforms the real stress tensor, $\boldsymbol{\sigma}$, found in the damaged space into an effective stress tensor $\boldsymbol{\sigma}_0$, found in an equivalent undamaged space. This is:

$$\boldsymbol{\sigma} = \mathbf{M} : \boldsymbol{\sigma}_0 \quad (3.14)$$

In the case of an isotropic damage, all directions of the stress tensor have the same degradation. Therefore, the damage internal variable can be transformed into an scalar parameter, and the relation between the real and the effective stresses can be written as:

$$\boldsymbol{\sigma} = [(1 - d)\mathbf{I}] : \boldsymbol{\sigma}_0 = (1 - d)\boldsymbol{\sigma}_0 \quad (3.15)$$

Being d the damage scalar internal variable. The value of this variable is ranged between 0 and 1. When the material is not damaged, the value of the damage variable is 0. In this case the real stresses in the material are equal to the effective stresses. When the material is completely damaged, $d = 1$. In this case the real stresses in the material become zero.

The relation between the real and the effective stresses is represented in figure 3.9. This figure shows that the deformation associated to a damaged state is equivalent to the deformation

associated to an equivalent undamaged state, which stress is the effective stress σ_0 (Oller, 2001). This situation corresponds to the strain equivalence assumption, that is when the strain is the same in the damaged and effective configurations. A different set of equations would be obtained if one assumes energy equivalence between both configurations.

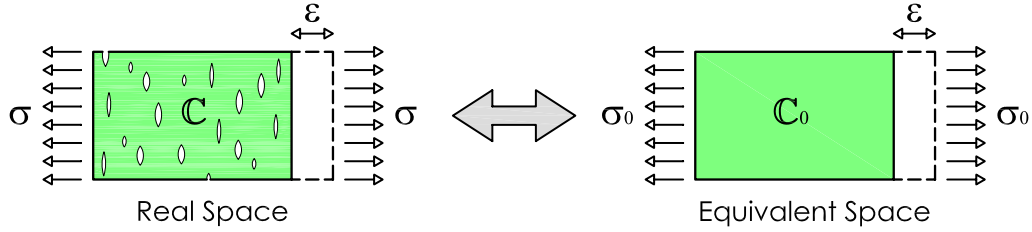


Figure 3.9: Real damaged space and equivalent space (Oller, 2001)

With the strain equivalence assumption, the effective stress can be obtained from the strains in the material using the effective stiffness tensor of the material, that corresponds to the elastic undamaged tensor:

$$\sigma_0 = \mathbb{C}_0 : \varepsilon \quad (3.16)$$

The real stress tensor is obtained coupling equations (3.15) and (3.16):

$$\sigma = (1 - d)\sigma_0 = \underbrace{(1 - d)\mathbb{C}_0}_{\mathbb{C}} : \varepsilon \quad (3.17)$$

The model defined by equation 3.15 is fully determined if the value of the damage parameter, d , can be evaluated at every time of the deformation process. Therefore, it is required to define a damage threshold, or damage criterion, that will determine the stress state for which the damage parameter (d) becomes different of zero; and a law providing the evolution of this parameter along the loading process.

Damage constitutive law

The damage constitutive law defines the evolution of the stress tensor in the material. This law has to be able to describe when the damage process begins to take place in the material. This is, the stress state in which the material elastic behavior is lost and degradation starts. And it has to be able to define which is the stress evolution once the stress threshold has been reached. The damage constitutive law is defined with the stress tensor and the damage internal variable. Its expression is:

$$\mathbb{F}(\sigma_0, \mathbf{q}) = f(\sigma_0) - c(d) \leq 0 \quad \text{with} \quad \mathbf{q} \equiv \{d\} \quad (3.18)$$

Where $c(d)$ is a function defining the damage threshold and $f(\sigma_0)$ is a scalar function, dependent on the stress tensor, that provides the equivalent stress value. This function is used to

compare different stress states. Damage in the material starts the first time that the equivalent stress $f(\boldsymbol{\sigma}_0)$ exceeds the initial value of the damage threshold, $c(d) = c^{\max}$, defined as a material property (Oliver et al., 1990).

Usually, instead of working with equation (3.18), the damage criterion is converted to an equivalent one by using a scalar function G which is positive and with its derivative positive, monotonously increasing and invertible:

$$\mathbb{F}^*(\boldsymbol{\sigma}_0, d) = G[f(\boldsymbol{\sigma}_0)] - G[c(d)] \leq 0 \quad (3.19)$$

In order to have fully determined the damage constitutive law, it is necessary to know the evolution of the damage threshold $c(d)$ and the damage internal variable d . This is described in the following.

Evolution of the damage variable. Softening behaviour

The mechanical problems that are dependent of internal variables require the definition of the evolution law of these variables. In the damage problem, the law that defines the evolution of the damage variable is (Oller, 2001):

$$\dot{d} = \dot{\mu} \frac{\partial \mathbb{F}^*(\boldsymbol{\sigma}_0, d)}{f(\boldsymbol{\sigma}_0)} \equiv \dot{\mu} \frac{\partial G[f(\boldsymbol{\sigma}_0)]}{f(\boldsymbol{\sigma}_0)} \quad (3.20)$$

being μ a non-negative scalar called damage consistency parameter. This parameter is used to define the load, unload and reload Kuhn–Tucker conditions:

$$\dot{\mu} \geq 0 ; \quad \mathbb{F}^*(\boldsymbol{\sigma}_0, d) \leq 0 ; \quad \dot{\mu} \cdot \mathbb{F}^*(\boldsymbol{\sigma}_0, d) = 0 \quad (3.21)$$

The Kuhn–Tucker condition states that if the damage criterion is lower than zero, then $\dot{\mu} = 0$ and the damage parameter remains constant, this situation is found when the damage threshold has not been reached or in unloading conditions. On the other hand, when the stress tensor has reached the damage threshold, $\mathbb{F}^* = 0$, and then $\dot{\mu} \geq 0$. In the case of having $\dot{\mu} = 0$, stresses and damage in the material must be constant and when $\dot{\mu} > 0$, according to equation 3.20, the damage parameter increases, which means that the material is under loading conditions. These situations are represented in figure 3.10, in which is represented the stress-strain evolution of a material defined with a damage model.

From the definition of the variation of the damage parameter (equation 3.20) and making use of the Kuhn–Tucker relations, it can be proved (Oller, 2001, 2002) that the evolution of the internal variables may be explicitly integrated to obtain:

$$\begin{aligned} c(d) &= \max \{c^{\max}, \max \{f(\boldsymbol{\sigma}_0)\}\} \\ d &= G[f(\boldsymbol{\sigma}_0)] \end{aligned} \quad (3.22)$$

Therefore, the evolution of the damage parameter depends on the definition of the function G . Oller (2001) propose two different softening models, defined by two different G functions. Both of them are described in the following:

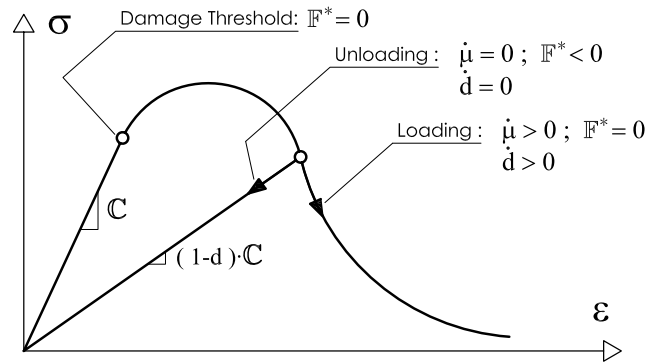


Figure 3.10: Uniaxial stress-strain curve for a damage model (Oliver et al., 1990)

Linear softening: The evolution of the damage parameter, in case of considering a linear softening, is defined by the following expression of the G function:

$$d = G[f(\sigma_0)] = \frac{1 - \frac{c^{\max}}{f(\sigma_0)}}{1 + A} \quad (3.23)$$

Exponential softening: This function was first proposed by Oliver et al. (1990), to obtain an exponential softening in the material. The expression of the damage parameter is:

$$d = G[f(\sigma_0)] = 1 - \frac{c^{\max}}{f(\sigma_0)} e^{-A \left(1 - \frac{f(\sigma_0)}{c^{\max}}\right)} \quad (3.24)$$

The softening functions defined in equations 3.23 and 3.24 depend on the parameter A . Parameter A is obtained in function of the fracture energy of the material. The evolution of the material stresses obtained with the linear and exponential softening laws is shown in figure 3.11. Figure 3.11a shows the stress-strain relation obtained for a material with a linear softening; and figure 3.11b shows the evolution of the same material when an exponential softening is applied to it.

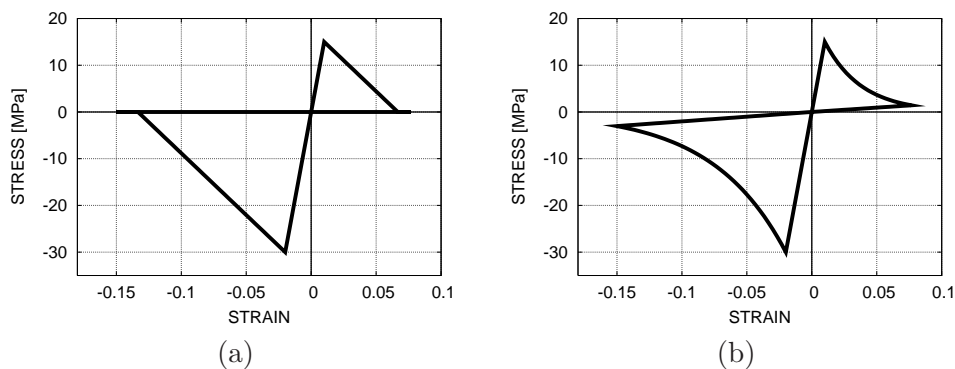


Figure 3.11: Stress-strain graph obtained with the damage formulation. (a) Linear softening (b) Exponential softening

Figure 3.11 shows a different value of the maximum stress that can be reached by the material if the stresses are found in the tension or compression sections of the plot. Damage starts for a compression stress of 30 MPa and it starts for a tensile stress of 15 MPa. This difference is achieved with the function used to obtain the equivalent stress value, $f(\boldsymbol{\sigma}_0)$. This function is defined in the following.

Equivalent stress

The equivalent stress is provided by a function that transforms the stress tensor of the material into a scalar value that is compared with the damage threshold, $c(d)$. The damage constitutive law described in equation 3.18 is equivalent to those used in plasticity (Malvern, 1968; Kachanov, 1971; Lubliner, 1990; Oller, 2002). Therefore, any criterion already defined for plasticity can be used in the damage formulation described. Some of the most known damage yield criteria defined in literature are: Rankine, Tresca, Von-Mises, Mohr-Coulomb and Drucker-Prager. All these criteria are fully described in the previously cited references.

Each one of these criteria combine the different components of the stress tensor to obtain the equivalent stress, which is compared with a threshold value. The election of one yield criterion or another depends on the material that is simulated, as each criterion provides failure for a different combination of the stresses found in each direction of the material. In example, Von-Mises criterion is commonly used for metallic materials. This compares the maximum octahedral shear stress with a threshold value:

$$\mathbb{F}(\boldsymbol{\sigma}, \tau_{oct}^{\max}) = \sqrt{J_2} - \tau_{oct}^{\max} \quad (3.25)$$

Being J_2 the second invariant of the stress tensor. If this criterion wants to be used in the damage formulation described,

$$\begin{aligned} f(\boldsymbol{\sigma}_0) &= \sqrt{J_2(\boldsymbol{\sigma}_0)} \\ c^{\max} &= \tau_{oct}^{\max} \end{aligned} \quad (3.26)$$

The same procedure used to adapt the Von-Mises yield law can be used with any other of the mentioned criteria. However, the criterion that is used in the present work is the one defined by Oliver et al. (1990) which is based in the norm of the principal stresses and provides a different degradation path for tension and compression cases (as has been shown in figure 3.11). This model defines the equivalent stress value with the following function:

$$f(\boldsymbol{\sigma}_0) = \varrho \cdot \|\boldsymbol{\sigma}_I\| \quad (3.27)$$

being $\boldsymbol{\sigma}_I$ the principal stress tensor and ϱ a function that weighs the amount of tension and compression efforts found in the stress tensor. This function is defined as:

$$\varrho = r_0 N + (1 - r_0) \quad (3.28)$$

Where

$$N = c_c^{\max}/c_t^{\max} \quad (3.29)$$

is the material ratio between the compression and tension threshold values. This parameter is a material property. And r_0 is a scalar function that defines the relation between the compression and the tension state of the stress tensor. This last function is defined with the following expression,

$$r_0 = \frac{\sum_{I=1}^3 \langle \sigma_I \rangle}{\sum_{I=1}^3 |\sigma_I|} \quad (3.30)$$

with $\langle x \rangle = 0.5 [x + |x|]$ the McAully function.

The compression-tension weight function has been defined to obtain a damage surface to be compared with a compression stress. Hence, when using this damage criterion, the value of $c(d)$ must be referred to compression stresses. Also, the value c^{\max} that appears in the softening functions 3.23 and 3.24, must be the maximum compression that can be achieved in the material.

This yield criterion provides a different failure strength for tensile and compression forces. The relation between both strengths is defined by parameter N . The material performance obtained with this criterion has been already shown in figure 3.11. This figure shows the stress-strain relation obtained for a material in which $N = 2$.

Parameter A

The parameter A that appears in equations (3.23) and (3.24), is obtained from the dissipation equation of the material, considering an uniaxial process under a monotonous increasing load. The total energy that can be dissipated by the system, by unit volume, is:

$$g_c = \int_0^\infty \Xi dt = \int_0^\infty \Psi_0 \dot{d} dt \quad (3.31)$$

Being Ψ_0 the Helmotz free energy of the system, which expression is (Oller, 2002),

$$\Psi_0 = \frac{1}{2} \varepsilon C_0 \varepsilon = \frac{1}{2} \frac{(c^{\max})^2}{C_0} \quad (3.32)$$

with C_0 the uniaxial stiffness of the material.

The integral defined in equation 3.31 is evaluated for the two damage laws that will be used in present work. The solution of this integral provides the expression of parameter A , which depends on the total energy that can be dissipated by the material by unit volume. In case of using an linear softening law, the integral defined in equation 3.31 has to be evaluated using the expression of the Helmotz free energy defined by equation 3.32 and the linear damage law defined by equation 3.23. On the other hand, the expression of A for an exponential softening is obtained with the damage law defined by equation 3.24. The evaluation of the integral defined in 3.31 for this two cases provides the following expressions for parameter A :

$$\begin{aligned}
\text{Linear softening :} \quad & A = -\frac{1}{2} \frac{(c^{\max})^2}{g_c C_0} \\
\text{Exponential softening :} \quad & A = +\frac{1}{\frac{g_c C_0}{(c^{\max})^2} - \frac{1}{2}}
\end{aligned} \tag{3.33}$$

where C_0 is the uniaxial stiffness of the material and g_c corresponds to the maximum energy per unit volume that can dissipate the material, in a compression case.

Classical fracture mechanics defines the fracture energy of a material as the energy that has to be dissipated to open a fracture in an unitary area of the material. This energy is defined as:

$$G_f = \frac{W_f}{A_f} \tag{3.34}$$

where W_f is the energy dissipated by the fracture at the end of the process and A_f is the area of the surface fractured. When coupling the fracture mechanics theory with the continuum mechanics, the relation defined to relate W_f with g_f is:

$$W_f = G_f \cdot A_f \equiv \int_{V_f} g_f dV \tag{3.35}$$

And the relation between the fracture energy defined as a material property, G_f , and the maximum energy per unit volume required by the damage formulation, g_f , becomes:

$$g_f = \frac{W_f}{V_f} = \frac{W_f}{A_f l_f} = \frac{G_f}{l_f} \tag{3.36}$$

Thus, the fracture energy per unit volume is obtained as the fracture energy of the material divided by the fracture length. This fracture length corresponds to the length, perpendicular to the fracture area. This length tends to be infinitesimal.

When damage mechanics is applied to a finite element code, in which a continuum formulation is transformed into a discrete formulation, the fracture length has to be transformed also from a continuum to a discrete space. This means that the fracture length cannot be infinitesimal but has to have a finite number. In a finite element code, the value defined to this length corresponds to the smallest value in which the structure is discretized: the length represented by a gauss point. Figure 3.12 shows a representation of this fracture length.

The use of a fracture length dependent on mesh size provides a different value of parameter A for each mesh and, therefore, a different stress evolution depending on the mesh size. Although the first impression can be that the problem becomes mesh dependent, this is not the case. There is a different stress evolution because larger elements have a lower fracture energy per unit volume, as their fracture length is larger. However, the global performance of the structure provided by the simulation is the same, independently of the mesh size used.

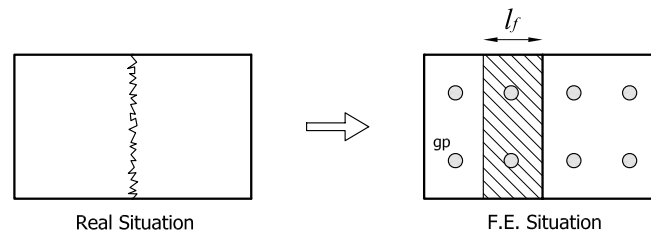


Figure 3.12: Fracture in a real body and in its finite element discretization. Fracture length description

This is shown in figure 3.13, in which the stress-strain performance (fig. 3.13b) is plotted for a tensile simulation made with two different mesh sizes (fig. 3.13c). Figure 3.13a shows that, although the stress path obtained with each mesh is different, the global performance of the structure is the same for both meshes. The global performance of the structure is represented with a capacity curve (force-displacement graph).

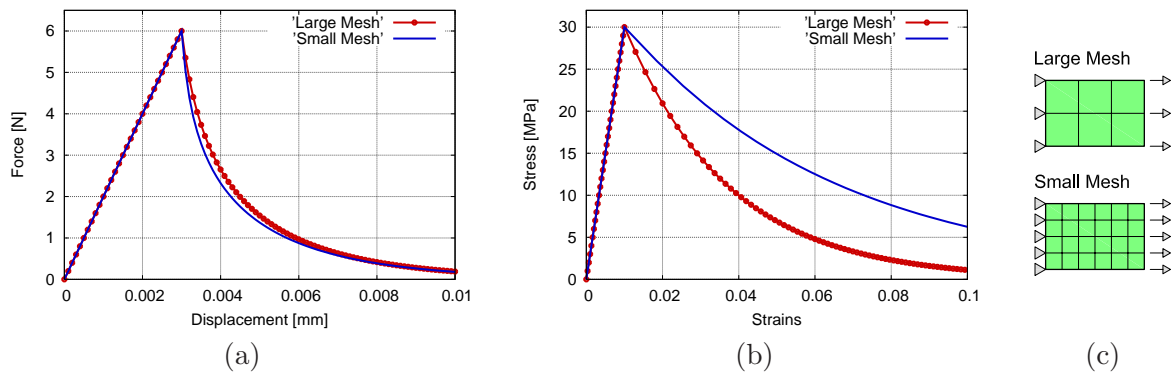


Figure 3.13: Damage simulation performed with two different mesh sizes: (a) Force-displacement plot, (b) stress-strain plot and (c) mesh discretization.

3.3.2 Friction damage constitutive law

As has been described, the damage parameter d provides the grade of deterioration of the material. When $d = 1$ the material is considered to be fully deteriorated, being unable to provide any strength to the structure. Stresses in the material are null. In a finite element simulation, this situation implies that the elements found around the damaged element can move freely, without any structural restriction. This mechanical performance is correct if the fractured surface is perpendicular to the forces applied to the structure, which corresponds to a fracture mode I (figure 3.14a). However, if the fracture is in mode II or mode III (figure 3.14b), this statement is not fully correct, as the fracture surface can still develop some strength through effects such as friction.

Despite all existing research dealing with the delamination problem, few of this research assess the effects of friction in the delamination phenomenon. A first approach to this problem is performed by Stringfellow and Freund (1993) in which the effect of friction is evaluated in the delamination of a thin from a substrate. In their approach, the authors develop an analytical model that is based on the dislocations found crystal materials, which are represented by the

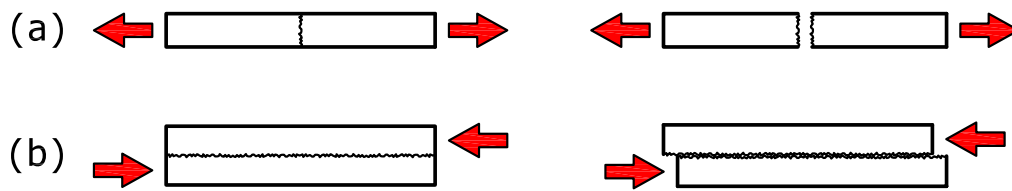


Figure 3.14: Structures that can be modeled with a damage constitutive law and which behavior when they are completely damaged is different

Burger's vector (Dieter, 1988). The model is implemented in a finite element code and is used to prove that friction is one of the main responsible effects determining the toughness strength of mode II fractures.

Regarding the effect of friction in delamination of composite laminates, Davidson and Sun (2005) and Sun and Davidson (2006) have studied the role of friction, among other parameters such as geometry and fixture compliance, in the delamination toughness obtained in mode II delamination tests. These authors add a new term to the energy balance used to obtain the energy release rate predicted by the mode II delamination tests,

$$G = \frac{1}{B} \left[\frac{\partial(W_e - U)}{\partial a} - \frac{\partial W_f}{\partial a} \right] \quad (3.37)$$

with W_e the work done by the external forces, U the strain energy, W_f the work of the frictional forces, B the sample width and a the length propagation of the fracture. The variation of the work done by frictional forces is obtained as the product of the tangential force by the tangential displacement. The authors include the effect of friction, among others, in the finite element simulation of three- and four-node bending tests in order to determine the reliability of the results obtained with each one of these tests.

A similar study has been performed by Fan et al. (2007), also with the objective to characterize the role of friction in mode II delamination tests. In this case, a non-dimensional parameter is defined to characterize friction:

$$e = \frac{G_0 - G_f}{G_0} = \frac{F_{C0}^2 - F_C^2}{F_{C0}^2} \quad (3.38)$$

with G_0 and F_{C0} the energy release rate and the force at the crack tip, respectively, obtained in absence of frictional effects and G_f and F_C are the energy release rate and the force at the crack tip when frictional effects are considered. The force containing frictional effects is obtained as:

$$F_C = F_{C0} - \int \mu p(x) dA \quad (3.39)$$

being μ the friction coefficient and $p(x)$ the normal force to the fracture surface. The authors propose different analytical expressions for obtaining F_{C0} and F_C for the different mode II delamination tests.

The objective of all the studies presented above is to assess the effects of friction in delamination toughness. However, no study has been found in which frictional effects are considered to take into account the residual strength provided by the fractured surface in mode II delamination. Hereafter is proposed a first approach to take into account this phenomenon, based on the addition of an empirical parameter to the damage formulation previously presented.

Addition of friction to the damage formulation

In order to take into account the residual strength provided by the fractured surface in mode II delamination, a friction damage parameter, d^{fric} , has been introduced into the damage formulation. This parameter defines the residual stress that remains in the material due to friction effects. The definition of this residual stress is equivalent to define a maximum value that can be reached by the damage parameter d . Therefore, the relation between the real damaged stress tensor σ and the effective stress tensor σ_0 becomes:

$$\sigma = (1 - d^*)\sigma_0 \quad \text{with} \quad d^* = \min \{d, d^{fric}\} \quad (3.40)$$

The frictional damage parameter d^{fric} is obtained from the value of the residual stress that will be found in the material:

$$d^{fric} = 1 - \frac{\sigma^{RS}}{f(\sigma_0)} \quad (3.41)$$

The residual stress σ^{RS} is defined as a percentage of the the stress threshold σ^0 . This percentage is a material property that has to be defined from empirical analysis.

Figure 3.15 shows an example of the material behavior that is obtained, in an unidirectional case, when a residual stress is defined for the material. The material considered has a threshold stress of 250 MPa and a residual stress of a 10% of the threshold stress (25 MPa). This figure shows the stress-strain graphs obtained for the same material when the friction parameter is applied to it and when it is not applied.

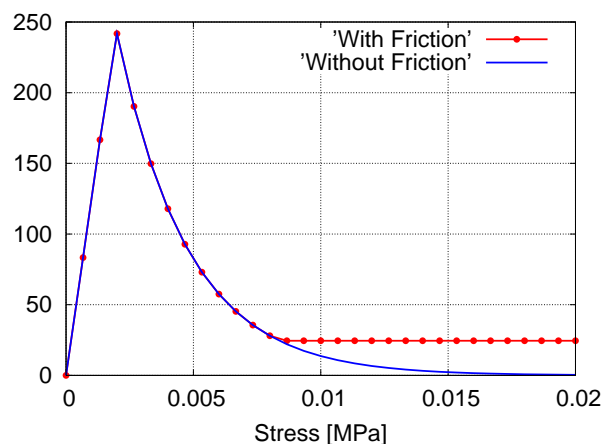


Figure 3.15: Comparison of the material performance when the the friction parameter is applied to it and when it is not

It is important to notice that with the definition made of the friction parameter the constitutive damage equation continues being isotropic. Consequently, the same level of damage is applied in all stress directions. This implies that in structural simulations like the one depicted in figure 3.14b, the formulation considers the friction effect but also a contact effect, as the remaining stress of the fractured elements in vertical direction (according to the figure) avoids the interpenetration of the top piece of the structure into the bottom one.

3.4 Numerical Example: End Notch Flexure (ENF) test

To prove the ability of the serial/parallel mixing theory, together with a damage constitutive law, to simulate delamination processes this section compares the numerical results obtained from the simulation of the *End Notch Flexure* (ENF) test with experimental results. This test is defined by the *European Structural Integrity Society* (ESIS) and the Japanese standard JIS (K-7086) and is used to obtain the toughness for crack propagation in mode II, corresponding to a shear crack, in unidirectional fibre reinforced polymer composites (FRPC).

The experimental results have been obtained from the tests made by CIMEP (*Centre per a la Innovació en Materials, Estructures i Processos*) and the University of Girona for the project GRINCOMP (ref. MAT2003-09768-C03) (Corbella et al., 2004).

3.4.1 Experimental test description

The End Notch Flexure test is based in the flexure of a beam with an initial crack in one of its ends. The test has been applied to a composite made of carbon fibres with an epoxy polymeric matrix. Fibres are oriented in the longitudinal direction of the beam and the initial crack is created introducing an insert in the laminate during its fabrication. The width of the gap generated by this insert must be smaller than $50 \mu\text{m}$. The span of the beam is 100 mm and it is loaded with a concentrated load at its mid-span. The test is made with a displacement controlled mechanism. Three different series, GRIN006, GRIN015 and GRIN024, each one containing five different samples, were tested during the experimental campaign. To perform the numerical simulation, the first sample of series GRIN006 has been considered (beam 3M101, according to the notation used in the tests). The dimensions of this sample, as well as the dimensions considered for the numerical simulation, are shown in figure 3.16.

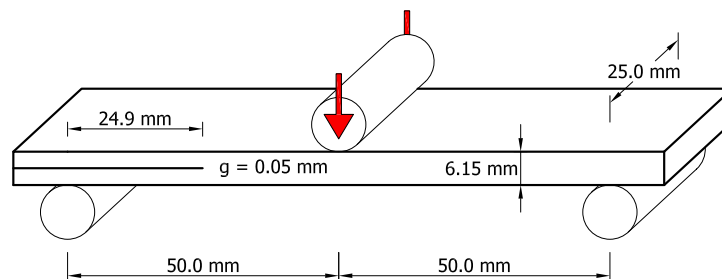


Figure 3.16: Sample geometry used for the ENF test

The experimental test applies a vertical displacement to the beam, as shown in figure 3.16, until the initial crack starts its propagation. The imposed displacement is applied until the

crack progression stops and the beam recovers its linear behavior. At this point, the sample is unloaded. The main results obtained from this test are two: The force–displacement graph, which shows the structural performance of the composite beam, and the final length of the initial crack. These two results are the ones that will be compared with the numerical model developed.

The exact properties of the composite material used in the experimental simulations were unknown when the experimental tests were performed (Corbella et al., 2004). However, the composite is known to be made of carbon fibres and an epoxy polymeric matrix from Hexcel composites. For the numerical simulation, the mechanical values considered to define the composite are the ones described in table 3.1, obtained from Hexcel Product data description. The fibre (AS4) and matrix considered are the ones found in HexPly 8552 UD carbon prepegs.

Matrix Properties		Fibre Properties	
Tensile Strength	120.66 MPa	Tensile Strength	4278 MPa
Tensile Modulus	4.67 GPa	Tensile Modulus	228 GPa
Poisson Modulus	0.30	Poisson Modulus	0.0
Mode I Fracture Energy	0.68 kJ / m ²	Volume Content	57.4 %
Volume Content	42.6 %		

Table 3.1: Composite components mechanical properties

3.4.2 Numerical model description

Two different numerical models have been developed to simulate the End Notch Flexure Test. One using a plain stress two dimensional formulation and a second one using a three dimensional formulation. The 2D model has been defined with 627 linear quadrilateral elements while the 3D model has 5016 linear brick elements. The mesh defined for the three dimensional model is shown in figure 3.17.

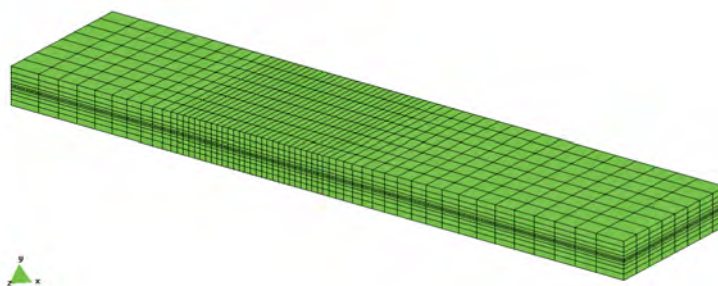


Figure 3.17: Three dimensional model developed. Mesh description

Two different materials have been defined in the numerical simulation. One corresponding to the composite material and another one corresponding to the insert material. The composite material is defined using the properties of the epoxy matrix and the carbon fibres shown in table 3.1. Fibre material is defined as an elastic material. Matrix material is characterized by the damage constitutive law described in section 3.3.

The damage model used requires knowing the relation between the compression strength and the tension strength of the material in order to obtain the correct damage evolution. As

these parameters are unknown, the simulation is performed considering that both strengths are identical ($N = 1$, equation 3.29). The fracture energy defined corresponds to the mode II fracture energy obtained from the experimental tests. The value of this energy, for the 3M101 beam, is: $G_{II} = 1.02 \text{ kJ/m}^2$.

The definition of the insert material properties has been done taking into account its structural performance. The main effect of this material in the beam is allowing the sliding of the section found above the insert along the section found below it. To do so, a material with a shear modulus nearly zero has been defined (it has not been defined as strictly zero to avoid numerical instabilities during the simulation). On the other hand, the longitudinal and transversal elastic modulus have been defined with a high value to avoid the penetration of the section above the insert into the section below it. This material has been defined as an elastic material. Its main mechanical properties are described in table 3.2

Insert Material Properties	
Tensile Modulus	1000 GPa
Shear Modulus	10^{-9} GPa
Poisson Modulus	0.0
Volume Content	100 %

Table 3.2: Insert material mechanical properties

3.4.3 Comparison between the numerical and the experimental results

The numerical and the experimental results are compared with the force–displacement graph obtained for both cases. The displacement represented corresponds to the vertical deflection of the point where the load is applied. This graph is shown in figure 3.18, in which the results for the 2D and 3D numerical simulations and the experimental test are represented.

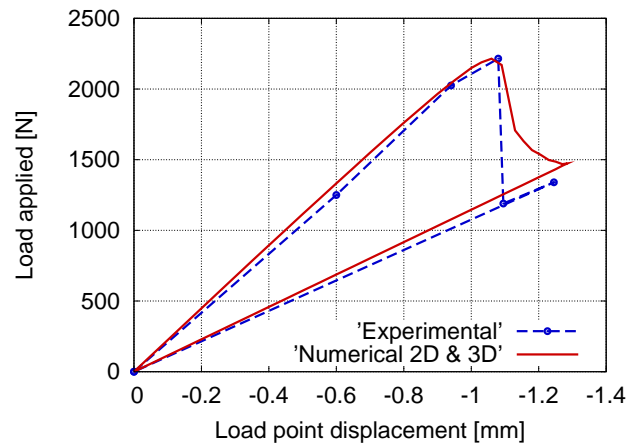


Figure 3.18: Force–displacement graph obtained for the different models.

Figure 3.18 shows that the two dimensional simulation provides exactly the same results as the three dimensional one, thus, for these kind of problems, 2D simulations are preferable, as the computer cost is much lower. However, the most important result shown in figure 3.18 is the agreement between the numerical and the experimental results. The beam initial elastic stiffness obtained in the numerical simulation is nearly the same that is obtained from the

experimental test. And this agreement between results is even better when comparing the beam maximum load capacity or failure point. The only result that differs in the numerical simulation is the final beam stiffness, when the crack has reached its maximum length. In this case, the numerical beam is a 6 % stiffer than the experimental one (the stiffness obtained in each case is, respectively, 1146 N/mm and 1076 N/mm).

The other result to be compared is the final crack length. The experimental values obtained for this final crack length for the sample being compared (3M101) is of 50.34mm, and the mean value of the crack length for all the GRIN006 serie is around 49.0mm; this is, a bit less than half the beam.

In the numerical simulation, the crack points correspond to those in which the damage parameter, in matrix material, is equal to one. These points have a matrix stiffness equal to zero. This implies that the composite serial stiffness is also zero, due to the iso-stress condition imposed by the serial/parallel mixing theory. The points in which matrix is completely damaged cannot develop any shear strength; hence, the final crack length can be obtained by finding the point, closer to the beam mid-span, with a value of the damage parameter, in matrix material, equal to one. Figure 3.19 shows the damage parameter in matrix in the load step in which the beam reaches its maximum deflection. This figure shows that the crack length obtained with the numerical simulation nearly reaches the mid-span section, agreeing with the results reported in the experimental test.

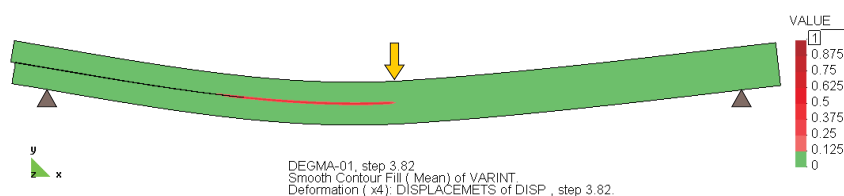


Figure 3.19: Damage in matrix material when the maximum deflection has been reached

The exact value of the damage parameter is shown, for the points represented in figure 3.20a, in figure 3.20b. In this figure can be seen that point 13 (corresponding to mid-span) reaches a damage value of 0.6, while the value of point 12 is approximately 0.98. Considering this last value close enough to one and thus, the section completely broken, the numerical crack length obtained is of 48mm. The point found at 49mm of the support has a damage value in matrix material of 0.89, which is also close enough to one to consider that the numerical results are exactly the same as the experimental ones.

In this last figure is also represented the force-displacement graph (with the force normalized for a value of 2500N). It can be seen that the main crack is developed just after the beam reaches its maximum strength capacity. The lost of stiffness suffered by the beam due to the crack propagation is stabilized as the crack reaches the mid-span section because the crack cannot pass through it. The sign of the shear stresses is reversed at mid-span and, just in it, shear stresses are zero; so, there are no efforts to damage the mid-span section.

3.4.4 Detailed study of the numerical results

According to the force-displacement graph obtained for the beam (figure 3.18), the results obtained with the three dimensional simulation match exactly with the results obtained with

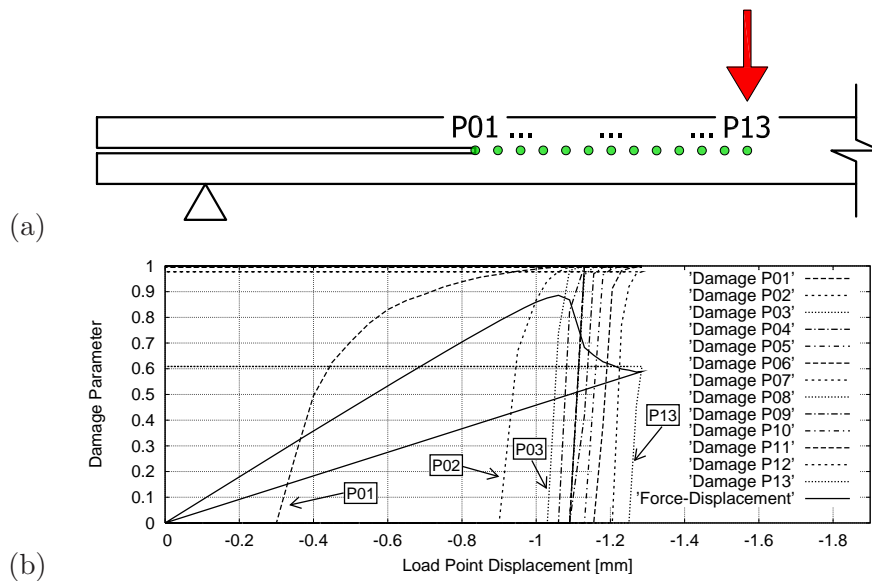


Figure 3.20: Evolution of the damage parameter in the beam

the two dimensional simulation. Thus, for the sake of simplicity, the detailed study of the numerical results is preformed using only the two dimensional simulation.

The first thing to study of the results obtained from the numerical simulations is if the supposition made to define the insert material is accomplished, this is: that it allows a free sliding between the section above and below it, by reducing to nearly zero its shear stiffness. To verify that this is the behaviour found in the insert material, the horizontal gap that appears between the upper and lower nodes (nodes A and B respectively in figure 3.21a) has been represented in figure 3.21b. This figure shows a linear increment of the gap between both nodes for the first load steps. This gap increment proves the validity of the material defined, as it shows that the section above the insert of the beam slides over the section below it. This gap increment remains linear until the displacement of the load point is a bit larger than 1.0mm, at this point the gap increases exponentially doubling its size. This point corresponds to the load for which the crack propagation begins and it ends when the crack has reached the section at mid-span. Afterwards, when unloading the beam, the horizontal gap size recovers the linear behaviour found before the crack propagation.

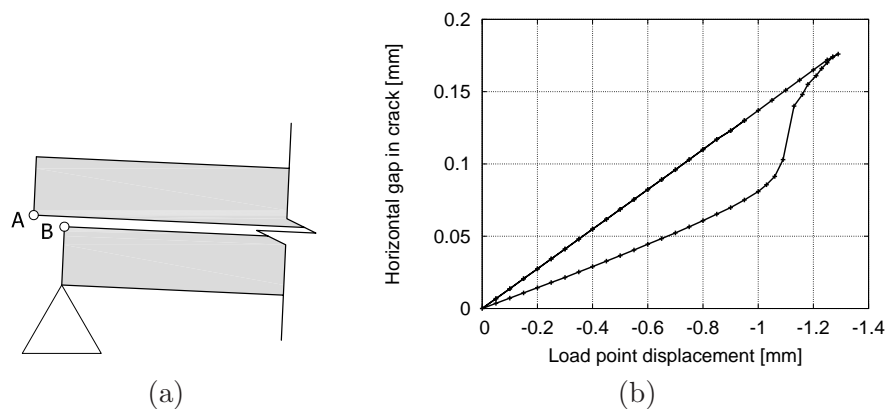


Figure 3.21: Evolution of the horizontal gap in the beam along the loading-unloading process

A better comprehension of the process that takes place in the beam can be obtained studying the evolution of the horizontal gap along the beam longitudinal axis, and the evolution of the shear stresses in the same region. Both results are displayed in figure 3.22 for different load steps. Each load step represented corresponds to a displacement of the load point of the same magnitude (i.e. step 1.06 corresponds to a load point displacement of 1.06mm). Figure 3.22 show that for the load step 0.60, when the crack propagation has not begin, the only gap found is in the sections where the insert is applied and that all shear stresses are concentrated at the first section without insert (point P01 of figure 3.20a). However, when the crack begins its propagation, the gap initiation, as well as the shear stresses peak, move towards the beam mid-span. The final step represented, step 1.28, corresponds to the load step in which the crack has reached the mid-span section. Figure 3.22 also shows that the behaviour of the composite, when matrix is completely damaged, is the same found in the insert material. So, as damage in matrix increases and its stiffness is reduced, the composite cannot develop shear stresses and the section above the mid-width plane slides freely over the section below.

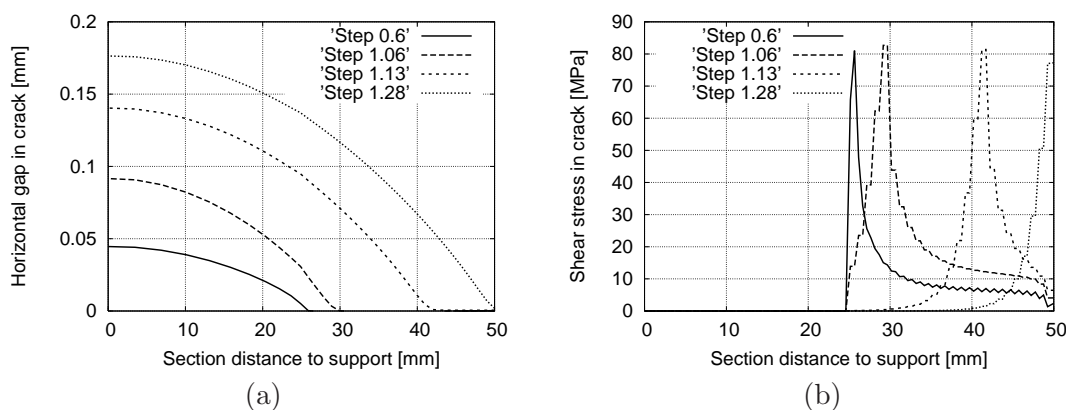


Figure 3.22: Evolution of the horizontal gap (a) and the shear stresses (b) along the beam mid-width for different load steps

The composite performance is obtained using the serial/parallel mixing theory, which imposes an iso-strain condition in the fibre direction and an iso-stress condition in the remaining directions. As the shear stresses are developed in the direction in which the iso-stress condition is applied, when matrix is completely damaged and cannot develop more shear stresses, the same happens with the rest of composite components (fibre, in this case). This is the reason because the shear stress of the composite, shown in figure 3.22b, is zero although fibre is an elastic material and still has the capacity to develop stresses.

The effect of the crack propagation on the beam can also be seen by studying the longitudinal stresses in the composite (figure 3.23). The contour map of the longitudinal stresses shown in figure 3.23a corresponds to step 0.6, when crack propagation has not started. This figure shows that the distribution of longitudinal stresses in the sections with the insert corresponds to the case of having two beams, one disposed over the other, while the complete section (i.e. at mid-span) behave like just one beam: the top section of the beam is in compression while the bottom section is in tension. On the other hand, when the crack has reached the mid-span section (figure 3.23b), the two beams behavior is extended to all the cracked sections, as it can be seen along the whole left side of the beam.

Finally, a last numerical test has been performed to validate the fracture length parameter, required by the damage formulation used to simulate matrix material. According to what has

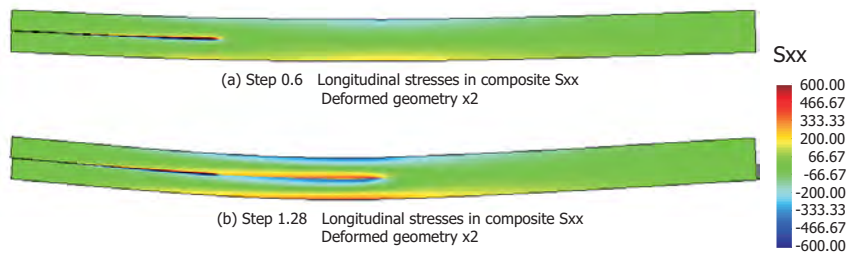


Figure 3.23: Longitudinal stresses in the composite for two different load steps

been explained in section 3.3, the fracture length represents the distance, perpendicular to the fracture surface, in which the fracture will be developed in the finite element formulation. The mesh used in the finite element simulation has a single element beside the gap opened by the insert, as it is shown in figure 3.24. This figure also shows the gauss points found in the finite element.

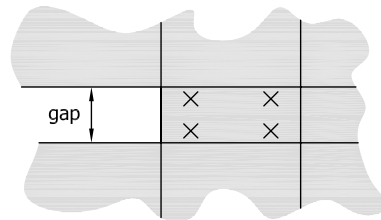


Figure 3.24: Finite elements and gauss points found around the gap opened by the insert in the beam

With the gauss point distribution shown in figure 3.24, the fracture length to be defined is half the gap size, as this is the gauss point length perpendicular to the fracture plane. Three different simulations have been performed with different gap sizes and fracture lengths. Model *Delam-2D-g20* has a gap size of $20\mu\text{m}$ and a fracture length of $10\mu\text{m}$, model *Delam-2D-g50* has a gap size of $50\mu\text{m}$ and a fracture length of $25\mu\text{m}$ and, finally, model *Delam-2D-g80* has a gap size of $80\mu\text{m}$ and a fracture length of $40\mu\text{m}$. The force-displacement graph obtained for these models is displayed in figure 3.25a, and a detail of this same graph in 3.25b. This figure shows that the results are practically identical in all cases and that only few differences are found in the crack propagation zone. This agreement among the different models allows considering the formulation defined, and the fracture length considered, correct.

3.5 Numerical Example: Ply drop-off test

Numerical simulation of large structures made of laminated composites are usually performed using a lamination formulation, as this formulation provides an accurate approximation of the structure mechanical performance, taking into account the through-the-thickness configuration of the laminate (layer orientation and stacking sequence), with a reasonable computational effort. Because delamination is one of the main failure causes of this structural types, some numerical procedure is required to take into account the delamination phenomenon when large scale simulations of composite laminate structures are performed.

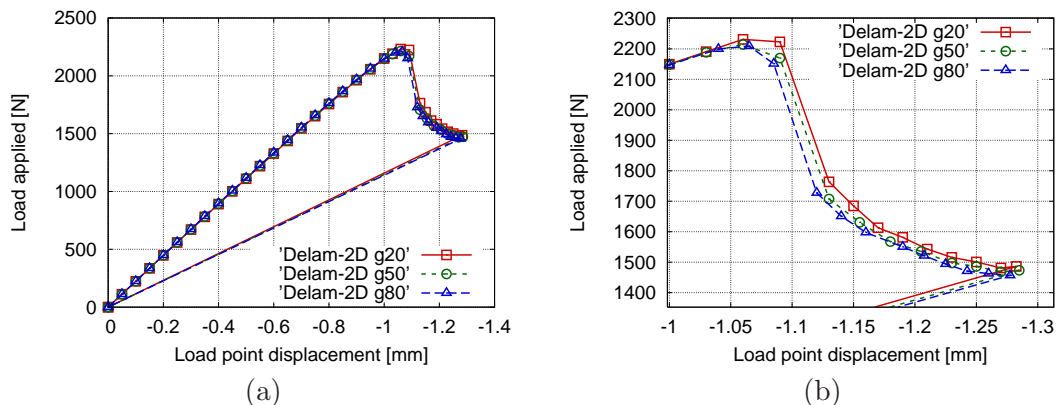


Figure 3.25: Force–displacement graph obtained for three different gap size models. General view and detail of the crack propagation zone

The purpose of present simulation is to describe a new procedure to take into account the delamination failure in large scale simulations of laminated composites. This procedure is described in the following section. The simulation is also used to assess the effects of the friction parameter added, to the damage formulation in order to take into account the residual strength of the delaminated surface.

The simulation has been performed with ComPack-Aero finite element code (CIMNE and Quantech, 2008), specially developed for the FEMCOM project, “*An innovative finite element method for non linear analysis of composite structures – CIMNE-AIRBUS*”. The results of the simulation have been already described in a delivered report of the project (Martinez et al., 2007). This code has been developed by the different members working in the FEMCOM project. Among them, it has to be remarked the work performed by F. Flores, developing the finite elements technology and the work developed by F. Rastellini, with the implementation of a simplified version of the serial/parallel mixing theory.

3.5.1 New procedure to take into account delamination in large scale simulations of laminated composites

ComPack-Aero finite element code

ComPack-Aero (CIMNE and Quantech, 2008) is an explicit finite element code developed by many researchers at the International Center for Numerical Methods in Engineering (CIMNE) in Barcelona, Spain. The code has a professional version commercialized by Quantech. A new version of ComPack-Aero code is in development to fulfill the objectives of FEMCOM project. The main aim of this project is to develop a non-linear finite element code capable of solving large scale structural problems of laminated composites, taking into account their micro-mechanical failures such as delamination or fibre buckling.

Although ComPack-Aero code contains a large number of different elements (such as truss elements, two- and three-dimensional solids, shells, beams, etc.), developed to solve different structural problems, in this work only two different elements are used: the LBST shell element (Flores and Oñate, 2005; Oñate and Flores, 2005; Flores and Oñate, 2007) and a three-dimensional solid element (Zienkiewicz and Taylor, 1991; Oñate, 1995). The LBST shell element is formulated as Total Lagrangean assumed strain element without rotational degrees

of freedom, the computation of the curvatures is made resorting to the geometry of the adjacent element. This element has two main advantages that make it the most adequate for the purpose sought. The first advantage is that it reduces significantly the computational cost of the simulation, as the rotation degrees of freedom are removed from the element. This feature improves the capacity of the code to deal with large scale simulations. And the second advantage is that, removing the rotation degrees of freedom, its coupling with solid elements can be done straightforward, as the degrees of freedom existing in both elements are the same. The numerical procedure used to couple both elements is described in detail in Flores (2007).

Despite all advantages provided by the LBST shell element, it has the drawback that shear stresses are not included in its formulation, therefore it is not possible to take into account structural failures produced by shear stresses. An example of this sort of failure is, precisely, delamination. To solve this drawback, a new numerical procedure has been developed in which the shear stresses are obtained from the angular momentum equations, as a residual product of the bending forces in the element (Oñate et al., 2007).

The new developed version of ComPack-Aero deals with composite materials using a simplified version of the serial/parallel mixing theory (Oñate et al., 2007). The simplified version of the serial/parallel mixing theory considers that the effects fiber in serial directions are negligible. Therefore, matrix is the only material that collaborates to the composite strength in these directions. In the parallel direction, the iso-strain relation is used for both component materials. Thus, the compatibility and equilibrium equations for the composite can be written as:

$$\begin{aligned}
 \text{Parallel direction :} \quad & \begin{aligned}
 {}^c\varepsilon_P &= {}^m\varepsilon_P = {}^f\varepsilon_P \\
 {}^c\sigma_P &= {}^mk^m\sigma_P + {}^fk^f\sigma_P
 \end{aligned} \\
 \text{Serial direction :} \quad & \begin{aligned}
 {}^c\varepsilon_S &= {}^m\varepsilon_S \\
 {}^c\sigma_S &= {}^m\sigma_S
 \end{aligned}
 \end{aligned} \tag{3.42}$$

Finally, laminates are treated with the two different procedures described in section 2.3. LBST shell elements use the classical lamination theory (Barbero, 1999) while solid elements use the parallel mixing theory to obtain the strain field in each layer and the simplified serial/parallel mixing theory to obtain the stresses associated to the strain field.

New procedure proposed

Delamination in laminated composites is a failure that, as has been already described in this work, can be simulated as the total loss of shear strength in some layers of the composite; this failure is produced by the shear stresses developed between the composite layers. It has been proved, with the previous numerical example (section 3.4), that this failure phenomenon can be simulated using the serial/parallel mixing theory together with a damage formulation. The damage formulation is applied to matrix material and provides its failure due to shear stresses, if the delamination phenomenon takes place. And, the compatibility equations used by the simplified serial/parallel mixing theory (equation 3.42) leads to the total loss of shear capacity by the composite in its serial directions, among them, the shear direction.

Knowing that the formulation used is capable to reproduce the delamination phenomenon, a new procedure is developed to take into account this micro-mechanical failure in large scale

simulations of laminated composites, performed with the LBST shell element and the classical lamination theory.

The first thing to be said is that the delamination phenomenon cannot be properly captured if the finite element simulation is made using the LBST shell elements; as the LBST rotation-free shell element used does not contain in its formulation the shear stresses that cause delamination failure. Therefore, the material cannot lose its shear capacity because it does not have it, neither can be damaged by shear stresses because they are not included in the formulation. However, shear stresses can be obtained from the angular momentum equations, as a residual product of the bending forces in the element (Oñate et al., 2007). These stresses are included in the composite constitutive equation, to be taken into account by the damage formulation used to simulate matrix material. Because the damage formulation used to simulate matrix material is isotropic, the failure of matrix is represented by a strength reduction in all matrix shear stresses. And, consequently, by a loss of the composite stiffness.

So, the introduction of shear stresses in the composite constitutive equation, which are transferred to matrix constitutive equation by the serial/parallel mixing theory, provides a loss of the structural capacity of the composite in its serial directions and a global reduction of its stiffness. Therefore, damage produced by delamination can be taken into account with the LBST shell element, although there is no way to know if this damage is produced by delamination effects or by any other cause (such as tension or compression stresses).

In the case of the Ply Drop-off test, the visualization of the delamination phenomenon using shell elements is even harder, as the main stresses applied to the composite are in fiber direction, which makes nearly imperceptible the stiffness reduction of matrix material when studying the composite structural response: although matrix is completely damaged, fibres continue providing strength in the direction in which they are oriented, that coincides with the direction in which the load is applied. For this reason it is necessary to post-process the damage parameter in matrix material, acting as a indicator of damage in the composite.

Most of the structural simulations of composite structures are made to obtain the mechanical performance of the structure in its service configuration, this is, when no point in the composite is damaged. In this simulations, the representation of the damage parameter provides enough information as it shows the regions where the structure has to be reinforced. However, there are some cases in which it is necessary to know the exact damage cause. In these cases, the damaged shell elements can be replaced by solid elements, using the solid-shell connection interface included in ComPack-Aero code (Flores, 2007). The new simulation, performed with shell and solid elements, will show if the damage obtained is produced by a delamination phenomenon or by any other mechanical failure mode.

Thus, the methodology proposed to solve delamination problems with the numerical code developed consist on solving the problem using shell elements and, afterwards, replace the most damaged sections with three dimensional solid elements to obtain a more detailed result of the critical section of the structure. In the case of the Ply Drop-off test, the section to be replaced is the section where the variation of thickness in the laminate is found. Figure 3.26 shows this procedure. This methodology can be extended to the calculation of larger structures such as plane wings. Figure 3.27 shows a schematic representation of the procedure that should be followed in those cases.

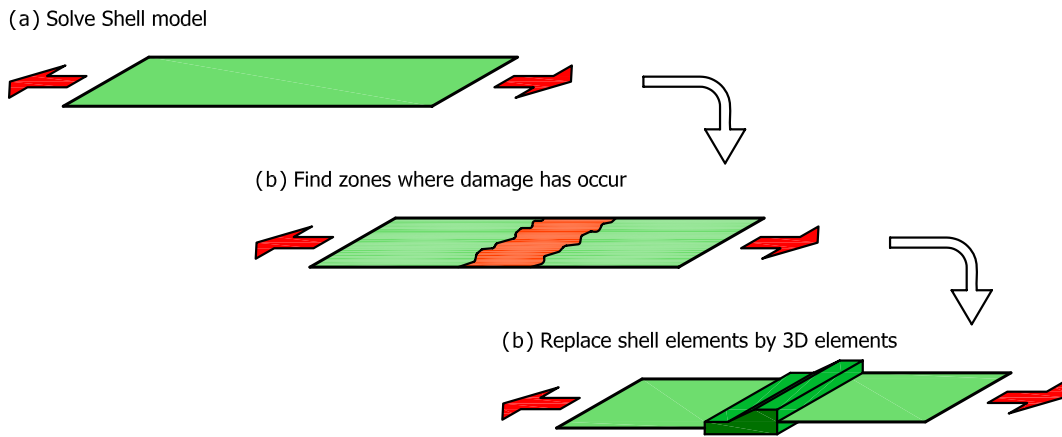


Figure 3.26: Resolution procedure to solve delamination problems with the code developed

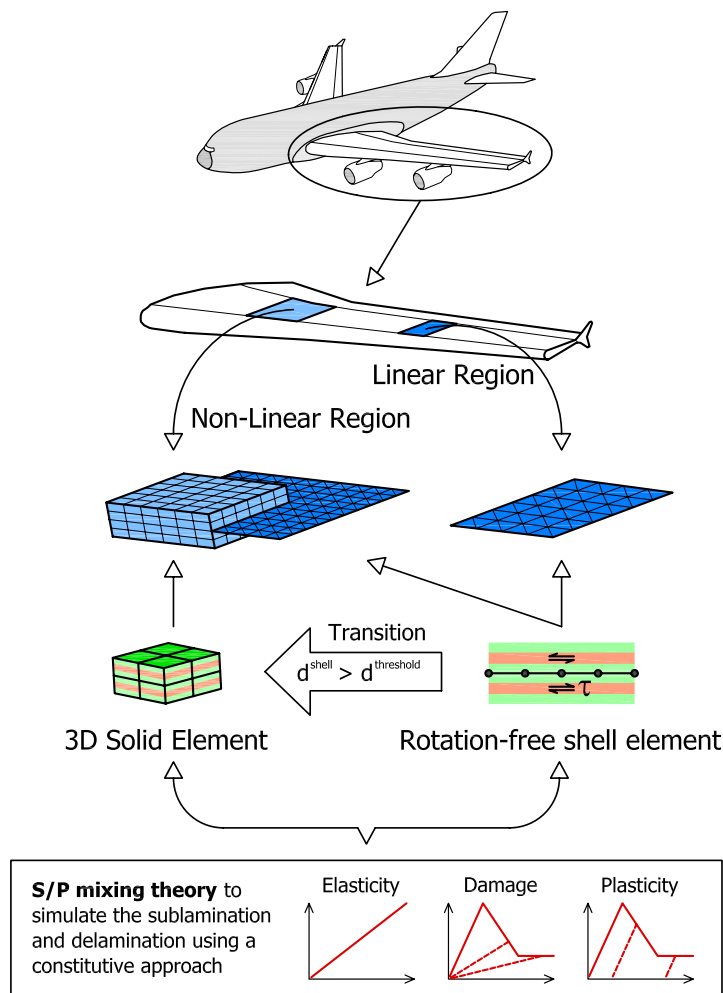


Figure 3.27: Schematic representation the procedure that should be followed to solve large structural problems

3.5.2 Description of the ply drop-off test

The Ply Drop-off test consist on applying a tensile stress to a composite laminate that has a thickness variation at its mid-span. Figure 3.28 shows an schematic representation of the test set-up and the sample dimensions. The laminate under study is composed by several layers (varying its number from 18 to 27) of the unidirectional prepreg IMS/977.2. The stacking sequence of the laminate, each layer orientation and the geometry of the section in which the thickness increases can be seen in figure 3.29. The properties of the prepreg layers are exposed in table 3.3.

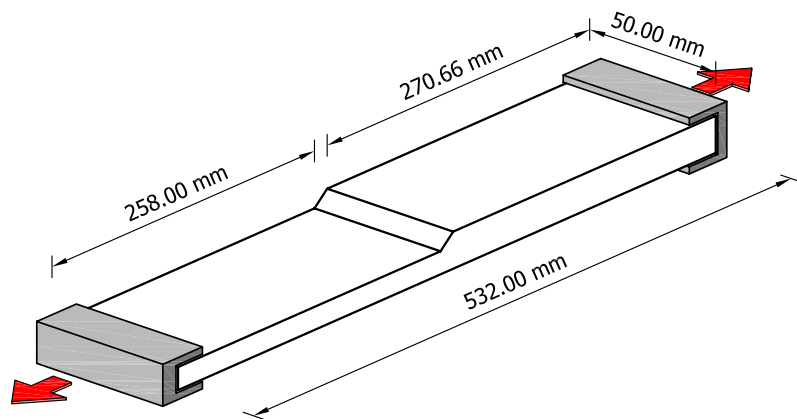


Figure 3.28: Ply Drop-off model dimensions

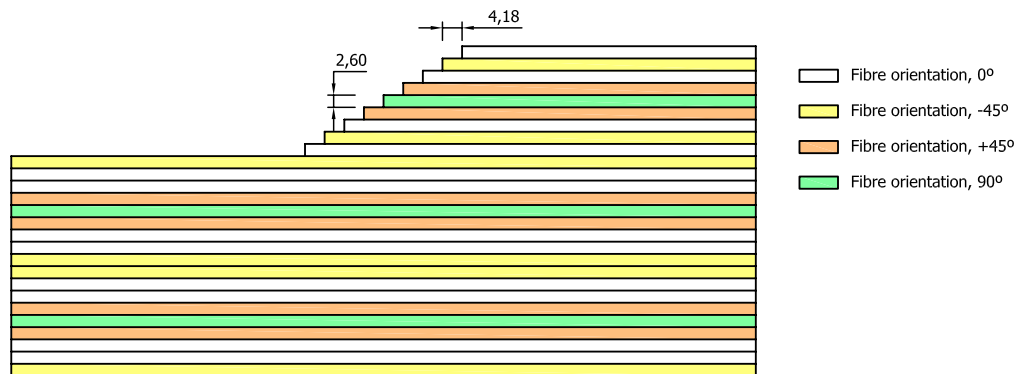


Figure 3.29: Stacking sequence and thickness variation of the sample used in the Ply Drop-off test

E_1 [GPa]	E_2 [GPa]	E_3 [GPa]	G_{12} [GPa]	G_{13} [GPa]	G_{23} [GPa]
175.0	7.9	7.9	4.3	4.3	4.3
G_{Ic} [J/m ²]	G_{IIc} [J/m ²]	G_{IIIc} [J/m ²]	ν	t [mm]	
555.0	738.0	738.0	0.3	0.26	

Table 3.3: Mechanical properties of the UD prepreg IMS/977.2

All these sample properties (material properties, geometry, etc.) have been used to construct and define the different finite element models to be used to perform the numerical simulation of the Ply Drop-off test. The characteristics of these finite element models are explained in the following section.

3.5.3 Numerical models developed

Three different models are developed to perform the numerical simulation of the Ply Drop-off test. According to the complexity of the model, the results obtained will be more or less accurate. The models developed are:

1. **Shell model:** This model simulates the ply drop-off test using a lamination formulation. Because shell elements are defined using their mid-plane, in order to simulate the effect of the thickness variation of the sample, a bending moment has been imposed in the elements where the thickness variation occurs.
2. **Solid-Shell model:** In this model, the region where the thickness variation takes place has been simulated with solid elements while, the rest of the structure, is simulated with shell elements.
3. **Solid model:** This model is made completely with three dimensional solid elements. This model is used to verify the results obtained with the two other simulations and to compare the computational improvement obtained with them.

Each one of these models has two versions. One in which the friction effect is included in the damage equation and another one in which friction is considered zero. The value of the friction considered is 2.5% of the matrix tensile strength.

In order to be able to compare the computational cost of each model, the meshes developed for each one of them have the same number of elements along the longitudinal and the transversal directions of the sample. In figure 3.30 is shown the number of elements defined in those directions.

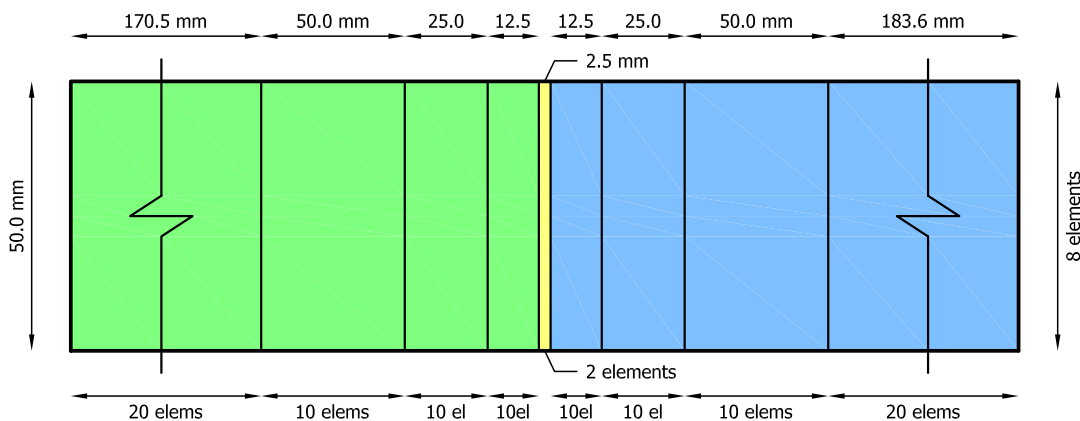


Figure 3.30: Zones in which the model has been divided and number of finite elements defined in each zone

As can be seen in figure 3.30, the model is divided in three main zones (each one displayed with a different color), depending on the number of layers existing in each zone. The green zone contains 18 layers; the yellow zone corresponds to the area where the thickness variation is found and the number of layers in it varies from 18 to 27; finally, the blue zone has 27 layers. This figure also shows that the region where the thickness variation occurs only has defined two finite elements in length. This is because, in order to reduce the computational cost of the solid models, layers have been grouped in stacks of three. Proceeding in this way, not only the number of elements required is reduced, but also the number of materials to be defined. This is shown in figure 3.31, where the geometry and materials considered are represented in the region where the thickness variation is found.

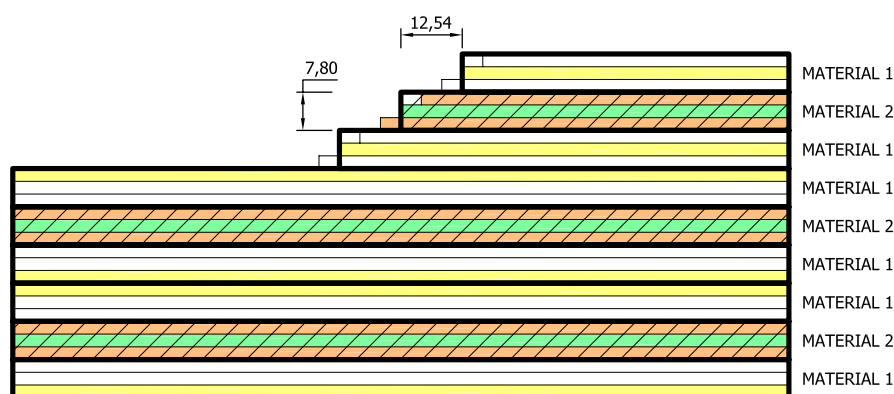


Figure 3.31: Materials defined in the numerical models

This figure shows that the materials defined in the solid models are:

- Material 1: Composed by two layers oriented at 0° and one layer oriented at -45°
- Material 2: Composed by two layers oriented at 45° and one layer oriented at 90°

These both materials are only used in the solid elements. In the case of shell elements, each layer is modeled independently along the laminate thickness. However, the thickness variation region is defined also with two finite elements in order maintain the similarity with the solid models.

Materials definition

The material properties described in table 3.3 correspond to the homogenized properties of the unidirectional prepreg IMS/977.2. Although these properties are useful, the mixing theory does not work with the composite homogenized mechanical parameters but with each component material properties. In this case, with the matrix and the fibre properties.

To obtain the mechanical properties of each one of the prepreg components, the values of the homogenized composite have been used considering:

1. Both composite components, fibre and matrix, have the same volumetric participation in the composite (50%).

2. Matrix is an isotropic material.
3. According to the simplified serial/parallel mixing theory formulation, fibre only collaborates to the composite strength and stiffness in its longitudinal direction.

With these three considerations in mind, the mechanical properties of each component material can be computed from the prepeg homogenized properties, obtaining the material characteristics displayed in table 3.4.

Matrix Properties		Fibre Properties	
Young Modulus	7.90 GPa	Young Modulus	342.1 GPa
Shear Modulus	4.30 GPa	Poisson Modulus	0.0
Poisson Modulus	0.30	Volume Content	50.0 %
Tensile Strength	85.0 MPa		
Fracture Energy	738 J / m ²		
Volume Content	50.0 %		

Table 3.4: Composite components mechanical properties. The value of the matrix tensile strength has been obtained from the brochure of CYCOM[®] 977-2 Toughened Epoxy Resin.

Description of the shell model

The shell model defined is composed by 1632 linear triangle shell elements and 927 nodes. The mesh developed is displayed in figure 3.32.

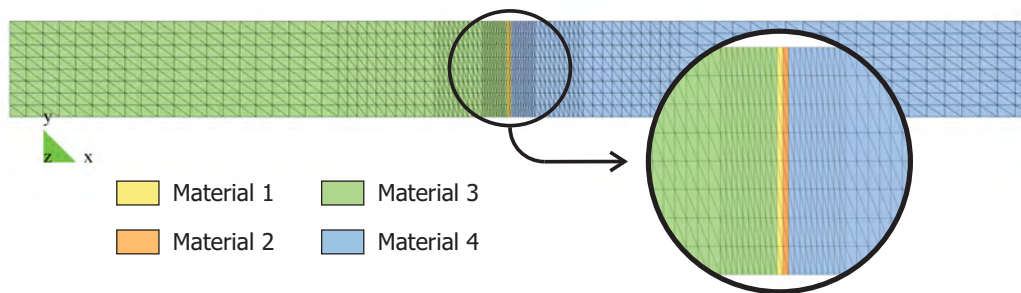


Figure 3.32: Mesh defined for the shell model. This figure also shows the different materials defined in the numerical model

Figure 3.32 shows that four different materials are defined in the shell model. The difference between materials consist in the number of layers defined and the orientation of these layers. Table 3.5 shows the number of layers and their orientation for each material defined.

As boundary conditions, the movement of the left end is restricted in directions x , y and z and the right end is restricted in directions y and z . An increasing in time longitudinal force is applied to the right end of the structure. The simulation has been run for a computational time of $4.0 \cdot 10^{-3}$ seconds with a time step of $2.5 \cdot 10^{-8}$ seconds. The final load applied to the structure, at the last time step, is of 155.2 kN.

Due to the fact that shell elements are coplanar, in order to simulate the thickness variation in the structure, the effect of eccentric forces has to be converted to an external load that will

Layer Num.	Material 1	Material 2	Material 3	Material 4
1	-45	-45	-45	-45
2	+ 0	+ 0	+ 0	+ 0
3	+ 0	+ 0	+ 0	+ 0
4	+45	+45	+45	+45
5	+90	+90	+90	+90
6	+45	+45	+45	+45
7	+ 0	+ 0	+ 0	+ 0
8	+ 0	+ 0	+ 0	+ 0
9	-45	-45	-45	-45
10	-45	-45	-45	-45
11	+ 0	+ 0	+ 0	+ 0
12	+ 0	+ 0	+ 0	+ 0
13	+45	+45	+45	+45
14	+90	+90	+90	+90
15	+45	+45	+45	+45
16	+ 0	+ 0	+ 0	+ 0
17	+ 0	+ 0	+ 0	+ 0
18	-45	-45	-45	-45
19	+ 0	+ 0		+ 0
20	-45	-45		-45
21	+ 0	+ 0		+ 0
22		+45		+45
23		+90		+90
24		+45		+45
25				+ 0
26				-45
27				+ 0

Table 3.5: Number of layers and fibre orientation defined in the different materials of the shell model

be applied to the shell elements. This eccentricity generates a bending moment, depending on the axial force applied to the structure, where the thickness variation occurs. This bending moment is applied as a pair of forces in the shell model. Figure 3.33 shows how the initial eccentric load is transformed to the applied pair of forces. The value of the bending moment and the pair of forces displayed in figure 3.33 is the following,

$$\begin{aligned}
 M &= F \cdot e \\
 F^+ &= -F^- = \frac{M}{d} = \frac{F \cdot e}{d}
 \end{aligned}
 \tag{3.43}$$

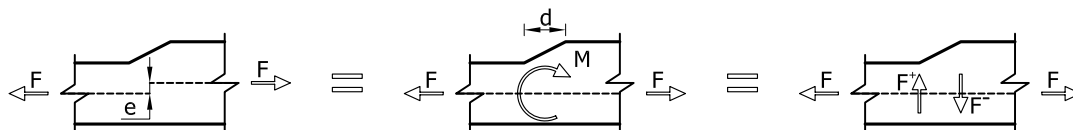


Figure 3.33: Conversion of the eccentric forces to a pair of forces

Description of the solid-shell model

The formulation of three dimensional solid elements can provide a better comprehension of the phenomenons that occur in the structural region where the thickness variation is found. With this aim, shell elements in this region have been replaced by solid elements. Figure 3.34 shows the mesh developed. This mesh has 2520 linear hexahedrons in the thickness variation region and 960 linear triangles at each side of this region. The number of nodes is 3852.

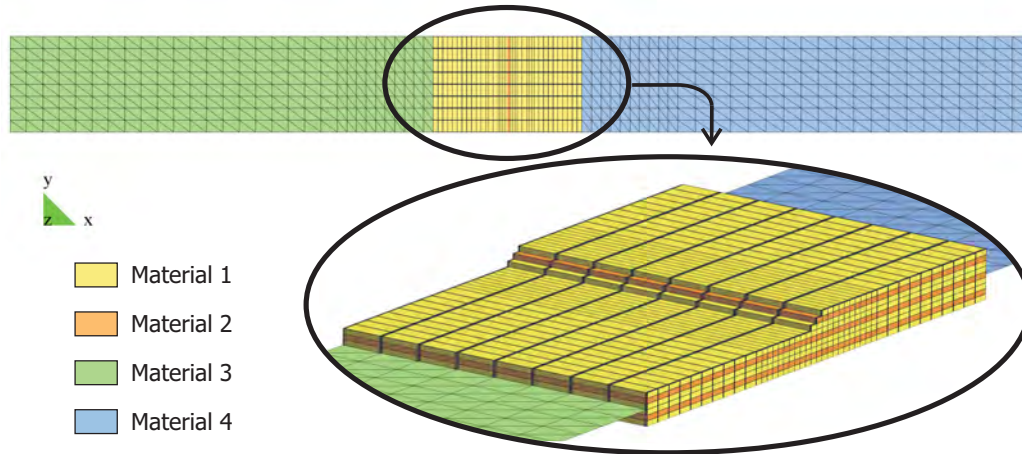


Figure 3.34: Mesh defined for the solid-shell model. This figure also shows the different materials defined in the numerical model

Shell elements found at each side of the three dimensional mesh are attached at the mid plane of the solid, which provides the eccentricity e shown in figure 3.33.

Figure 3.34 shows that four different materials are defined in the model. Materials three and four correspond to the shell materials already defined for the shell model and exposed in table 3.5. Materials defined in the solid elements, materials one and two, are based in the lamination formulation for solid elements of the mixing theory. This formulation considers that in a solid element composed by different layers, the deformation found in all layers is the same (and variation of deformation occurs between the different solid elements). With this consideration in mind, it can be written:

$$S_{\varepsilon} = {}^{L1} \varepsilon = {}^{L2} \varepsilon = \dots = {}^{Ln} \varepsilon \quad (3.44)$$

Where S_{ε} is the solid deformation and ${}^{Li} \varepsilon$ is the deformation of layer i . Having the deformation of each layer, the serial/parallel mixing theory can be applied to obtain its stress state.

Materials defined in solid elements are composed by several layers of the composite material exposed in table 3.4, each layer with a different orientation. According to the discretization made along the laminate thickness and shown in figure 3.31, materials 1 and 2 have the following number of layers and orientations:

As boundary conditions, all displacements of both ends of the structure have been restricted, except the longitudinal displacement of the right end (according to figure 3.34), where an increasing displacement has been applied defining a constant velocity. The simulation has

Material	Num. of layers	Orientation of layers		
Material 1	3	+ 0	-45	+ 0
Material 2	3	+90	+45	+90

Table 3.6: Laminated solid materials defined in the solid-shell model

been run for a computational time of 4.0^{-3} seconds with a time step of 3.21^{-8} seconds. The final displacement reached, by the right end of the structure at the last time step, is 3.0 mm.

Description of the solid model

The three dimensional solid model developed is used to obtain detailed results of the mechanical phenomenons taking place in the structure when it is loaded, as this model contains the complete strain and stress tensors. Thus, its main function is to provide results to be compared with the results obtained from the models previously described, to validate their ability to simulate the mechanical behavior of the structure and the accuracy of the results obtained with them. Also the computational times obtained with the three dimensional solid models will be compared with the times obtained with the simplified simulations, as the three-dimensional times are considered a highest values that can be reached solving the problem.

The mesh developed for the three dimensional solid model is composed of 6120 linear hexahedrons and 7893 nodes. As is shown in figure 3.35, two different materials have been defined. Both materials are the ones defined for the solid-shell model and described in table 3.6.

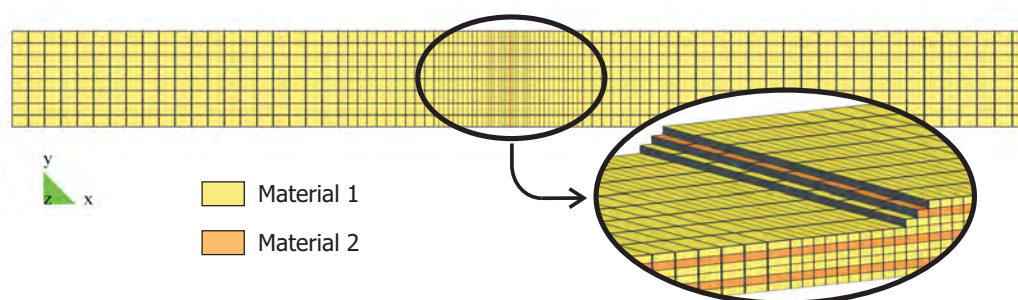


Figure 3.35: Mesh defined for the solid model. This figure also shows the different materials defined in the numerical model

The boundary conditions applied to the structure, as well as the computational times and time steps defined, are exactly the same that have been used in the solid-shell model.

3.5.4 Results obtained

The results of the six different simulations performed, corresponding to the three different finite element models developed: shell, solid-shell and solid; and if friction has been considered or not in the matrix damage equation; are shown and compared in this section. In the following table are exposed the names given to each simulation.

Model name	Description
3D-nF	Solid model without friction
3D-F	Solid model with friction
3D-Sh-nF	Solid-shell model without friction
3D-Sh-F	Solid-shell model with friction
Sh-nF	Shell model without friction
Sh-F	Shell model with friction

Table 3.7: Notation used for each finite element simulation

The firsts results presented are the ones obtained from the simulation made with the three dimensional solid models. These results show with detail the different phenomenons that take place in the structure and provide a good comprehension of the results obtained with the other models. Once knowing the structural performance of the laminate in the Ply Drop-off test, the results corresponding to the shell models are presented and compared with the solid ones. This comparison shows all the information obtained, and missing, when a shell finite element model is used to simulate a delamination phenomenon. Afterwards the results of the solid-shell element are explained and used to study the improvement obtained when adding solid elements to an already existing shell structure. Finally, all simulations will be compared among them. This comparison is made studying the structural performance obtained with all models, using a force-displacement graph. It is also compared the different CPU times required to run each simulation. The comparison between the results obtained with the friction and non-friction models is done when studying each single simulation by its own.

Solid model simulation

In the Ply Drop-off test, when the structure is loaded with a tensile force, the thickness variation found in the middle of the sample generates a bending moment that bends the structure as shown in figure 3.36. Results obtained in this figure correspond to an applied displacement of 0.9 mm to the right end of the structure.

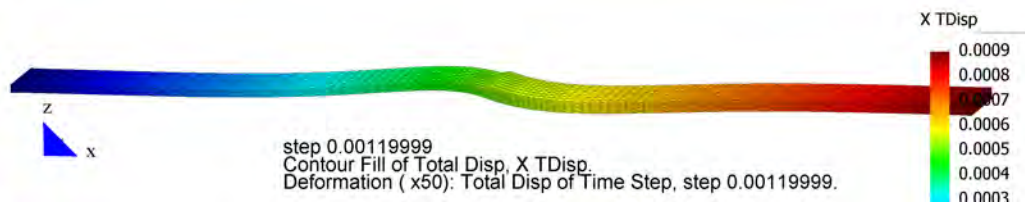


Figure 3.36: Deformation of the 3D-nF simulation when a displacement of 0.9 mm is applied to the right end of the structure

This thickness variation generates not only a bending moment but also shear stresses, which are concentrated in the layers of the laminate where the thickness variation takes place. These shear stresses are represented, also for an applied displacement of 0.9 mm, in figure 3.37.

According to the simplified serial/parallel mixing theory, fibres only collaborate to the composite strength in its longitudinal direction. Thus, all shear stresses affect only the matrix material. When stresses in matrix reach its maximum elastic value, the stress allowed in the material falls according to the damage constitutive law. And, when the total fracture energy has been achieved, the element cannot support more stresses, its contribution to the

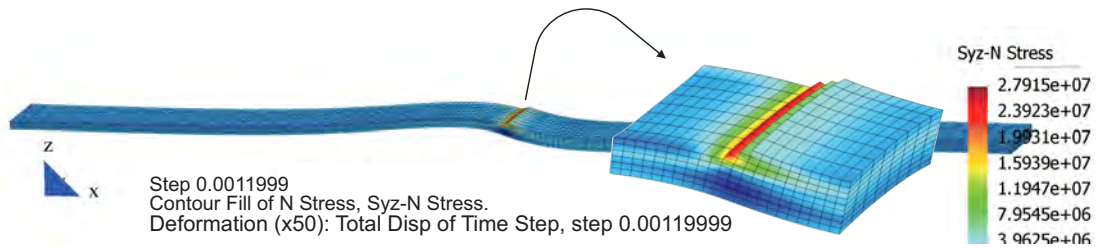


Figure 3.37: Shear stresses in the 3D-nF simulation

structure strength disappears and all stresses jump to the finite element found beside the cracked one. Also, the lack of strength of the element, in all directions except the fibre's longitudinal one (because fibre is not damaged), implies the disconnection between the finite elements found above and below the completely damaged element. The mechanical response of a structure with this sort of failure is exactly the same that is found in a structure when delaminates. Hence, this procedure localizes delamination without the computational cost of breaking the mesh, remesh the new delaminated area and add a contact condition to avoid interpenetration.

This effect is fully shown in figure 3.44 (included at the end of this section), where the shear stresses found in the structure are shown in one column and, in the column beside it, is displayed the evolution of the damage parameter. In this figure can be seen that, as the simulation advances, the maximum shear stresses move to the next element that can still provide some strength. The damage parameter moves in the same direction and with the same path as the shear stresses advance.

The damage parameter shown in figure 3.44 can take values between 0.0 and 1.0, both inclusive. When the damage parameter is 0.0 means that the element is not damaged at all and when its value is 1.0 represents that the element is completely damaged, being unable to provide more strength, neither stiffness, to the structure. In the case of laminated solids, the damage parameter represented keeps its limits between 0 and 1, and is defined as:

$$d = \frac{1}{v_e} \sum_{i=1}^n V_{L_i} d_{L_i} \quad (3.45)$$

Where V_e is the element volume, n the number of layers found in the element, V_{L_i} the volume of layer L_i and d_{L_i} the damage parameter of layer L_i .

When friction is applied to the matrix damage constitutive law, the residual strength provided by friction does not allow the delamination to grow until the end of the sample, as happens with the model when no friction is applied (figure 3.44, *e* to *g*). The delamination phenomenon stops when all damaged elements can provide, with their residual strength, enough shear stresses to equilibrate the shear effort that appears due to the thickness variation. Figure 3.45 shows the shear stress evolution and the damage evolution in the 3D-F model.

The differences found between the model in which the residual friction strength is applied and the model without it can be seen also in the force-displacement graph of the structure, shown in figure 3.38

This figure shows that for an applied displacement of, approximately, 1.6mm the effect of damage due to delamination begins to be perceptible in both models as a reduction of the

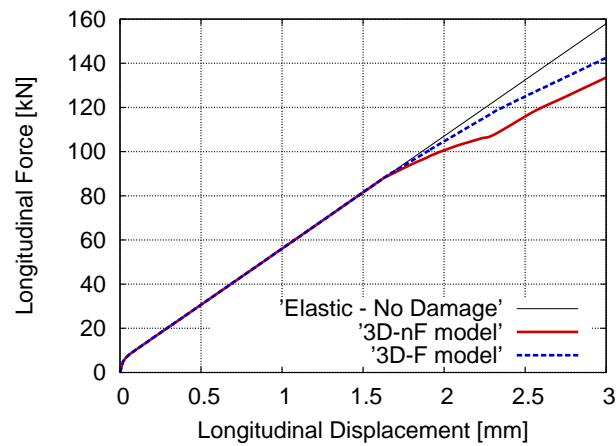


Figure 3.38: Force-displacement results for the solid models with and without friction

structure stiffness. However, this reduction is much larger in the case in which friction is not considered while, when friction is considered, the stiffness reduction is smaller because of the residual strength imposed in the constitutive equation of matrix material.

Shell model simulation

Once knowing the structural behavior that is expected from the laminate when the Ply Drop-off test is applied to it, in this section are shown the results obtained from this test when performing a numerical simulation using shell elements.

As a result of the bending moment applied to the structure (to simulate the thickness variation of the sample), the structural deformation is the same found in the case of the three dimensional model. In figure 3.39 can be seen this deformation for an applied displacement of nearly 0.9 mm.

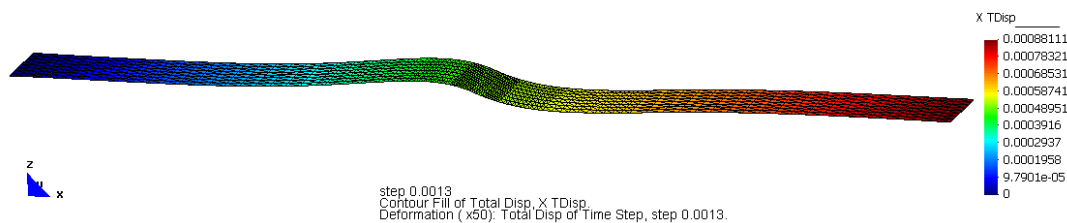


Figure 3.39: Deformation of the Sh-nF simulation when a displacement of 0.9 mm is applied to the right end of the structure

When studying the failure criteria of the structure, the first thing that must be noticed is that, as the rotation-free shell elements do not have shear stresses in their formulation, the effect of delamination will not be observed in the same way as is observed in the case of a three dimensional simulation. In the case of shell elements, what can be observed is the evolution of damage in the material due to delamination.

Although shear stresses are not included in the element formulation, a good estimation of their

value can be obtained from the angular momentum equations. These stresses are included in the composite constitutive equation. Following this procedure, the simulation shows that damage appears in the structure in the same place that appears when performing a three dimensional simulation, in the section where the thickness variation occurs. This can be seen in figure 3.46 in which the damage value is shown for different time steps. The damage parameter represented in this figure has been computed with the same expression described when studying the results of the three dimensional solid model (equation 3.45).

As can be seen in figure 3.46, damage starts in the structure for an applied displacement of 1.72 mm. Thus, the error in the damage initiation when simulating the Ply Drop-off test with shell elements is, approximately, of a 15%, when compared with the solid model, in which damage starts for an applied displacement of 1.50 mm.

The other main difference when comparing both models is that damage moves from right to left, instead of moving from left to right as happens with the solid model. The explanation for this effect is the following,

1. Damage starts as a result of the delamination produced by the shear stresses that appear due to the thickness variation in the structure. In the shell model, this shear stresses do not advance from left to right because the bending moment is always applied in the same section of the structure. On the other hand, in the solid model, the bending moment moves following the crack tip, which also moves the stresses that will propagate the delamination.
2. When delamination stabilizes, for a displacement of 3.0 mm in 3D-nF model and 2.625 mm in 3D-F model, the damage in the structure moves towards the left end of the structure, as this region of the structure is weaker than the other one. And this is exactly what happens in the shell simulation, as delamination crack cannot advance to the right end of the structure (delamination gets stabilized where the thickness variation occurs, because the bending moment is always applied in the same section), damage moves towards the left end.

Hence, the results obtained with the shell model are, with the limitations of the element formulation, completely coherent with the results obtained from the three dimensional solid model. In case of requiring a better accuracy and detailed prediction from the simulation, some shell elements must be replaced by solid elements, as is shown with next simulation.

Finally, the comparison between the model with and without friction shows that, in the case of a shell simulation, no difference is obtained between both models. Efforts affecting the structure are mainly longitudinal and matrix collaboration is not as relevant to the final strength of the structure. So, the effect of residual strength is practically imperceptible. This can be seen in the force displacement graph obtained from both simulations. This graph is shown in figure 3.40. In this figure, the results of the model in which friction is not considered, red line, cannot be seen because they are below the blue line.

Solid-Shell model simulation

This model improves significantly the comprehension of the different mechanical phenomenons that take place in the Ply Drop-off test, without increasing substantially the CPU time required to run the simulation. The addition of three dimensional elements in the region where damage begins, according to the shell model, provides a good prediction of the mechanical

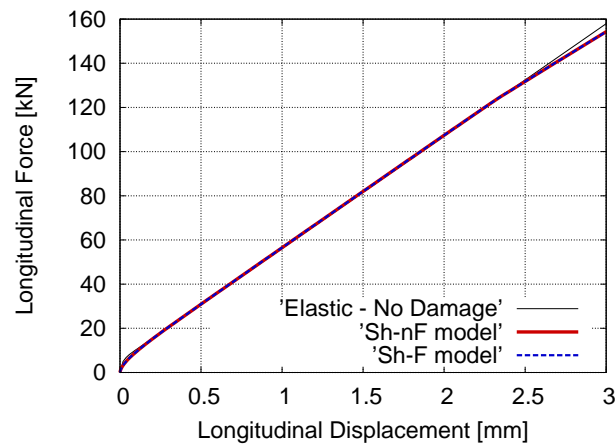


Figure 3.40: Force-displacement results for the shell models with and without friction

effect that takes place. When discussing the shell models results, damage was associated with delamination at all time because the phenomenology of this damage was known from the three dimensional solid model. However, in other cases, the reason because damage starts can be unknown. The addition of three dimensional solids to the shell mesh will provide this information.

First result to be shown is that the thickness variation in the structure provides, with the solid-shell model, the same deformation shown for the previous two simulations. This deformation is displayed in figure 3.41.

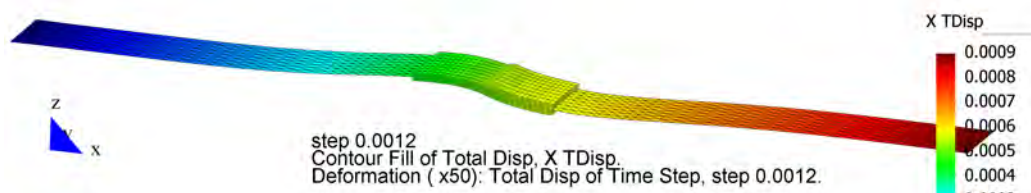


Figure 3.41: Deformation of the 3D-Sh-nF simulation when a displacement of 0.9 mm is applied to the right end of the structure

Besides the agreement in the displacement field among this model and the previous ones presented, the most important information to be obtained from this simulation are the mechanical effects that lead to the apparition of damage in the structure. This can be seen in figure 3.47, in which the evolution of shear stresses and damage parameter is shown along the loading process for the 3D-Sh-nF model.

This figure shows that damage appears in the structure due to a delamination phenomenon: the layer where the thickness variation starts is completely damaged due to shear stresses. Thus, the damage cause predicted by the solid-shell model is exactly the same found in the solid three dimensional model. This agreement between models is also found in the load step in which damage starts, for an applied displacement of 1.50mm in the right end of the structure. However, in this case, delamination stops for an applied displacement lower than 2.625 mm, coincident with the displacement in which the delaminated area reaches the end of the solid mesh and cannot continue through the shell element. At this point, as has been also obtained with previous models, damage starts increasing from the last delaminated section

towards the left end of the structure. This evolution of the damage region can be observed better in figure 3.48, in which the damage parameter in shell elements are depicted. This figure shows that damage has been already extended along the left side shell elements for an applied displacement of 2.400 mm.

When comparing the results obtained between the models with and without friction, figure 3.42, it can be seen that in the model in which friction is not considered the stiffness is slightly lower when damage due to delamination starts. However, results between both simulations are practically coincident because the delaminated area is too small to provide larger differences between both models.

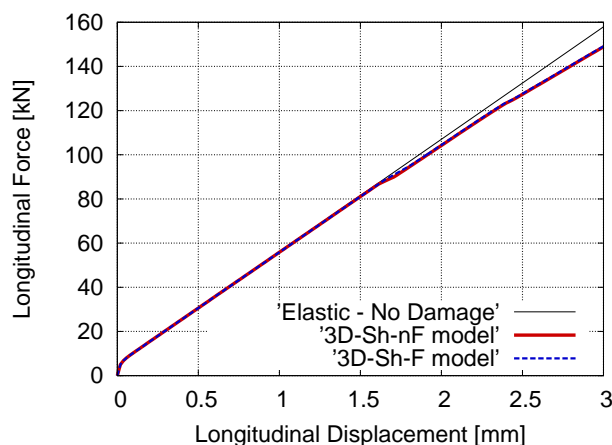


Figure 3.42: Force-displacement results for the solid-shell models with and without friction

Comparison among all simulations

Up to this point, the results obtained with the different simulations performed prove the ability of shell models to predict the apparition of damage in the structure as a consequence of delamination phenomenons, and how the structure behaves when this damage appears. Also the solid-shell model has been proved to be a good complement to the shell formulation, as it can show the exact failure criteria that originates the damage shown by the shell model.

The structure performance is similar in all models developed, as can be seen in figure 3.43. In this figure the results obtained with the different finite element meshes (shell, solid-shell and solid) are compared, for the friction models and the non-friction ones, using the force-displacement graphs obtained for each simulation. These graphs show that in the elastic range all models have the same stiffness and, when delamination starts, the stiffness reduction is proportional to the formulation accuracy of the model. However, the final load reached does not differ significantly among the different simulations and, when friction is considered, this difference is even lower.

All results shown so far prove the validity of the procedure proposed to take into account delamination phenomenons in laminated structures. This is, localize the damaged regions in the structure using shell elements simulated with a lamination theory and replace these elements for solid elements to obtain a detailed representation of the failure cause. However, to justify the convenience of using this procedure instead of modeling from the beginning the structure with three dimensional solids, the CPU times required to solve the problem with

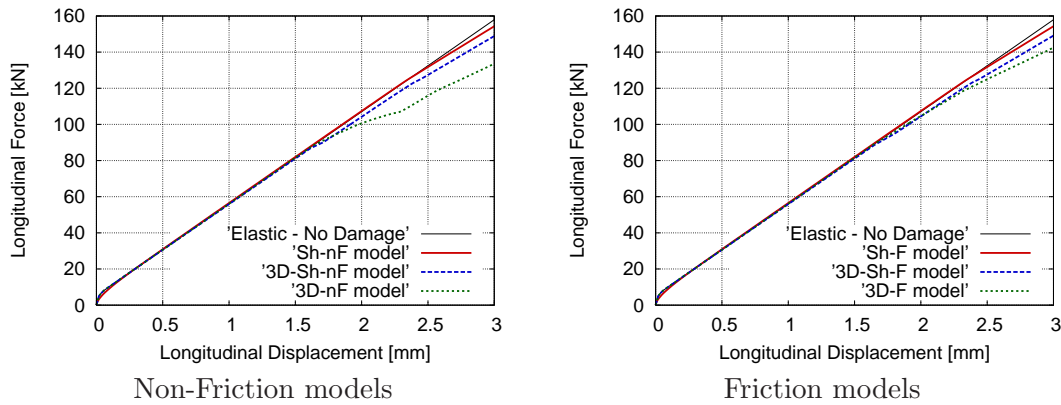


Figure 3.43: Force-displacement graph comparing the results obtained for the non-friction models and the friction ones

the new formulation proposed must improve significantly the CPU times required with a 3D simulation.

In the following table, the CPU times required to solve each one of the simulations are exposed. All calculations have been made with a Dell laptop that has an Intel Core 2 Duo T7200 CPU working at 2.0 GHz and with a RAM memory of 2GB.

Model name	CPU Time	Num. iterations
3D-nF	6h 51m	128750
3D-F	6h 51m	127500
3D-Sh-nF	4h 10m	137500
3D-Sh-F	3h 59m	131250
Sh-nF	2h 29m	160000
Sh-F	2h 21m	160000

Table 3.8: Notation used for each finite element simulation

Results presented in table 3.8 show that running the simulation with shell elements reduce nearly by three the time required by the three dimensional model. And, even when the model is refined adding solid elements where the thickness variation is found, the CPU time required is still considerable lower than in the three dimensional simulation, as the reduction of the CPU time is a bit larger than a 40%.

With the CPU times shown, the cost of running both models proposed to solve the problem, the shell model and, afterwards, the solid-shell model, is lower than the time required to run a complete three dimensional model. And, as has been seen, the results obtained with the methodology proposed are as good as the ones provided by the solid three dimensional models. It also has to be said that the structure considered in this simulation is quite small and that the benefits of the procedure proposed will be substantially more visible when applying this procedure to larger structures such a plane wing, in which the section that will be damaged is unknown.

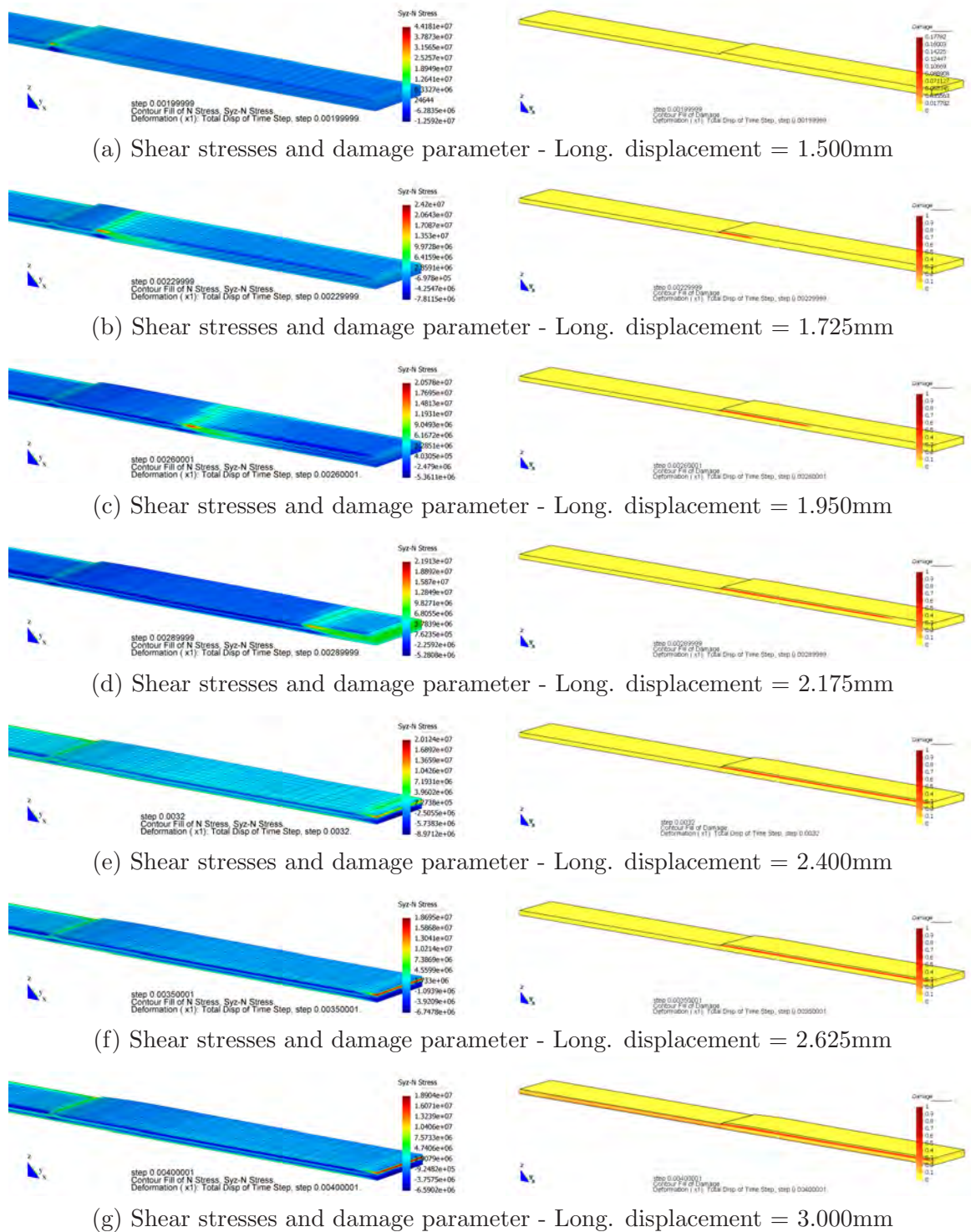


Figure 3.44: Shear stresses and damage parameter in the **3D-nF** model. This figure shows the evolution of both variables as the applied displacement increases

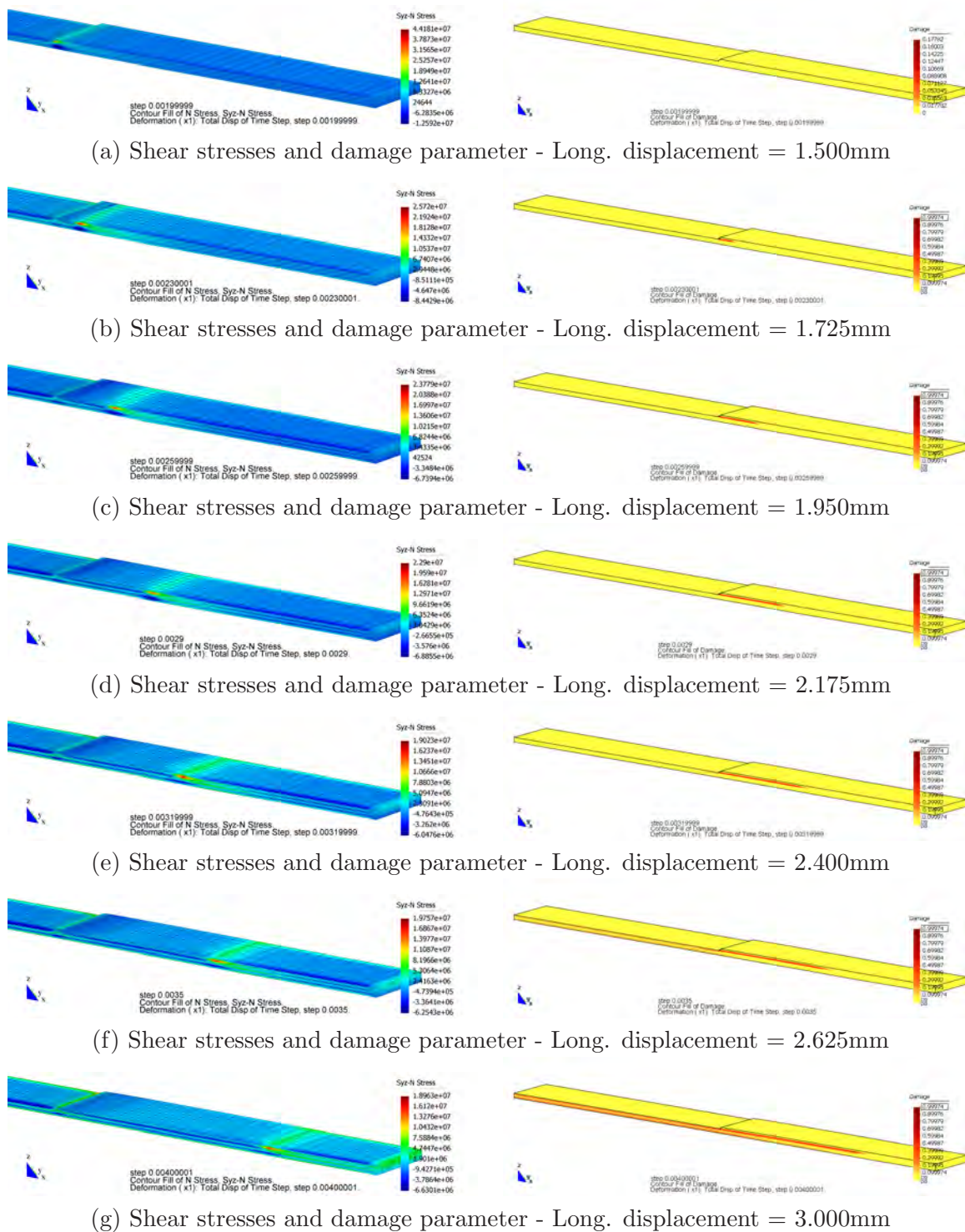


Figure 3.45: Shear stresses and damage parameter in the **3D-F** model. This figure shows the evolution of both variables as the applied displacement increases

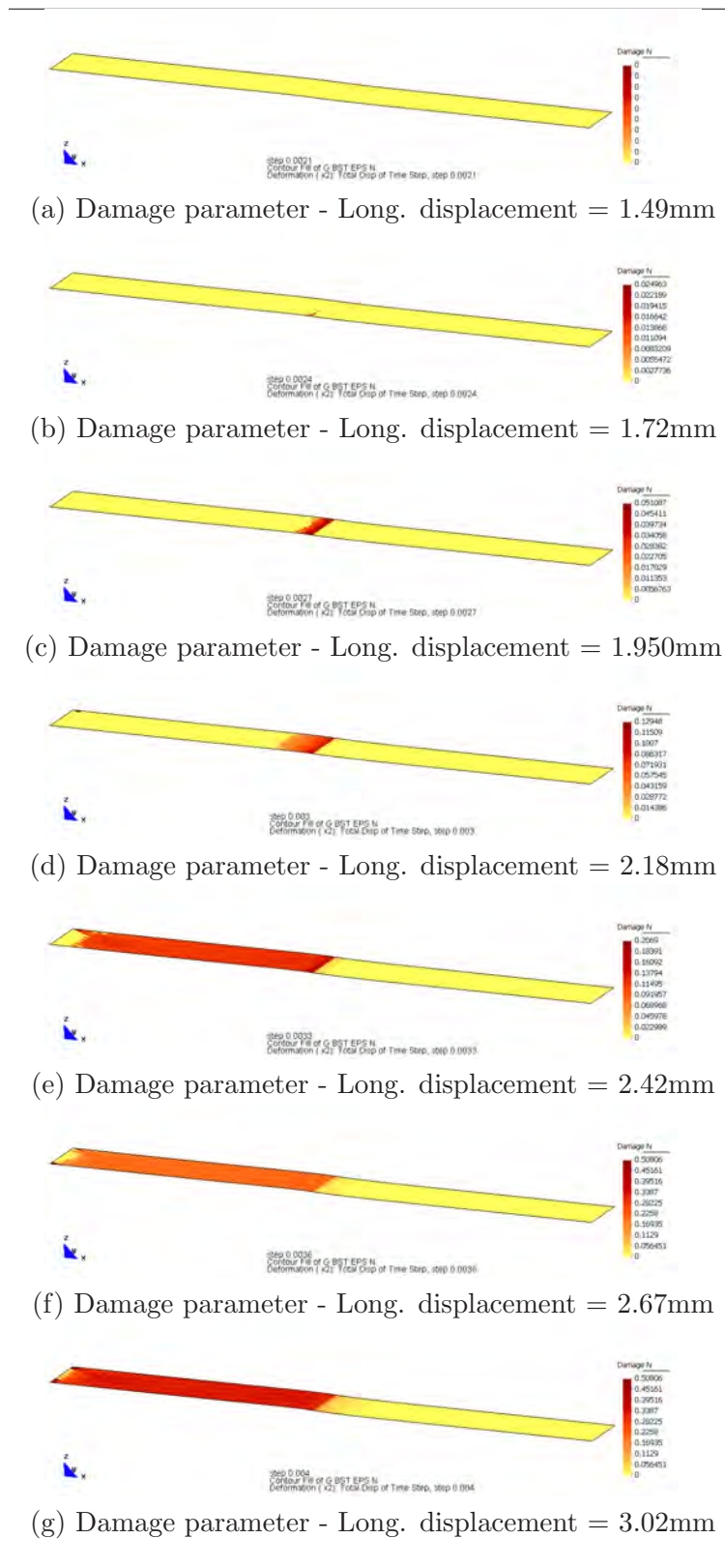


Figure 3.46: Damage parameter in the **Sh-nF** model. This figure shows the evolution of damage parameter as the applied displacement increases

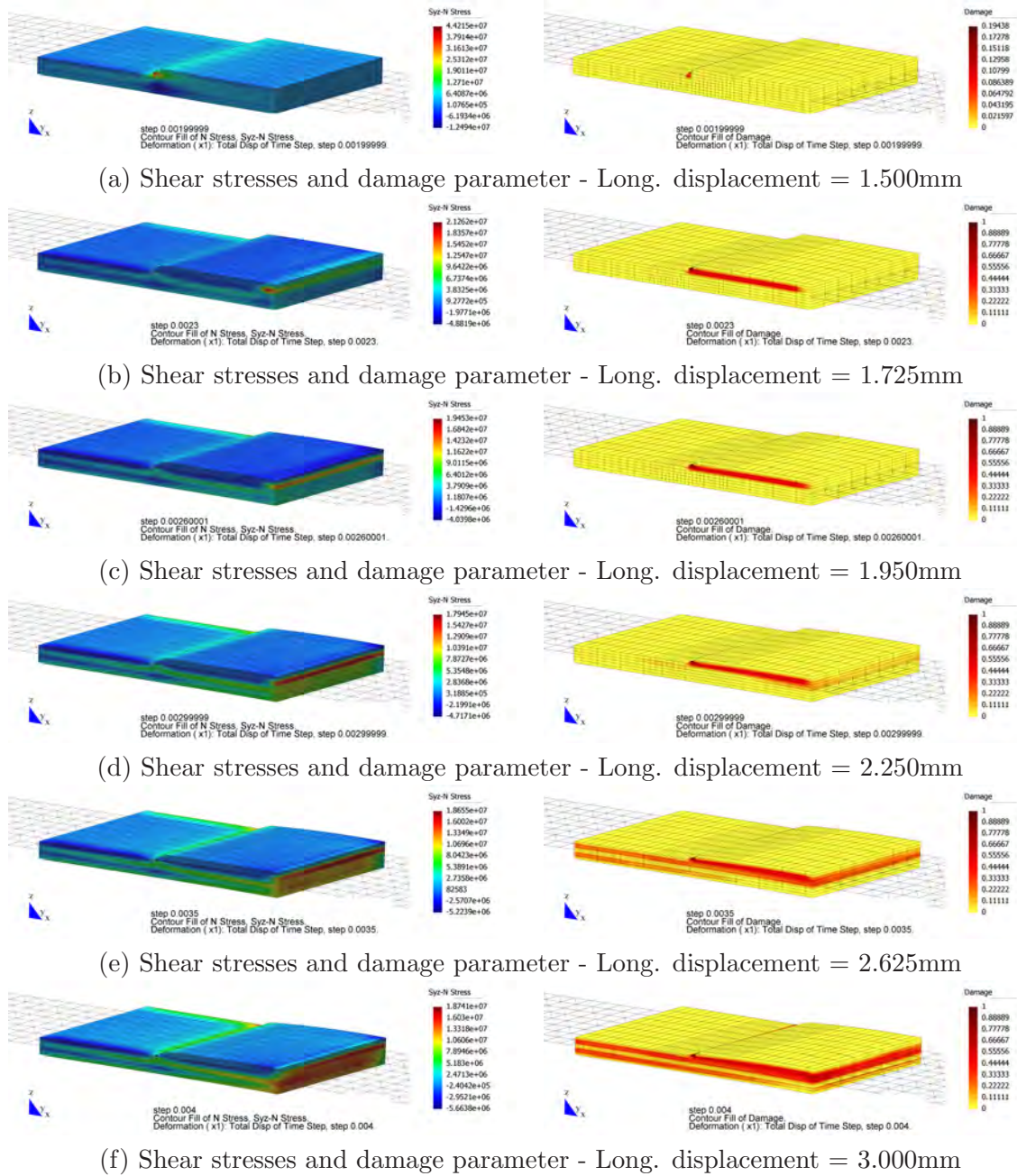


Figure 3.47: Shear stresses and damage parameter in the solid elements of the **3D-Sh-nF model**. This figure shows the evolution of both variables as the applied displacement increases

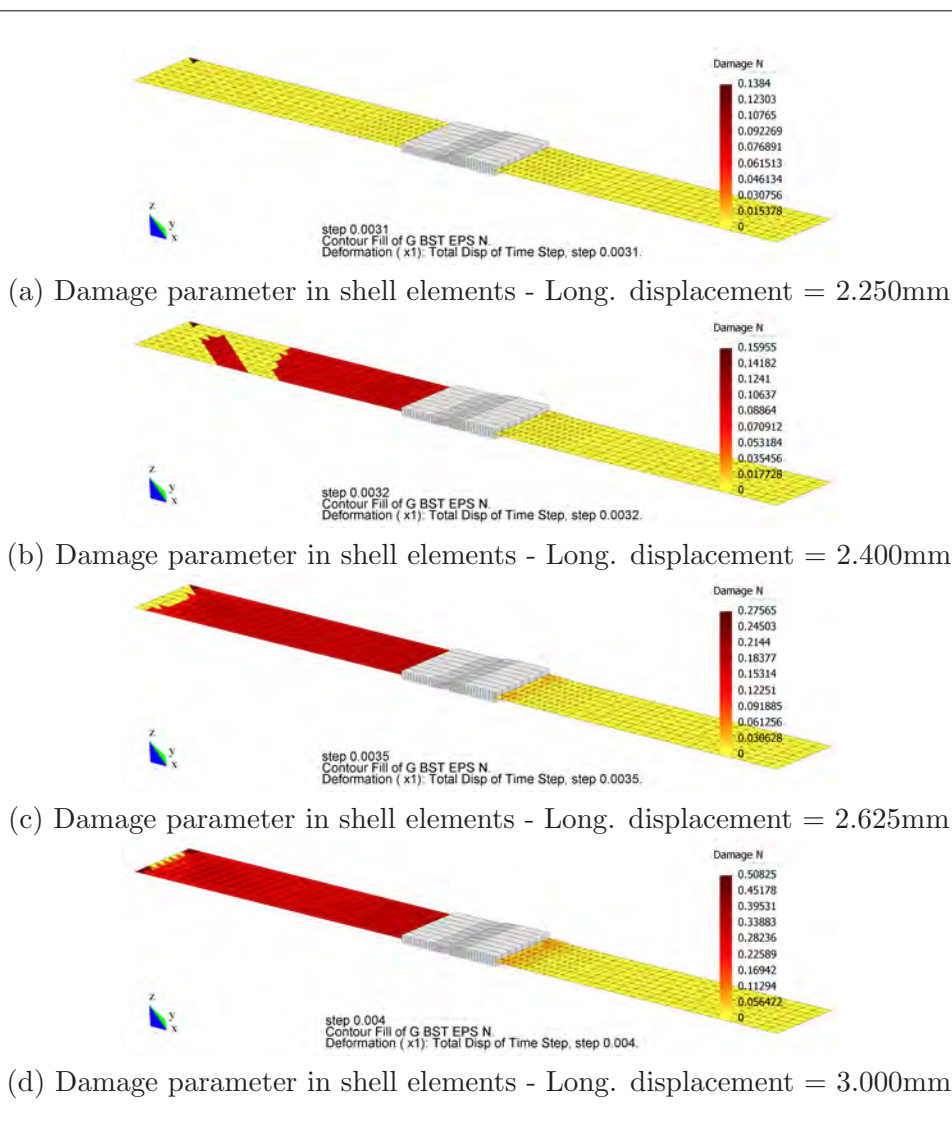


Figure 3.48: Damage parameter in the shell elements of the **3D-Sh-nF** model. This figure shows the evolution of both variables as the applied displacement increases

3.6 Conclusions and further work

In this chapter two different numerical procedures have been proposed related to the delamination problem. The first one consist on using the serial/parallel mixing theory to obtain the mechanical performance of the composite. It has been shown that this theory is capable to simulate delamination in the composite without the need of any additional formulation. The second procedure proposed provides a methodology to perform large scale simulations of composite materials, using shell elements and the classical lamination theory, taking into account delamination failure.

This section describes the main conclusions obtained from the numerical examples used to prove the performance of the two procedures proposed. It also contains a section in which are described some research lines that can be followed from the present work.

3.6.1 Conclusions

The main conclusion that can be inferred from the numerical simulations performed in this chapter, the end-notch flexure (ENF) test (section 3.4) and the ply drop-off test (section 3.5), is that the serial/parallel mixing theory is capable to simulate a delamination process by using the appropriate constitutive equations to predict the material behavior of the composite components. No other help or formulation is needed. This assessment has been proved when comparing the numerical with the experimental results for the ENF test. As the results obtained with the numerical simulation are practically identical to the results obtained from the experimental tests.

The structural behavior of the materials, obtained from the numerical simulations, shows that the delamination phenomenon occurs as a result of the lost of stiffness in matrix material due to the damage produced by the shear stresses in it. This lost of stiffness in matrix material implies that no other component material can develop serial stresses, due to the iso-stress condition of the serial/parallel mixing theory in the serial direction. This is translated in a lost of stiffness of the composite in all serial directions. In the case considered, the serial directions are all directions non coincident with fibre orientation. Thus, the composite is unable to avoid the shear deformations produced by the external loads, allowing a perfect sliding between the materials existing over and below it.

This procedure to deal with delamination provides an almost perfect simulation of the phenomenon without making any material distinction of the section expected to delaminate. Thus, the formulation becomes a good tool to study problems in which the delamination is known to occur but it is not known in which structural component or section will happen. Also, with the procedure developed, no remeshing formulation, neither contact, is needed to obtain the delamination effects on the structure; which reduces significantly the computational cost of the simulation.

The simulations performed have proved, also, that the damage formulation developed to simulate the matrix material constitutive behavior requires knowing the properties of the mesh generated to perform the simulation, as the fracture energy that can be developed by the model depends on the fracture length of it. This fracture length corresponds to the dimension perpendicular to the fracture surface. However, once knowing this dimensional parameter, the results obtained are mesh independent.

The second numerical procedure proposed in this chapter is focused in using the methodology developed to predict delamination failure in large scale simulations of laminated composites.

This sort of simulations are usually performed using shell elements and the classical lamination theory. Most of the shell elements implemented in finite element codes do not include in their formulation the interlaminar shear stresses components, in particular, the LBST element used in this work does not have them. However, this drawback can be solved obtaining the shear stresses as a residual product of the simulation, from the angular momentum equations. These stresses are included afterwards in the constitutive equation of the composite; which permits to take into account the delamination failure in the material constitutive performance and localize the elements in which some sort of damage takes place. Once damage has been localized, the damaged elements can be replaced by solid elements to obtain the type mechanical failure obtained in the material.

This methodology has been applied to the ply drop-off test, which has proved that, despite the possible differences in the final values of the different simulations performed (shell, solid-shell and solid simulations), all of them provide the same qualitative results. All models have shown that the failure cause of the laminate in the ply drop-off test is due to delamination, found in the first layer where the thickness of the sample begins to increase. And, when this delamination stops, damage propagates from the last laminated section in the structure to the left end of it. The force-displacement graphs have shown that this process is not followed by a significant reduction of the stiffness, neither the strength, of the laminate.

The results obtained have proved the good performance of shell element simulations, as they are capable to localize where and when damage starts, as well as the structure behavior as a result of this damage. The ability to make these predictions works even in cases in which the failure cause is due to shear stresses (such as delamination), not included explicitly in the element formulation as they have to be obtained as a residual result from the element momentums. And, if a better prediction and comprehension of the failure mechanisms wants to be obtained from the numerical simulation, the code allows replacing some shell elements with solid three dimensional elements, which will provide a more detailed representation of the region where damage occurs.

Thus, these results validate the procedure proposed to solve composite laminated structures: First running a shell model that will localize the regions of the structure where damage occurs for, afterwards, replacing some shell elements for solid elements in case of requiring knowing the exact mechanical causes of the damage found with the shell elements. Results obtained with this procedure, for the Ply Drop-off test, have been compared with a three dimensional simulation of the test obtaining a perfect agreement among the models.

Also, this new methodology proposed reduces significantly the CPU time required to perform the simulation, as shell model requires a third of the time needed to perform the three dimensional simulation. The advantages of the proposed methodology to solve laminated structures will be more perceptible when dealing with larger simulations, in which the areas that are damaged are unknown, as it is also unknown the type of damage suffered by the structure.

Finally, it has to be said that the friction parameter included in the damage formulation has proved that friction can play an important role in the delamination toughness, as it stabilizes the fracture propagation. However, this effect is only visible when the delamination is simulated with solid elements.

3.6.2 Further work

The good results obtained with the new procedures proposed to simulate delamination in composites using the serial/parallel mixing theory, together with a damage formulation, justify further research of the delamination phenomenon, following the path began in this work. Some possible research lines are described hereafter.

- The version of the serial/parallel mixing theory used to simulate delamination only uses two constituent materials to characterize the composite: fiber and matrix. With this scope, delamination relies on matrix material. It can be interesting to develop a new version of the serial/parallel mixing theory capable to deal with three constitutive materials. The new material added to the formulation can be defined as an interface material, which will contain all the mechanical parameters required to characterize the delamination phenomenon (fracture energies, stiffness, etc.)
- The damage constitutive law used to characterize matrix material in the presents simulations have been proved to work satisfactorily, according to the results obtained from the simulations. However, further research can be performed trying to improve this formulation, or studying how the delamination phenomenon is characterized when different yield criterions are used, such Mohr-Coulomb or Drucker-Prager.
- The constitutive laws used to simulate delamination should be improved with a large strain formulation. The stiffness reduction suffered by the structure due to delamination leads to large displacements. These should be taken into account in order to obtain more accurate prediction of the delamination phenomenon and, what is even more important, to obtain a more accurate prediction of the mechanical performance of the structure, once delamination has taken place.
- Friction effects. Despite the relevance that have friction effects in the fracture toughness of mode II delamination, few studies have been found in which friction is used to simulate delamination phenomenons. Therefore, this field is completely opened for further research. In this work a friction parameter has been introduced in the damage formulation. The new damage formulation has proved that friction can stabilize delamination propagation. However, this parameter is based on an empirical value difficult to obtain. The friction parameter should be improved, making it dependent on the material friction coefficient. Also friction formulation should be improved to take into account its directional behavior (the formulation developed considers this effect isotropic) and to make it dependent on the forces normal to the fracture surface.
- Finally, the simulations included in this work have proved the ability of the numerical procedures proposed to deal with the delamination problem, but they are small simulations that do not take advantage of all capabilities provided by the proposed procedures. Now these procedures should be used to perform simulations of large scale laminate structures, obtaining their structural performance taking into account possible micro-mechanical failures, such as delamination. These simulations will increase the existing knowledge of how laminated structures behave and will reveal possible drawbacks of the procedures proposed, hidden when these are used in small scale simulations.

References

- Allix, O. and Ladev ze, P. (1995). Damage analysis of interlaminar fracture specimens. *Composite Structures*, 31(1):61–74.
- ASTM D-5528. *Standard test method for mode I interlaminar fracture toughness of unidirectional fiber-reinforced polymer matrix composites*.
- ASTM D-6671. *Standard test method for mixed mode I-mode II interlaminar fracture toughness of unidirectional fiber reinforced polymer matrix composites*.
- Balac  de Morais, A. and Pereira, A. (2006a). Mixed mode I+II interlaminar fracture of glass/epoxy multidirectional laminates – part 1: Analysis. *Composites and Science Technology*, 66(13):1889–1895.
- Balac  de Morais, A. and Pereira, A. (2006b). Mixed mode I+II interlaminar fracture of glass/epoxy multidirectional laminates – part 2: Experiments. *Composites and Science Technology*, 66(13):1896–1902.
- Balzani, C. and Wagner, W. (2007). An interface element for the simulation of delamination in unidirectional fiber–reinforced composite laminates. *Engineering Fracture Mechanics*, doi:10.1016/j.engfracmech.2007.03.013.
- Barbero, E. J. (1999). *Introduction to composite materials design*. Taylor & Francis, Philadelphia, USA.
- Benzeggagh, M. L. and Kenane, M. (1996). Measurement of mixed-mode delamination fracture toughness of unidirectional glass/epoxy composites with mixed-mode bending apparatus. *Composites and Science Technology*, 56(4):439–449.
- Blanco, N. (2004). *Variable mixed-mode delamination in composite laminates under fatigue conditions: testing & analysis*. PhD thesis, Departament d’Enginyeria Mec nica i de la Construcci  Industrial – Univeristat de Girona. Directors: Josep Costa.
- Bolotin, V. V. (1996). Delamination in composite structures: its origin, buckling, growth and stability. *Composites Part B: Engineering*, 27(2):129–145.
- Borg, R., Nilsson, L., and Simonsson, K. (2001). Simulation of delamination in fiber composites with a discrete cohesive failure mode. *Composites and Science Technology*, 61(5):667–677.
- Borg, R., Nilsson, L., and Simonsson, K. (2002). Modeling of delamination using a discretized cohesive zone and damage formulation. *Composites and Science Technology*, 62(10–11):1299–1314.
- Borg, R., Nilsson, L., and Simonsson, K. (2004). Simulating DCB, ENF, and MMB experiments using shell elements and cohesive zone model. *Composites and Science Technology*, 64(2):269–278.
- Brunner, A. J., Blackman, B. R. K., and Davies, P. (2007). A status report on delamination resistance testing of polymer-matrix composites. *Engineering Fracture Mechanics*, doi:10.1016/j.engfracmech.2007.03.012(2).
- Camanho, P. P. and D vila, C. G. (2002). Mixed-mode decohesion finite elements for the simulation of delamination in composite materials. Technical Report TM-2002-211737, NASA.

- Camanho, P. P., Dávila, C. G., and de Moura, M. F. (2003). Numerical simulation of mixed-mode progressive delamination in composite materials. *Journal of Composite Materials*, 37(16):1415–1438.
- CIMNE and Quantech (2008). *ComPack-Aero. Innovative finite element methods for non linear analysis of composite structures*. Explicit finite element code developed by CIMNE & Quantech ATZ. www.cimne.com; www.quantech.es/QuantechATZ/Stampack.html.
- Corbella, B., Vicens, J., and Costa, J. (2004). Informe de los resultados de los ensayos de propagación de grieta en modo II del "round robin test" del proyecto grincomp (mat2003-09768-c03). Technical Report 2004-CYT-01-IT01, CIMEP.
- Davidson, B. D. and Sun, X. (2005). Effects of friction, geometry and fixture compliance on the perceived toughness from the three- and four-point bend end-notched flexure tests. *Journal of Reinforced Plastics and Composites*, 24(15):1611–1628.
- Davies, P., Blackman, B. R. K., and Brunner, A. J. (1998). Standard test methods for delamination resistance of composite materials: Current status. *Applied Composite Materials*, 5(6):345–364.
- de Moura, M. F. S. F., Gonçalves, J. P. M., Marques, A. T., and de Castro, P. M. S. T. (2000). Prediction of compressive strength of carbon-epoxy laminates containing delamination by using a mixed-mode damage model. *Composite Structures*, 50(2):151–157.
- Dieter, G. E. (1988). *Mechanical metallurgy*. McGraw-Hill Book Company, London, UK.
- Fan, C., Ben Jar, P. Y., and Roger Cheng, J. J. (2007). A unified approach to quantify the role of friction in beam-type specimens for the measurement of mode II delamination resistance of fibre-reinforced polymers. *Composites and Science Technology*, 67(6):989–995.
- Flores, F. G. (2007). Imposición de restricciones multipunto en la modelización con elementos sin grados de libertad rotacionales. In *Mecánica computacional, Vol. XXVI*, October, Córdoba, Argentina.
- Flores, F. G. and Oñate, E. (2005). Improvements in the membrane behaviour of the three node rotation-free BST shell triangle using an assumed strain approach. *Computer Methods in Applied Mechanics and Engineering*, 194(6–8):907–932.
- Flores, F. G. and Oñate, E. (2007). A rotation-free shell triangle for the analysis of kinked and branching shells. *International Journal for Numerical Methods in Engineering*, 69(7):1521–1551.
- Iannucci, L. and Willows, M. L. (2006). An energy based damage mechanics approach to modelling impact onto woven composite materials - part I. Numerical models. *Composites Part A: Applied science and manufacturing*, 37(11):2041–2056.
- Iannucci, L. and Willows, M. L. (2007). An energy based damage mechanics approach to modelling impact onto woven composite materials - part II. Experimental and numerical results. *Composites Part A: Applied science and manufacturing*, 38(2):540–554.
- Jansson, N. E. and Larsson, R. (2001). A damage model for simulation of mixed-mode delamination growth. *Composite Structures*, 53(4):409–417.
- JIS K-7086. *Testing methods for interlaminar fracture toughness of carbon fibre reinforced plastics*.

- Kachanov, L. M. (1971). *Foundations of the theory of plasticity*. Applied mathematics and mechanics. North-Holland Publishing Company, Amsterdam, Netherlands.
- Kachanov, L. M. (1986). *Introduction to continuum damage mechanics*. Mechanics of elastic stability. Martinus Nijhoff, Dordrecht, Netherlands.
- Kedward, K. T. (2002). *Mechanical design handbook*, chapter Section 15: Composites, pages 15.01–15.29. McGraw-Hill, New York, USA.
- Krueger, R. (2002). The virtual crack closure technique: History, approach and applications. Technical Report CR-2002-211628, NASA.
- Krueger, R. (2004). Virtual crack closure technique: history, approach and applications. *Applied Mechanics Reviews*, 57(2):109–143.
- Lubliner, J. (1990). *Plasticity theory*. MacMillan Publishing Company, New York, USA.
- Malvern, L. E. (1968). *Introduction to the mechanics of a continuous medium*. Prentice-Hall, Englewood Cliffs, NJ, USA.
- Martínez, X., Oller, S., and Barbero, E. (2007). Study of delamination in composites by using the serial/parallel mixing theory and a damage formulation. In *Composites 2007 – ECCOMAS thematic conference on mechanical response of composites*, September, Porto, Portugal.
- Martínez, X., Oller, S., and Barbero, E. (2008). *Mechanical response of composites*, chapter Study of delamination in composites by using the Serial/Parallel mixing theory and a damage formulation. Springer, ECCOMAS series edition.
- Martinez, X., Rastellini, F., Flores, F., Oller, S., and Oñate, E. (2007). FEMCOM: Benchmark 01: Ply drop-off test. damage propagation due to delamination. Technical report, CIMNE.
- Obreimoff, I. W. (1930). The splitting strength of mica. *Proceedings of the Royal Society of London A*, 127(805):290–297.
- Oliver, J., Cervera, M., Oller, S., and Lubliner, J. (1990). Isotropic damage models and smeared crack analysis of concrete. In Mang, H. and Bićanić, N., editors, *Second International Conference on Computer Aided Analysis and Design of Concrete Structures*, pages 945–958, April, Zell am See, Austria.
- Oller, S. (2001). *Fractura mecánica. Un enfoque global*. CIMNE (Centro Internacional de Métodos Numéricos en Ingeniería), Barcelona, Spain.
- Oller, S. (2002). *Dinámica no-lineal*. CIMNE (Centro Internacional de Métodos Numéricos en Ingeniería), Barcelona, Spain.
- Oller, S. (2003). *Simulación numérica del comportamiento mecánico de los materiales compuestos*. CIMNE (Centro Internacional de Métodos Numéricos en Ingeniería), Barcelona, Spain.
- Oñate, E. (1995). *Cálculo de estructuras por el método de elementos finitos. Análisis estático lineal*. CIMNE (Centro Internacional de Métodos Numéricos en Ingeniería), Barcelona, Spain, 2nd edition.
- Oñate, E. and Flores, F. G. (2005). Advances in the formulation of the rotation-free basic shell triangle. *Computer Methods in Applied Mechanics and Engineering*, 194(21–24):2406–2443.

- Oñate, E., Oller, S., Flores, F., Rastellini, F., and Martinez, X. (2007). FEMCOM: An innovative finite element method for non linear analysis of composite structures. First annual report project. Technical report, CIMNE.
- Pagano, N. J. and Schoeppner, G. A. (2000). *Comprehensive composite materials*, chapter Delamination of polymer matrix composites: Problems and assessment, pages 433–528. Elsevier, London, UK.
- Paiva, J. M. F. d., Mayer, S., and Rezende, M. C. (2005). Evaluation of mechanical properties of four different carbon/epoxy composites used in aeronautical field. *Materials Research*, 8(1):91–97.
- Pinho, S. T., Iannucci, L., and Robinson, P. (2006). Formulation and implementation of decohesion elements in an explicit finite element code. *Composites Part A: Applied science and manufacturing*, 37(5):778–789.
- Rastellini, F. (2006). *Modelización numérica de la no-linealidad constitutiva de laminados compuestos*. PhD thesis, Departament de Resistència de Materials i Estructures a l'Enginyeria (RMEE) – UPC. Directors: Sergio Oller and Eugenio Oñate.
- Rastellini, F., Oller, S., Salomon, O., and Oñate, E. (2007). Composite materials non-linear modelling for long fibre reinforced laminates: Continuum basis, computational aspects and validations. *Computers and Structures*, doi:10.1016/j.compstruc.2007.04.009.
- Reeder, J. R. and Crews, J. H. (1991). Nonlinear analysis and redesign of the mixed-mode bending delamination test. Technical Report TM-102777, NASA.
- Rice, J. F. (1968). *Fracture, an advance treatise. Vol 2*, chapter Mathematical analysis in the mechanics of fracture, pages 192–311. Associated Press, New York, USA.
- Stringfellow, R. G. and Freund, L. B. (1993). The effect of interfacial friction on the buckle-driven spontaneous delamination of a compressed thin film. *International Journal of Solids and Structures*, 30(10):1379–1395.
- Sun, X. and Davidson, B. D. (2006). Numerical evaluation of the effects of friction and geometric nonlinearities on the energy release rate in three- and four-point bend end-notched flexure tests. *Engineering Fracture Mechanics*, 73(10):1343–1361.
- Turon, A. (2006). *Simulation of delamination in composites under quasi-static and fatigue loading using cohesive zone models*. PhD thesis, Departament d'Enginyeria Mecànica i de la Construcció Industrial – Universitat de Girona. Directors: Pedro P. Camanho and Josep Costa.
- Turon, A., Camanho, P. P., Costa, J., and Dávila, C. G. (2006). A damage model for the simulation of delamination in advanced composites under variable-mode loading. *Mechanics of Materials*, 38(11):1072–1089.
- Turon, A., Camanho, P. P., and Dávila, C. G. (2004). An interface damage model for the simulation of delamination under variable-mode ratio in composite materials. Technical Report TM-2004-213277, NASA.
- Turon, A., Dávila, C. G., Camanho, P. P., and Costa, J. (2007). An engineering solution for mesh size effects in the simulation of delamination using cohesive zone models. *Engineering Fracture Mechanics*, 74(10):1665–1682.
- Zienkiewicz, O. C. and Taylor, L. R. (1991). *The finite element method*. McGraw–Hill Book Company, London, UK.

Chapter 4

Compression Strength of Composite Materials

4.1 Introduction

The failure criteria of long fibre composites subjected to compressive forces can be due to two main reasons, fibre buckling and/or composite delamination (Welsh and Adams, 1997). Regarding the fibre buckling phenomenon, first studies correspond to Rosen (1965) who defined two different buckling modes and the compression stress at which this buckling occurs; this expression depends on matrix shear strength and on the volumetric participation of fibres in the composite. Rosen initial formulation lead to new studies which tried to predict with more accuracy the composite critical compression stress due to fibre buckling. Of those, its worth to mention the works of Barbero and Tomblin (1996), Balacó de Morais and Torres Marques (1997) and Drapier et al. (1999). The models proposed by these authors are based on energetic equilibriums between the composite components, these equilibriums lead to a final expression of the maximum compression stress that can be applied to the composite. It is also interesting the scope used by Parnes and Chiskis (2002) or Kosker and Akbarov (2003); in both cases the fibre buckling problem is solved studying the compatibility between the strain–stress state of fibre and matrix materials.

The expressions found in all models agree in the dependence of the critical compression stress on three main parameters:

1. Matrix shear strength
2. Fibre initial misalignment
3. Proportion between fibre and matrix in the composite

Thus, the limit compression stress of these new formulations depends on the same parameters pointed out by Rosen and on a new one: fibre initial misalignments. It can be concluded that any formulation regarding fibre micro–buckling must take into account fibre initial misalignments to predict accurately composite compression limit stress.

According to Jochum and Grandidier (2004), fibre misalignments are produced in the composite manufacturing process, during the matrix curing. These misalignments are regular in frequency and amplitude along the whole fibre length and can be represented by a sinusoidal shape. Figure 4.1 shows a photograph of the misalignments found in a carbon fibre embedded in an epoxy matrix.

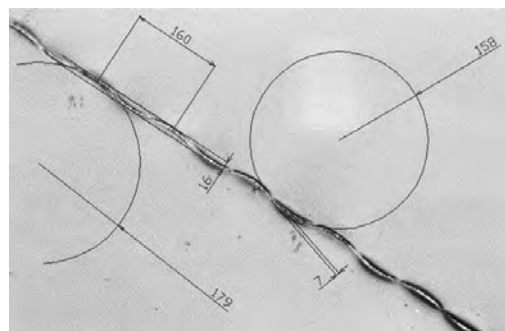


Fig. 2. Example of microbuckling measurements (in micrometers) done on a T300 carbon fibre inside of an LY556 epoxy matrix.

Figure 4.1: Initial fibre misalignments (Jochum and Grandidier, 2004)

There are two main problems in all known formulations developed to obtain the compression strength of the composite. The first one is that most of them only provide an expression to obtain the maximum stress can be applied to the composite before fiber buckling occurs. However, in a structural problem, a local failure does not imply the total failure of the structure, being necessary to know the post-critical behavior of the material to continue the simulation, in order to obtain the global structure performance.

The second problem appears because the composite is treated as a single material with average properties from its constituents. A formulation based only in the composite, forces to pre-define the constitutive performance of the composite constituents in order to obtain the expressions that will provide the critical buckling strength of the material. In example, Drapier et al. (1999) consider that the fibers are an elastic material and the matrix is modeled with a J2 law. Thus, the application range of the formulation developed is reduced to those composites which constituents have an specific constitutive performance, being necessary to reformulate the whole problem if a different constitutive law is required.

These two problems: impossibility to obtain the post-critical strength of the composite and pre-defined constitutive behavior of the composite components, can be solved simulating the composite material with the serial/parallel mixing theory developed by Rastellini et al. (2007) and described in chapter 2. This theory can be understood as a constitutive equations manager that obtains the composite constitutive performance by combining the mechanical behavior of its different constituents. Therefore, the main aim of this chapter is to develop a compression strength formulation to be included in the serial/parallel mixing theory and capable of taking advantage of all the benefits provided this theory. A first attempt to include the fiber buckling phenomenon in the mixing theory has been already made by Puig et al. (2001), with promising results.

The fiber buckling phenomenon is included into the serial/parallel mixing theory by modifying the constitutive performance of the composite constituent materials (fiber and matrix) according to the micro-structural interaction that exist between them. The modification of the constitutive performance of both components is made using an homogenization method (Sánchez-Palencia, 1987; Oller et al., 2005).

Homogenization methods deal with the global problem of composite material in a two scale context. The macroscopic scale works with the composite material to obtain the global structural response; composites are treated as homogeneous materials in this scale. The microscopic scale corresponds to an elemental characteristic volume in which the microscopic fields inside the composite are obtained, this scale works with the component materials of the composite, studying the behavior of a Representative Volume Element (RVE). Homogenization theory assumes a periodical repetition of the RVE in the composite material to relate these two scales.

The study of the fibre buckling problem using an homogenization method would consist on obtaining the composite performance by solving an RVE with a finite element model of the fibre-matrix system, using a large displacement theory to obtain the moment in which fibre buckles, and taking into account the initial fibre misalignments. Figure 4.2 shows a possible finite element model of the RVE. Results obtained from this model would be extrapolated to the composite to solve the structural problem.

However, homogenization methods are unaffordable to be used nowadays due to their computational cost: obtaining the response of a real structure with this methods implies solving a complex finite element model for each point in which the structure is discretized. Thus all efforts are focused on the study of the structural performance of RVE's (González and Llorca,

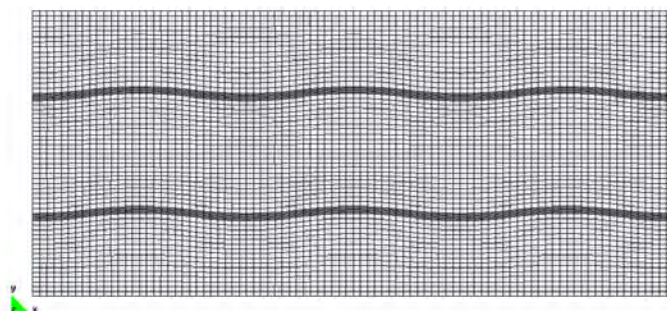


Figure 4.2: Finite element model of a RVE that takes into account fibre initial misalignments

2007) or on how the information can be transferred from the micro-scale to the macro-scale (Zalamea, 2001; Car et al., 2002). To improve the computational efficiency of the formulation developed, the RVE shown in figure 4.2, is simplified to an unidirectional case using the existing analogy between the micro-structural performance of the RVE and a Curved Bar under unilateral Elastic Restrain (CuBER problem, figure 4.3). It will be shown that this simplification makes a significant reduction on the computational cost without reducing the amount of information obtained, neither the accuracy of it.

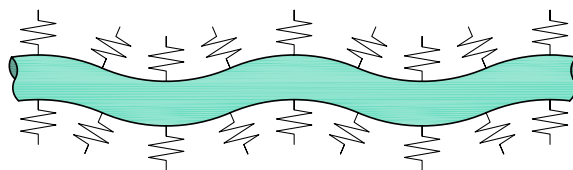


Figure 4.3: Problem of a curved bar under unilateral elastic restriction (CuBER problem)

The homogenization method used consist in transforming the structural solution provided by the CuBER problem, characterizing the interaction between fiber and matrix, into some parameters to be included in the constitutive equations of both components of the composite: fibre and matrix. Thus, what is homogenized is not the composite but its constituents performance. Once having a modified constitutive behavior of the composite constituents, the serial/parallel mixing theory can be used to obtain a composite performance that will take into account the micro-structural interaction of fibre and matrix due to fibre initial misalignments. It will be shown that the new constitutive performance of both materials, together with the mixing theory formulation, is capable to simulate the fiber buckling phenomenon and, thus, to obtain the critical compression stress of the composite and its post-critical behavior. Also, the formulation developed establishes a direct relation between the compression capacity of the composite and the three main parameters defined in literature to obtain this final compression strength: fibre initial misalignments, matrix shear strength and proportion between fibre and matrix in the composite.

The new homogenized constitutive equations are included in an algorithm that do not only provides the compression strength of composite materials made of long fibers with initial misalignments but goes a step further, taking into account all possible situations that can be found in the numerical simulation of structures. The algorithm takes into account the direction of the stresses applied to the fibers: compression or tension, and is capable to obtain the composite performance when it is unloaded. Also, the algorithm provides a solution to the case in which fiber initial misalignments are too small to affect the composite performance, in this case the buckling formulation of a straight bar is applied to obtain the constitutive

performance of the composite components.

This chapter is structured as follows. Section 4.2 contains a brief state of the art of the different theories and formulations existing nowadays to obtain the compression strength of composite materials. Afterwards, in section 4.3 is described the formulation required to solve the CuBER problem, as well as the methodology used to transform the structural performance of this problem into two homogenized constitutive laws, one for the fibre and the other for the matrix. These modified constitutive laws are used by the mixing theory. The validation of the new homogenized constitutive equations is shown in section 4.4. In this section the results obtained with the new formulation are compared with the results that are obtained from a micro-model of the RVE cell considered. Once having proved the correct performance of the methodology proposed, section 4.5 defines the algorithm used to implement, in a finite element code, the effect of fiber buckling to reduce the compression strength of composite materials. This algorithm includes the homogenized constitutive equations for matrix and fiber in the serial/parallel mixing theory, taking into account the different loading cases that can be found in the composite as well as the level of fiber misalignment in the composite. The validation of the algorithm proposed to obtain the compression strength of composite materials is described in section 4.6. This validation compares the numerical results with experimental data existing in literature and includes a numerical example in which a composite structure is solved with the new formulation developed. Finally, section 4.7 includes the conclusions obtained from the formulation described and validations performed in this chapter.

4.2 Compression strength of composite materials

Since the first investigation made by Rosen (1965), many authors have studied the problem of long fiber composites under compression efforts. These studies have lead to different formulations that provide an approximation to the maximum compression stress that can be applied to the composite. The present section summarizes the most relevant formulations found in literature dealing with the problem of compression strength in long fiber composites, due to the fiber buckling phenomenon.

4.2.1 Rosen model

The first known study in which the compression strength of long fiber composites was related to the fiber buckling problem corresponds to Rosen (1965). This study has been summarized by Jones (1999). To obtain the compression strength of the composite, Rosen considered the fiber as a column on an elastic foundation. With this model in mind, two different buckling modes were defined: extensional and shear buckling (see figure 4.4).

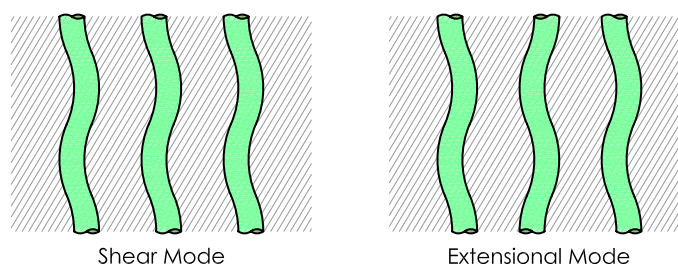


Figure 4.4: Shear and extensional buckling modes defined by Rosen (1965)

To obtain the compression strength of the composite Rosen defined a two dimensional model in which fibers are considered plates infinitely wide. With this assumption, the Timoshenko and Gere (1961) energy method was applied to obtain the buckling load of the plate considering m transversal restrictions along its length. Minimizing the resulting expression in function of m , the equations obtained to compute the composite maximum compression stress are, for each buckling mode:

Extensional mode:

$$\sigma_{c, \max} = 2 \left[V_f + (1 - V_f) \frac{E_m}{E_f} \right] \sqrt{\frac{V_f E_m E_f}{3(1 - V_f)}} \quad (4.1)$$

Being V_f the fiber volumetric participation and E_m and E_f the matrix and fiber elastic modulus, respectively. This equation considers an iso-strain condition in fiber direction. If $E_m \ll E_f$, it can be considered that matrix stresses are nearly zero and expression 4.1 can be simplified to:

$$\sigma_{c, \max} = 2V_f \sqrt{\frac{V_f E_m E_f}{3(1 - V_f)}} \quad (4.2)$$

Shear mode:

$$\sigma_{c, \max} = \frac{G_m}{1 - V_f} \quad (4.3)$$

Where G_m is the shear stiffness of matrix material.

The buckling mode that will lead to the failure of the composite depends on the volume content of fiber in the composite. The plot of the results obtained with expressions 4.1 and 4.3 in function of the fiber volumetric participation for an E-Glass composite, is displayed in figure 4.5. This figure shows that for fiber volume contents lower than 0.18 the buckling mode that will lead to the composite failure is the extensional mode and, for fiber contents larger than 0.18, the maximum compression strength is produced by the shear mode.

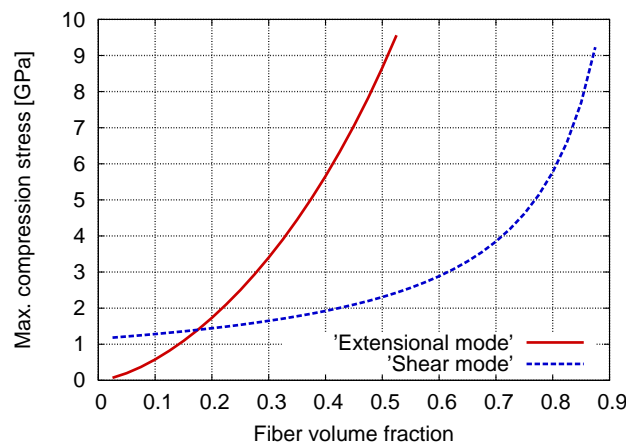


Figure 4.5: Maximum compression stress that can be applied to an E-Glass composite using Rosen's formulation

The most known expression known of the Rosen model corresponds to the maximum compression of the composite due to shear buckling (equation 4.3). This is because the fiber volume content in the most commonly used composites, is in the range of 50 – 60%. Therefore,

according to figure 4.5, the failure in the most commonly used composites will be produced by shear buckling.

Following the same idea used by Rosen to formulate his model, Lo-Chim and Xu-Reifsnider developed two different models that try to improve Rosen's one. Hereafter are both of them briefly explained.

Lo-Chim model

The model proposed by these authors follows the same procedure used by Rosen but reduce the number of assumptions. They add a term, during the derivation of the result, to account for unknown boundary conditions. This term is obtained by fitting the model to the experimental results. Therefore, the equation proposed to obtain the compression strength of the composite is (Lo and Chim, 1992):

$$\sigma_{c, \max} = \frac{G_{12}}{1.5 + 12 \left(\frac{6}{\pi}\right)^2 \left(\frac{G_{12}}{E_{11}}\right)} \quad (4.4)$$

where the variables G_{12} and E_{11} are obtained using the elastic mechanical parameters of fiber and matrix and their volumetric participation in the composite.

Xu-Reifsnider model

The model proposed by Xu and Reifsnider (1993) replace the Timoshenko beam formulation used to obtain the compression strength of a column by the problem of a column embedded in an elastic foundation. With this substitution, the expression obtained by these authors to characterize the maximum strength that can be applied to the composite becomes:

$$\sigma_{c, \max} = G_m \left[V_f + \frac{E_m}{E_f} (1 - V_f) \right] \left(2(1 + \nu_m) \sqrt{\frac{\pi \sqrt{\pi} \eta r_f}{3 \left(\frac{E_m}{E_f}\right) \left(V_f \frac{E_m}{E_f} + 1 - V_f\right) (1 + V_f \nu_f + \nu_m (1 - V_f))}} + 1 - \xi - \frac{\sin \pi \xi}{2\pi} \right) \quad (4.5)$$

From the first model developed by Rosen, and the updates proposed by Lo-Chim and Xu-Reifsnider, different authors have studied the fiber buckling problem in composites obtaining more accurate expressions to compute the maximum compression strength that can be applied to the composite. All new formulations maintain the dependence of fiber buckling in fiber volume fraction and matrix shear stiffness but they do also introduce a new parameter in the equation: fiber initial misalignments.

4.2.2 Fiber initial misalignments

The effect of fiber initial imperfections on the compression performance of long fiber composites has been assumed and proved by all authors studying the problem. Therefore, the measurement of fiber initial misalignments appears essential to obtain an accurate prediction of the compression strength of the composite (Jochum and Grandidier, 2004).

Yurgartis (1987) developed an optical technique which consist on cutting the composite at an angle and measuring the major axis of the ellipse formed by the intersection of a cylindrical fiber with the cutting plane. The determination of the cutting angle was made assuming a symmetric distribution of fiber misalignment. This technique has been refined afterwards by Barbero and Tomblin (1996), which accurately measured the angle of cut by measuring the major and minor axes of the ellipse formed by the rod specimen.

A first attempt to obtain a three dimensional measurement of fiber initial misalignments was made by Paluch (1996) by taking a stack of sections of the composite and matching the fibers found in each XY image of each section. From this first attempt, Clarke et al. (1995) developed a new technique in which the three dimensional spatial distribution of fiber misalignments could be obtained. This technique uses a confocal laser scanning microscope (CLSM) to obtain the each fiber position along the Z axis of the sample. The main advantage of using a CLSM is that the data acquisition is non-destructive, therefore the composite does not have to be cut at different Z sections, being more easy to correlate the fiber position between sections.

Finally, its worth to mention the work made by Jochum and Grandidier (2004). These authors made several single fiber specimens of a Torray T300 carbon fiber embedded in an epoxy matrix. The apparition of initial fiber misalignments where recorded during the curing process using an optical microscope, thanks to the transparency of the matrix. These authors propose an elastic microbuckling model to explain the apparition of fiber initial misalignments during the curing process of the composite.

4.2.3 Barbero and Tomblin model

Being aware of the importance of fiber initial misalignments in the compression performance of composite materials, Barbero and Tomblin (1996); Tomblin et al. (1997); Barbero (1998), developed a formulation, based on continuous damage mechanics, to predict the compression strength of composite materials taking into account fiber initial imperfections.

The model developed is based in the following hypothesis: (a) Matrix shear stiffness is non-linear and can be characterized by an hyperbolic tangent function. (b) Fiber misalignments in the composite follow a Gaussian distribution. Taking into account these two hypothesis, the relation between the buckling stress in the composite and the fiber imperfection is obtained using the principle of total potential energy. The final expression obtained to calculate the critical compression stress in the composite is (Barbero, 1998):

$$\sigma(\alpha, \gamma) = \frac{\tau_u}{2(\gamma + \alpha)} \frac{(\sqrt{2} - 1)(e^{\sqrt{2}g} - e^{2g}) + (\sqrt{2} + 1)(e^{(2+\sqrt{2})g} - 1)}{1 + e^{2g} + e^{\sqrt{2}g} + e^{(2+\sqrt{2})g}} \quad (4.6)$$

With $g = \gamma G_{LT} / \tau_u$. And being τ_u the maximum shear strength of matrix material, G_{LT} the matrix shear stiffness (defined by an hyperbolic tangent function), γ the shear strain in the composite and α the misalignment angle of fibers.

Expression 4.6 provides the maximum compression strength that can be applied to the composite considering that fibers have a misalignment angle α . Once having this expression, a continuum damage model is applied to the compression stress of the composite to obtain the composite performance. Therefore,

$$\sigma_C = \sigma(\alpha)[1 - \omega(\alpha)] \quad (4.7)$$

Where $\omega(\alpha)$ is the area of buckled fibers per unit of initial fiber area. The area of buckled fibers is proportional to the area under the normal distribution located beyond the misalignment angle $\pm\alpha$, and it can be computed as:

$$\omega(\alpha) = 2 \int_{\alpha}^{\infty} f(\alpha') d\alpha' \quad (4.8)$$

with $f(\alpha)$ the probability density of the normal distribution.

Thus, the model developed by Barbero and Tomblin not only provides the maximum compression strength that can be applied to the composite before fiber buckling (for a given misalignment angle, equation 4.6), but also provides the stress evolution of the composite. This stress evolution depends on the number of fibers that have buckled; fibers with large misalignments will buckle for lower loads. This last equation is important because there are few models that provide the post-critical performance of the composite once the maximum compression stress has been reached.

4.2.4 Balacó de Morais model

Another approximation to the compression strength of composite materials due to fiber microbuckling is the one provided by Balacó de Morais (Balacó de Morais, 1996; Balacó de Morais and Torres Marques, 1997; Balacó de Morais, 2000). This author considers that fiber misalignments have a sinusoidal shape and assumes a shear buckling mode of the fibers. The compression strength is derived from the variational principle of the minimum potential energy of the system, which is defined as:

$$\Pi = U_f + U_m - W \quad (4.9)$$

Being U_f the fiber bending strain energy, U_m the matrix shear strain energy and W the work done by the compression load. To obtain the shear strain energy of matrix material a Drucker-Prager yield model has been considered. The work done by the compression load is obtained using a large displacement formulation.

Once having defined all parameters of equation 4.9, the minimum potential energy equation is numerically solved for successive increments of the stress acting on the fiber, to obtain the lamina compression strength:

$$\sigma_L = V_f \sigma_f + (1 - V_f) \sigma_m \quad (4.10)$$

The main problem with this approach is that it is computationally very expensive. To solve this inconvenience, the model is simplified to a linear formulation (Balacó de Morais, 2000).

The new model assumes small displacements to compute the work done by the compression load, matrix strain energy is obtained considering linear elasticity and fiber strain energy is neglected. With these assumptions, a fourth order polynomial equation is obtained that provides the compression strength of the composite.

A further simplification is made with the consideration that if fibers are considerably stiffer than matrix, when matrix fails, matrix compression stress is much smaller than the compression yield stress and thus negligible. This assumption leads to a close form expression in which the composite compression strength is obtained as:

$$\sigma_C = \frac{\tau_{um}}{\theta_0 + \frac{1-V_f}{1+V_f} \frac{\tau_{um}}{G_m}} \quad (4.11)$$

Being, τ_{um} the maximum shear stress that can take the matrix, θ_0 the initial fiber misalignment angle and G_m the matrix shear stiffness. According to Balacó de Morais (2000), this expression works well with composites made with stiff fibers such as Kevlar or Carbon but loses its accuracy with less stiff fibers as E-Glass.

4.2.5 Drapier model

An interesting approach to obtain the compression strength of composite materials is the one developed by Drapier et al. (1999, 2001), who solves the fiber microbuckling problem in a two scale context. The displacement field is formulated taking into account the meso-displacements of the structure and the micro-displacements obtained due to fiber initial misalignments. Therefore, the displacement is written as,

$$u(x) = u_G(x) + u_L(x) \quad (4.12)$$

being u_G the displacement related to the structural scale, which is modulated by the u_L , the displacement at the ply scale.

With this scope, an specific finite element is developed which formulation is obtained by coupling the equilibrium in both scales, which is defined using the principle of virtual work. The micro scale equilibrium takes into account fiber bending stiffness.

In this formulation, fibers are considered elastic. Thus, the composite failure is obtained by the failure of matrix material (simulated with a J2 model), produced by the efforts obtained from the micro and the meso scales.

The results obtained with the proposed model provide a good agreement with theoretical and experimental data. The model developed can also take into account the stacking sequence, stiffness effects and the type of loading and boundary conditions.

4.2.6 Other authors dealing with the problem. Structural models

Another scope used to solve the problem, different of all the formulations shown above, is the one used by Parnes and Chiskis (2002) or Akbarov and Kosker (2001); Kosker and Akbarov (2003). In both cases the problem is solved studying the structural compatibility between fibre and matrix stress-strain fields.

Parnes and Chiskis use the Euler-Bernoulli beam equations and consider fibres as a bar embedded in an elastic foundation. According to the authors, the formulation obtained can be used for composites with low fiber content or in composites in which fibers have an infinite wave-length.

On the other hand, the solution of Akbarov and Kosker follow the path defined by Guz and Lapusta (1999), based on using the three dimensional linearized equations of stability and the model of a piecewise uniform medium. The matrix (uniform medium) is simulated with a viscoelastic model. The formulation developed obtains the time required to buckle the fibers when a uniform pressure is applied to the composite. Fiber buckling is considered to occur when its initial imperfection starts growing indefinitely.

4.2.7 Puig and Oller model

The model developed by Puig and Oller (Puig, 2001; Puig et al., 2001, 2002) to obtain the compression strength of composite materials due to fiber buckling can be considered the point of departure for the formulation that is presented in this chapter.

These authors deal with the compression strength problem using a continuum mechanics approach and obtaining the constitutive performance of the composite using the mixing theory. Up to this point, all authors studying the fiber microbuckling problem obtain expressions that provide the maximum compression stress that can be applied to the composite, which is treated as a single material. These formulations cannot provide solutions for composites in which its constituent materials show a non-linear behavior and, when non-linearities are considered, fibers are defined as elastic materials and the non-linearities are introduced in matrix, that is simulated with a pre-defined constitutive model that cannot be modified without modifying the formulation developed.

Therefore, the main advantage of the model proposed by Puig and Oller is that, using the mixing theory, composite constituents can be simulated with any existing constitutive model. This increases the applicability of the formulation developed, being possible to use it for simulating any possible composite in which the compression strength due to fiber buckling has to be taken into account.

The formulation proposed by these two authors is based in a modification of the isotropic damage model defined by Kachanov (Kachanov, 1986; Oliver et al., 1990), introducing a new internal variable related to the fiber buckling phenomenon. Therefore,

$$\sigma = (1 - d_f)(1 - d_p)\mathbb{C} : \varepsilon \quad (4.13)$$

Being \mathbb{C} the composite constitutive tensor, d_f the mechanical damage parameter and d_p the buckling damage parameter. The expression for this last parameter is:

$$d_p = f_1(\text{fibre})f_2(\text{matrix}) \quad (4.14)$$

Where $f_1(\text{fibre})$ is a function that depends on fibre buckling stress and $f_2(\text{matrix})$ is the matrix damage parameter. Function f_1 is obtained from the critical Euler load that can be applied to a column. Its final expression is (Oller, 2003):

$$f_1(\text{fibre}) = \left(\frac{4l}{n\pi d} \right)^2 \varepsilon \quad (4.15)$$

Being l the length of the fiber, which is a parameter required by the formulation, n the buckling mode, d the fiber diameter and ε the longitudinal strain of fiber material. The buckling mode that will lead to fiber buckling is computed as:

$$n = \frac{4l}{\pi d} \sqrt{\varepsilon} \quad (4.16)$$

Although the model developed by Puig and Oller provides a good numerical performance, it fails in not considering important parameters related to the fiber microbuckling problem such as fiber initial misalignments. Also, the buckling stress of fiber material is obtained without considering the restraint provided by matrix. This restraint effect is introduced afterwards, with the f_2 function.

4.3 Homogenized constitutive equations. CuBER problem

This section provides the procedure and formulation used to include the effects of fiber misalignments and the interaction between fiber and matrix in the constitutive equations of both composite components. This is done homogenizing the constitutive equations of fiber and matrix using the results obtained from the solution of a representative volume element (RVE) of an initially misaligned fiber embedded in a matrix. The solution of the RVE is obtained using the existing analogy with the problem of a curved bar under unilateral restriction (CuBER problem).

This section includes a description of the problem to be solved and the formulation used to solve it, as well as the boundary conditions and the parameters required from the composite to obtain this solution. Afterwards the procedure used to homogenize the constitutive equations of fiber and matrix materials, using the results obtained from the CuBER formulation, is described.

4.3.1 Representative Volume Element to solve the fibre buckling problem

According to the different authors that have studied the problem, a micro-model able to simulate the fibre buckling phenomenon must take into account fibre initial misalignments, the proportion of fibre and matrix in the composite and matrix shear strength. A representative volume element, depending on these three parameters, can be the one shown in figure 4.6. This figure shows also, in dashed lines, the final position of that would be expected in fibres after applying the compression force to the composite.

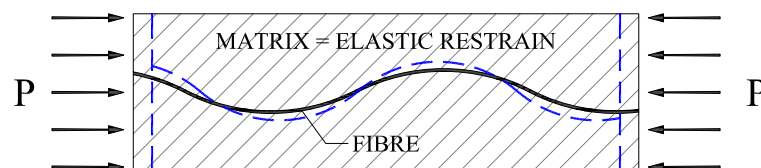


Figure 4.6: Fibre-matrix system. Fibre behaviour when the composite is compressed

The performance that is obtained from fibre and matrix materials when solving the RVE shown in figure 4.6 must be translated to constitutive properties in order to include them in

a mixing theory formulation. Figure 4.6 shows that when the composite is compressed, fibre initial misalignments tends to increase due to fibre structural deformation. This deformation is restrained by matrix material. Thus, the constitutive performance expected in each material is:

Fibre: Its structural stiffness is reduced due to its original misalignment: for a fixed value of compression force P , fibre longitudinal strain is increased due to its structural deformation. This structural deformation depends on matrix elastic restraint

Matrix: Stresses in it are increased due to the restriction made over fibre movement. These stresses correspond to shear stresses and transversal stresses. Both components are found in the serial direction of the composite.

It will be shown that these two performances can be obtained also by solving a simplified unidirectional model consisting in a curved bar under unilateral elastic restraint (CuBER), like the one shown in figure 4.7. The solution to the structure shown in this figure has already been used by other authors to solve similar problems. Naik et al. (2003) used it to study weave fabric composites and Wang and Shenoi (2004) to study curved sandwich beams.

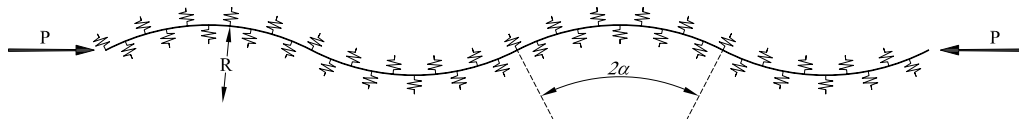


Figure 4.7: Curved bar under unilateral elastic restraint problem

4.3.2 CuBER equations

The problem of a curved bar under unilateral elastic restraint was first formulated and solved by Hetényi (1971). Figure 4.8 shows the geometry considered.

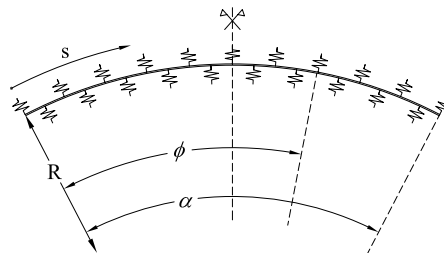


Figure 4.8: Geometry of the bar to be considered in the CuBER problem

The hypothesis in which the curved bar under unilateral restriction problem is solved are the following:

1. All components defining the problem, the bar and the foundation in which it is supported, have an elastic behavior.
2. The the axis of the bar is contained in an arch of a circle of radius R . The arch length is defined by its internal angle α (figure 4.8).

3. The reaction forces of the foundation are proportional to the radial deflection of the bar.
4. The deformation of the bar due to normal stresses is negligible.

According to the hypothesis exposed, the elastic restraint of the bar can be idealized as a continuous spring which produces a radial load in the bar, proportional to its radial displacement:

$$q = k \omega \quad (4.17)$$

Being q the radial load produced by the elastic restriction over the bar, ω the bar radial displacement and k the elastic restraint.

The equations describing the bar behavior are obtained studying an infinitesimal section of the bar, such the one displayed in figure 4.8, in which acts a normal force N , a shear force Q and a bending moment M . These are displayed in figure 4.9.

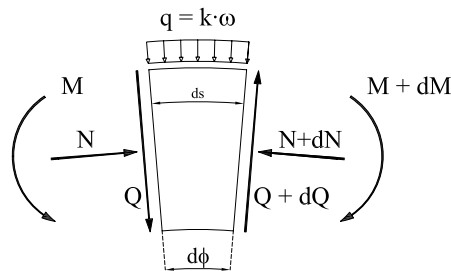


Figure 4.9: Forces acting on an infinitesimal section of the curved bar

The study of the equilibrium of forces in the beam infinitesimal section lead to three different equilibrium equations. The equilibrium equation in the radial direction can be written as:

$$qds - Nd\phi = dQ \quad (4.18)$$

The equilibrium equation in the tangential direction is:

$$Qd\phi = dN \quad (4.19)$$

And the momentum equilibrium equation is written as:

$$QRd\phi = dM \quad (4.20)$$

Neglecting the axial deformation of the bar due to the normal force N (hypothesis 4), the differential bending equation of a circular arch of radius of curvature R and flexural rigidity EI is, according to Hetényi (1971),

$$EI \left(\frac{d^2\omega}{ds^2} - \frac{\omega}{R^2} \right) = -M \quad (4.21)$$

Rearranging equations 4.18 to 4.21, the bar displacement in its radial direction is defined by the differential equation:

$$\frac{d^5\omega}{d\phi^5} + 2\frac{d^3\omega}{d\phi^3} + \eta^2\frac{d\omega}{d\phi} = 0 \quad (4.22)$$

where

$$\eta = \sqrt{\frac{R^4 \cdot k}{EI} + 1} \quad (4.23)$$

The general solution for equation 4.22 is:

$$\begin{aligned} \omega(\phi) = & C_0 + [C_1 \cosh(\eta_1\phi) + C_2 \sinh(\eta_1\phi)] \cos(\eta_2\phi) + \\ & + [C_3 \cosh(\eta_1\phi) + C_4 \sinh(\eta_1\phi)] \sin(\eta_2\phi) \end{aligned} \quad (4.24)$$

Being C_0, C_1, C_2, C_3, C_4 the integration constants of the differential equation, which value is obtained when imposing the boundary conditions of the problem; and η_1 and η_2 :

$$\eta_1 = \sqrt{\frac{\eta - 1}{2}} \quad \eta_2 = \sqrt{\frac{\eta + 1}{2}} \quad (4.25)$$

Once having obtained the general expression for beam displacement, equations 4.18 to 4.21 can be derived to obtain the general expressions for the bending moment, the shear force and the normal force in the bar. These are:

$$\begin{aligned} M(\phi) = & -\frac{EI}{R^2} \{ C_0 - 2\eta_1\eta_2 [\{ C_1 \sinh(\eta_1\phi) + C_2 \cosh(\eta_1\phi) \} \sin(\eta_2\phi) + \\ & + 2\eta_1\eta_2 [\{ C_3 \sinh(\eta_1\phi) + C_4 \cosh(\eta_1\phi) \} \cos(\eta_2\phi)] \} \\ Q(\phi) = & -\frac{EI}{R^3} 2\eta_1\eta_2 \{ + [(\eta_1 C_1 + \eta_2 C_4) \cosh(\eta_1\phi) + (\eta_1 C_2 + \eta_2 C_3) \sinh(\eta_1\phi)] \sin(\eta_2\phi) + \\ & + [(\eta_2 C_1 - \eta_1 C_4) \sinh(\eta_1\phi) + (\eta_2 C_2 - \eta_1 C_3) \cosh(\eta_1\phi)] \cos(\eta_2\phi) \} \\ N(\phi) = & RkC_0 + \frac{EI}{R^3} 2\eta_1\eta_2 \{ + [C_1 \sinh(\eta_1\phi) + C_2 \cosh(\eta_1\phi)] \sin(\eta_2\phi) - \\ & - [C_3 \sinh(\eta_1\phi) + C_4 \cosh(\eta_1\phi)] \cos(\eta_2\phi) \} \end{aligned} \quad (4.26)$$

These equations can be simplified using the arch symmetry shown in figure 4.8. Defining the axis of symmetry as the origin of ϕ angle, it can be easily verified that in this axis the following boundary conditions must be fulfilled:

$$\left. \frac{d\omega}{d\phi} \right|_{\phi=0} = 0 \quad \text{and} \quad Q(\phi=0) = 0 \quad (4.27)$$

The result of applying these two conditions to the previous equations is that the integration constants C_2 and C_3 disappear and equations 4.24 and 4.26 become:

$$\begin{aligned}
\omega(\phi) &= C_0 + C_1 \cosh(\eta_1 \phi) \cos(\eta_2 \phi) + C_4 \sinh(\eta_1 \phi) \sin(\eta_2 \phi) \\
M(\phi) &= -\frac{EI}{R^2} \{C_0 - 2\eta_1 \eta_2 [C_1 \sinh(\eta_1 \phi) \sin(\eta_2 \phi) - C_4 \cosh(\eta_1 \phi) \cos(\eta_2 \phi)]\} \\
Q(\phi) &= -\frac{EI}{R^3} 2\eta_1 \eta_2 \{(\eta_1 C_1 + \eta_2 C_4) \cosh(\eta_1 \phi) \sin(\eta_2 \phi) + (\eta_2 C_1 - \eta_1 C_4) \sinh(\eta_1 \phi) \cos(\eta_2 \phi)\} \\
N(\phi) &= RkC_0 + \frac{EI}{R^3} 2\eta_1 \eta_2 \{C_1 \sinh(\eta_1 \phi) \sin(\eta_2 \phi) - C_4 \cosh(\eta_1 \phi) \cos(\eta_2 \phi)\}
\end{aligned} \tag{4.28}$$

The final expression for the bar radial displacement ω as well as for the bar efforts (M , Q and N) depends on the value of the integration constants: C_0 , C_1 and C_4 . Their value will be determined applying to the problem three more boundary conditions.

According to Hetényi (1971), the angular deflection of the beam can be obtained as the integral of the elementary rotations M/EI along the bar. If this integral starts in the axis of symmetry shown in figure 4.8, the initial rotation is zero and the value of the angular deflection becomes:

$$\theta(\phi) = \int_0^S \frac{M(s)}{EI} ds = \int_0^\phi \frac{M(\varphi)}{EI} R d\varphi \tag{4.29}$$

And the vertical and horizontal displacement of the beam can be obtained as,

$$\begin{aligned}
u(\phi) &= u_0 - \int_0^\phi \theta(\varphi) R \sin(\varphi) d\varphi \\
v(\phi) &= v_0 - \int_0^\phi \theta(\varphi) R \cos(\varphi) d\varphi
\end{aligned} \tag{4.30}$$

Including the angle definition (equation 4.29) in equation 4.30, and defining the initial horizontal displacement u_0 equal to zero (as a result of the symmetry existing in the problem), the final expression obtained to calculate the horizontal displacement, for a defined angle ϕ , is:

$$u(\phi) = C_0 (\sin \phi - \phi \cos \phi) - C_1 \Upsilon (\eta_1 I_{211} - \eta_2 I_{121}) + C_4 \Upsilon (\eta_1 I_{121} + \eta_2 I_{211}) \tag{4.31}$$

with,

$$\begin{aligned}
\Upsilon &= \frac{2\eta_1 \eta_2}{\eta_1^2 + \eta_2^2} \\
I_{211} &= \int_0^\phi \cosh(\eta_1 \varphi) \sin(\eta_2 \varphi) \sin \varphi d\varphi \\
I_{121} &= \int_0^\phi \sinh(\eta_1 \varphi) \cos(\eta_2 \varphi) \sin \varphi d\varphi
\end{aligned}$$

To obtain the vertical displacement for any desired angle ϕ first it is necessary to obtain the vertical displacement in the bar for $\phi = 0.0$. This vertical displacement corresponds to the radial displacement of the bar and its value is:

$$\begin{aligned}\omega(\phi = 0) &= C_0 + C_1 \cosh(0.0) \cos(0.0) + C_4 \sinh(0.0) \sin(0.0) \\ &= C_0 + C_1\end{aligned}\quad (4.32)$$

The final expression for the vertical displacement is:

$$v(\phi) = C_0 (\sin \phi - \phi \cos \phi) + C_1 [1 - \Upsilon (\eta_1 I_{212} - \eta_2 I_{122})] + C_4 \Upsilon (\eta_1 I_{122} + \eta_2 I_{212}) \quad (4.33)$$

with,

$$\begin{aligned}I_{212} &= \int_0^\phi \cosh(\eta_1 \varphi) \sin(\eta_2 \varphi) \cos \varphi \, d\varphi \\ I_{122} &= \int_0^\phi \sinh(\eta_1 \varphi) \cos(\eta_2 \varphi) \cos \varphi \, d\varphi\end{aligned}$$

These two bar displacements are related to the radial deflection in the following manner:

$$\omega = u(\phi) \sin(\phi) + v(\phi) \cos(\phi) \quad (4.34)$$

4.3.3 Boundary conditions and solution of the CuBER problem

The final expressions defining the behavior of the CuBER problem require the definition of three boundary conditions, that will allow finding the value of the integration constants C_0 , C_1 and C_4 .

Using all symmetries existing in the geometry shown in figure 4.7, the problem can be simplified to the following one:

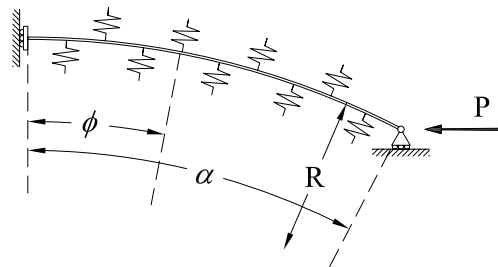


Figure 4.10: Boundary conditions to be applied to the CuBER problem

In which the boundary conditions to be applied are:

$$\begin{aligned}1\text{st BC:} & \quad M(\phi = \alpha) = 0 \\ 2\text{nd BC:} & \quad N(\phi = \alpha) \cos(\alpha) - Q(\phi = \alpha) \sin(\alpha) = P \\ 3\text{rd BC:} & \quad v(\phi = \alpha) = 0\end{aligned}\quad (4.35)$$

When the expressions of M , N , and Q , defined in equation 4.28, and the expression of v , defined in equation 4.33, are included in the boundary conditions defined in equation 4.35, a linear system of three equations with three unknowns, as the following, is obtained:

$$\begin{cases} a_1 C_0 + b_1 C_1 + c_1 C_4 = d_1 \\ a_2 C_0 + b_2 C_1 + c_2 C_4 = d_2 \\ a_3 C_0 + b_3 C_1 + c_3 C_4 = d_3 \end{cases} \quad (4.36)$$

The constants a_i , b_i , c_i and d_i , $i = 1 \div 3$ depend on the fibre misalignment geometry, and the fibre and matrix stiffness. These constants can be easily computed when the misalignment parameters are defined. The linear system shown in equation 4.36 is solved using a factorization method.

After solving the linear system shown in equation 4.36, the value of the integration constants can be added to the different equations described in this section in order to obtain the efforts and displacements of the bar for any desired angle ϕ . The values obtained can be used to include the structural effects provided by the CuBER problem in the constitutive equations of fibre and matrix, so the initial fibre misalignments can be taken into account in the composite constitutive performance.

4.3.4 Definition of the CuBER problem using the composite properties

The formulation described in previous section provides a simplified methodology to solve the RVE that is used to obtain the compression strength of composite materials. This section describes the properties required from the composite in order to define the parameters required by the CuBER problem.

The fibre buckling problem is formulated for composite materials composed by long fibres embedded in a matrix. Thus, the fibre buckling problem will be characterized by the properties of fibre and matrix materials. Most of the fibre reinforced composites used nowadays are composed by multiple layers. These layers can have different fibre orientations. Therefore, the described properties will be required for each layer.

Matrix characteristics

When solving the CuBER problem, matrix is considered an isotropic material. This supposition allows defining the elastic restraint k defined in equation 4.17, as a constant variable with the same value in all space directions.

Even the serial/parallel mixing theory allows considering any kind of material evolution to define the materials that compose the composite, the formulation developed to solve the fibre-buckling phenomenon uses the isotropic damage formulation described in section 3.3 (Oliver et al., 1990; Oller, 2001) to obtain the post-critical performance of matrix material. This formulation provides a damage variable that reduces the real stresses in the material according to the damage existing in it:

$${}^m \sigma = (1 - d)^m \sigma_0 \quad (4.37)$$

Being σ the real stress tensor and σ_0 an effective stress tensor. In an isotropic damage formulation, this relation between stresses is also applied to the stiffness parameters of the material. Therefore, the restraint that will be applied by matrix to the fibre depends on the level of damage existing in the matrix and is computed as:

$$k = (1 - d)k_0 \quad (4.38)$$

Where k_0 corresponds to the initial elastic restraint, which value is defined as the matrix Young Modulus, ${}^m E$, and k is the effective restraint that can be applied in function of the level of damage existing in matrix material.

Although the performance of matrix material has been defined using a damage formulation, in the procedure developed this formulation can be easily replaced by other material evolution laws such as plasticity. In the particular case of a plastic law, the internal variable d used in equation 4.38 must be replaced by κ (with κ the plastic damage variable).

Fibre characteristics

The equations describing the CuBER problem take also in consideration the elastic stiffness of fibre material. Usually, fibre buckling occurs before the material reaches its yield stress, so the initial Young Modulus of fibre will characterize its elastic stiffness. However, in order to take into account possible damages in fibre material (i.e. if a tensile stress is applied to the composite before compressing it), the elastic stiffness used in the CuBER problem for fibre material will be, at every stage of the load process:

$${}^f E = (1 - d) {}^f E_0 \quad (4.39)$$

Being d the fiber damage parameter (if a damage formulation is used to characterize fiber material). As has been already commented with matrix, this parameter can be preplaced by a plastic damage parameter of for any other, depending on the formulation used to simulate this material.

Fibre Misalignments

Fibre misalignments are commonly defined in literature as a sinusoidal form, characterized by its amplitude (A) and wave length (λ). To be able to use the CuBER problem formulation, it is necessary to transform this shape into an arch of circumference. It is considered that both curves are similar enough.

Figure 4.11 shows with a continuous line the original sinusoidal shape and with a dashed line the circumferential arch to be used in the calculations. As can be seen, both geometries are very similar.

Applying the circumferential equation, the radius and the arch angle can be obtained from the amplitude and wavelength values as:

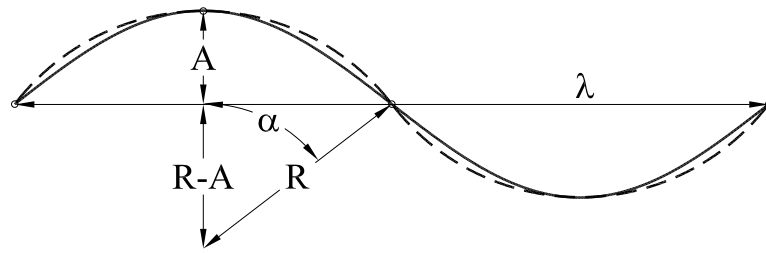


Figure 4.11: Transformation of a sinusoidal shape into a circumferential one

$$R = \frac{A^2 + (\lambda/4)^2}{2A} \quad (4.40)$$

$$\alpha = \arcsin\left(\frac{\lambda}{4R}\right)$$

Non-linear performance of the CuBER problem

As has been described in the hypothesis defined to solve the CuBER problem, one of its main conditions is that all components acting in the problem are considered to be elastic. Thus, when solving the CuBER problem to modify the constitutive laws of fibre and matrix, the behavior expected in both materials is an elastic one. However, both materials are simulated using a damage formulation, which provides a non-linear material behavior.

In order to be able to solve the CuBER problem formulation when any of the composite components reach its elastic yield stress, an explicit incremental approach is used to solve the CuBER equations. This approach is based on the assumption that during a load step, the variation in the stiffness of the composite components is small enough to provide the same results obtained when using a constant stiffness value. The stiffness values considered in each time step for the matrix and the fibre are the ones exposed in equations 4.38 and 4.39, respectively.

Considering correct the assumption that the stiffness variation is negligible in a load step, what must be taken into account is the stiffness variation of both materials along the whole loading process. To do so, an incremental approach is used: At each load step, the fibre misalignment geometry is actualized according to the results obtained when solving the CuBER problem. This procedure requires that the load P , defined in equation 4.35, must be the load increment corresponding to the current load step, and not the total load applied to the element.

Applying this explicit incremental methodology, the fibre misalignments will vary according to the real material properties of the composite components and the linear formulation of the CuBER problem becomes non-linear. Figure 4.13 shows schematically the expected variation of fibre misalignments as the compression load increases in the composite.

4.3.5 Fibre homogenized constitutive equation

The effects of fibre misalignment and its interaction with matrix material, obtained from the solution of the CuBER problem, must be included in the fibre constitutive equation so the

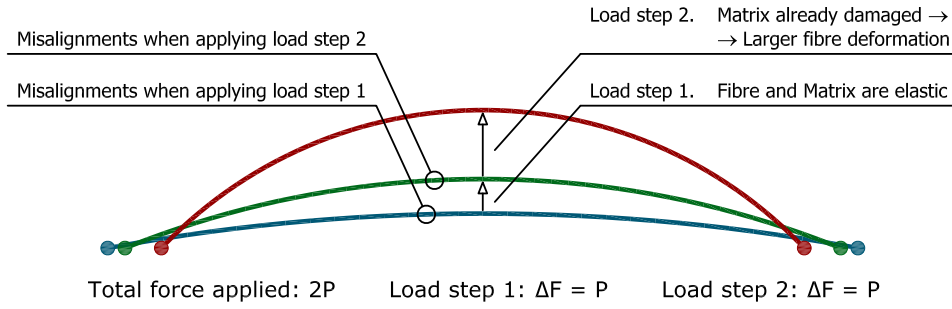


Figure 4.12: Evolution of fibre misalignments in the loading process

serial/parallel mixing theory can take them into account. These effects are applied only to the longitudinal direction of the fibre (or parallel direction) as this is the only component of the strain and stress tensors that is affected by fibre buckling.

The solution of the CuBER problem provides a structural displacement of fibres due to its initial misalignments. To include this effect into the constitutive equation of fibre material, this displacement must be transformed into a strain value. As the CuBER problem does not take into account the normal deformation of the bar due to the compression force (Hetényi, 1971), the total parallel strain in fibre material is divided in two components, a structural strain, $f^s \varepsilon_P$, provided by the CuBER problem and a constitutive strain, $f^c \varepsilon_P$, due to the compression force applied to the composite. Thus, the total parallel strain in the composite, $f \varepsilon_P$, is:

$$f \varepsilon_P = f^c \varepsilon_P + f^s \varepsilon_P \quad (4.41)$$

Equation 4.41 considers a serial distribution of the two mechanical phenomena, constitutive and structural, that take place in the fibre material. Therefore, the effect of fibre misalignment introduces a new structural stiffness to the fibre material, as it is shown in the following diagram:

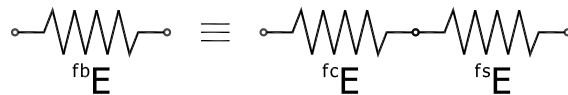


Figure 4.13: Serial coupling of the fibre structural and constitutive stiffness

With the configuration shown in figure 4.13, the new fibre buckling stiffness of fibre material $f^b E$, in its longitudinal direction, can be computed as the serial composition of the fibre constitutive ($f^c E$) and structural ($f^s E$) stiffness.

$$\frac{1}{f^b E} = \frac{1}{f^c E} + \frac{1}{f^s E} \quad (4.42)$$

Where the fibre constitutive stiffness corresponds to the Young Modulus of fibre material in its longitudinal direction, and fibre structural stiffness is obtained from the results provided when solving the CuBER problem.

The new fibre buckling stiffness, $f^b E$, is introduced in the constitutive equation of fibre material using a damage formulation. Thus, a new fibre buckling damage parameter, $f^b d$ is defined as:

$$f^b E = (1 - f^b d) f^c E \quad \rightarrow \quad f^b d = 1 - \frac{f^b E}{f^c E} \quad (4.43)$$

The fiber buckling damage parameter affects the constitutive performance of fibre material as any other damage formulation, with the only difference that the fibre buckling damage is not an isotropic damage but an anisotropic damage: it only affects the longitudinal direction of the stress tensor. Thus, the real stresses in fibre will be obtained from the elastic prediction of the stresses as:

$${}^f \boldsymbol{\sigma} = (I - f^b D) \cdot {}^f \boldsymbol{\sigma}_0 \quad (4.44)$$

with,

$$f^b D = \begin{bmatrix} f^b d & 0 & \dots & 0 \\ 0 & 0 & & 0 \\ \vdots & & \ddots & \vdots \\ 0 & 0 & \dots & 0 \end{bmatrix} \quad (4.45)$$

This definition of the fibre buckling damage matrix is correct considering that the first component of the fibre stress tensor corresponds to the parallel direction. If the parallel component is found in any other position, the fibre buckling damage parameter must be moved to the diagonal term where the stress parallel component is found.

The fiber buckling damage formulation described above can be coupled easily with the constitutive damage formulation used to characterize fiber material. Thus, the final stress in fibre material, when coupling the effects of fibre buckling and the constitutive effects, is:

$${}^f \boldsymbol{\sigma} = (1 - d) \cdot (I - f^b D) \cdot {}^f \boldsymbol{\sigma}_0 \quad (4.46)$$

Being d the damage parameter obtained from the damage constitutive equation applied to the fibre material.

Fibre structural stiffness, ${}^{fs} \mathbf{E}$

The fibre structural stiffness that appears in equation 4.42 is obtained when solving the CuBER problem, from the relation obtained between the force applied as a boundary condition and the displacement obtained as a result of the force applied. As the problem is elastic, the relation between the displacement obtained when solving the CuBER problem and the force applied will be always the same. However, in order to apply a force proportional to the dimensions of the problem, the force P that will be defined as a boundary condition correspond to the force corresponding to the total deformation found in the RVE to be solved. Being the total deformation of the element ${}^f \varepsilon_P$, the stresses in the fibre will be:

$$\boldsymbol{\sigma} = f^c E \cdot {}^f \varepsilon_P \quad (4.47)$$

and, the force in one fibre:

$$P = \sigma \cdot A_{fib} \quad (4.48)$$

Being, A_{fib} the area of one fibre of the composite. The force computed with this procedure will be applied to the CuBER problem to obtain a longitudinal displacement of the fibre, $u(\phi = \alpha)$ (see figure 4.10). This displacement can be transformed into a strain dividing by the total length of the bar considered in the CuBER problem which, according to figure 4.10, corresponds to one quarter of the wave-length defined as a misalignment property. This is:

$$\varepsilon = \frac{u(\phi = \alpha)}{0.25\lambda} \quad (4.49)$$

The structural stiffness can be computed from the strain stress relation:

$$f^s E = \frac{\sigma}{\varepsilon} = \frac{P}{A_{fib}} \frac{0.25\lambda}{u(\phi = \alpha)} \quad (4.50)$$

Equation 4.50 shows that the structural stiffness varies in function of the relation between P and u , which depends of fibre initial misalignments and the matrix stiffness. This relation will remain constant while these both parameters remain constant but, as soon as fibre misalignments suffer a large variation or matrix stiffness is reduced, the structural stiffness will vary, modifying also the constitutive performance of fibre in the composite.

Once having the structural stiffness due to fibre misalignments, the real structural deformation can be computed using equations 4.41 and 4.42, obtaining:

$$f^s \varepsilon = \frac{f^c E}{f^c E + f^s E} \cdot f^c \varepsilon \quad (4.51)$$

Although the only parameter required to modify the fibre constitutive equation is the structural stiffness, it is important to obtain the real strains affected by the fibre buckling problem in order to scale other parameters obtained from the resolution of the CuBER problem. To take into account the material non-linearities of the problem, it is necessary to know the exact deformation of the fiber in each load step. When solving the CuBER problem, the variation obtained for fiber misalignments (amplitude and wave-length) correspond to an input strain of $f^c \varepsilon$, while the real strain that should be considered is $f^s \varepsilon$. Thus, the values of the results obtained must be scaled by:

$$SF = \frac{f^s \varepsilon}{f^c \varepsilon} \quad (4.52)$$

To obtain the new amplitude of fibre misalignments, the vertical displacement of the CuBER bar, for $\phi = 0$, has to be added to the previous amplitude (see figure 4.10). The new wave length is obtained subtracting four times the horizontal displacement u (as only a quarter of the wave length has been considered when solving the cuber problem). Therefore, the regularized misalignment value becomes:

$$\begin{aligned} new A &= A + SF \cdot v(\phi = 0) \\ new \lambda &= \lambda - 4SF \cdot u(\phi = \alpha) \end{aligned} \quad (4.53)$$

4.3.6 Matrix homogenized constitutive equation

The structural displacement of fibres due to their initial misalignment generates stresses in the matrix material that surrounds the fibre when the composite is loaded with a compression force. This effect can be seen in figure 4.14, where are shown the transversal stresses (respect fibre direction) and the shear stresses found in matrix material when a finite element micro-model of the RVE is compressed.

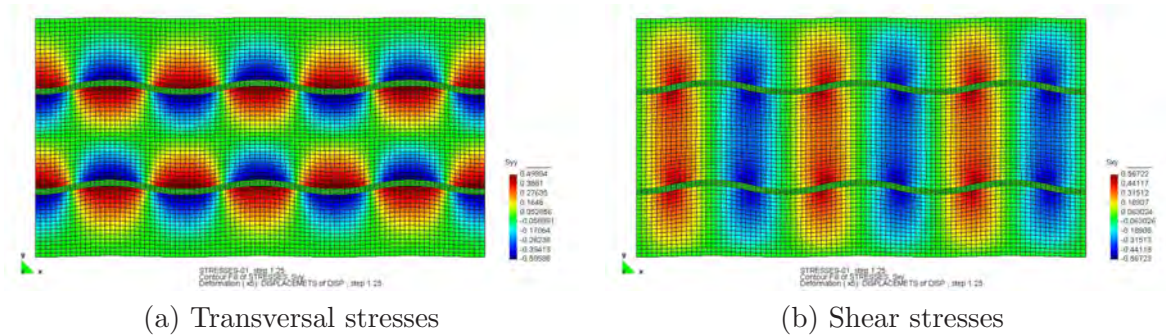


Figure 4.14: Matrix structural stresses produced by fibre displacements

These structural stresses, that do not exist in the case of aligned fibres, lead to a matrix failure for lower compression efforts. The stress state for which the matrix failure will occur is defined by the constitutive equation defined for matrix material. In this case, a damage constitutive law. Therefore, in order to obtain the new matrix homogenized constitutive equation, the structural stresses produced by the interaction of matrix with fibre, must be included in the damage constitutive law. Two different structural stresses must be considered: transversal and shear stresses.

Again, as happened when obtaining the homogenized constitutive performance of fibre material, the structural results (loads and displacements) provided by the CuBER problem must be transformed into parameters that can be understood by a constitutive equation, this is: stresses and strains.

As has been pointed out by González and Llorca (2007), final fracture in reinforced composites usually occurs due to stress concentrations or localized failures. Thus, when extracting the stress results from the CuBER problem to modify the matrix constitutive law, the values that would be sought are the maximum values of shear and transversal stress provided by the model.

Matrix structural transversal stress

Matrix structural transversal stresses will be obtained from the elastic restriction applied by matrix over fibre when solving the CuBER problem. Fibre displacement and the elastic restrain provided by matrix are related by matrix elastic constant:

$$q = k\omega$$

Where q is the radial load produced by the elastic restriction over the fibre, k is the matrix Young Modulus and ω is the fibre radial displacement. This last parameter can be computed, according to equations presented when solving the CuBER problem, as:

$$\omega = C_0 + C_1 \cosh(\eta_1 \phi) \cos(\eta_2 \phi) + C_4 \sinh(\eta_1 \phi) \sin(\eta_2 \phi)$$

To convert the structural problem into a mechanical one, the radial load q must be transformed into a stress, which can be done dividing it by the affected area. This area is obtained using a finite element micro-model of a transversal section of the fibre-matrix system. In it, a vertical displacement has been applied to fibre material to see the stress distribution in matrix due to its elastic restriction.

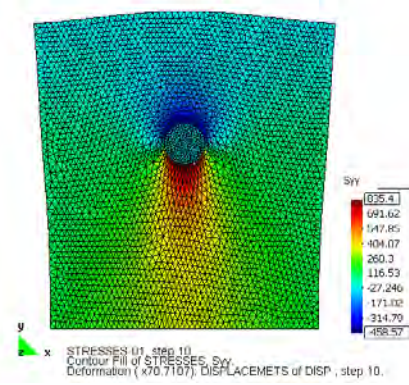


Figure 4.15: Stresses in a transversal section

Figure 4.15 shows transversal stresses in matrix. As can be seen, the acting force of fibre over the matrix can be distributed uniformly along whole fibre diameter. Also, the resultant stress must be divided by two, as half of it correspond to the compression stress produced by the fibre over the upper matrix and the other half corresponds to the tensile stress produced over the lower matrix. Therefore, the matrix transversal stresses can be computed, from the equilibrium in the solid, as:

$$\sigma_{yy} = \frac{k \omega}{2\varnothing_f} \quad (4.54)$$

With \varnothing_f the fiber diameter. With the transversal stress appears also a perpendicular one due to Poisson effects, which value is:

$$\sigma_{\perp} = -\nu \sigma_{yy} = -\nu \frac{k \omega}{\varnothing_f} \quad (4.55)$$

According to figure 4.14, the maximum transversal stress in matrix material due to fibre misalignments is found where the misalignment amplitude is maximum. In these places, the fibre displacement corresponds to $\omega(\phi = 0)$ (figure 4.10) and can be obtained from equation 4.28 when solving the CuBER problem. Considering x the direction in which fibers are oriented, the transversal stress is found in y direction and the perpendicular stress in x direction. Thus, the final matrix structural (ms) transversal stress state found in $\phi = 0$ is:

$$\begin{cases} ms \sigma_{xx} = -\nu \frac{k \omega(\phi = 0)}{2\varnothing_f} \\ ms \sigma_{yy} = \frac{k \omega(\phi = 0)}{2\varnothing_f} \end{cases} \quad (4.56)$$

Matrix structural shear stress

The unidimensional model developed to simulate the fibre-matrix interaction of the RVE considered cannot obtain directly the matrix structural shear stress, as there are not tangential springs in the model for simulating the matrix shear behavior. This is solved computing matrix shear stress value from the fibre deformation. Shear stresses are produced by the distortion of an infinitesimal element due to a stress state. This distortion is defined as (Timoshenko, 1940a):

$$\gamma = \frac{du_x}{dy} + \frac{du_y}{dx} \quad (4.57)$$

Where the values of u_x and u_y , as well as their derivatives, can be obtained from equation 4.30. Once the value of the distortion is known, the shear stress is obtained as the product of the distortion by the matrix shear stiffness modulus, mG , thus:

$${}^{ms}\sigma_{xy} = {}^mG \gamma \quad (4.58)$$

According to figure 4.14, the maximum value of matrix shear structural stress is found at the inflection point between the convex and concave arches of circumference. This point corresponds, in the CuBER problem (figure 4.10), to the angle $\phi = \alpha$. Therefore, the maximum expected shear stress is:

$${}^{ms}\sigma_{xy} = {}^mG \left(\left. \frac{du_x}{dy} \right|_{\phi=\alpha} + \left. \frac{du_y}{dx} \right|_{\phi=\alpha} \right) \quad (4.59)$$

Addition of matrix structural stresses in its constitutive equation

The obtained matrix structural stresses cannot be introduced as real stresses in the matrix constitutive equation, as the equilibrium between the internal and external forces will be lost. If the RVE is loaded with a compression force (in the direction of fibres), the only stresses that can appear in matrix material are in that same direction. Stresses in other directions cannot appear as there is no external force to equilibrate them. However, if the simulation done with the CuBER problem has to include the same parameters that the finite element simulation of the RVE, the effect of these stresses must be included.

The effect of matrix structural stresses on the RVE is that the elastic limit of matrix material is reached for lower loads, matrix is not only affected by the longitudinal stress but also by transversal and shear stresses, which leads to a faster failure of the composite. Thus, it is not necessary to know the exact value of structural stresses as long as their effect on matrix can be reproduced. To do so, the structural stresses are defined as fictitious stresses and are included directly in the matrix constitutive equation as internal variables. These internal variables will lead to a matrix failure for lower compression loads. Defining the initial matrix yield function as (Oller, 2002):

$${}^m\mathbb{F}({}^m\sigma, q_i) \leq 0 \quad (4.60)$$

Where ${}^m\sigma$ is matrix stress tensor and q_i matrix internal variables. When introducing matrix structural stresses in the yield function equation 4.60 becomes,

$${}^m\mathbb{F}^*({}^m\sigma, q_i, {}^{ms}\sigma) \leq 0 \quad (4.61)$$

with ${}^{ms}\sigma$ the matrix structural stresses or fictitious stresses. This new matrix yield function is defined as:

$${}^m\mathbb{F}^*({}^m\sigma, q_i, {}^{ms}\sigma) = {}^m\mathbb{F}({}^m\sigma + {}^{ms}\sigma, q_i) \quad (4.62)$$

Figure 4.14 shows that transversal and shear fictitious stresses are located at different points of the RVE geometry. Hence, the value of matrix fictitious stresses to be included as internal variable will be the most critical of the following two, in a 2D case:

$$\begin{cases} {}^{ms}\sigma_1 = \text{SF} \begin{pmatrix} {}^{ms}\sigma_{xx} & {}^{ms}\sigma_{yy} & 0 \\ 0 & 0 & {}^{ms}\sigma_{xy} \end{pmatrix} \\ {}^{ms}\sigma_2 = \text{SF} \begin{pmatrix} {}^{ms}\sigma_{xx} & {}^{ms}\sigma_{yy} & 0 \\ 0 & 0 & {}^{ms}\sigma_{xy} \end{pmatrix} \end{cases} \quad (4.63)$$

With FS the scale factor defined in equation 4.52. This scale factor is necessary to adjust the values obtained when solving the CuBER problem to the real strain that is applied to the RVE due to fibre misalignments.

The two cases to be considered in a two dimensional simulation must be increased to five in the case of a three dimensional simulation. This is because fibre initial misalignments can be found either in the plane xy or in the plane xz (unless it is known and defined the plane in which they are found). Thus, as the fictitious stresses interact with the stresses found in matrix material due to the loading process, it is not possible to know *a priori* which configuration will damage more the matrix and all of them must be taken into account. Considering that the matrix stress tensor is defined by the following components:

$$\mathbf{m}\sigma = [\sigma_{xx} \ \sigma_{yy} \ \sigma_{xy} \ \sigma_{zz} \ \sigma_{xz} \ \sigma_{yz}] \quad (4.64)$$

The fictitious stresses that has to be considered in the new constitutive equation are:

$$\begin{cases} {}^{ms}\sigma_1 = \text{SF} \begin{pmatrix} {}^{ms}\sigma_{yy} & {}^{ms}\sigma_{yy} & 0 & 0 & 0 & 0 \\ {}^{ms}\sigma_{yy} & 0 & 0 & {}^{ms}\sigma_{yy} & 0 & 0 \end{pmatrix} \\ {}^{ms}\sigma_2 = \text{SF} \begin{pmatrix} {}^{ms}\sigma_{yy} & 0 & 0 & {}^{ms}\sigma_{yy} & 0 & 0 \\ 0 & 0 & {}^{ms}\sigma_{xy} & 0 & 0 & 0 \end{pmatrix} \\ {}^{ms}\sigma_3 = \text{SF} \begin{pmatrix} 0 & 0 & {}^{ms}\sigma_{xy} & 0 & 0 & 0 \\ 0 & 0 & 0 & 0 & {}^{ms}\sigma_{xy} & 0 \end{pmatrix} \\ {}^{ms}\sigma_4 = \text{SF} \begin{pmatrix} 0 & 0 & 0 & 0 & {}^{ms}\sigma_{xy} & 0 \\ 0 & 0 & 0 & 0 & 0 & {}^{ms}\sigma_{xy} \end{pmatrix} \\ {}^{ms}\sigma_5 = \text{SF} \begin{pmatrix} 0 & 0 & 0 & 0 & 0 & 0 \\ 0 & 0 & 0 & 0 & 0 & {}^{ms}\sigma_{xy} \end{pmatrix} \end{cases} \quad (4.65)$$

Matrix affected by fibre misalignments

In function of the fibre volumetric participation in the composite, not all matrix material will be affected by the structural stresses produced by fibre misalignments. As it is shown the results from the micro-model (figure 4.14), only matrix that surrounds the fibre is affected by fibre misalignments.

To take into account this situation, matrix damage parameter is divided in two components, a structural damage and a constitutive one. Obtaining:

$$d^m = {}^A k^A d + {}^{nA} k^{nA} d \quad (4.66)$$

Where ${}^A k$ and ${}^{nA} k$ are the proportion of matrix affected and not affected by fibre misalignments, respectively, and ${}^A d$ and ${}^{nA} d$ are the damage parameters obtained for the affected and not affected matrices, respectively.

The proportion of matrix affected by fibres is obtained considering that fibres affect matrix in a region equal to the amplitude of the misalignment. This region is displayed in figure 4.16.

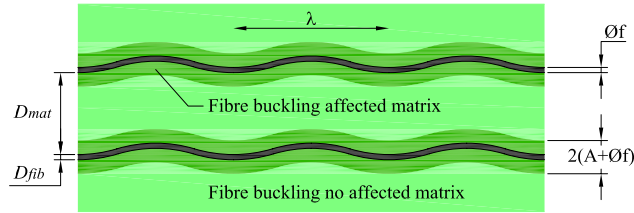


Figure 4.16: Matrix volume affected by fibre buckling effects

Assuming an homogenized distribution of fibre and matrix in space, the proportion of affected matrix can be obtained considering only one of the directions perpendicular to the fibre longitudinal axis. Therefore, the length D_{mat} can be computed using the fibre and matrix volumetric participation (${}^f k$ and ${}^m k$ respectively), as:

$${}^m k = \frac{D_{mat}}{D_{mat} + D_{fib}} = \frac{D_{mat}}{D_{mat} + \text{Ø}f} \quad \rightarrow \quad D_{mat} = \frac{{}^m k \text{Ø}f}{1 - {}^m k} \quad (4.67)$$

According to figure 4.16, the length of matrix matrix affected by fibre misalignments is:

$${}^A D_{mat} = 2A \quad (4.68)$$

With these two lengths, the proportion of matrix affected by fibre misalignments is obtained as the quotient between the affected matrix and the total length of matrix in the composite:

$${}^A k = \frac{{}^A D_{mat}}{D_{mat}} = 2A \frac{1 - {}^m k}{{}^m k \text{Ø}f} \quad (4.69)$$

And the proportion of not affected matrix becomes:

$${}^{nA} k = 1 - {}^A k \quad (4.70)$$

To compute the matrix damage parameter, the constitutive equation must be verified twice. The first time introducing a fictitious stresses equal to zero in the yield function ${}^m \mathbb{F}^*$ (equation 4.62) to obtain the non affected damage parameter. And the second time introducing the fictitious stresses defined in equation 4.63 or in equation 4.65, depending on the dimension of the problem, to obtain the affected damage parameter.

When solving for second time the damage constitutive equation, with the structural fictitious stresses, another parameter to be changed in the damage formulation is the fracture length

considered (see section 3.3). In this case the fracture length do not depend on the dimension of the finite element but on the dimensions of fibre misalignments. When homogenizing a structural behaviour, each gauss point contains all information of the RVE, independently of the dimension of the gauss point. Thus, even the dimension of the finite element is of, i.e. $5.0\mu\text{m}$, if the wave length of the misalignment is of $400.0\mu\text{m}$, the fracture energy released in the micro-model will correspond to damaging all the wave length of the fibre misalignment.

The model developed in the CuBER problem represents half the wave length of fibre misalignments. Therefore, the fracture length considered when adding the structural fictitious stresses to the constitutive equation is:

$$l_f = 2R\alpha \quad (4.71)$$

4.4 Validation of the homogenization method

In this section, the approach used to include the effects of fibre misalignment and the interaction between fibre and matrix due to this particular geometric configuration, is validated. To do so, the results of a finite element micro-model of the representative volume element (RVE) to be simulated are compared with the results obtained with the formulation proposed. It will be shown that the behavior of the RVE is the same in both models. This result agreement justifies the use of the constitutive equation homogenization approach to obtain the performance of the RVE.

4.4.1 Models description

A basic composite configuration has been defined to verify the agreement between the finite element micro-model and the composite model that uses the serial/parallel mixing theory to obtain the composite performance, with the homogenized constitutive laws for fibre and matrix materials. The composite defined is made of glass-fibres embedded in an epoxy matrix. The values considered for each component material are average values, obtained from literature. These are shown in table 4.1.

Matrix Properties		Fibre Properties	
Elastic Modulus	3.00 GPa	Elastic Modulus	80.00 GPa
Poisson Modulus	0.30	Poisson Modulus	0.00
Tensile Strength	90.00 MPa		
Fracture Energy	1.00 kJ/m ²		

Table 4.1: Composite components mechanical properties used to validate the homogenized constitutive equations

Matrix material has been described with the modified damage constitutive law defined in previous section. The yield function used to obtain the stress state in which damage starts in matrix material is based in the norm of the principal stresses (see section 3.3), which non-homogenized expression is (Oliver et al., 1990; Oller, 2001):

$$\mathbb{F}(\sigma, q_i) = \sqrt{\sigma_1^2 + \sigma_2^2 + \sigma_3^2} - \sigma^{max} \leq 0 \quad (4.72)$$

Being σ_i the principal stresses values obtained from the matrix stress tensor and σ^{max} the matrix maximum stress, which value has been defined as 90 MPa (table 4.1).

Using the fact that fibre buckling becomes before fibres reach their limit elastic strength, fibres are considered to be an elastic material. The other parameter required to define fibre elastic properties is the Poisson modulus, which is considered equal to zero. This is done because fibre transversal deformations, due to their longitudinal strains, are considered negligible.

The misalignment properties considered for the basic model are the ones defined by Jochum and Grandidier (2004). These authors obtain fibre misalignment properties from different samples using an optical microscope. The results obtained from these observations are:

1. The diameter of the fibre is of $7.0 \mu\text{m}$
2. Amplitude is one to twice the fibre diameter
3. Wave length is comprehended between 150 and $300 \mu\text{m}$
4. Undulations have a periodic form along the fibre length

With these values in mind, the misalignment configuration defined for the basic model of the RVE are the ones shown in figure 4.17 and described in table 4.2. The volumetric participation of fibre and matrix in the composite is obtained from the geometry shown in figure 4.17. This figure shows that only two fibres are considered in the RVE model. This small fibre proportion has been chosen in order to see more clearly the interaction between fiber and its surrounding matrix.

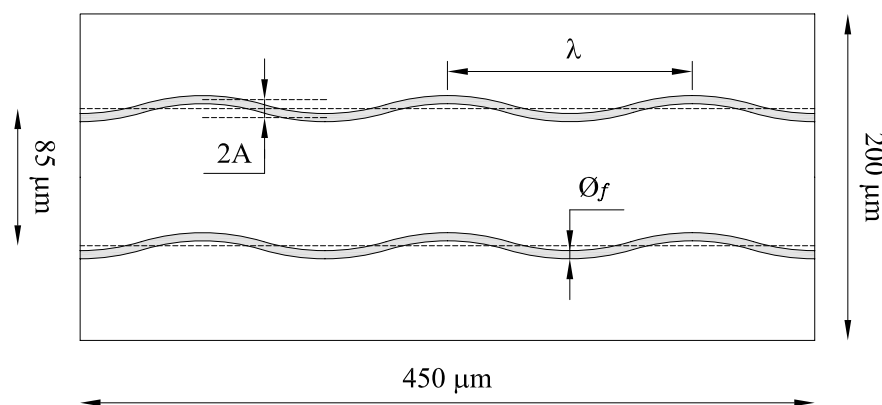


Figure 4.17: Geometry of the Representative Volume Element simulated

Fibre diameter	$7.0 \mu\text{m}$
Amplitude	$10.5 \mu\text{m}$
Wave length	$225.0 \mu\text{m}$
Fibre Vol. particip.	7.0 %
Matrix Vol. particip.	93.0 %

Table 4.2: Misalignment properties and volumetric participations used to validate the homogenized constitutive equations

To be certain of the good performance of the formulation proposed, six different variations of the basic RVE model have been defined. Each one modifying the different parameters that affect the micro-mechanical behavior of the RVE. These are: fibre initial misalignment geometry, which depends on misalignment amplitude (A) and wavelength (λ), fibre diameter (\varnothing_f) and stiffness properties of fibre and matrix materials ($^f E$ and $^m E$, respectively). Each one of these parameters have been increased and reduced respect the basic model, in order to see the dependence of the developed formulation in all of them. The values of the different parameters applied to the geometry, as well as the name assigned to each model developed, are described in table 4.3.

RVE	\varnothing_f [μm]	A [μm]	λ [μm]	$^f E$ [GPa]	$^m E$ [GPa]
Bmod	7.0	10.5	225.0	80.0	3.0
DfiM	5.0	10.5	225.0	80.0	3.0
DfiL	9.0	10.5	225.0	80.0	3.0
AmpM	7.0	7.0	225.0	80.0	3.0
AmpL	7.0	14.0	225.0	80.0	3.0
FreM	7.0	10.5	150.0	80.0	3.0
FreL	7.0	10.5	300.0	80.0	3.0
Wmat	7.0	10.5	225.0	80.0	1.5
Sfib	7.0	10.5	225.0	230.0	3.0

Table 4.3: Parameters defining the different RVE models developed

All different RVE configurations described in table 4.3 have been modeled with a finite element micro-model and with the new formulation proposed. Each micro-model is labeled with the word *micro*, thus, the micro-model of Bmod RVE is named *micro-Bmod*. On the other hand, the models developed with the new formulation will be labeled with the word *RoM* which names, the Bmod RVE, as *RoM-Bmod*.

Finite element micro models

The finite element micro-models have been defined using a two dimensional plane stress formulation. The geometry has been modeled using linear quadrilateral elements, which number varies between 2880 elements in the *FreM* and *FreL* models to 3185 elements in all other models. All models have 48 elements in direction y (each fibre is modeled with four elements in its transversal direction to capture with more accuracy its bending stiffness) and 60 or 64 elements, depending on the RVE cell simulated, in direction x . The mesh used for the *micro-Bmod* model is displayed in figure 4.18.

The difference between the mesh shown in figure 4.18 and the meshes developed for all the other RVE models is found in the fibre geometry. Which is modified in order to follow the different fibre misalignments defined.

Figure 4.18 also shows the boundary conditions defined in all micro-models. The longitudinal movement in left boundary is fixed to zero while the longitudinal movement right one, displayed with a dashed line, is moving towards the fixed one. This movement generates a compression on the RVE. The two points plotted in both boundaries correspond to the points in which the transversal displacement has been fixed to zero, in order to stabilize the model and avoid undesired translations of it. In the moving boundary it has been applied a fixed displacement, instead of a compression load, so the models can provide their post-critical strength, avoiding a sudden finish of the numerical simulation because the model cannot

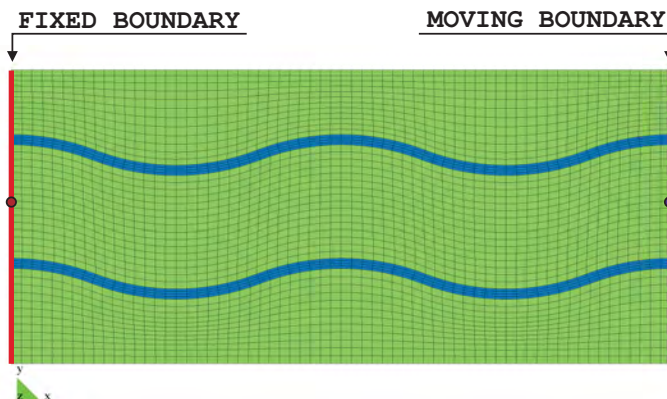


Figure 4.18: micro-Bmod finite element model. Mesh and boundary conditions defined

reach the applied load.

Two different materials have been defined in each micro-model. The green material shown in figure 4.18 corresponds to the matrix material, which is characterized by a damage constitutive law. The blue material corresponds to fibre which, as it has been already said, is characterized using an elastic law. The mechanical properties of both are described in table 4.1.

Finite element RoM models

The RoM models obtain the performance of the different RVE defined using the homogenized constitutive equations for matrix and fibre presented in section 4.3. The finite element models developed also use a plain stress formulation. The mesh used for these simulations contains only eight linear quadrilateral finite elements. This mesh is shown in figure 4.19.

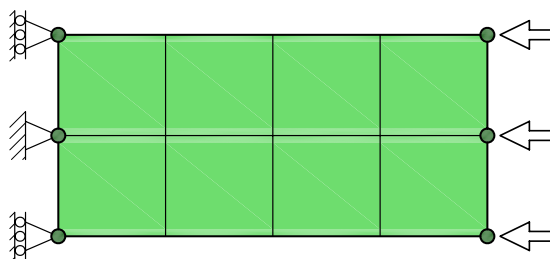


Figure 4.19: RoM finite element models. Mesh and boundary conditions defined

The arrows shown in the right side nodes define the displacement direction applied to those nodes. This displacement is the same that has been applied to the RVE micro models. Again, the election of applying displacements instead of forces is made with the aim of obtaining the post-critical behavior of the composite once the maximum compression load has been reached.

It is important to remark the difference in the number of mesh elements required by the micro models and the RoM models. The number of elements required by the micro models is three orders of magnitude larger than the number of elements required by the RoM models. Therefore, if the results provided by both procedures are similar, the new formulation proposed will offer the possibility to do large scale simulations taking into account the fibre-matrix

micro-structural interaction due to fibre initial misalignments. Possibility that is unbearable by nowadays personal computers if a complete homogenization method wants to be used.

The model is defined with a single composite material, which constitutive performance is obtained using the serial/parallel mixing theory. The fibre and matrix defined for the composite, as well as their constitutive laws, are defined at the beginning of this section. The volumetric participation considered for each component material has been obtained from figure 4.17. However, fibre volumetric participation has been reduced approximately 1.5% of the total composite volume in all models. This has been done because RoM models turned out to be slightly stiffer than the micro models, when the composite is still in its elastic range. Applying the new fibre volumetric participation, the stiffness difference is reduced and the comparison among the different models can be made easily. As this modification has been done proportionally in all RoM models, the results obtained do not lose their validity, as the reduction can be understood as the calibration required in all finite element simulations in order to obtain a better agreement with real results.

Another particularity of the RoM models is the proportion of affected matrix considered in the simulations. The value of affected matrix is computed automatically by the code using expression 4.69. However, in the RVE considered, as the amount of fibre in the composite is very small, the quantity of affected matrix shown by the micro models exceed the computed value. The implementation of the CuBER problem in the finite element code (which will be described in section 4.5) allows providing user-defined value of the affected matrix due to fibre buckling. The value defined for the RoM models is 0.75. Which is, approximately, the amount of matrix affected according to the micro model results.

4.4.2 Results to be studied in the code validation

The study of the results obtained with the different models developed to validate the proposed formulation must be done comparing the global performance of the micro models with the RoM models. The comparison of the specific performance of each model cannot be made because the results obtained are completely different in both simulations: a single finite element do not provide all information obtained from a model with thousands of elements. However, as the interest lays on the global performance of the RVE cell, if the global results are similar, the formulation can be considered to be valid.

The global performance expected from the RVE when including fibre misalignments is a reduction on the composite stiffness and an initial failure on the composite for lower loads, due to the failure of matrix material. Therefore, these two effects are the ones to be compared. The reduction of composite stiffness is produced by the reduction of fibre stiffness due to its micro-structural displacements and the failure for lower loads is produced because matrix stresses are increased with the shear transversal structural stresses that appear as result of the fibre structural displacements.

Even the main interest, when comparing the results obtained with each formulation, lays into the RVE global behavior; it is also interesting the comparison of the parameters used by the serial/parallel mixing theory to include the results of the *CuBER* problem in its constitutive behavior. These parameters are the matrix maximum stresses and the fibre stiffness reduction due to its structural displacements. Matrix stresses will be compared using the maximum shear and transversal stress found, nearby the fibre, in the micro model and the structural stresses provided by the RoM model, which are stored as internal variables.

On the other hand, the reduction of fibre stiffness cannot be compared between both models.

Fibres are modeled as an elastic material and their stiffness is not modified at any load step in the micro models while, in the RoM models, its stiffness is modified due to the structural damage defined in section 4.3. Thus, fibre stiffness will be constant in the micro models and will vary in the RoM models. However, as one of the main parameters defining the stiffness reduction in the RoM models are fibre misalignments, what can be compared is the evolution of fibre amplitude and wave-length with both models. It is important to remark that these two parameters, by themselves, are not a direct indicator of how fibre stiffness will change, as it also depends on fibre diameter, matrix stiffness and fibre constitutive stiffness.

Hence, the validation of the formulation proposed is made comparing the structural results of both RVE models, micro and RoM, studying the load for which composite failure starts and the stiffness of the composite before and after the failure. This comparison is made using the force-displacement curves obtained for the RVE. The results obtained with both models for matrix structural stresses and the evolution of fibre misalignments are also compared. This second validation, although less relevant, will provide a better comprehension of the behavior of the developed formulation. These two validations are performed in detail for one of the RVE models: the Bmod model. Afterwards, with a more general view, all other RVE cells simulated are also compared.

4.4.3 Detailed comparison of the results obtained with the micro-Bmod and RoM-Bmod simulations

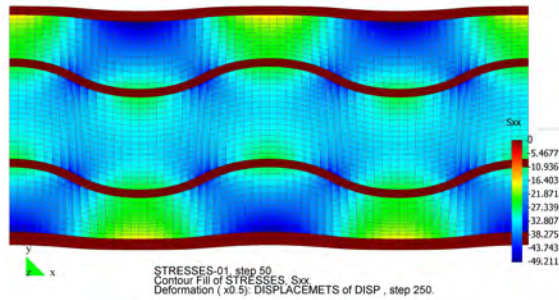
In order to obtain a better comprehension of the performance of the RVE studied and of the performance of the new formulation developed, in this comparison the micro-mechanical behavior of both models is studied first. This performance is studied comparing the two main parameters to be used when defining the homogenized constitutive equations of fibre and matrix in the RoM models: matrix structural stresses and the evolution of fibre initial misalignments. Afterwards, the global behavior of the RVE simulated obtained with both models will be compared.

Matrix structural stresses

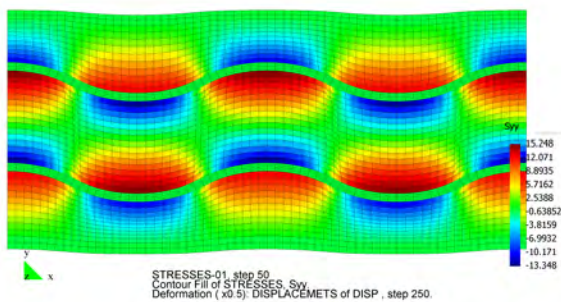
If fibre initial misalignments are not present in the RVE (case of straight fibres) the matrix stresses that are obtained when the structure is loaded with a compression force are constant along the whole element in the longitudinal direction and zero in the transversal and shear directions. Otherwise, when fibre initial misalignments are present, the interaction between fibre and matrix modifies the constant stress field in longitudinal direction and generates stresses in the transversal and shear directions, as can be seen in figure 4.20.

Figure 4.20 shows the effect of fibre misalignments in matrix material and the distribution of the transversal and shear stresses that appear when the composite is compressed. The results represented correspond to an applied displacement on the composite material of $5.0 \mu\text{m}$. When applying this displacement, the composite is still under elastic conditions: no damage has appeared in matrix material. It has been chosen this load step because, once damage appears in matrix, the comparison between the stresses found in the micro model and the RoM models is no longer valid, as matrix damage has a different meaning in each formulation.

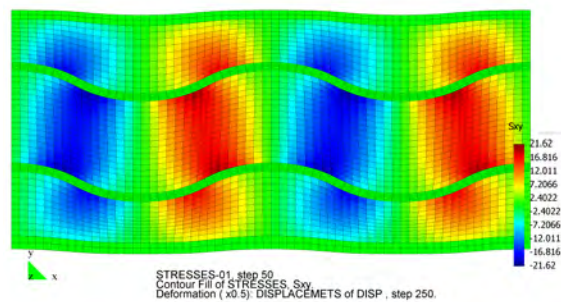
The results of these figure have been also used to obtain the proportion of matrix that is considered to be affected by fibre misalignments, which is set as a 75%.



(a) Longitudinal stresses



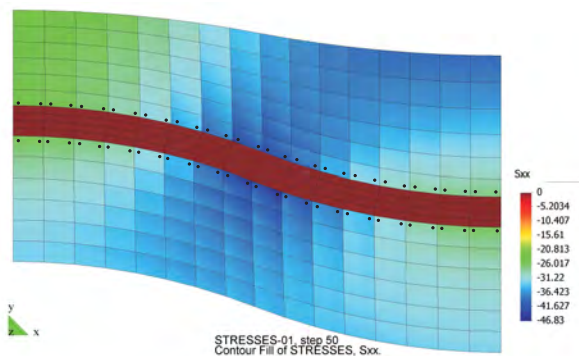
(b) Transversal stresses



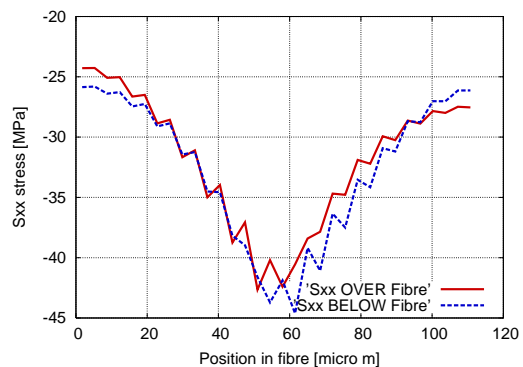
(c) Shear stresses

Figure 4.20: Matrix stresses in micro-Bmod for a compression displacement of $5.0 \mu\text{m}$

To obtain the maximum stress values that are found in matrix material, a section of the composite has been studied (figures 4.21, 4.22 and 4.23). From the contour plot obtained from the finite element model, it has been obtained the exact values of the stresses in the gauss points (marked with a point in the figures) found in the element just above and below the fibre. The values of the stresses in those gauss points are plotted in the graphs displayed beside the contour plot figure.



(a) FEM Contour plot



(b) Exact values in gauss points

Figure 4.21: Matrix S_{xx} stresses in micro-Bmod for a compression displacement of $5.0 \mu\text{m}$

From the graphs displayed in figures 4.21, 4.22 and 4.23 the transversal and shear stresses can be obtained to be compared with the structural fictitious stresses computed with the RoM model. Longitudinal stresses have been also obtained in order to verify the reduction made, due to poisson effects, of these stresses when they are included in the transversal fictitious stress vector (equation 4.63) used in the homogenized constitutive law. The maximum shear stress obtained with the finite element micro-model is found in the elements above the fibre and its value is 18.2 MPa. And the maximum transversal stress is found in the elements

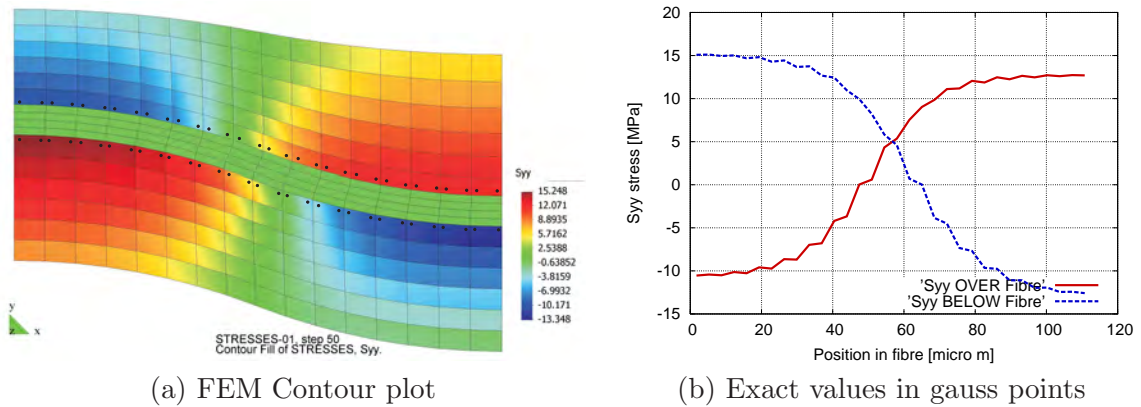


Figure 4.22: Matrix S_{yy} stresses in micro-Bmod for a compression displacement of $5.0 \mu\text{m}$

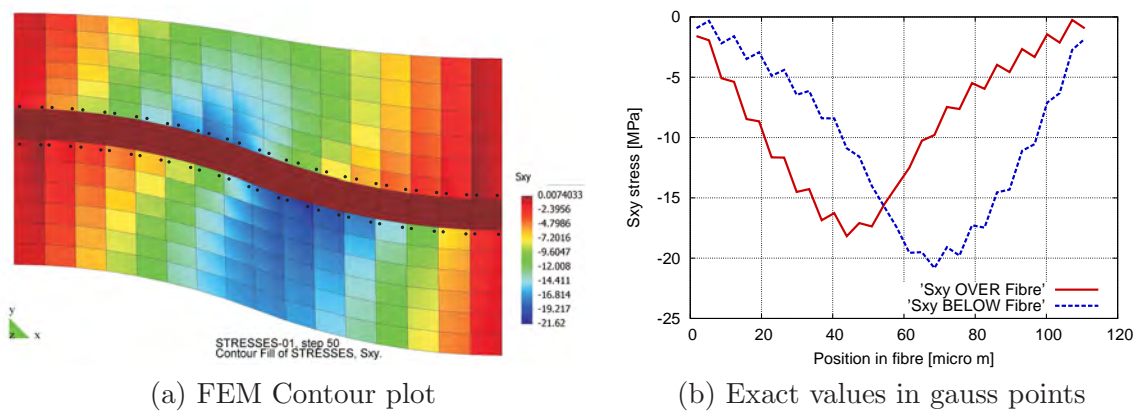


Figure 4.23: Matrix S_{xy} stresses in micro-Bmod for a compression displacement of $5.0 \mu\text{m}$

below the fibre and its value is 15.1 MPa . The longitudinal stress associated to this value is of 25.9 MPa .

When studying the structural stresses obtained with the RoM model for matrix material, only one value is obtained from the solution of the CuBER problem for each load step. This value corresponds to the maximum shear or transverse value that can be obtained in a micro-structural simulation of the RVE cell. Figure 4.24a shows the fictitious stress values obtained with the RoM simulation and the homogenized longitudinal stress value obtained for the matrix material. It is worth to remark the two changes in the stiffness slope observed in the longitudinal stress values (S_{xx}). This effect can be better understood looking at the damage parameters in matrix material displayed in figure 4.24b. The first stiffness reduction appears due to the structural damage (for an applied compression displacement slightly larger than 0.01mm) and the second stiffness reduction is found when damage starts also in the matrix not affected by fibre misalignments, plotted as constitutive damage in figure 4.24b. The apparition of the structural damage before the constitutive one proves that the fictitious stresses applied to the homogenized constitutive equation of matrix leads to a faster degradation of this material.

However, to validate the accuracy of the stress values obtained from the CuBER problem, the stress comparison must be done for the same applied compression displacement used to obtain the stresses in the micro model. This is, for an applied displacement of $5.0 \mu\text{m}$. The value of these fictitious stresses for the RoM-Bmod are displayed in table 4.4. This table also contains the stresses found with the micro-Bmod model and the error obtained when using the

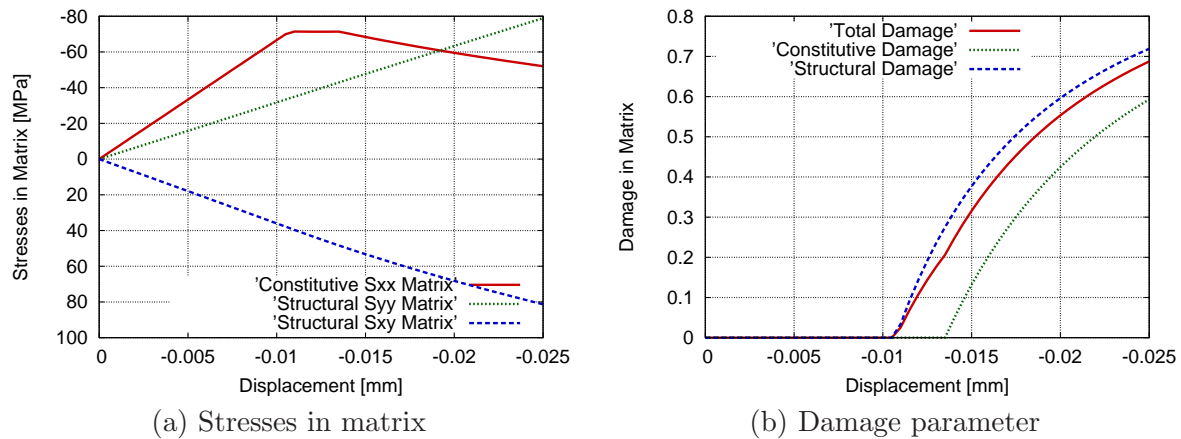


Figure 4.24: Stresses in matrix and evolution of the damage parameter in RoM-Bmod model

proposed formulation, considering that the real results are the ones obtained with the finite element micro simulation. An error with a positive value means that the stresses obtained with the RoM model are larger than the stresses provided by the micro simulation and vice versa.

Stress	micro	RoM	Error
Sxx	25.9 MPa	28.6 MPa	10.4 %
Syy	15.1 MPa	15.8 MPa	4.6 %
Sxy	18.2 MPa	17.9 MPa	-1.6 %

Table 4.4: Stress comparison between micro-Bmod and RoM-Bmod

Results displayed in table 4.4 show the good agreement among the stresses obtained with each simulation. Having the same stress tensor in both models assures that the apparition of damage in all of them will begin for the same applied compression load. Although in the micro model the damage is localized in the element with maximum stresses and in the RoM model the damage is applied in all the matrix material affected by fibre misalignments.

Fibre initial misalignments

The evolution of fibre misalignments has been obtained for both simulations of the RVE cell. Fibre misalignments in the micro-Bmod model have been computed from the displacement along the loading process of the nodes A and B shown in figure 4.25. Fibre misalignments in the RoM-Bmod model are obtained as an output result of the CuBER problem.

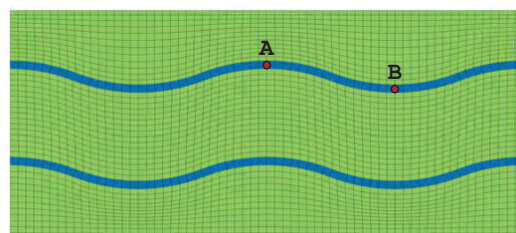


Figure 4.25: Nodes from which fibre misalignments are obtained

The agreement between both simulations is not, in this case, as good as it was in the case

of structural stresses. The micro model provides larger values for the increment of amplitude and wave length than the RoM model. However, the trend obtained with both simulations is similar. In order to appreciate better this trend, the amplitude and wave length increment of the results obtained with the micro model have been divided by 10. Figure 4.26a shows the evolution of misalignment amplitude along the loading process while figure 4.26b shows the evolution of the wave length. It can be seen that the trend in both cases is very similar.

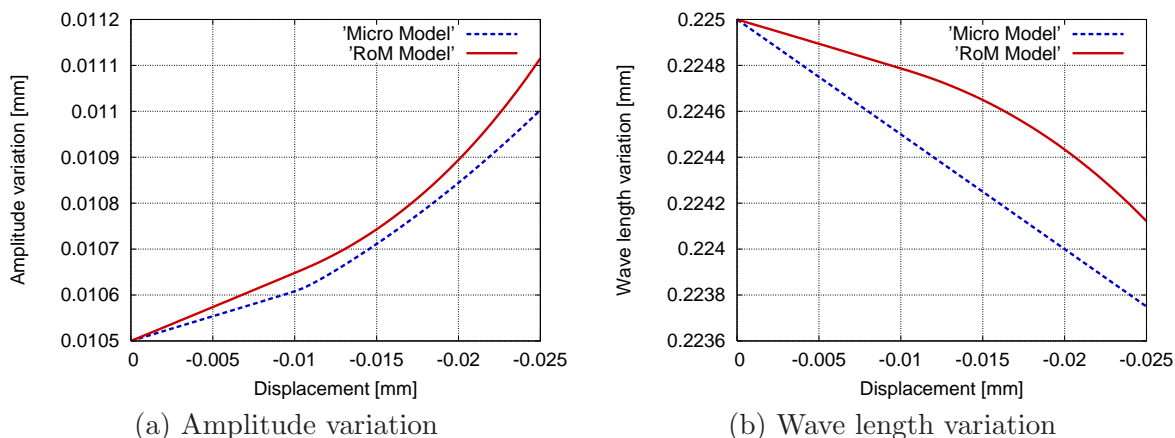


Figure 4.26: Evolution of fibre misalignments along the loading process in micro-Bmod and RoM-Bmod models

When comparing the amplitude variation it is important to point out that when damage appears in matrix material, for an applied displacement slightly larger than $0.01 \mu\text{m}$ (see figure 4.24b), the amplitude starts increasing faster than it did when matrix behavior was elastic. This effect is shown by both RVE simulations and proves the effect of matrix stiffness in the CuBER problem: as matrix damage increases, its capacity to restrain fibre displacements is reduced and fibre misalignments start increasing faster. On the other hand, the evolution of the wave-length follows this same pattern in the RoM model but not in the micro model, in which a constant reduction of this parameter is observed. This last result, which was not expected, proves that although the micro model provides, in theory, a better approximation of the composite RVE cell, the results obtained with it do not have to be trusted at a 100%.

Global behavior of the RVE

Despite of all the resemblances and differences obtained when comparing specific parameters provided by both models: micro and RoM, the most important issue to compare is the global behavior of the RVE. Although is not the case, even having partial results completely different, if the new formulation proposed is capable to reproduce a global behavior of the RVE similar to the one obtained with the micro-model, the formulation can be considered valid to include the effect of fibre misalignments and fibre interaction with matrix material in the serial/parallel mixing theory, in order to obtain the compression strength of composite materials.

The global performance of the RVE is defined by two main parameters: the load for which damage appears in matrix and the stiffness of the composite, before and after, matrix failure. These two parameters can be studied with the force-displacement graph obtained for each simulation of the RVE. Both graphs are represented in figure 4.27.

Figure 4.27 shows that the initial stiffness of the RVE cell is exactly the same for both the micro-Bmod and RoM-Bmod models. It is also the same the load for which damage starts,

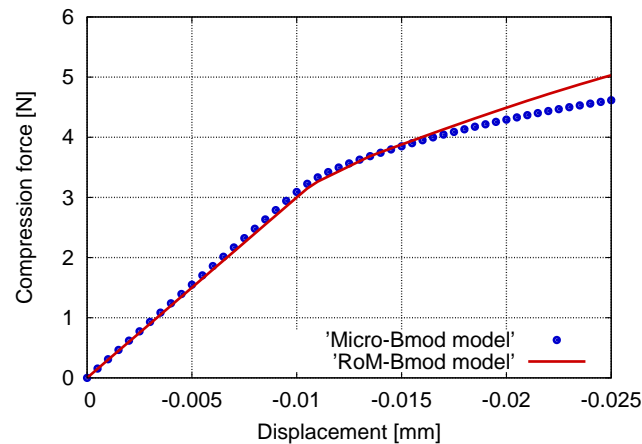


Figure 4.27: Force-displacement graph showing the global behavior of the Micro-Bmod and RoM-Bmod models

which corresponds to the load in which the stiffness changes its slope. This agreement is produced thanks to the agreement in the transversal and shear stresses of matrix material, shown in table 4.4. The parameter that differs more in both models is the final stiffness slope, developed once matrix degradation has started. The RoM-Bmod model is slightly stiffer than the micro-RoM model. However, the difference found in this last slope is small enough to consider that the RoM model performance is correct and practically the same as the performance shown by the micro model. Thus, it can be conclude that the global behavior of both models is equivalent.

A better comprehension of the global performance shown by the RoM-Bmod model can be obtained from the stress-strain graphs, of the composite and of its constituent materials, obtained from the simulation. The stresses and strains represented correspond to the longitudinal direction of the RVE. These graphs, shown in figure 4.28, are displayed together with the results obtained from the same RVE simulation when the fibre misalignment phenomenon is not considered. Opposing these both graphs, the effects using the homogenized constitutive equations for fibre and matrix can be seen more clearly.

Figure 4.28b shows that matrix degradation appears, due to the effect of fibre misalignment, for a longitudinal stress which is more than 20% lower than the stress in which damage starts if the misalignments are not considered. Of the two different fictitious stress tensors added to the homogenized constitutive law (equation 4.63), damage is produced by the stress tensor containing the fictitious structural shear stress. This is a relevant issue as provides another agreement with the fibre buckling theories existing in literature: one of the main parameters that defines the fibre buckling problem is the shear strength of matrix. This shear strength is represented in the proposed formulation by the homogenized constitutive law and, as has been seen, the fictitious stresses that lead to matrix failure are the shear stresses.

Fibres in the misaligned model show a small reduction of their elastic stiffness from the beginning of the stress-strain graph, when they are compared with the aligned model. However, this reduction becomes more important, and keeps increasing, when damage appears in matrix (figure 4.28c). The stiffness reduction can be seen more clearly with the fibre structural damage parameter. This is represented in figure 4.29 together with the matrix damage parameter. This figure shows how an initial damage is present in fibre material due to the initial misalignment and how damage remains constant until matrix degradation starts. At this point, fibre structural damage starts increasing exponentially.

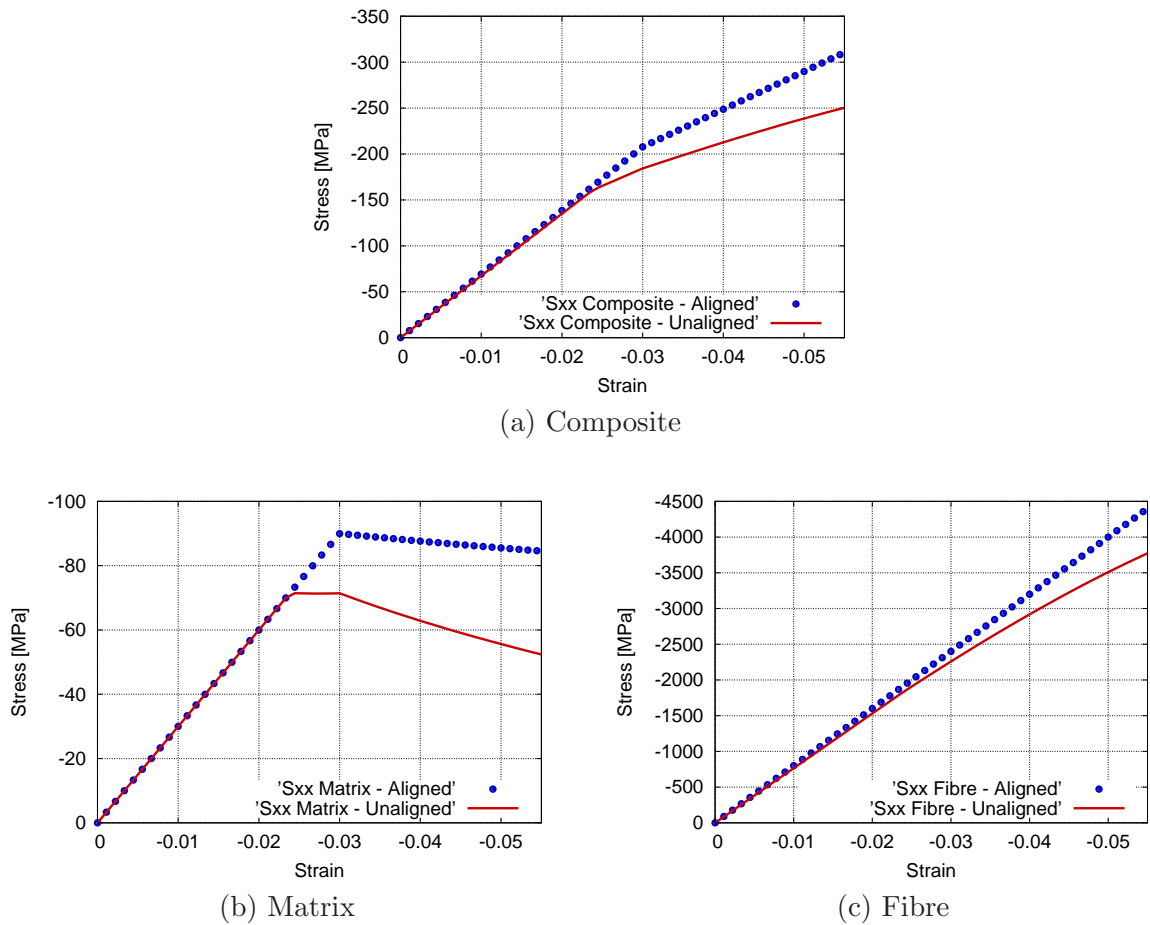


Figure 4.28: Stress-strain graphs obtained for the RVE with the serial/parallel mixing theory, with aligned and misaligned fibres

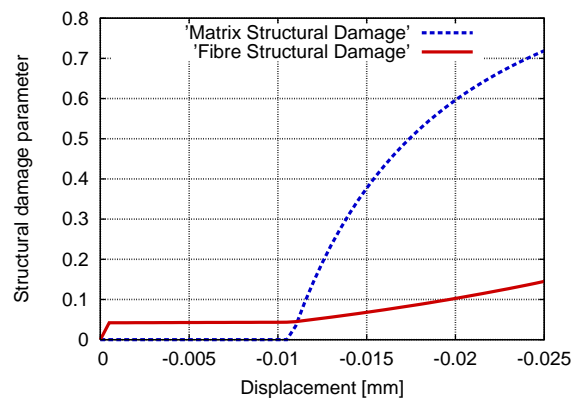


Figure 4.29: Fibre and matrix structural damage. RoM-Bmod model

Finally, when comparing the stress-strain behavior of the composite between the aligned and the misaligned case (figure 4.28a), it can be seen clearly the effects of fibre and matrix materials. Degradation starts before in the RVE with misalignments, as damage degradation starts before, and the stiffness reduction of the composite after matrix degradation is rather larger in the case in which misalignments are considered because the fibre contribution to the composite stiffness is smaller, as its stiffness is also reduced.

4.4.4 Comparison of the results obtained with the micro and RoM models for the different RVE considered

This section validates the performance of the developed formulation, to homogenize the constitutive equations of fibre and matrix material, by studying the global behavior of the RVE when the different parameters included in the CuBER problem are modified. This parameters are fibre initial misalignments (amplitude and wave length), fibre diameter and fibre and matrix stiffness.

A detailed description of the different RVE models developed has been already shown in table 4.3. However, here is described briefly the parameters modified in each model, respect the Bmod configuration, and the name given to the model:

AmpL:	Misalignment amplitude is decreased to $7.0 \mu\text{m}$
AmpM:	Misalignment amplitude is increased to $14.0 \mu\text{m}$
FreL:	Misalignment wave length is decreased to $150.0 \mu\text{m}$
FreL:	Misalignment wave length is increased to $300.0 \mu\text{m}$
DfiL:	Fibre diameter is decreased to $5.0 \mu\text{m}$
DfiM:	Fibre diameter is increased to $9.0 \mu\text{m}$
Wmat:	Matrix stiffness is decreased to 1.5 GPa
Sfib:	Fibre stiffness is increased to 230.0 GPa

As has been done with the Bmod simulation, the global behavior of the composite will be studied with the force-displacement graph obtained for each RVE simulation. It will be also presented the comparison of the matrix structural stresses with the maximum stresses found in the micro models, as these stresses have been proved a good parameter to verify the load at which composite degradation starts due to fibre buckling.

Matrix structural stresses

The firsts results that will be compared are the matrix shear and transversal stresses obtained for each RVE simulation. The stresses provided by the micro models as well as the stresses provided by the RoM models and the error obtained with these last models (if the micro model stresses are considered to be correct) are displayed in table 4.5 for the models in which amplitude is modified, table 4.6 for the models in which wave length is modified, table 4.7 for models with different fibre diameter and, finally, in table 4.8 for the models in which the composite components stiffness is modified.

Model	Stress	micro	RoM	Error
AmpL	Sxx	30.0 MPa	30.1 MPa	0.3 %
	Syy	11.4 MPa	10.7 MPa	-6.1 %
	Sxy	14.1 MPa	11.5 MPa	-18.4 %
AmpM	Sxx	25.2 MPa	27.1 MPa	7.5 %
	Syy	16.3 MPa	20.6 MPa	26.4 %
	Sxy	22.3 MPa	25.3 MPa	13.5 %

Table 4.5: Stress comparison between RVE simulations in which the amplitude is modified

Results shown in tables 4.5 to 4.8 show that the new formulation proposed captures with a good accuracy the modification of matrix structural stresses when the different parameters involved in the CuBER problem are modified. If the stresses increase in the micro model, also increase in the RoM model. Also, the error obtained when comparing the exact value of the

Model	Stress	micro	RoM	Error
FreL	Sxx	23.0 MPa	23.6 MPa	2.6 %
	Syy	21.8 MPa	32.4 MPa	48.6 %
	Sxy	23.9 MPa	38.0 MPa	59.0 %
FreM	Sxx	27.4 MPa	30.6 MPa	11.7 %
	Syy	10.4 MPa	9.1 MPa	-12.5 %
	Sxy	14.6 MPa	9.9 MPa	-32.2 %

Table 4.6: Stress comparison between RVE simulations in which the wave length is modified

Model	Stress	micro	RoM	Error
DfiL	Sxx	26.4 MPa	29.8 MPa	12.9 %
	Syy	11.5 MPa	11.6 MPa	0.9 %
	Sxy	13.7 MPa	13.2 MPa	-3.6 %
DfiM	Sxx	26.1 MPa	27.3 MPa	4.6 %
	Syy	18.1 MPa	20.2 MPa	11.6 %
	Sxy	21.4 MPa	22.3 MPa	4.2 %

Table 4.7: Stress comparison between RVE simulations in which the fibre diameter is modified

Model	Stress	micro	RoM	Error
Wmat	Sxx	18.0 MPa	20.3 MPa	12.8 %
	Syy	32.4 MPa	43.4 MPa	34.0 %
	Sxy	34.6 MPa	36.6 MPa	5.8 %
Sfib	Sxx	10.4 MPa	12.0 MPa	15.4 %
	Syy	12.8 MPa	15.4 MPa	20.3 %
	Sxy	14.3 MPa	14.4 MPa	0.7 %

Table 4.8: Stress comparison between RVE simulations in which the fibre and matrix stiffness are modified

structural stresses computed is, in most cases, lower than a 5%. This error tends to be lower for the shear structural stresses than for the transversal ones. This is an important issue as the fictitious stress tensor which leads to the apparition of damage in matrix material corresponds, in all simulations performed, to the stress tensor defined by shear stresses. Again, this result agrees with all existing literature treating the fibre buckling problem.

Concerning the error obtained when computing the shear structural stresses, it can be said that the two cases in which larger errors are found are when the fibre misalignment parameters are modified: amplitude and wave length. Being quite larger when modifying the wave length parameter. Although differences are important, and are reflected in the force-displacement graph, it has to be reminded that this is a partial result that do not imply obtaining a wrong global behavior of the RVE cell.

Global behavior comparison

The comparison of the global behavior of all the RVE cells simulated with the micro and RoM models is performed using the force-displacement graphs obtained from the calculations. As has been done when comparing the structural stresses, four different graphs will be shown, each one containing the simulations in which one of the parameters defining the CuBER

performance is modified. All graphs contain also the result obtained with the **Bmod** models which works as a reference of the two other results displayed.

Figure 4.30 includes the global performance of the models in which the amplitude is increased or reduced, related to the value defined by the **Bmod** model. In figure 4.31 the results for the models in which the wave length is modified are displayed. Figure 4.32 shows the results for the models with different fibre diameters and, figure 4.33 includes the results for the models in which the stiffness of matrix and fibre are modified.

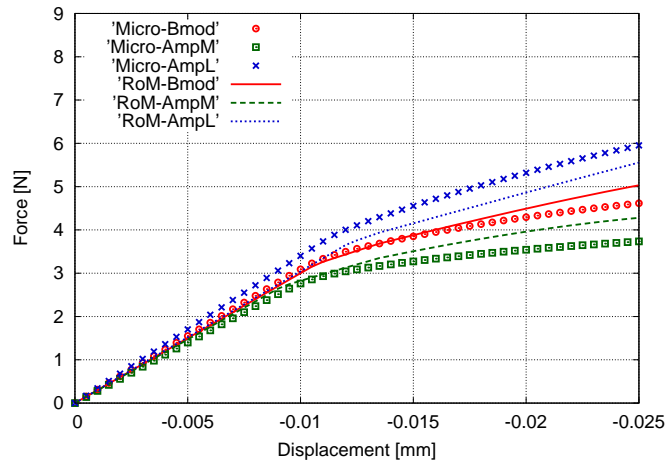


Figure 4.30: Force-displacement graph showing the global behavior of the models in which the amplitude is modified

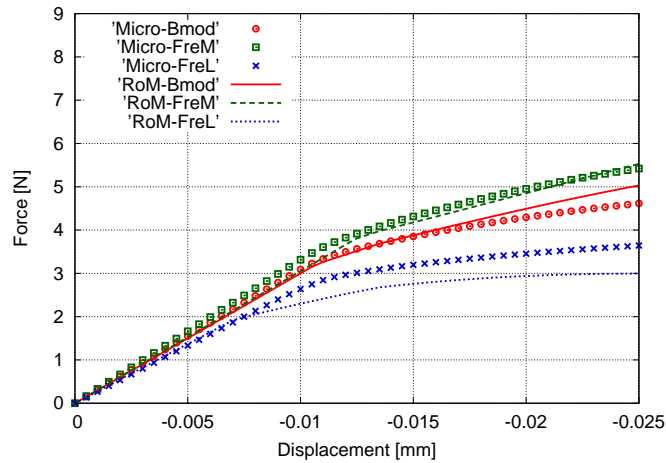


Figure 4.31: Force-displacement graph showing the global behavior of the models in which the wave length is modified

As can be seen in figures 4.30 to 4.33, the global behavior of the RVE obtained with the new proposed formulation and the global behavior obtained from the micro models is nearly the same in all cases. When one of the parameters defining the CuBER problem is modified, it also modifies the point in which damage appears in the composite, as well as the composite stiffness before and after damage apparition. The force-displacement graphs represented show that the modification of these three mechanical performances of the composite is the same in the micro and in the RoM models.

Figure 4.30 shows that the elastic stiffness of the composite suffers small variations when the misalignment amplitude is modified. Despite of the error found in the fictitious structural

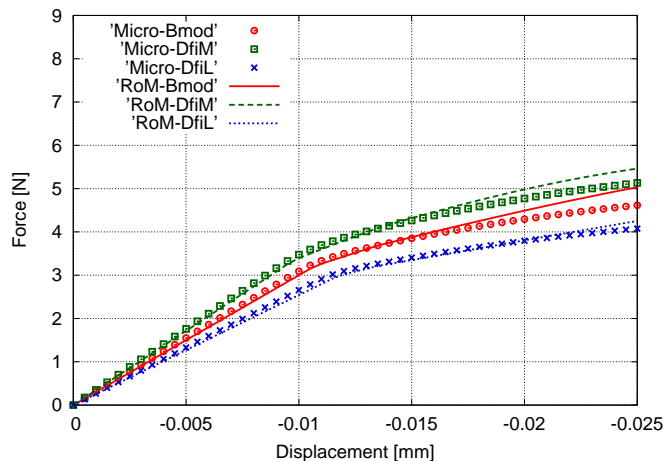


Figure 4.32: Force-displacement graph showing the global behavior of the models in which the fibre diameter is modified

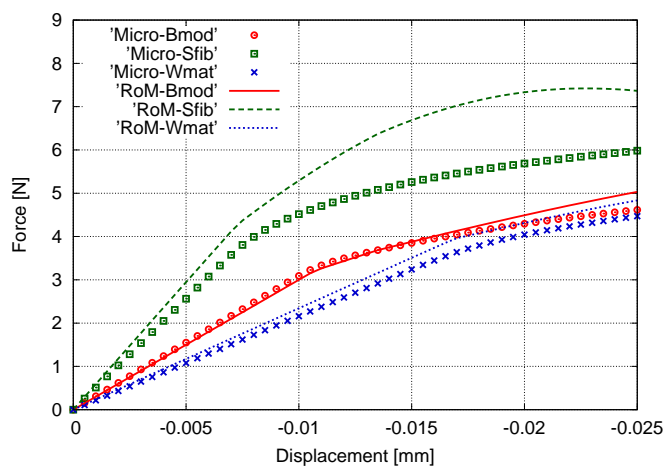


Figure 4.33: Force-displacement graph showing the global behavior of the models in which the stiffness of the composite constituents is modified

stresses, the differences between the load for which degradation starts in the composite is nearly unnoticeably when comparing the global behavior of the micro and the RoM models. And, finally, the error obtained in the composite stiffness after the apparition of damage seems to increase as fibre amplitude is increased. However, the error is small enough to consider the results correct.

When comparing the RVE performance when misalignment wave length is increased or reduced (figure 4.31), the error obtained in the calculation of matrix structural stresses is clearly reflected. Specially when the wave length is reduced. On the other hand, the prediction of the two stiffnesses shown by the composite, before and after fibre damage, are very accurate in all cases.

The comparison of the results obtained for the models in which fibre diameter is modified (figure 4.32) shows a perfect agreement between the micro and the RoM model. This agreement is found in all the composite stiffnesses and in the load for which the composite degradation starts.

The last parameters modified are the fibre and matrix stiffness, which results are shown

in figure 4.33. This figure shows that even the matrix structural stress prediction is quite accurate, the accuracy of the results cannot be guaranteed. While the prediction of the RVE performance with the RoM model is nearly the same that the one obtained with the micro model when matrix stiffness is reduced, the prediction for the case in which fibre stiffness is increased is not as accurate. Specially the stiffness obtained after the apparition of damage in the composite. Thus, composites with larger fibre stiffness will require a better calibration to adjust the micro-structural performance of both models.

With all results shown, it can be concluded that the developed formulation to include the micro-structural effects of fibre misalignment in the serial/parallel mixing theory, using the homogenized constitutive equations obtained from the solution of the CuBER problem, provide accurate results when they are compared with the performance of a finite element micro model. The formulation developed is able to capture modifications in fibre misalignments and fibre and matrix properties; being those the parameters defined in literature related to the fibre buckling problem. Also, the failure cause of matrix material has been found to be due to shear stresses in all simulations performed.

4.5 Numerical procedure to obtain the compression strength of composites

4.5.1 General description of the numerical procedure developed

According to the different authors that have studied the problem of compression strength of long fibre composites (Rosen (1965), Barbero and Tomblin (1996), Balacó de Moraes and Torres Marques (1997) or Drapier et al. (1999), to name a few), this type of failure is produced by the fibre buckling phenomenon. The formulation proposed by these authors depends on three main parameters: fibre initial misalignments, shear strength of matrix material and the proportion between fibres and matrix in the composite. Using these parameters, different formulations are proposed to obtain the maximum compression stress that can be applied to the composite before it fails due to fibre buckling.

In this work, the composite performance is obtained with the serial/parallel mixing theory, which obtains the composite constitutive behavior from the constitutive behavior of its constituent components (section 2.3, Rastellini (2006)). Using the serial/parallel mixing theory, the formulations proposed in literature cannot be used, as they have to be applied to the composite and not to its different constituents. Moreover, as the serial/mixing theory provides the stress-strain for each component material, it is worth take advantage of this extra information (not provided by other composite formulations) to obtain a formulation capable to provide results for tensional states beyond the maximum compression load, and more similar to the real micro-mechanical phenomenons taking place in the composite.

Up to this point, it has been described a new methodology and formulation to take into account the effect of the micro-structural interaction between fibre and matrix, due to fibre initial misalignments, in the serial/parallel mixing theory (section 4.3). To do so, the effects of this micro-structural interaction have been included in the constitutive equations of fibre and matrix defining an homogenized constitutive law for each material. The good performance of this new methodology has been proved in the numerical validation shown in section 4.4.

Therefore, the effects of fibre initial misalignments, as well as the interaction between fibre and matrix due to these misalignments, can be included in the serial/parallel mixing theory

with the formulation developed. It will be shown in this section that if the new formulation is properly included in a finite element code, the compression strength of the composite is obtained straightforward from the constitutive performance of the composite constituents (this ability of the formulation has been already proved in Martínez et al. (2007)).

However, to obtain a general procedure to calculate the compression strength of composite materials, there are other cases that have to be considered that are not included in the homogenized constitutive equations for fibre and matrix obtained in section 4.3. These cases are the situation in which fibres do not have initial misalignments or the situation in which fibre initial misalignments are too small to affect significantly the constitutive behavior of fibre and matrix. A general procedure to obtain the compression strength of composite has also to be able to deal with unloading processes and must provide a different composite performance depending on the sign of the load applied to it: tensile load or compression load.

The procedure proposed to obtain the compression strength of composites, is based in a phenomenological representation of the micro-mechanical performance of the composite constituents. This procedure, besides including fibre initial misalignments in the constitutive equations of fibre and matrix, it also considers other fibre configurations and it takes into account the loading history of the composite.

The two first subjects described in this section are the methodologies used by the new procedure to deal with fibres without initial misalignments and with initial misalignments. In the case of misaligned fibres two different situations are considered: large and small misalignments. Afterwards it is described the numerical implementation of the different formulations developed to obtain the compression strength of the composite. First it is shown how the new procedure is included in the serial/parallel mixing theory and after it is explained how all the formulation is included in a finite element code. Finally, some numerical examples are shown to illustrate the performance of the new fibre buckling theory developed.

4.5.2 Compression strength in fibres without initial misalignments

One of the main parameters defining the fibre buckling phenomenon is fibre initial misalignments. However, there are situations in which these misalignments can be small enough to be imperceptible to the testing methodologies used to record them. There can be also other situations in which their wave length is too large to be considered a proper misalignment. An example of this last situation can be the case of steel reinforcements in a concrete column; according to Barbat and Cardona (1999), the buckling of steel reinforcements in reinforced concrete columns (figure 4.34) is one of the main failure causes of these structural elements in the case of an earthquake. This situation can be understood as a compression failure of a composite (reinforced concrete) due to the fiber buckling phenomenon. In those cases, although misalignments exist, the wave lengths are too large and amplitudes too small to consider the geometric imperfections of the bar fibre misalignments.

To take into account these two particular cases, or any other case in which fiber misalignments can be considered non-existent, it is necessary to obtain a formulation to obtain the maximum compression force that can be applied to the composite due to fibre buckling effects.

The main task of matrix in fibre reinforced composites is to transmit the loads applied to the composite to fibres, which are the elements that will support the load (Oller, 2003). However, if the load applied to the composite is a compression force, matrix also has the function of confining fibres avoiding them to buckle. Fibres are very slender elements that, without the surrounding matrix, will buckle for an infinitesimal load.



Figure 4.34: Buckling of the steel reinforcement of a reinforced concrete column (Barbat and Cardona, 1999).

Although matrix is restraining fibres from buckling, the relation of both materials when fibres do not have initial misalignments is, before fibre buckling, the one provided by the serial/parallel mixing theory: both composite constituents have the same strain in parallel direction and the same stresses in serial directions. But, at a certain load, is possible that matrix cannot restrain fibres any more and fibre buckling occurs.

As has been done with misaligned fibres (section 4.3), this problem can be solved using the existing analogy between the fibre-matrix system and the case of a bar in an elastic foundation. Thus, the fibre buckling load can be computed considering fibres a bar and the matrix in which they are embedded the elastic foundation. Matrix stiffness provides the elastic variable of the foundation. If damage appears in matrix material, the elastic variable defining the foundation will be reduced proportionally to the degradation found in matrix.

The procedure developed to obtain the compression strength of composite materials do not only finds the maximum load that can be applied to the composite but also its post critical strength. Therefore, once fibres without misalignment have buckled, it is necessary to find their new configuration and constitutive performance.

Once the fibre has buckled it will adopt a new geometry. This new geometry is similar to the one found in the case of fibres with initial misalignments and can be defined by a wave length and an amplitude. Therefore, after fibre buckling, the new fibre geometry will be computed and the composite post-critical behavior will be obtained using the formulation already developed for fibres with an initial misalignment.

This section defines the buckling stress for which fibre buckling will occur and the geometric configuration expected in fibre when it has reached this limit buckling stress. At the end of the section is included brief summary of the procedure to be followed and the parameters required by it.

Buckling stress for fibres without initial misalignments

In the case of fibres without initial misalignment, the buckling stress is obtained from the critical buckling load of a straight bar in an elastic foundation. The geometry of the problem is shown in figure 4.35.

To obtain the critical buckling load of a bar under unilateral elastic restriction the energy

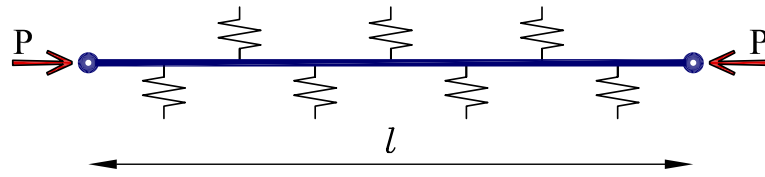


Figure 4.35: Geometry considered to obtain the buckling load of straight fibres

method described by Timoshenko (1940b) will be used. This is an approximate method in which the strain energy of bending (ΔU) is compared with the decrease in the potential work of the load (ΔT). A lower value of ΔT than ΔU means that the deflection of the bar requires an increase of the potential energy of the system; or, which is the same, means that the system is stable. On the other hand, if $\Delta U < \Delta T$, the deflection of the bar is accompanied by a decrease in the potential energy of the system, which makes it unstable. The load that separates both situations is defined as the critical buckling load and can be obtained defining:

$$\Delta U = \Delta T \quad (4.73)$$

According to Timoshenko and Gere (1961), in the case of a bar on an elastic foundation, to obtain the buckling load of the bar its necessary to add the strain energy of the foundation to the energy of bending. Thus, equation 4.73 becomes:

$$\Delta U_1 + \Delta U_2 = \Delta T \quad (4.74)$$

Where U_1 is the bending energy and U_2 is the strain energy of the foundation.

In order to obtain the critical load from equation 4.74, it is necessary to know the deflection that will have the bar when buckling. The general equation for the deflection curve of the beam can be expressed by the fourier series:

$$\omega = \sum_{n=1}^{\infty} a_n \sin\left(\frac{n\pi x}{l}\right) \quad (4.75)$$

Once knowing the expected deflection, the expression that provides the energy of bending is:

$$\Delta U_1 = \frac{EI}{2} \int_0^l \left(\frac{d^2\omega}{dx^2}\right)^2 dx = \frac{\pi^4 EI}{4l^3} \sum_{n=1}^{\infty} n^4 a_n^2 \quad (4.76)$$

And the strain energy of the elastic foundation is:

$$\Delta U_2 = \frac{k}{2} \int_0^l \omega^2 dx = \frac{kl}{4} \sum_{n=1}^{\infty} a_n^2 \quad (4.77)$$

Being k the elastic modulus of the foundation and n the buckling mode shape.

Considering that the beam is loaded with a normal compressive force, the decrease in the potential work of the load can be written as:

$$\Delta T = \frac{P}{2} \int_0^l \left(\frac{d\omega}{dx} \right)^2 dx = \frac{\pi^2 P}{4l} \sum_{n=1}^{\infty} n^2 a_n^2 \quad (4.78)$$

The substitution of expressions 4.76 to 4.78 into equation 4.74 leads to the expression that will provide the critical buckling load of a bar on an elastic foundation, which is:

$$\frac{\pi^4 EI}{4l^3} \sum_{n=1}^{\infty} n^4 a_n^2 + \frac{kl}{4} \sum_{n=1}^{\infty} a_n^2 = \frac{\pi^2 P}{4l} \sum_{n=1}^{\infty} n^2 a_n^2 \quad (4.79)$$

To obtain the critical value of load P , the deflection curve of the beam can be simplified defining all a_n parameters equal to zero except one (Timoshenko and Gere, 1961). So, writing the deflection of the bar as,

$$\omega = a_n \sin \left(\frac{n\pi x}{l} \right) \quad (4.80)$$

Equation 4.79 becomes,

$$\frac{\pi^4 EI}{4l^3} n^4 a_n^2 + \frac{kl}{4} a_n^2 = \frac{\pi^2 P}{4l} n^2 a_n^2 \quad (4.81)$$

This last expression must be valid for any value of a_n . Thus, the critical buckling load of a beam under unilateral elastic restriction can be written as,

$$P_{cr} = \frac{\pi^2 EI}{l^2} \left(n^2 + \frac{kl^4}{n^2 \pi^4 EI} \right) \quad (4.82)$$

Where the n value defines the buckling mode of the bar. According to equation 4.82 the value of n that makes P_{cr} minimum depends on the elastic modulus of the foundation and the length and stiffness of the bar. So, the buckling mode of the bar will depend on the value of these parameters.

One of the main problems found with the formulation described to obtain the buckling load of a bar in an elastic foundation is the definition of the buckling length l to be used. In the case considered, fibre vertical movement is restrained with the same intensity along the whole fibre length.

In order to consider the most unfavorable situation, the buckling length that will be assumed is the buckling length that minimizes the critical buckling load. This buckling length can be obtained searching the value of l that minimizes the function $P_{cr}(l)$ defined in equation 4.82:

$$\frac{dP_{cr}}{dl} = 0.0 \quad \longrightarrow \quad -2\pi^2 EI \left(\frac{n^2}{l^3} - \frac{kl}{n^2 \pi^4 EI} \right) = 0.0 \quad (4.83)$$

Expression 4.83 defines a critical buckling length, which value is:

$$l_{cr} = n\pi \sqrt[4]{\frac{EI}{k}} \quad (4.84)$$

If the buckling length defined in equation 4.84 is replaced in expression 4.82, the critical buckling load obtained is:

$$P_{cr} = 2\pi\sqrt[2]{kEI} \quad (4.85)$$

This last expression is interesting to be analyzed because, as it can be seen, the dependence on the buckling mode disappears from the critical load value, which provides a unique buckling load value for all buckling modes. The only dependence in the buckling mode is found in the critical length, which increases linearly with the value of n . A better understanding of these results can be obtained looking at table 4.9 in which the buckling load, buckling length and final bar deformation are displayed for different buckling modes. This table has been made considering the following values defining the problem: $E = 78.0$ GPa, $\varnothing_f = 15 \mu\text{m}$ (from the fibre diameter can be obtained its inertia) and $k = 3.0$ GPa.





Buckling mode	Buckling load	Buckling length	Bar deflection
1	4.71 N	50.0 μm	
2	4.71 N	100.0 μm	
3	4.71 N	150.0 μm	
4	4.71 N	200.0 μm	

Table 4.9: Critical buckling load and length for different buckling modes

Table 4.9 shows that for the same buckling load, different bar deformations can be obtained depending on the buckling length or buckling mode considered. All deformations obtained are a combination of the first buckling mode deformation. Thus, if an infinite fibre is considered, the buckling load provides a deformation that follows a periodic misalignment path. This effect validates the assumption that after fibre buckling, the formulation developed for fibres with initial misalignments can be used to predict the post-critical behavior of straight fibres.

Once knowing the critical buckling load for which fibres will buckle, this load must be converted to a critical stress in order to be verified by the constitutive equation of fibre material. This conversion is made dividing the critical load by fibre area. Therefore, the critical stress that will lead to fibre buckling is:

$$\sigma_{cr} = \frac{2\pi\sqrt[2]{kEI}}{\pi\varnothing_f^2/4} = \frac{8\sqrt[2]{kEI}}{\varnothing_f^2} \quad (4.86)$$

The critical stress defined in equation 4.86 corresponds to the critical stress in fibre longitudinal direction. Thus, it has to be compared with the parallel component of the stress tensor obtained for fibre material provided by the serial/parallel mixing theory.

Geometry of fibres after buckling

Once fibres have reached their buckling stress, their geometry must change from aligned to misaligned in order to apply the misaligned fibre formulation and obtain their post-critical

performance. The new geometry configuration of fibres is provided by the the bar deflection equation used to obtain the buckling stress (equation 4.75), which is defined by the amplitude a_n and the wave length l_{cr} .

The value of l_{cr} that is considered corresponds to the first buckling mode of the fibre. Therefore, to determine the fibre new geometry is necessary to determine the value of the amplitude a_1 . The value of this parameter is obtained using the existing equilibrium between the critical buckling load applied to the fibre and the restrain effort made by matrix material to avoid fibre displacement.

Two different equations are defined to obtain the new fibre geometry. These equations are deduced using the following hypothesis:

1. Fibre new geometry is considered to be contained in an arch of circumference. This approximation has been already used when solving the CuBER problem and it has been already proved its validity.
2. When fibre buckles it increases its length. This length increment implies a reduction of the longitudinal stress found in fibre material.
3. New fibre geometry is determined by the equilibrium between matrix efforts over fibres and fibre normal stresses.
4. Only longitudinal stiffness is considered in fibre to obtain its new geometry. Flexural stiffness is considered negligible in the mechanical effects that provide new fibre configuration.

Based on the hypothesis mentioned above, the first equation used to calculate the new fibre geometric configuration is based on geometry assumptions. The length of the fibre before applying any load to the composite is, as it is shown in figure 4.36, l_{cr} .

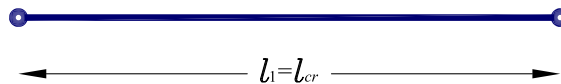


Figure 4.36: Fibre geometry before applying any load to the composite

As the compression load increases in fibre, its length is reduced according to the longitudinal strains applied to the composite. Thus, just before buckling, the fibre geometry is the one shown in figure 4.37, and its length is l_2 :

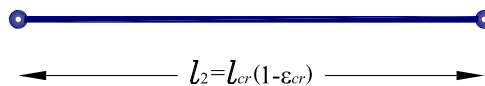


Figure 4.37: Fibre geometry just before reaching the critical buckling load

$$l_2 = l_{cr}(1 - \varepsilon_{cr}) \quad (4.87)$$

where ε_{cr} , is obtained from the critical buckling stress:

$$\varepsilon_{cr} = \frac{\sigma_{cr}}{E} \quad (4.88)$$

When fibre buckles its geometry must change from the geometry shown in figure 4.37 to a curved geometry. At this point, the first hypothesis defined is used to obtain the new fibre geometric configuration. Thus, the new fibre shape must be contained in an arch of circumference and the new fibre length can be obtained from the arch equation. Figure 4.38 shows the new geometry of the fibre and the most relevant parameters defining the geometry. It is important to notice in this figure that the distance between the ending nodes of the fibre remains l_2 : the longitudinal length of the fibre must remain constant and what varies its transversal geometry.

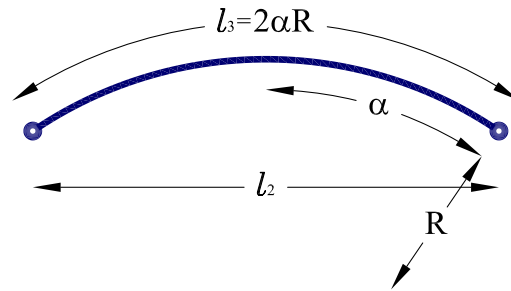


Figure 4.38: Fibre geometry just after reaching the critical buckling load

From the final geometry of the fibre, shown in figure 4.38, can be obtained the relation between the internal angle α and the radius R . This is:

$$\sin(\alpha) = \frac{l_2}{2R} = \frac{l_{cr}(1 - \varepsilon_{cr})}{2R} \quad (4.89)$$

The other equation required to calculate the final configuration of the fibre is obtained imposing the second and third hypothesis. The second hypothesis says that the length increment of fibre after buckling implies a reduction of the applied force in the fibre. The length increment in fibre due to the change in its geometry is obtained losing some of the longitudinal strains existing before fibre buckling. Therefore, the new longitudinal strain in fibre is:

$$\hat{\varepsilon} = \frac{l_1 - l_3}{l_1} = \frac{l_{cr} - 2\alpha R}{l_{cr}} \quad (4.90)$$

This variation in the longitudinal strain of fibre material produces a variation in the longitudinal stress and, consequently, a variation on the axial force applied to the fibre. The value of the new axial force is:

$$\hat{\sigma} = E\hat{\varepsilon}; \quad P = \hat{\sigma}A_f; \quad \rightarrow \quad P = EA_f \frac{l_{cr} - 2\alpha R}{l_{cr}} \quad (4.91)$$

According to the third hypothesis, the new axial force in the fibre must be in equilibrium with the external load, q , result of the restraint of matrix material over fibre (figure 4.39). The external load is proportional to the fibre radial displacement ω :

$$q = k\omega \quad (4.92)$$

The expression of the radial displacement suffered by the fibre can be obtained from the circumferential properties of the new fibre geometry. Thus,

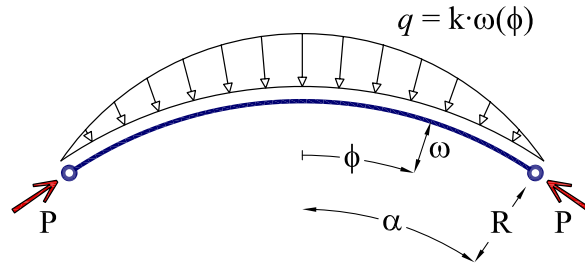


Figure 4.39: Equilibrium defined between compression force in fibre and elastic restraint of matrix

$$\omega(\phi) = R \left(1 - \frac{\cos \phi}{\cos \alpha} \right) \quad (4.93)$$

In order to have the system displayed in figure 4.39 in equilibrium, the sum of the external forces made by matrix over the fibre must be equal to the axial force existing in fibres. Therefore,

$$P = \int_0^\alpha qR \, d\phi = \int_0^\alpha kR^2 \left(1 - \frac{\cos \phi}{\cos \alpha} \right) \, d\phi \quad (4.94)$$

Being P the axial force in fibre defined in equation 4.91. Replacing the expression of this force in equation 4.94 the second equation required to obtain the fibre new geometric configuration is obtained:

$$EA_f \frac{l_{cr} - 2\alpha R}{l_{cr}} = \int_0^\alpha kR^2 \left(1 - \frac{\cos \phi}{\cos \alpha} \right) \, d\phi \quad (4.95)$$

The new fibre geometry, defined by the arch radius R and the internal angle α can be obtained with the non-linear system defined by equations 4.89 and 4.95. After solving the integral defined in equation 4.95 and rearranging both equations, the system to be solved becomes:

$$\begin{cases} \frac{l_{cr}(1 - \varepsilon_{cr})}{2 \sin \alpha} - R = 0 \\ kR^2 \left(\alpha - \cos \alpha \ln \left[\tan \left(\frac{\pi}{4} + \frac{\alpha}{2} \right) \right] \right) - EA_f \frac{l_{cr} - 2\alpha R}{l_{cr}} = 0 \end{cases} \quad (4.96)$$

This non-linear system of equations is solved using a Newton Raphson method (Hoffman, 2001). To do so, the second equation of 4.96 is transformed into the function $f(\alpha)$ that has to be minimized:

$$f(\alpha) = kR^2 \left(\alpha - \cos \alpha \ln \left[\tan \left(\frac{\pi}{4} + \frac{\alpha}{2} \right) \right] \right) - EA_f \frac{l_{cr} - 2\alpha R}{l_{cr}} \quad (4.97)$$

The procedure starts with an initial prediction of α equal to the maximum angle allowed by the equations: $\alpha = \pi/2$. From this initial prediction the value is corrected following the Newton Raphson scheme,

$$\alpha^{i+1} = \alpha^i - \frac{f(\alpha^i)}{f'(\alpha^i)} \quad (4.98)$$

until the desired tolerance is obtained:

$$f(\alpha^n) \leq \text{toler} \quad (4.99)$$

With this procedure in less than seven iterations the error is smaller than 10^{-10} .

Once having the new geometry radius and internal angle, both values must be converted to the amplitude, A , and wave-length, λ required by the CuBER formulation (equation 4.100). With the new misalignment parameters, the formulation of fibres with initial misalignments can be applied to obtain the post-critical behavior of the fibre.

$$\begin{aligned} A &= R(1 - \cos \alpha) \\ \lambda &= 4R \sin \alpha \end{aligned} \quad (4.100)$$

Parameters required by the formulation developed for fibres without initial misalignments and procedure summary

The equations described previously provide the constitutive performance of composite materials made of fibres without initial misalignments under compression efforts. This section reviews the most important expressions obtained to solve the problem and defines the main parameters required by the formulation from the finite element code.

To verify if fibre buckling occurs or not in the composite is required to compare the parallel stresses of fibre material with the critical buckling stress obtained in equation 4.86.

$${}^f\sigma_P \leq \sigma_{cr} = \frac{8\sqrt[2]{kEI}}{\phi_f^2} \quad (4.101)$$

Thus, to know if fibre buckling occurs it is necessary provide to the formulation the fibre parallel stress component. It is also required the fibre longitudinal stiffness, E , and the matrix stiffness, k . Both stiffnesses are defined by each material young modulus when the material is still under elastic conditions. However, if damage has appeared in any of the composite constituent materials, the damage effect must be included in the stiffness value (see equations 4.38 and 4.39 in section 4.3 for matrix and fibre, respectively). Finally, it is also necessary to know the fibre diameter, which is required by the equation and to obtain the moment of inertia I .

If fibre buckling occurs, the new fibre geometry will be obtained using the non-linear system of equations 4.96. Which requires, to be solved, the same information used to obtain the fibre buckling stress.

Once the fibre new geometric configuration is known, to obtain the post-critical performance of the composite the code uses the formulation developed for composites in which fibers have initial misalignments. The parameters required by this problem are fully described in next section.

4.5.3 Compression strength in fibres with initial misalignments

The procedure used to obtain the compression strength of composite materials in which fibres have initial misalignments is based in the composite performance obtained with the homogenized constitutive equations presented in section 4.3 of the present chapter. Section 4.4 has shown the mechanical performance obtained in the composite when fibre and matrix are simulated using the homogenized constitutive equations developed: degradation in matrix appears for lower compression stresses and fibre stiffness is reduced. This reduction of fibre stiffness becomes more significant as matrix damage increases because the confinement effect provided by matrix is weaker.

As the load in the composite increases, it is possible that the damage in matrix and the structural damage in fibre makes the the composite unable to support the applied load. At this point the maximum compression force that can be applied to the composite is reached and the stress-strain relation begins to decrease providing the post-critical path of the composite.

This situation is shown in figure 4.40 in which the force-displacement graph obtained for the composite and the damage evolution in matrix and fibre are represented. In this graph it has been marked the displacement in which the maximum load is reached in the composite ($\text{disp} = -35.5 \mu\text{m}$). The composite properties defined to obtain this graph correspond to the properties of the RoM-Bmod model defined in section 4.4.

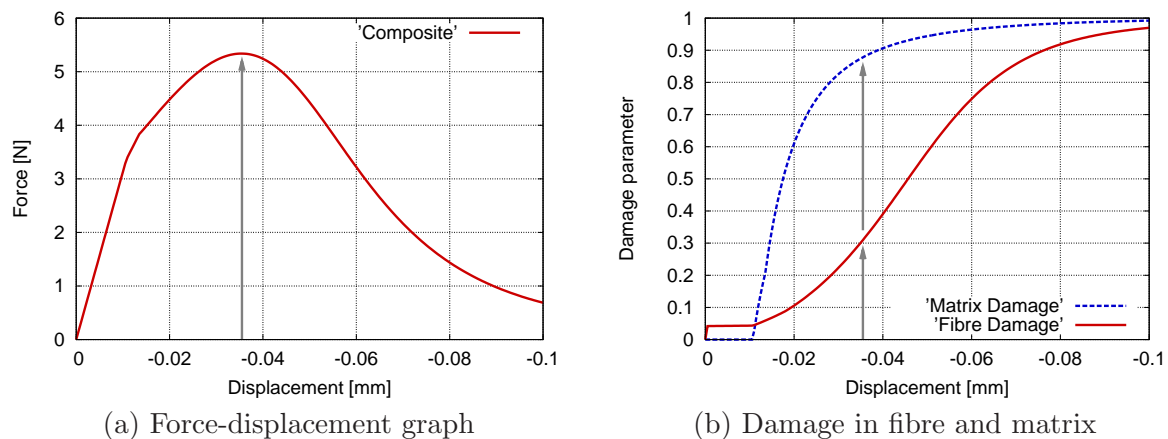


Figure 4.40: Post critical performance of a composite with fibres with initial misalignments

Figure 4.40 shows that the formulation developed to take into account fiber initial misalignments and the interaction between fiber and matrix provides the buckling strength of the composite without requiring any additional formulation. When matrix cannot restrain fibers any more, their initial misalignment starts increasing indefinitely, being unable to provide more strength to the composite. This state is taken as fiber buckling. This approach to obtain the fiber buckling load has already been used in the work of Akbarov and Kosker (2001).

Eventually, damage in matrix can reach a level in which the confinement effect becomes non-existent. When this situation is reached, the equations that provide the structural displacement of the fibre are not longer valid and must be replaced by the equations of a curved bar.

Another situation that must be considered in the case of fibres with initial misalignments corresponds to the case in which the misalignments are too small (very large wave length with small amplitudes) to affect significantly the composite performance. In these situations

is possible that fibre buckle like a straight fibre before the homogenization procedure affects the composite performance. As there is no way to know *a priori* if the compression strength of composites with misaligned fibres will be determined by the homogenized constitutive equations or if fibres will buckle because misalignments are too small, it is necessary to verify at each load step if the stresses applied over the misaligned fibre are larger than the buckling stresses.

In the case of misaligned fibres, the buckling stress is obtained using the existing analogy between the composite micro-structural configuration and the case of a curved bar in an elastic foundation, for which the buckling load can be obtained.

Therefore, to obtain the compression strength of fibres with initial misalignments it has to be included, to the numerical procedure based in the homogenized constitutive equations, the performance of the fibre when there is no more matrix to restrain it and the calculation of the buckling stress in the case of curved fibres. The formulations required for these two last calculations are described in the following. Afterwards it will be drawn a brief summary of the procedure used to obtain the compression strength of composite with misaligned fibres.

Fibre performance when matrix is completely damaged

As has been already commented, when matrix is completely damaged the equations used to solve obtain the constitutive performance of fibre and matrix due to fibre initial misalignments are no longer valid. Therefore, the CuBER formulation must be replaced by the formulation of a curved bar. The geometric configuration of the problem considered is shown in figure 4.41.

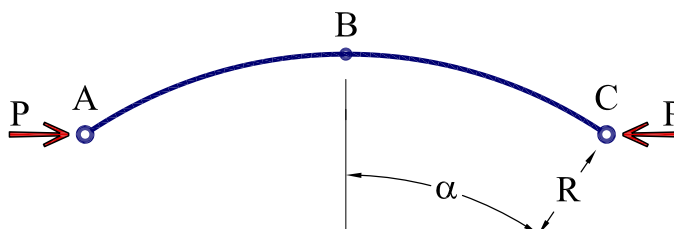


Figure 4.41: Geometry of the curved bar problem when matrix is completely damaged

The displacements of the bar shown in figure 4.41, for the applied force P can be obtained easily using the unit force method described in (Cervera and Blanco, 2004). This method is based in the principle of virtual work. In order to obtain the displacement in a specific point of the structure, a unit force, in the same direction of the displacement sought, must be applied to the point in which the displacement is required. Therefore, the displacement becomes:

$$d_i = \int_0^L \frac{MM^*}{EI} dS \quad (4.102)$$

Being M the bending moments law of the structure, M^* the bending moments law obtained from the unit force applied and L the total length of the structure.

Using the existing symmetry of the problem, and transforming the axis to polar coordinates, the horizontal displacement of the curved bar in point C is obtained with the following expression:

$$\begin{aligned}
u_C &= -\frac{PR^3}{EI} \int_0^\alpha (\cos \phi - \cos \alpha)^2 d\phi \\
&= -\frac{PR^3}{EI} \left[\alpha \left(\frac{1}{2} + \cos^2 \alpha \right) - \frac{3}{2} \cos \alpha \sin \alpha \right]
\end{aligned} \tag{4.103}$$

And the vertical displacement of point B is obtained as:

$$\begin{aligned}
v_B &= -\frac{PR^3}{EI} \int_0^\alpha (\cos \phi - \cos \alpha) (\sin \alpha - \sin \phi) d\phi \\
&= -\frac{PR^3}{EI} \left[\frac{1}{2} \sin^2 \alpha - \alpha \cos \alpha \sin \alpha + \cos \alpha - \cos^2 \alpha \right]
\end{aligned} \tag{4.104}$$

The displacement values obtained for the case of a curved bar, without any kind of restriction, can be used as were used the displacements obtained when solving the CuBER problem to obtain the homogenized constitutive law of fibre material. Therefore, the new structural stiffness for fibre becomes:

$$f^s E^* = \frac{P}{A_{fib}} \frac{0.25\lambda}{u_C} \tag{4.105}$$

This new value of fibre structural stiffness is used to obtain the homogenized constitutive performance of fiber material if the matrix confinement of fibres becomes negligible. This situation is considered to occur when the new fibre structural stiffness is larger than the structural stiffness obtained with the CuBER problem (equation 4.50). The values for the amplitude and wave-length are actualized with the values obtained for u_C and v_B .

It is important to point out that if this new fiber stiffness replaces the stiffness obtained when solving the CuBER problem, no structural stresses must be added to the matrix homogenized constitutive law, as matrix collaboration has been assumed non-existent.

Buckling stress of misaligned fibres

The critical buckling stress for fibres with initial misalignments is obtained following the same procedure used to obtain the buckling stress of straight fibres. The buckling load is obtained from the energy equilibrium:

$$\Delta U_1 + \Delta U_2 = \Delta T \tag{4.106}$$

In this case, the radial deflection of the beam produced by a small perturbation of the load applied is:

$$\omega = \omega_0 + \delta\omega \tag{4.107}$$

Where ω_0 is the beam deflection in the equilibrium state and $\delta\omega$ is the perturbation of this deflection, that can be expressed by Fourier series as,

$$\delta\omega = \sum_{n=1}^{\infty} a_n \sin\left(\frac{n\pi\phi}{\alpha}\right) \quad (4.108)$$

Wang and Shenoi (2004) define the following expressions to characterize the energy variation in the case of a curved beam. The expression for the change in the bending strain energy is:

$$\Delta U_1 = \frac{EI}{2} \int_0^\alpha \left(\frac{1}{R^2} \frac{d^2\omega}{d\phi^2} + \frac{\omega}{R^2} \right)^2 R d\phi - U_1 \quad (4.109)$$

Being $U_1 = (EI/2R^3)\omega_0^2\alpha$ the bending strain energy of the beam in its equilibrium state. If equation 4.109 is integrated and ω is replaced by its definition according to equations 4.107 and 4.108, the final expression for the change in the bending strain energy becomes:

$$\Delta U_1 = \frac{EI}{4R^3} \sum_{n=1}^{\infty} \left[1 - \left(\frac{\pi n}{\alpha} \right)^2 \right]^2 a_n^2 + \frac{2EI\omega_0\alpha}{\pi R^3} \sum_{n=1,3,5,\dots}^{\infty} \left[1 - \left(\frac{\pi n}{\alpha} \right)^2 \right]^2 \frac{a_n}{n} \quad (4.110)$$

The expression for the change in the elastic foundation strain energy is:

$$\Delta U_2 = \frac{1}{4} k\alpha R \sum_{n=1}^{\infty} a_n^2 + 2k\omega_0 R \sum_{n=1,3,5,\dots}^{\infty} \frac{a_n\alpha}{\pi n} \quad (4.111)$$

And, the work done by the external forces (considering the contribution of the normal force and the bending moment) can be written as:

$$\Delta T = \frac{\pi^2\omega_0}{4\alpha} \left(k + \frac{EI}{R^4} \right) \sum_{n=1}^{\infty} n^2 a_n^2 - \frac{2\pi EI\omega_0}{\alpha R^3} \sum_{n=1,3,5,\dots}^{\infty} n a_n \quad (4.112)$$

This last equation is obtained considering the bending moment and the normal force constants, with the following expression at the static equilibrium state:

$$P_0 = kR\omega_0 \quad M_0 = \frac{EI\omega_0}{R^2} \quad (4.113)$$

Replacing in equation 4.106 the expressions defined in 4.110 to 4.112 and rearranging the result, the critical buckling load of a curved beam in an elastic foundation can be written, in a general form, as:

$$P_0 = \frac{\frac{EI\alpha}{R^3} \sum_{n=1}^{\infty} \left[1 - \left(\frac{\pi n}{\alpha} \right)^2 \right]^2 a_n^2 + kR\alpha \sum_{n=1}^{\infty} a_n^2}{\frac{\pi^2}{R\alpha} \left(1 + \frac{EI}{kR^4} \right) \sum_{i=1}^{\infty} n^2 a_n^2 - \frac{8EI}{kR^4} \left\{ \frac{\alpha}{\pi} \sum_{n=1,3,\dots}^{\infty} \left[1 - \left(\frac{\pi n}{\alpha} \right)^2 \right] \frac{a_n}{n} + \frac{\pi}{\alpha} \sum_{n=1,3,\dots}^{\infty} n a_n \right\} - \frac{8\alpha}{\pi} \sum_{n=1,3,\dots}^{\infty} \frac{a_n}{n}} \quad (4.114)$$

Following the same procedure defined for the straight beam, the critical buckling load can be obtained considering only the contribution of one of the terms of the Fourier series. The solution for $n = 1$ will not be considered because it corresponds to a rigid body movement.

The critical buckling load for even n values is:

$$P_{cr} = \frac{\alpha^2 \frac{EI}{R^2} \left[1 - \left(\frac{\pi n}{\alpha} \right)^2 \right]^2 + kR^2}{\pi^2 \left(1 + \frac{EI}{kR^4} \right) n^2} \quad (4.115)$$

And the critical buckling load for odd n values is:

$$P_{cr} = \frac{\alpha^2 \frac{EI}{R^2} \left[1 - \left(\frac{\pi n}{\alpha} \right)^2 \right]^2 a_n + kR^2 a_n}{\pi^2 \left(1 + \frac{EI}{kR^4} \right) n^2 a_n - \frac{8\alpha^2}{\pi^3 n} \left(\frac{EI}{kR^3} + R \right)} \quad (4.116)$$

From this last equation can be obtained the value of a_n :

$$a_n = \frac{\frac{8\alpha^2 P_{cr}}{\pi^3 n} \left(\frac{EI}{kR^3} + R \right)}{\left(1 + \frac{EI}{kR^4} \right) n^2 P_{cr} - \frac{\alpha^2}{\pi^2} \left\{ \frac{EI}{R^2} \left[1 - \left(\frac{\pi n}{\alpha} \right)^2 \right]^2 + kR^2 \right\}} \quad (4.117)$$

The deflection amplitude a_n reaches its maximum value when the denominator of this expression becomes zero. This condition leads to the expression of the critical buckling load for odd n values, which is exactly the same as the one found for even n values (equation 4.115).

This result is coherent with the critical buckling load obtained for a straight beam. It can be easily verified that equation 4.115 becomes equation 4.82 when $\alpha R \rightarrow l$ and $R \rightarrow \infty$.

In the case of fibres with initial misalignments, the buckling length considered corresponds to the length between two consecutive inflection points of the misalignment. This is:

$$l = \lambda/2 \quad (4.118)$$

So, in order to obtain the critical buckling load of the system, is required to evaluate expression 4.115 for different n values until the minimum value of P_{cr} is found. The buckling stress will be calculated as:

$$\sigma_{cr} = \frac{P^*}{A_f} \quad \text{with} \quad P^* = \min \{ P(n = i); i \in \mathbb{N} \} \quad (4.119)$$

If at any load step fibre parallel stresses are larger than σ_{cr} , fibre buckling will occur and the new misalignment configuration should be computed. To obtain the new amplitude and wave length the same procedure used for straight fibres is used. However, in this case, the length used to obtain the new geometry corresponds to the buckling length l (defined in equation 4.118) divided by the n value defining the buckling mode. The reason for which this length is used can be easily understood looking at the buckling deformation obtained, for example, for $n = 2$. This deformation is shown in figure 4.42. This figure shows that the new misalignment is contained in half the buckling length used to verify the critical buckling stress in the fibre.

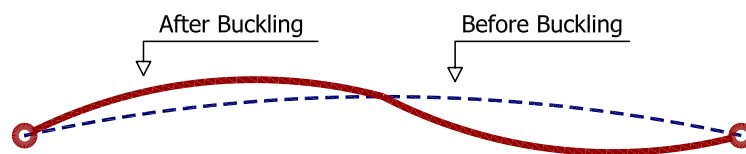


Figure 4.42: Second buckling mode of a curved beam in an elastic foundation

4.5.4 Parameters defining the fibre buckling problem

Having defined all the numerical procedures required to obtain the compression strength of composite materials and all the formulation involved, they must be included in a finite element code in order to perform numerical simulations of composites taking into account the fibre buckling phenomenon.

The numerical code in which the procedures are included is PLCd (CIMNE, 2008). This is a finite element code that works with two and three-dimensional solid geometries and with beam elements. Composite materials are treated in it using the serial/parallel mixing theory developed by Rastellini (2006). It can deal with kinematic and material nonlinearities. It uses various constitutive laws to predict the material behavior (Elastic, visco-elastic, damage, damage-plasticity, etc. Oller et al. (1990)) and uses different yield surfaces to control their evolution (Von-Mises, Mohr-Coulomb, improved Mohr-Coulomb, Drucker-Prager, etc. Malvern (1968); Lubliner et al. (1989)). The Newmark method (Barbat et al., 1997) is used to perform dynamic analysis. The beam element formulation included in PLCd is fully described in Mata et al. (2007, 2008).

The input data file required by PLCd contains all information related to a finite element method: mesh elements, mesh nodes, material properties, boundary conditions, etc. As PLCd code deals with composites using the serial/parallel mixing theory, it requires the definition of each composite material according to its constituent materials and their volumetric participation. Finally, to be able to obtain the compression strength of the composite with the new formulation developed, few more parameters must be defined for each composite used in the simulation. In the following these parameters are described, as well as the way in which the code uses them.

There are five misalignment parameters required by the formulation that must be included in the PLCd input data file. These are described in table 4.10.

Rfib:	Fibre radius
Ampl:	Misalignment amplitude
Freq:	Misalignment wave-length
AffM:	Proportion of matrix affected by fibre misalignments
FrLe:	Fracture Length to be considered in matrix damage formulation

Table 4.10: Parameters required by PLCd to obtain the compression strength of composites

There can be some simulations in which the compression strength of the composite is not a limitation factor, either because the composite is always loaded with tensile stresses, either because the compression forces applied to the composite are very small. In these cases, it is interesting to skip all the compression strength procedure to reduce the computational cost of the simulation. For this reason, the **Rfib** parameter not only provides to the code with the information of fibre radius but also tells the code if the compression strength procedure must be applied to the present simulation or not. If this parameter is defined as 0.0, the code

understands that the compression strength of the composite is not an important issue in the simulation and skips its verification.

The **Ampl** parameter does also have a double meaning as it tells the code if fibres have initial misalignments or not. If **Ampl** is defined as 0.0 the code considers the case of straight fibres. Otherwise, if an amplitude value is given to **Ampl**, the initial misalignment formulation will be applied in present simulation. In this case it is necessary to give a value different of 0.0 to **Freq** parameter.

Finally, the last two parameters defined in table 4.10, **AffM** and **FrLe**, should be defined as 0.0 except in exceptional cases. These two parameters, amount of matrix affected by fibre misalignments and fracture length to be applied to matrix damage formulation, are automatically computed by the code according to the expressions 4.69 and 4.71 defined in section 4.3. However, there can be some simulations in which these parameters must be defined manually. In these cases, they can be defined in the input data file replacing the 0.0 (which tells the code to calculate them) for the value that wants to be considered.

4.5.5 Implementation of the numerical procedure proposed in a finite element code

The numerical procedures and formulations developed to obtain the compression strength of composite materials due to the fibre buckling phenomenon are included in PLCd, a finite element code that deals with composite materials using the serial/parallel mixing theory. Therefore, the mixing theory algorithm (already described in section 2.3) must be modified to include the new formulations developed.

The fibre buckling formulation not only affects the constitutive performance of fibre and matrix materials but also requires to establish communication between both materials, as the degradation and the stress-strain state of each one affects the other one. This situation forces the compression strength procedure to interact in different places of the serial/parallel mixing algorithm to gather all information required by the fibre buckling formulation and to provide a correct constitutive performance of the composite.

This section describes, using flow charts, how the formulation defined in this section and in section 4.3 is implemented in the serial/parallel mixing algorithm. The first flow chart shown, in figure 4.43, provides a description of the modifications required in the serial/parallel mixing theory to include the fibre buckling procedure. In this flow chart all procedures related to the compression strength formulation are shaded in blue. As can be seen it is necessary to modify the serial/parallel mixing theory algorithm in two different places.

The first time in which the CuBER problem is solved is just after obtaining the prediction of the strain tensors for fibre and matrix, in order to obtain the fictitious structural stresses required by the matrix homogenized constitutive equation. It is important to remark that the CuBER problem is solved only if fibres are misaligned. In case of aligned fibres there is no need to solve the CuBER problem because matrix structural stresses are zero.

The second time in which the serial/parallel mixing theory algorithm has to be modified is after solving the matrix homogenized constitutive law. At this point, the code enters into the fibre buckling algorithm (or compression strength algorithm), described in figure 4.44, with the matrix damage parameter obtained from matrix constitutive law. This damage parameter is required to obtain the fiber homogenized constitutive performance. The code enters into the fibre buckling algorithm in each iteration performed by the serial/parallel mixing theory,

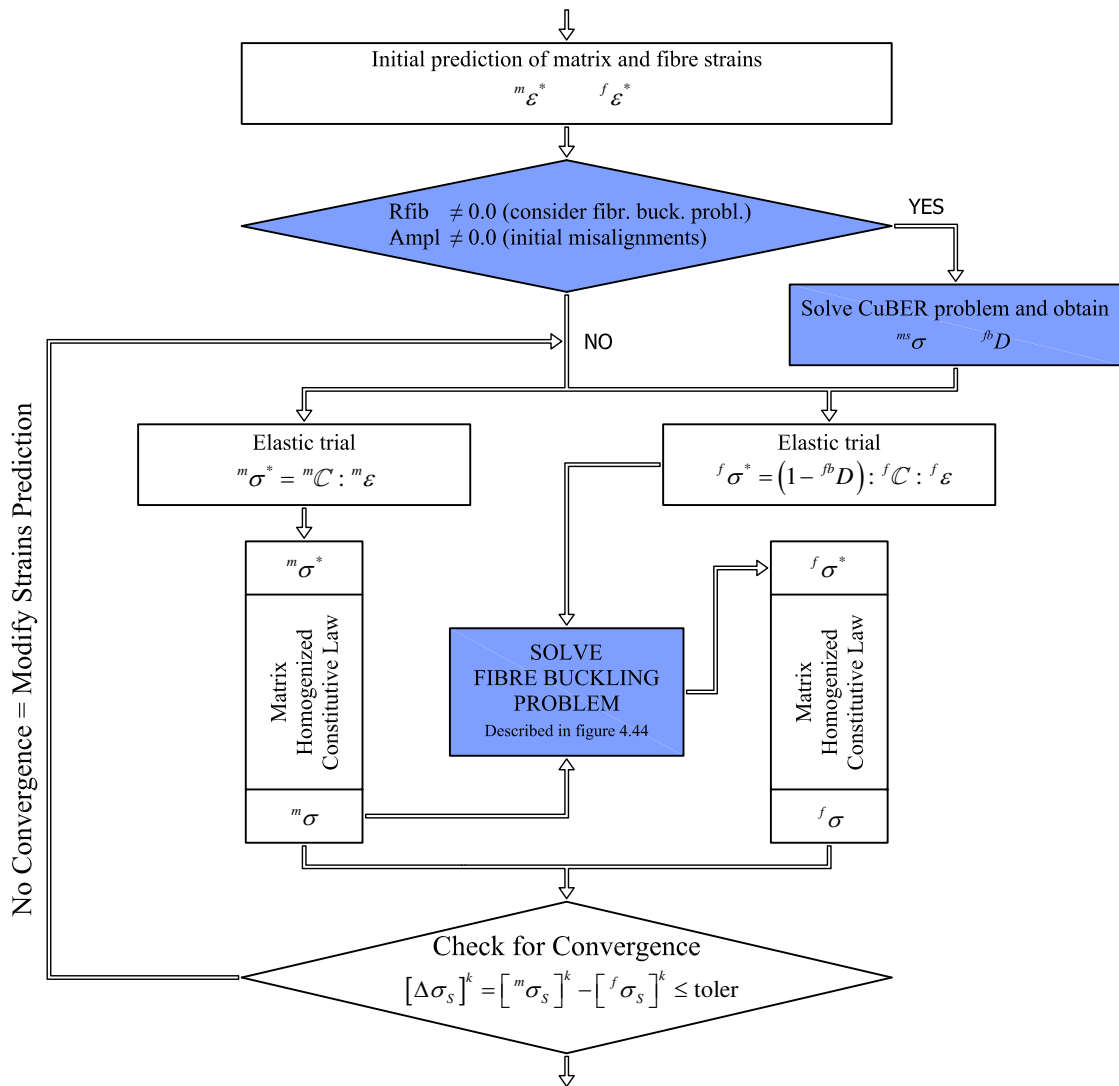


Figure 4.43: Flow chart with the implementation of the compression strength algorithm in the serial/parallel mixing theory. The algorithm used to solve the fibre buckling problem is described in figure 4.44

as the matrix damage parameter can be modified in each iteration, being possible that these modifications affect fibre constitutive performance.

The fibre buckling algorithm calculates the parameters required by fibre and matrix homogenized constitutive equations for all the possible situations considered to obtain the compression strength of composite materials. Therefore, three different numerical procedures can take place depending on the situation in which the fibre-matrix system enters the algorithm. This situation is described by three different parameters: fibre radius, misalignment amplitude and the parallel strain of fibre material.

Having a fibre radius equal to zero tells the program that the compression strength of the composite due to fibre buckling effects does not have to be considered. In this case no calculations are performed and the code leaves the algorithm. On the other hand, if fibre radius is non-zero, two different situations can be found: that fibres are aligned or misaligned.

In the case of aligned fibres, the code checks if they are in tension or compression ($f\varepsilon^* > 0$

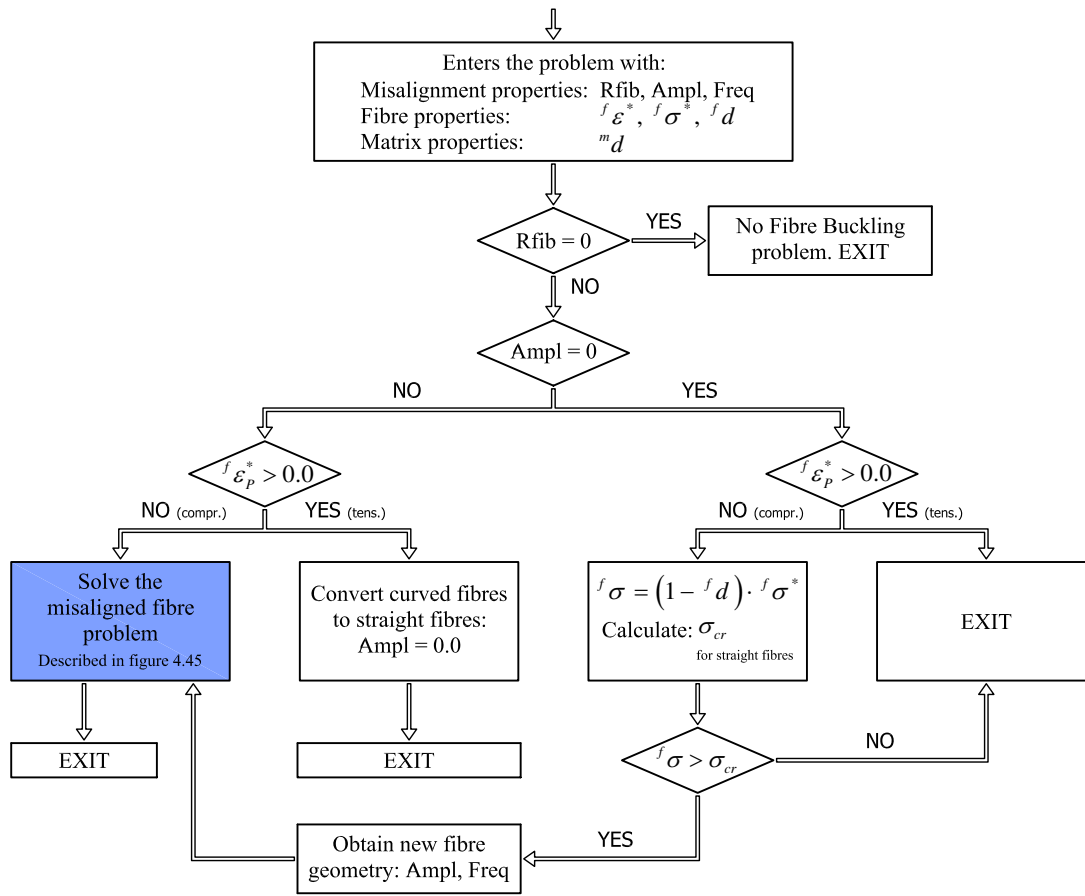


Figure 4.44: Fibre buckling algorithm included in the serial/parallel mixing theory. The procedure shaded in blue is described in the flow chart shown in figure 4.45

or $f\varepsilon^* < 0$, respectively). If fibres are in tension the code leaves the algorithm while, if they are in compression, the parallel component of the stress tensor of fibres is compared with the critical buckling stress for straight fibres. If fibre stress is smaller than the buckling stress the code leaves the algorithm but, in case of fibre buckling, the new fibre geometry is calculated and the misaligned fibre problem is solved.

The case in which the fibres enter the fibre buckling algorithm with some misalignment, either initial misalignment or a misalignment produced by fibre buckling of straight fibres, the code verifies if the parallel strain of fibre material is a compression or a tension strain. When a tensile load is applied to misaligned fibres, the micro-structural displacement suffered by them implies a reduction of their misalignment, transforming their curved geometry into a straight one. Thus, if the strain applied is a tensile strain, curved fibres are transformed into straight fibres defining their **Ampl** value as 0.0. On the other hand, if fibres are compressed, the problem of misaligned fibres is solved. The flow chart used to solve this problem is shown in figure 4.45.

This last flow chart shows the algorithm already described when defining the numerical procedure used to obtain the compression strength of fibres with initial misalignments. The CuBER problem is solved to obtain the structural damage parameter of fibre material. The fibre structural stiffness used to calculate the structural damage parameter must be larger than the structural stiffness obtained in the case in which matrix is not confining fibres

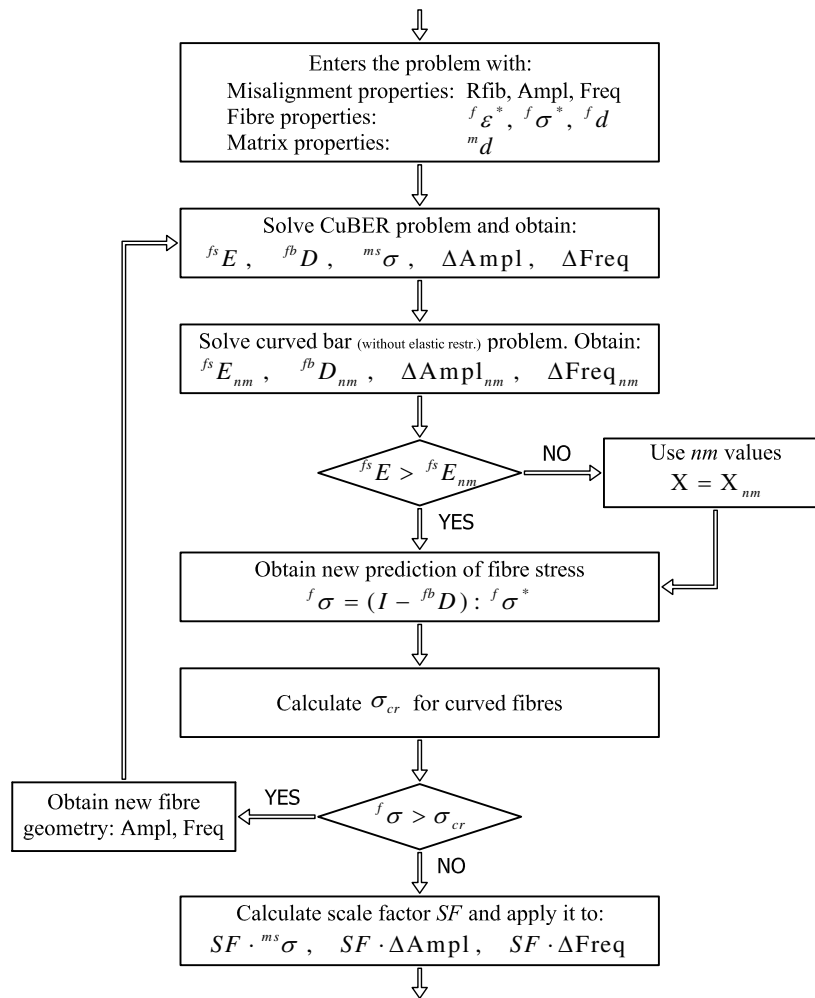


Figure 4.45: Flow-chart description of the numerical procedure used for misaligned fibres

any more. Having obtained fibre structural stiffness, the new parallel stress prediction of fibres is compared with the buckling stress of a curved bar in an elastic foundation. If fibre buckle ($f\sigma > \sigma_{cr}$) the new buckled geometry is calculated and the problem is solved again. Otherwise, the prediction of fibre stresses are considered correct and the code leaves the algorithm after modifying the amplitude, wave-length and matrix structural stresses according to the scale factor defined in equation 4.52.

4.5.6 Numerical performance of the procedure developed to obtain the compression strength of composite materials. Numerical examples

The main objective of this section is to illustrate the numerical performance of the new procedure developed to obtain the compression strength of composite materials. With this aim different numerical simulations of a RVE cell are studied. In each simulation some parameters are modified to obtain different RVE behaviors that will provide a better comprehension of how the numerical procedure developed works and the results that will be expected when performing numerical simulations of composite materials in which their compression strength is obtained with the developed methodology.

The RVE cell used to perform the different numerical simulations included in this section has the geometry shown in figure 4.46 and the material properties used for all simulations, except specified otherwise, are shown in table 4.11. Both materials, fiber and matrix, are defined as isotropic materials (the composite anisotropy is provided by the serial/parallel mixing theory). They are modeled using the homogenized constitutive equations obtained modifying the damage constitutive law defined in section 3.3.

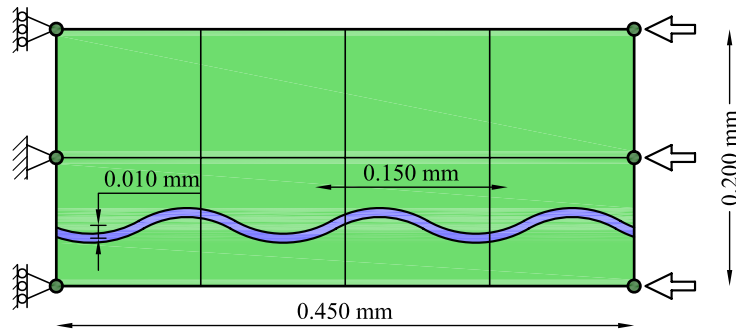


Figure 4.46: Geometry and mesh of the RVE used in the numerical simulations to study the procedure developed to obtain the composite compression strength

Matrix Properties		Fibre Properties	
Elastic Modulus	2.00 GPa	Elastic Modulus	70.00 GPa
Poisson Modulus	0.30	Poisson Modulus	0.00
Compression Strength	50.00 MPa	Compression Strength	2400.00 MPa
Fracture Energy	0.35 kJ/m ²	Fracture Energy	50.00 kJ/m ²
Volume fraction	0.50	Volume fraction	0.50
		Fibre diameter	7.00 μm

Table 4.11: Fibre and matrix mechanical properties used to study the performance of the numerical procedure developed to obtain the compression strength of composites

The compression force applied to the RVE is obtained with a displacement in the right nodes shown in figure 4.46. Applying a prescribed displacement instead of a force allows obtaining the post-critical path of the composite once the maximum compression load has been reached.

The numerical examples shown in this section can be classified in different groups depending on the results expected to be obtained from them. The first group compares the performance of the composite when fibres have initial misalignments, when fibres are straight and when the fibre buckling problem is not considered. Afterwards the influence of matrix stiffness is studied in the case of straight fibres and in the case of fibres with initial misalignments. Next group verifies that the results obtained with the numerical procedure developed are mesh independent. Finally, the performance of the composite is studied for different loading-unloading cases. These last simulations will show how the formulation developed behaves when unloading the composite or when tensile stresses are applied to composites in which fibres have initial misalignments.

Comparison of the compression strength obtained when fibres have or do not have initial misalignments

In this section the performance of the RVE cell shown in figure 4.46, with fibre initial misalignments, is compared with the performance obtained when fibres do not have initial misalignments and when the compression strength of the composite is not considered. This comparison provides a good understanding of the effects of fibre misalignments and of the reduction obtained in the composite compression strength due to fibre buckling.

Figure 4.47 shows the force-displacement response of the different RVE simulated for this comparison. This figure shows that fibre initial misalignments reduce the compression strength of the composite in more than a 50%. On the other hand, in the case considered, having aligned fibres does not reduce the compression strength of the composite, as fibre damage appears before the buckling stress is reached. However, the fibre buckling formulation provides a different unloading path, as fibre buckling occurs for an applied displacement of 22 μm , when matrix reach a damage level in which it cannot restrain fibres anymore.

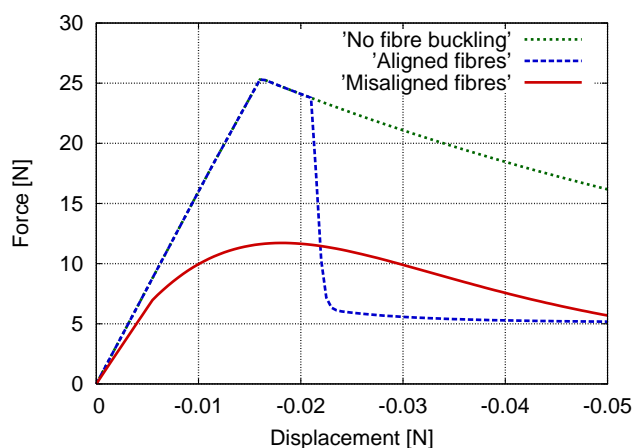


Figure 4.47: Comparison among the results obtained when fibres have original misalignments, when fibres are straight and when the fibre buckling problem is not considered

Another important information provided by figure 4.47 is the composite stiffness, which is lower in the case of fibre misalignments than in the other two simulations. This is because fibre initial misalignments introduce an initial structural damage in fibre material that reduce its stiffness. The evolution of fibre structural damage is represented in figure 4.48b. Figure 4.48a shows the evolution of matrix damage.

Figure 4.48 shows very clearly the effect of fibre buckling in the case of straight fibres. When fibre buckling occurs damage in matrix and in fibre suffers an instantaneous increase due to the new geometric configuration of fibres. This effect is also shown when studying the misalignment evolution in the different simulations performed (figure 4.49). This figure shows that while in the case of fibre with initial misalignments these increase continuously, in the case of aligned fibres the misalignment appears when fibre buckling occurs.

From the results shown in this last figure it is also interesting the study of the quotient between misalignment amplitude and wave length, which provides a good estimation of the grade of misalignment of fibre (larger values are obtained for larger misalignments). In the case of fibres with initial misalignments the values obtained for this quotient are comprehended between 0.07 and 0.11 at the beginning and at the end of the simulation, respectively. On the other hand, the values obtained for straight fibres are comprehended between 0.13

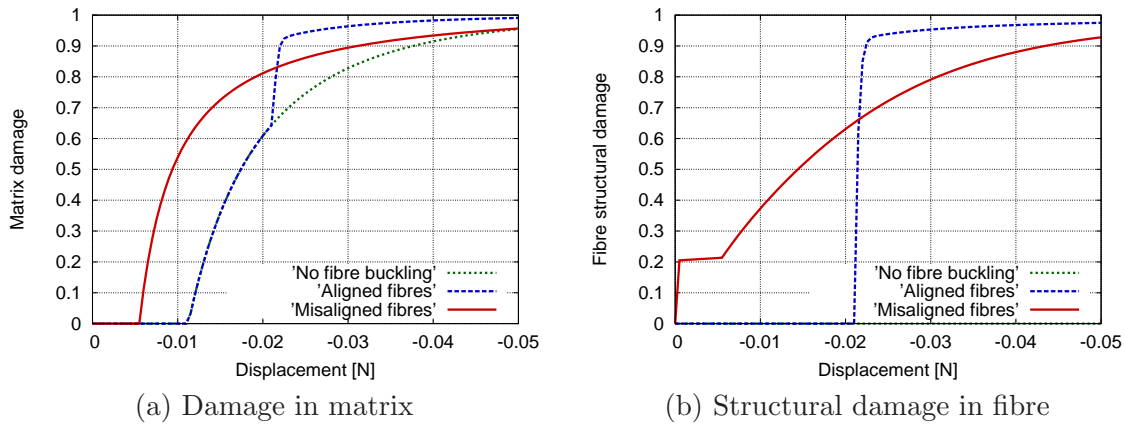


Figure 4.48: Evolution of matrix and fibre damage in the case of fibres with initial misalignments, straight fibres and when the fibre buckling problem is no considered

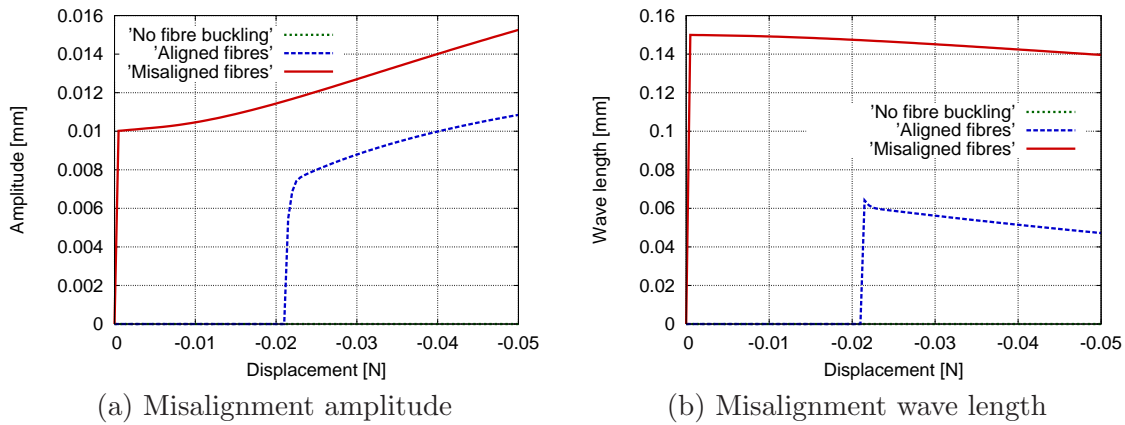


Figure 4.49: Evolution fibre misalignments in the case of fibres with initial misalignments, straight fibres and when the fibre buckling problem is no considered

and 0.23. This shows that when straight fibres buckle, their new geometric configuration provides misalignments that are always more pronounced than the misalignments defined for the composite with fibres initially misaligned. Having larger fibre misalignments provides a weaker fibre due to micro-structural effects.

This situation explains that the structural damage in fibre (figure 4.48b) is larger in the case of aligned fibres than when fibres have an initial misalignment. It also explains the result obtained in the force displacement graph (figure 4.47), which shows that the final load reached in the composite is lower in the case in which fibre buckling occurs than in the composite with initial misalignments. Hence, it can be concluded that although a composite with straight fibres can reach larger critical loads, its structural behavior is more brittle than the failure obtained in a composite which fibres have initial misalignments.

Misaligned fibres: Dependence on the level of initial misalignment

In this section the performance of two different RVE simulations containing fibres with initial misalignments is studied. The initial misalignments considered are defined varying the wave length shown in figure 4.46. Their mechanical performance is compared also with the results obtained for the RVE cell when the compression strength formulation is not used. To perform

these simulations, the compression strength of fibre material has been increased to 4500 MPa.

Two different wave length values have been consider to compare the effects of the level of initial misalignment in fibre materials. One of the RVE models has an initial wave length of $150 \mu\text{m}$ while the other has a wave length of $350 \mu\text{m}$. Thus, using the quotient between amplitude and wave length previously defined, the misalignments defined for the model with a wave length of $150 \mu\text{m}$ are 2.3 times more pronounced than in model with a wave length of $350 \mu\text{m}$.

Figure 4.50a shows the force displacement graphs obtained for the different simulations performed. This graph shows that if fibre initial misalignments are reduced, the composite performance is more similar to the performance obtained when no misalignments are considered. In fact, the situation of straight fibres can be understood as an initial misalignment with a wave length equal to inf . Therefore, the critical load for the simulation with a wave length of $350 \mu\text{m}$ is reached when fibre buckles and not because the misalignment level reaches the maximum load that can be taken by the composite. The effect of fibre buckling in the simulation with a wave length of $350 \mu\text{m}$ can be seen more clearly studying the fibre structural damage parameter (figure 4.50b). Fibre buckling occurs when the damage parameter increases suddenly, for an applied displacement of $26 \mu\text{m}$, varying its value from 0.08 (value obtained due to the initial misalignment defined) to 0.8.

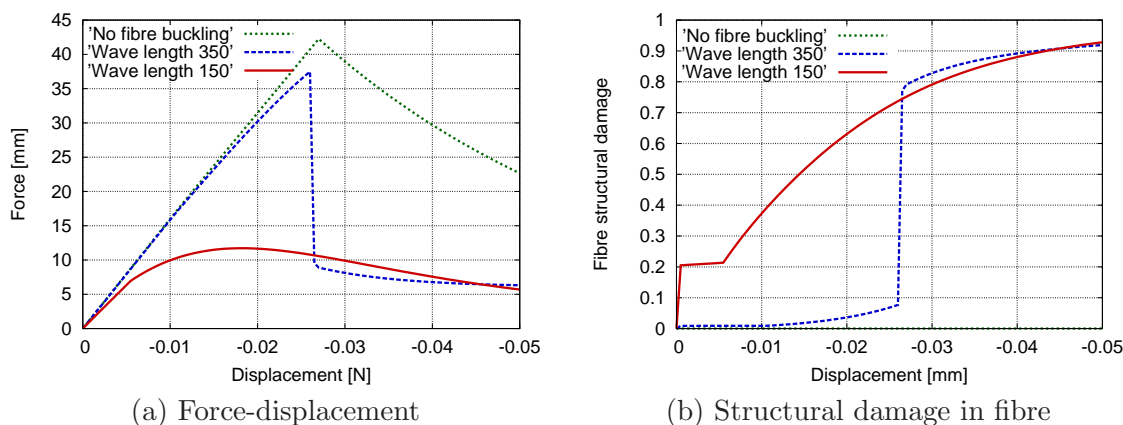


Figure 4.50: Composite performance for different levels of fibre initial misalignments

Aligned fibres. Effect of matrix confinement

This section shows the effect of matrix confinement in composites in which fibres do not have initial misalignments. Matrix confinement is directly proportional to matrix stiffness, therefore, two different simulations of the RVE cell described in figure 4.46 have been performed with two different matrix stiffnesses.

All material material properties considered in these simulations correspond to the properties defined in table 4.11, with the exception of matrix young modulus. The matrix defined in one of the simulations has a young modulus of ${}^mE = 2000 \text{ MPa}$ while, in the other simulation, the matrix material defined has a young modulus of ${}^mE = 200 \text{ MPa}$. Thus, the confinement capacity of this last matrix is reduced ten times compared to the first matrix defined.

The composite performance obtained for these two simulations is shown in the force displacement graph displayed in figure 4.51a. This graph shows that while the maximum compression load is defined by fibre compression strength when matrix is strongly confining fibres (case of

$mE = 2000 \text{ MPa}$), if this confinement capacity is reduced by ten fibre buckles before reaching its maximum compression stress. This figure also shows that, as fibre buckles before, its post-critical strength is slightly larger than when fibre buckles for larger loads. This is because the misalignments obtained are lower if the buckling load is lower. This affirmation is proved by the value of the fibre structural damage parameter, shown in figure 4.51b.

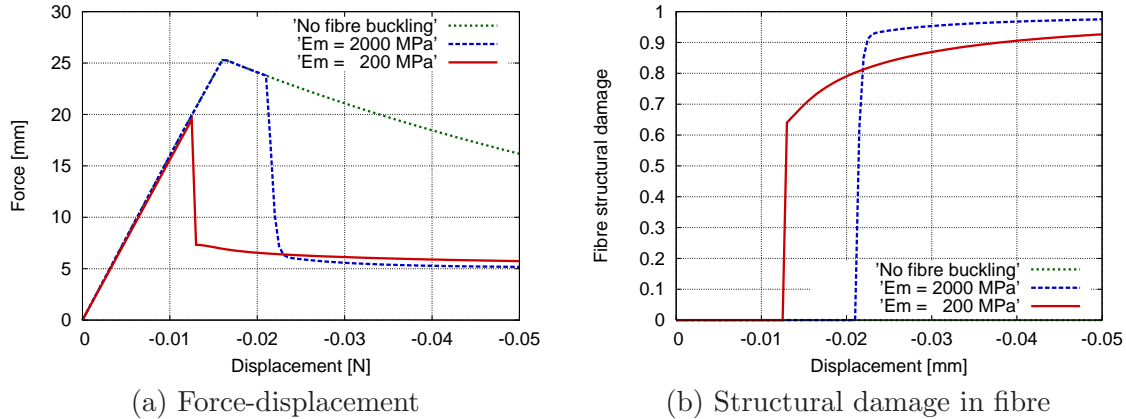


Figure 4.51: Fibre buckling load dependence on matrix confinement capacity in composites with initially aligned fibres

These simulations prove the ability of the numerical procedure developed to take into account the effect of matrix confinement when no fibre misalignments have been defined in the composite. This ability is rather important when simulating composite structures under cyclic loads. In these cases matrix degradation increase as the number of cycles increase; this degradation reduces matrix stiffness and, at a certain number of cycles, a sudden fracture of the composite can occur due to fibre buckling.

Dependence on mesh refinement

One of the main problems found when fracture mechanics is applied to the finite element method is that in most cases the results become mesh dependent. This happens because a continuum formulation (fracture mechanics) is being used in a discrete procedure (finite elements). Thus, many efforts must be done when implementing a continuum formulation in a finite element code to avoid these situation. When using the damage formulation described in section 3.3, the mesh independency is obtained with the definition of the fracture length parameter.

In the numerical procedure developed to obtain the compression strength of composite materials, the fracture length has been re-defined when formulating the matrix homogenized constitutive law (section 4.3), in order to adjust the physical meaning of fracture energy to the parameters included in the new constitutive equation. The fracture length of the matrix affected by fibre misalignments depends of the wave length of these misalignments instead of depending on the finite element size.

To prove the validity of the new fracture length considered, three different numerical simulations of the RVE cell defined in figure 4.46 and table 4.11 have been performed with three different meshes. Each mesh has a different number of finite elements: 8, 32 and 512. Figure 4.52 shows the finite element models developed.

The results provided by the three different simulations are exactly the same, as proves the

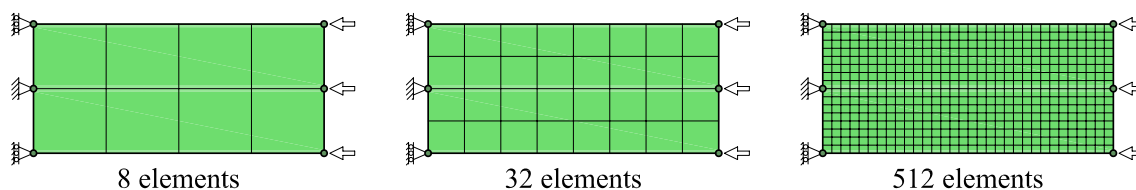


Figure 4.52: Finite element models used to prove the mesh independency of the new procedure developed

force displacement graph shown in figure 4.53. This agreement among the results obtained for all simulations shows the validity of the fracture length value defined for the new homogenized constitutive equation of matrix material.

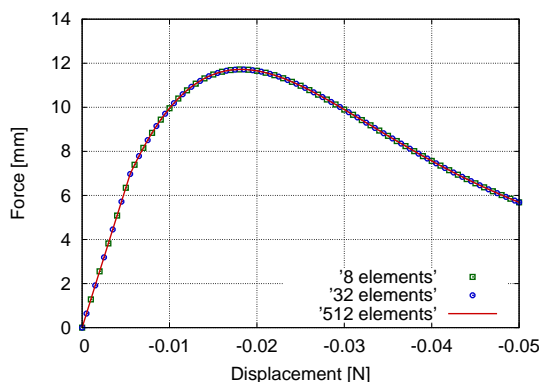


Figure 4.53: Force displacement graph for the different simulations performed

Numerical performance of the formulation for different loading paths

The last group of simulations carried out, in order to show the performance of the numerical procedure developed to obtain the compression strength of composites, apply different loading paths to the RVE models of the composite in which fibres have initial misalignments and the composite in which fibres do not have initial misalignments.

The main objective of these simulations is to show the performance of the numerical simulation developed when the composite is unloaded and when tensile stresses are applied to the composite. With this aim, two different loading paths have been defined. In the first one the RVE cell is loaded and unloaded several times but the composite remains always under compression efforts. The other loading path considered, the first unloading branch is extended until a tensile stress is applied to the RVE cell. Figure 4.54 shows both load paths. As the load is applied as an imposed displacement, the graphs displayed correspond to displacement vs. time curves.

The first results that are shown correspond to the composite in which fibres have initial misalignments when it is loaded following the first load path. The composite performance is studied using a force-displacement graph, which shows the maximum compression load that can be applied to the composite and its post-critical behavior once the maximum load has been reached. The force displacement graph obtained for the RVE cell in this case is shown in figure 4.55.

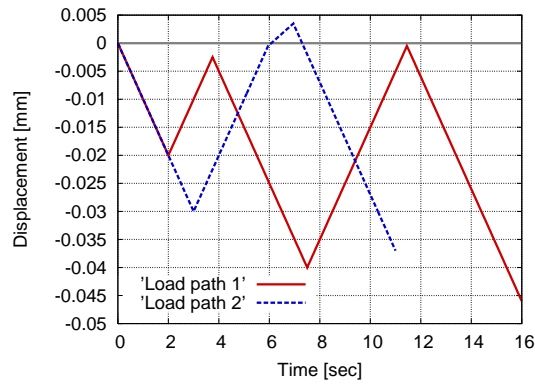


Figure 4.54: Load paths applied to the different RVE cell models

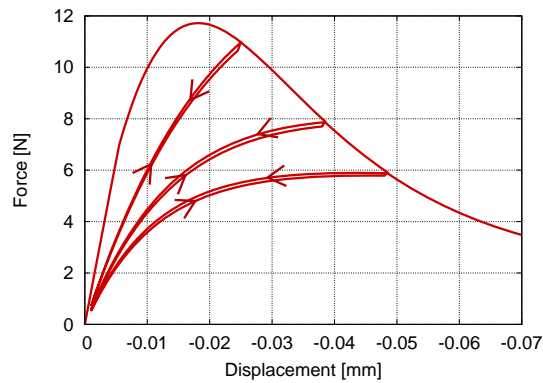


Figure 4.55: Composite with misaligned fibres under load path 1. Force-displacement graph

This graph shows that the unloading branches are not straight (as usually happens with a damage formulation) but, instead, the composite stiffness increases as the load is being reduced. This effect is produced by fibre misalignments: as the load is reduced, fibre misalignments are also reduced, which leads to a stiffer composite material. These effect can be seen more clearly when studying the variation of the misalignment amplitude and wave length, which is shown in figures 4.56a and 4.56b, respectively.

It is interesting to observe that not only the amplitude and wave length are recovered but also their final value is lower (amplitude) and larger (wave length), after the unloading process. Or, in other words, the level of misalignment is lower after unloading the RVE cell. This is because when the unloading process starts, matrix is already damaged and its capacity to confine fibres is reduced. Therefore, fibres can extend more easily and their level of misalignment is reduced.

This effect provides a damage formulation for the composite in which damage is recovered if the material is unloaded. Thus, unlike the damage formulation described in section 3.3, the structural damage due to fibre buckling does not remain constant in the structure. However, although composite stiffness is recovered, when it is compressed again the load does not follow the elastic branch but, instead, follow the path defined in the unloading process (figure 4.55). To explain this effect is useful plot the damage evolution of fibre and matrix, which are shown in figure 4.57.

As can be seen in this figure, although damage in fibre is partially recovered (due to the reduction of fibre misalignments), matrix damage remains constant during the unloading process. Thus, when the compression load is applied again, the confinement capacity of

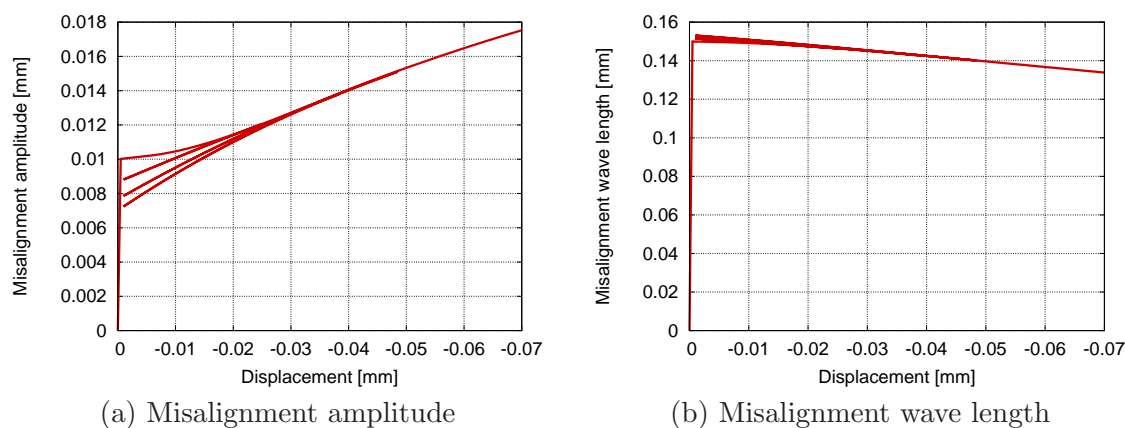


Figure 4.56: Composite with misaligned fibres under load path 1. Evolution of fibre initial misalignments

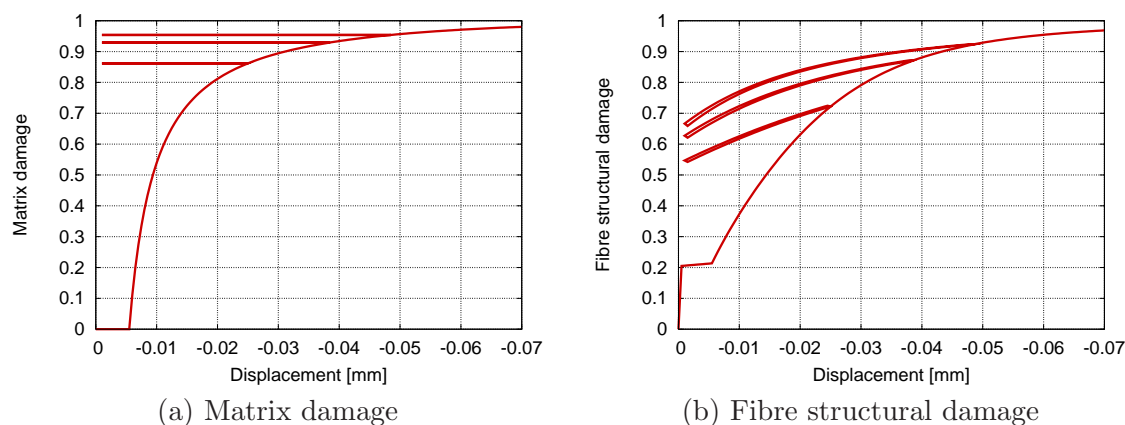


Figure 4.57: Composite with misaligned fibres under load path 1. Evolution of damage in matrix and fibre

matrix is lower than the confinement capacity provided by the matrix the first time that the composite was compressed, which leads to a faster increase of fibre initial misalignments.

A completely different composite performance is obtained if tensile stresses are applied to the composite when it is unloaded. In this case, the formulation developed converts curved fibres into straight fibres. Therefore, when the composite is loaded again, it follows the initial elastic branch because fibres have recovered their initial stiffness. This can be observed in the second simulation developed, in which the second loading path is applied to the composite in which fibres have initial misalignments. Figure 4.58 shows the force displacement graph obtained for this simulation.

In this case the performance of the composite, when it is compressed after having applied to it tensile stresses, is exactly the same that is obtained in a composite with fibres without initial misalignments. And the maximum compression strength is obtained for the load that leads to fibre buckling. This effect is fully described by the graphs showing the evolution of matrix and fibre damage (figure 4.59).

This figure shows that when the RVE cell is unloaded, matrix damage remains constant with a value of 0.90. On the other hand, during the unloading process, fibre structural damage is reduced from 0.82 to 0.60; and, when the applied displacement produces a tensile stress in the composite, this damage becomes zero and remains zero during the loading process,

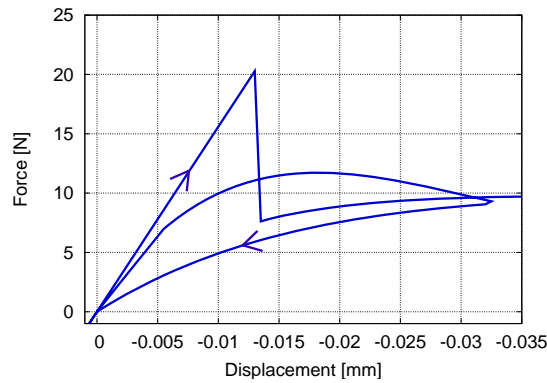


Figure 4.58: Composite with misaligned fibres under load path 2. Force-displacement graph

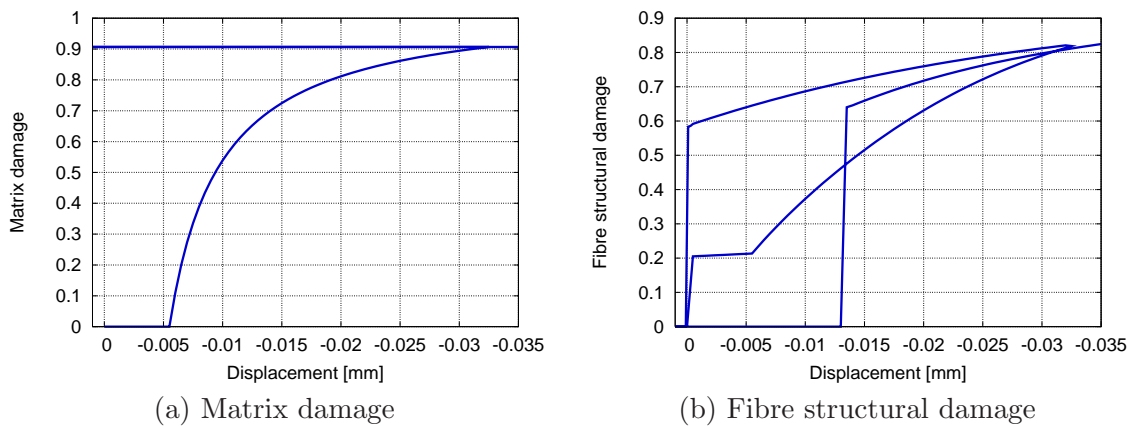


Figure 4.59: Composite with misaligned fibres under load path 2. Evolution of damage in matrix and fibre

until fibre buckling occurs for an applied compression displacement of 0.14 mm. After fibre buckling, fibre structural damage keeps increasing according to the performance provided by the formulation for fibres with initial misalignments.

The other two cases considered in this group of simulations obtain the performance of composites in which fibres do not have initial misalignments, when the load path 1 and 2 are applied to them. The first case shown corresponds to the load path 1. The force displacement graph obtained for the RVE displayed in figure 4.60. In this case, the first time the structure is unloaded fibre buckling has not yet occurred. Therefore, the unloading path and the following loading path have a constant stiffness. After fibre buckling, the performance of misaligned fibres is recovered: when the structure is unloaded it recovers its stiffness and when it is loaded again, it follows the unloading path.

This simulation is also useful to see that the buckling load obtained in the simulation with initially misaligned fibres, loaded following the second load path, is lower than the buckling load obtained when fibres are aligned and the composite is compressed for the first time. In the first case the buckling load is 20 N (figure 4.58), while when fibers are initially aligned the buckling load is 24 N. The difference found in the values for the maximum compression load that can be applied to the composite shows the effect of matrix damage the compression strength of the composite, and proves the ability of the numerical procedure developed to take into account this damage.

In this simulation is also interesting the study of fibre constitutive damage and fibre structural

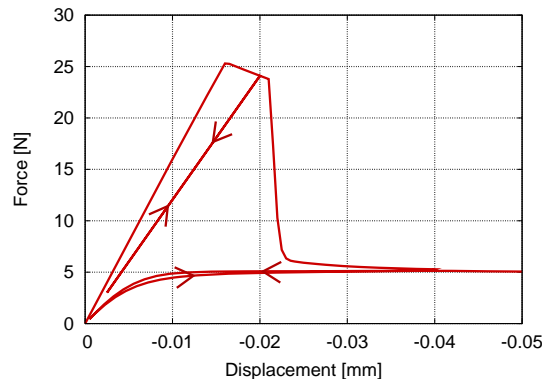


Figure 4.60: Composite with initially straight fibres under load path 1. Force-displacement graph

damage. Both parameters are represented in figure 4.61. This figure shows that while fibre constitutive damage remains constant during the unloading process, fibre structural damage is modified as the misalignments produced by fibre buckling are reduced during the unloading process.

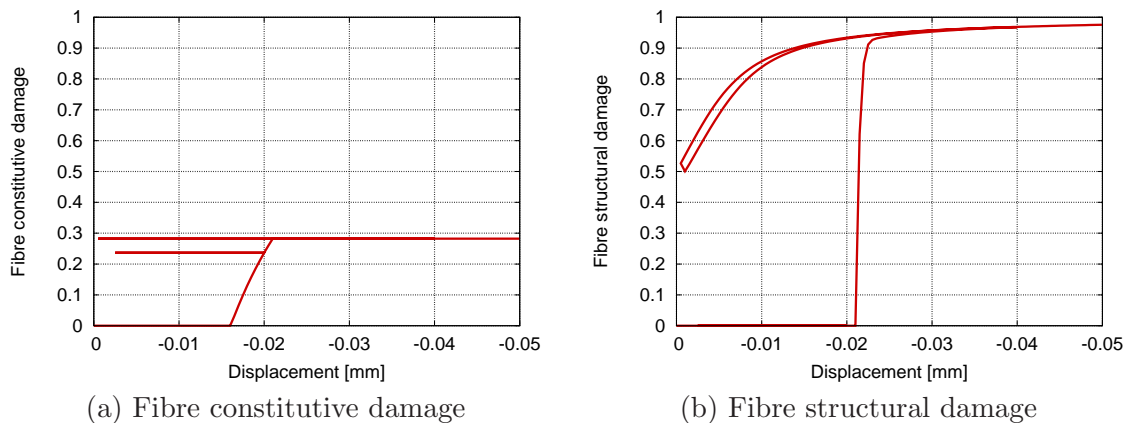


Figure 4.61: Composite with initially straight fibres under load path 1. Evolution of damage in fibre

Figure 4.61 provides also another important composite performance obtained with the simulation developed: when fibre buckling occurs, fibre constitutive damage do not increase anymore and all damage increment in fibre material is due to fibre structural damage. This behavior is consequence of the fibre buckling effect. The apparition of fibre structural damage reduces fibre longitudinal stresses due to fibre geometric configuration: part of the fibre deformation is used not to increase fibre stress but to increase fibre misalignment. Therefore, stresses in fibre do not reach the maximum stress value allowed by fibre constitutive law and fibre damage remains constant.

The last simulation performed corresponds to the composite in which fibres are originally aligned, when the second load path is applied to it. In this case, as can be seen in figure 4.62, the fibre buckling phenomenon occurs twice. The second time the RVE cell is compressed fibre geometric configuration corresponds again to the case of straight fibres, therefore, their structural performance is provided by the straight fibre buckling phenomenon. However, this second time, the load for which fibre buckling occurs is much lower than the first fibre buckling load (6.8 N and 24 N, respectively). This difference is obtained due to damage in matrix material, which is much larger the second time that the composite is compressed,

being reduced its confinement capacity.

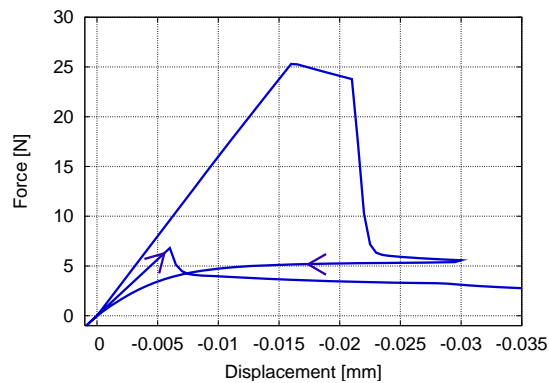


Figure 4.62: Composite with initially straight fibres under load path 2. Force-displacement graph

It is worth to notice that, in this last simulation, the buckling load obtained the second time the RVE cell is compressed is slightly larger, 6.8 N, than the compression load that would be obtained if no tensile stresses would have been applied to the composite, 5.6 N (this value corresponds to the minimum value obtained in the first loading branch, value that would have been recovered if no tensile stresses had been applied to the composite). However, although the compression load reached is larger, after fibre buckling the compression post-critical load is lower: 3.1 N against 5.6 N for an applied displacement of -0.03 mm. This result shows that the effect of fibre buckling reduces the post-critical compression capacity of the composite. This is because each time that fibre buckling occurs, a sudden damage increase is experienced by the composite components.

4.6 Validation of the formulation proposed and numerical example

In this section the formulation proposed to obtain the compression strength of composite materials is validated comparing the results obtained from the numerical prediction with the experimental data provided by Barbero and Tomblin (1996). This validation proves the ability of the numerical procedure developed to obtain the compression strength of real composite materials due to the fibre buckling phenomenon.

However, the main purpose of the fibre buckling formulation presented is not to obtain the compression strength of composites, performing finite element calculations of representative volume elements, but to be used in finite element simulations of structural elements. Therefore, after validating the formulation, the finite element simulation of a cantilever beam is described to show the performance of the developed code when used to calculate a structural element. To see more clearly how the fibre buckling formulation affects the structural behavior of the cantilever, the numerical results obtained with the new formulation are compared with the results obtained when the fibre buckling theory is not considered in the simulation.

4.6.1 Validation of the formulation developed to obtain the compression strength of composite materials

The validation of the formulation developed to obtain the compression strength of composite materials has been done comparing the compression load obtained with the new formulation with the experimental results described in the paper of Barbero and Tomblin (1996). First it is described how the experimental tests are performed and the compression values obtained with them, afterwards is defined the finite element model used to obtain the compression strength with the new formulation developed. Finally, the experimental results are compared with the numerical results.

Description of the experimental test

The experimental tests performed by Barbero and Tomblin (1996) and Tomblin et al. (1997) were made over cylindrical rods, with a diameter of 9.2 mm, pultruded by Creative Pultrusions Inc. The composite materials used were made of E-Glass fibers embedded in a polymeric matrix. Eleven different composites were tested, each one with a different combination of fiber, matrix and fiber volumetric participation. For each one of these materials, eight different compression tests were performed to obtain an average value of the compression strength for each one of them.

The compression tests were performed using short samples (38 mm) to prevent the global buckling of the sample and, as a result, avoiding the application of a lateral support. Strain gages with a length equal to the specimen size were applied to each sample. Half of the samples contained gages disposed back-to-back to verify the specimen alignment. The compression failure was observed at the center of the gage section for the 75% of the samples. The compression strength was obtained using a modified ASTM D-695 test fixture (Barbero and Tomblin, 1996).

From all the tests performed by Barbero and Tomblin, three of them (chosen as the most representative) are used to validate the proposed formulation. Their mean compression strength value and the 95% confidence interval is displayed in table 4.12.

Sample	σ_C [MPa]
ACA	560.90 (± 35.1)
CAA	477.74 (± 36.6)
CBB	521.56 (± 16.2)

Table 4.12: Compression strength of the samples that will be compared with the numerical results

The constituent materials, fiber and matrix, of each sample used to validate the formulation and their volumetric fractions are shown in table 4.13. As the materials properties were not defined in the paper of Barbero and Tomblin (1996), their value has been obtained from the most common values defined in literature for polymeric matrices and e-glass fibers. Matrix mechanical characteristics are described in table 4.14. Table 4.15 describes the mechanical characteristics of fibers. The constitutive law used to simulate all component materials is a damage law.

Misalignment measurements were performed with the optical technique proposed by Yurgartis (1987). This technique consist of cutting the composite at an angle and measuring the major axis of the ellipse formed by the intersection of a cylindrical fiber with the cutting plane. The

Sample: ACA	
Matrix material:	2036C Polyester with added styrene
Fibre material:	Glass fiber OC 102-AA-56
Fibre vol. fraction:	55.2 %
Sample: CAA	
Matrix material:	2036C Polyester
Fibre material:	Glass fiber OC 102-AA-56
Fibre vol. fraction:	40.2 %
Sample: CBB	
Matrix material:	D-1419 Vinyl Ester
Fibre material:	Glass fiber OC 366-AD-113
Fibre vol. fraction:	43.0 %

Table 4.13: Material components and volume fractions of the experimental samples used to validate the developed formulation

2036C Polyester		D-1419 Vinyl Ester	
Elastic Modulus	3.00 GPa	Elastic Modulus	3.50 GPa
Poisson Modulus	0.35	Poisson Modulus	0.35
Tensile Strength	35.00 MPa	Tensile Strength	40.00 MPa
Fracture Energy	0.17 kJ/m ²	Fracture Energy	0.31 kJ/m ²

Table 4.14: Matrix mechanical properties

E-Glass OC-102-AA-56		E-Glass OC-366-AA-113	
Elastic Modulus	80.00 GPa	Elastic Modulus	80.00 GPa
Poisson Modulus	0.20	Poisson Modulus	0.20
Tensile Strength	1500.00 MPa	Tensile Strength	1500.00 MPa
Fiber Diameter	13.00 μm	Fiber Diameter	23.00 μm

Table 4.15: Fiber mechanical properties

misalignment angle is computed from the major axis length, the fiber diameter (which can be measured as the minor axis of the ellipse), and the angle of the cutting plane.

The number of measurements made to each sample was determined so that the expected value of the half normal distribution had a 95 % confidence interval of $\pm 0.2^\circ$. The half normal distribution is considered because fiber micro-buckling occurs at the same load for positive or negative misalignment angles (Barbero and Tomblin, 1996). Therefore, the symmetric normal distribution was converted to a half normal distribution, in which the negative side gets folded onto the positive side. The number of measurements performed to each sample, as well as the half normal distribution expected angle, are displayed in table 4.16.

Finally, Barbero and Tomblin also obtained experimentally the value of the shear stiffness for the different composites with a torsion test (Sonti and Barbero, 1996). However, neither the test nor the values obtained are explained in this document because, in the current validation, the shear stiffness will be obtained from the young modulus value, using the

Sample	Half normal distribution expected value (degrees)	Number of measurements
ACA	2.87	1359
CAA	2.76	1271
CBB	2.63	1224

Table 4.16: Misalignment values and number of measurements performed by Barbero and Tomblin

elasticity formulation.

Description of the numerical simulation

To validate the proposed formulation to obtain the compression strength of composite materials, a numerical simulation of the three different samples previously described: ACA, CAA and CBB, has been performed. The numerical model developed corresponds to a representative volume element (RVE) in which a two dimensional iso-strain formulation has been used. The geometry of the RVE considered is displayed in figure 4.63. This figure also shows the finite element mesh used to perform the simulation and the boundary conditions applied to it.

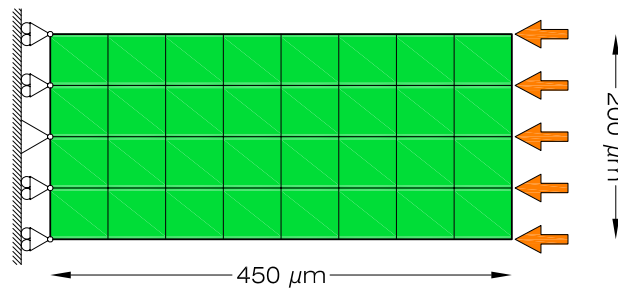


Figure 4.63: Geometry and mesh defined for the simulation used to validate the formulation developed

The compression effort on the finite element model has been applied as a constant displacement of the right side of the structure (figure 4.63). This boundary condition provides the post-critical performance of the composite once the maximum compression load has been reached.

Three different numerical simulations have been performed corresponding to the three experimental samples used to validate the formulation. The composite material defined in each simulation correspond to the composites defined in table 4.13. The properties of the matrix and fiber materials are the ones shown in tables 4.14 and 4.15, respectively.

In order to take into account fiber initial misalignments in the calculation of the compression strength of the composite three different parameters are required: fiber radius, misalignment amplitude and misalignment wave-length. Fiber radius is a known parameter dependent on the fibers used and its value is defined in table 4.15. Misalignment values are obtained from values provided by Barbero and Tomblin for the half normal distribution expected misalignment angle (table 4.16).

The angle defined in table 4.16 is defined as the angle found in the inflection point of the fiber geometry (point A in figure 4.64). This angle corresponds to the largest angle found in

the sinusoidal geometry defined for fiber misalignments. Although the physical meaning of the expected angle obtained by Barbero and Tomblin does not correspond to the angle that is defined in the numerical simulation, both angles are a measure of fiber initial misalignments. Results obtained with the performed simulations prove that these two angles can be considered equivalents.

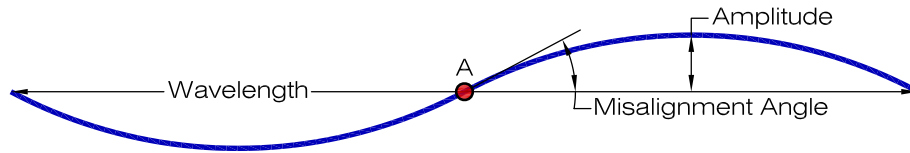


Figure 4.64: Fiber misalignment and misalignment angle considered

To obtain the misalignment parameters required by the formulation developed, another value is needed. An amplitude and a wave length must be defined but, at this point, only an angle is known. The amplitude required is obtained from the statement made by Jochum and Grandidier (2004), who define the amplitude value as one to two times the fiber diameter. Once having defined the misalignment amplitude, using the value of fiber diameter, the wavelength can be computed from the misalignment angle defined by Barbero and Tomblin as:

$$\lambda = 2A \frac{\sin \alpha}{1 - \cos \alpha} \quad (4.120)$$

Being λ and A the misalignment wave-length and amplitude (respectively) and α the misalignment angle. The misalignment parameters used to perform the finite element simulations are the ones displayed in table 4.17 for each sample considered. The amplitude value has been defined, randomly, slightly larger than one time the fiber diameter.

Sample	\varnothing_{fib}	A	λ
ACA	$13\mu\text{m}$	$15.0\mu\text{m}$	$1198\mu\text{m}$
CAA	$13\mu\text{m}$	$15.0\mu\text{m}$	$1246\mu\text{m}$
CBB	$23\mu\text{m}$	$25.0\mu\text{m}$	$2175\mu\text{m}$

Table 4.17: Misalignment parameters defined in the finite element models used to validate the developed formulation

As has been already said when describing the experimental test, shear stiffness is computed automatically by the finite element code using the elasticity formulation. Its value depends on the material Young modulus and Poisson ratio. The expression that defines the shear stiffness is:

$$\frac{1}{G_{ij}} = \frac{1 + \nu_{ji}}{E_i} + \frac{1 + \nu_{ij}}{E_j} \quad (4.121)$$

Being i and j the directions for which the stiffness modulus is computed. In the case of an isotropic material, the expression of the shear stiffness is simplified to:

$$G = \frac{E}{2(1 + \nu)} \quad (4.122)$$

Comparison among the experimental and the numerical results

The comparison between the experimental and the numerical results is made with the force-displacement graphs obtained from the numerical simulation. The force applied to the finite element structure is plotted against the displacement in the face where the load is applied. The stresses provided by Barbero and Tomblin are transformed into the force that would resist the RVE defined in figure 4.63.

The maximum experimental compression strength obtained for each composite is represented, in figure 4.65, with an horizontal line while, the numerical results, are represented as force-displacement graphs. This figure shows the agreement between the maximum compression strength obtained with the formulation developed and the experimental results.

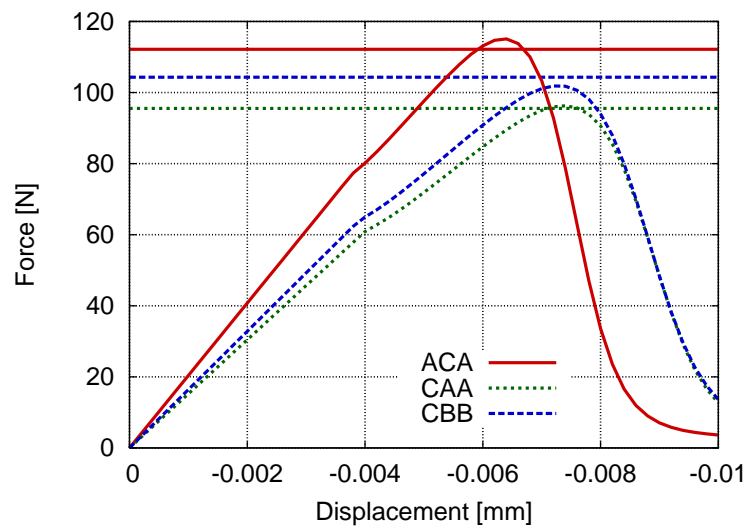


Figure 4.65: Comparison among the experimental and the numerical compression stress obtained for each sample

The maximum error obtained with the numerical simulations correspond to the ACA sample and is lower than a 2.6%. Also, it is worth to point out that the error obtained with all numerical models is inside the 95% confidence interval obtained with the experimental data. The maximum compression values, as well as the errors obtained with each model are displayed in table 4.18.

Sample	Experimental F max [N]	Numerical		
		F max [N]	Error [N]	Error [%]
ACA	112.18(± 7.02)	115.09	2.91	2.6%
CAA	95.55(± 7.32)	96.29	0.74	0.8%
CBB	104.31(± 3.24)	101.84	-2.47	-2.4%

Table 4.18: Maximum compression load of the experimental and numerical samples and error obtained with the numerical simulations

Figure 4.65 shows that when the composite reaches the maximum compression load, its post-critical strength falls abruptly. This is because the fibre buckling phenomenon. The maximum compression load is reached when matrix cannot restrain fibre micro-structural deformation any more (for an applied displacement of 0.006 mm, matrix damage is nearly 1.0). At this point fiber structural damage increases exponentially leading to the reduction of the compression load that can be applied to the composite material. This phenomenon is

shown in figure 4.66 in which the fiber and matrix structural damage parameters are plotted against the compression displacement applied to the RVE that simulates the ACA sample.

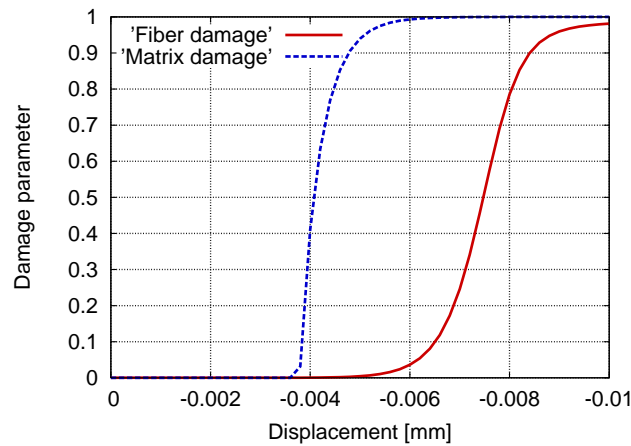


Figure 4.66: Structural damage in fiber and matrix materials. ACA sample

The developed formulation adds two different structural stresses to matrix material to increase its damage due to the fiber-matrix micro-structural interaction (see section 4.3). Of these two stresses the one that leads to the matrix damage shown in figure 4.66 is the one that increase the shear stresses in matrix material. This result is important as it agrees with all existing theories dealing with the fiber buckling problem (i.e. Rosen (1965); Tomblin et al. (1997); Balacó de Moraes and Torres Marques (1997); Drapier et al. (1999)), in which the compression strength of the composite has a strong dependence on the shear strength and stiffness of matrix material.

It is also interesting to compare the RVE response that is obtained if the compression strength algorithm is not used in the simulation. Figure 4.67 shows the performance of the ACA sample when it is simulated using the compression strength formulation and when this formulation is not considered. The composite performance is shown with a force-displacement graph.

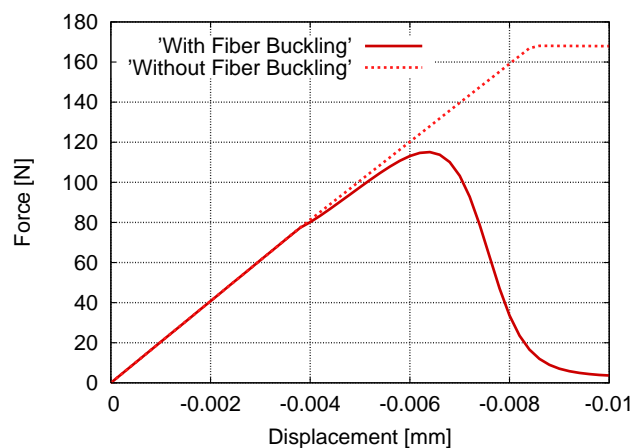


Figure 4.67: Comparison of the results obtained when the fiber buckling formulation is or is not considered in the numerical simulation. ACA sample

This last figure shows that, when matrix damage starts, for an applied displacement of 0.004 mm (see figure 4.66), the composite stiffness is slightly reduced when compared to the simulation in which the fiber buckling formulation is not used. This last figure also shows that the maximum compression load reached, in the simulation that does not use the

compression strength algorithm developed, is obtained when fibers reach their yield strength. Having defined a yield stress in fibers of 1500 MPa, the reduction in the compression capacity obtained with the developed formulation is larger than a 30%.

With these results, it can be concluded that the formulation developed to obtain the compression strength of composite materials can reproduce experimental results obtained with real composites. And that the reduction of the compression capacity in the composite is significant enough to be taken into account. Therefore, the theory can be used to simulate structures taking into account the reduction of the composite compression strength due to the fibre micro-buckling phenomenon.

4.6.2 Numerical simulation of a cantilever beam

Once having proved the validity of the formulation developed, in this section this formulation is used to obtain the structural performance of a cantilever beam when the fiber buckling phenomenon is taken into account. This numerical simulation proves the ability of the formulation proposed to be used in more complex simulations, in which the stresses found in the different elements used to discretize the structure are not only compression stresses. These stresses may vary from one element to the next one, forcing the formulation to provide different behaviors in each case.

Cantilever model

A cantilever beam has been chosen as the structural tipology to prove the ability of the formulation developed to be used in structural simulations. The beam is loaded in its free edge with a vertical force, which produces an increasing bending moment in the beam that reaches its maximum value in its clamped end. The dimensions of the beam considered are shown in figure 4.68. The election of a cantilever beam for this simulation has been made because in the clamped end coexist two different stress states: the bottom section is in compression while the top section is in tension. As the absolute value of both stresses is the same (varying only their direction), the differences between the compression and the tension performance in the beam, obtained with the developed formulation, will be shown very clearly.

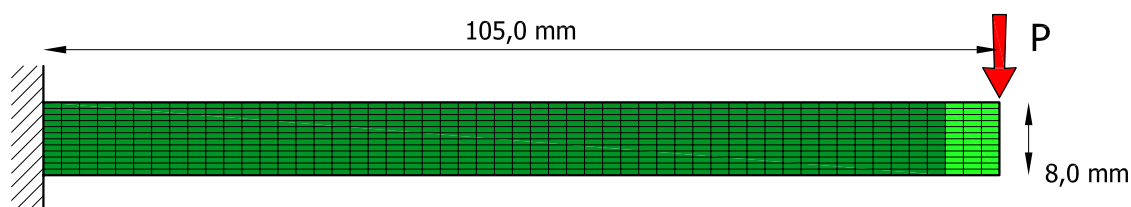


Figure 4.68: Cantilever geometry and mesh used for the numerical simulation

Figure 4.68 shows the geometry and the boundary conditions applied to the cantilever beam. The vertical load has been applied as a constant displacement in order to obtain the post-critical performance of the structure. This figure also shows the finite element mesh used to simulate the beam. The beam has been discretized with quadrilateral elements using a two-dimensional plane-stress formulation. It has 12 elements along its thickness and 53 elements along its length, which makes a total of 636 quadrilateral elements and 702 nodes.

Two different colors have been used to represent the cantilever beam displayed in figure 4.68, each one corresponding to a different material used in the simulation. The material drawn in darker green corresponds to the composite of sample CAA defined by Barbero and Tomblin (1996). The compounding materials of this composite and their volumetric participation are defined in table 4.13. The matrix and fiber mechanical properties are defined in tables 4.14 and 4.15 respectively. The second material used is represented in light green. This material is also the CAA composite but, in this case, both fiber and matrix are simulated with an elastic law. Because the interest of this simulation lays in obtaining the structural behaviour of the clamped end of the cantilever, an elastic material has been considered in the elements where the load is applied to avoid the distortion of the results because of local effects in those elements.

Two different numerical models have been performed for the structure defined: **Cant-FB** and **Cant-noFB**. The first model computes the structure using the formulation developed to obtain the compression strength of composites while, the second model, does not use this formulation. In this second model, the compression and the tensile strengths of the composite are equal and are defined by the damage law of each component material. The comparison of the results obtained with each model shows the effects of the new formulation when it is used in the simulation of structural elements.

Results obtained with the numerical simulations

To compare the structural performance obtained with both numerical simulations, a force-displacement graph has been used (figure 4.69). This graph contains in the x axis the vertical displacement of the free edge of the cantilever and in the y axis the vertical load applied to obtain this displacement. In red is represented the structural response of the model that uses the compression strength formulation developed (**Cant-FB** model) and in blue is represented the response obtained with the model that does not reduce the compression strength of the composite material due to the fiber buckling phenomenon (**Cant-noFB** model). This color criterion is used in all graphs shown in this section.

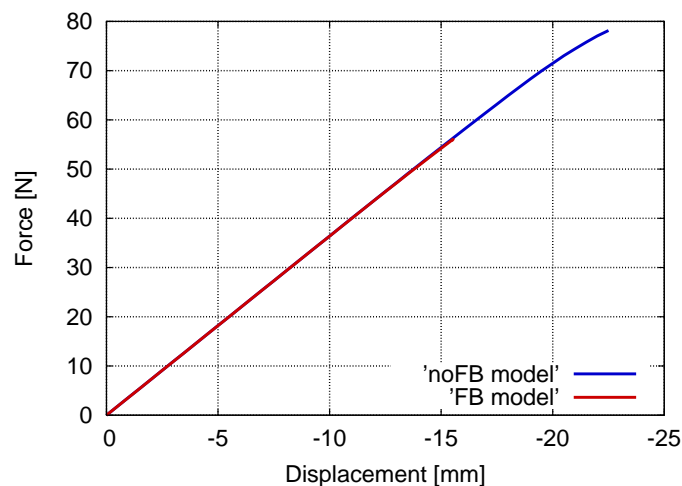


Figure 4.69: Force displacement graph obtained for the **Cant-FB** and the **Cant-noFB** models

Figure 4.69 shows that the structural performance of both models is practically the same. Both models have a linear relation between the force applied and the vertical displacement obtained in the free edge of the structure. However, the maximum load applied to the

Cant-FB model is 56.3 N while the maximum load applied to the Cant-noFB model is 78.2 N. This is, the maximum vertical load that can be applied to the structure when the fiber buckling phenomenon is not considered is 39% larger than when fiber buckling is taken into account.

The difference found in the maximum load that can be applied to the cantilever is due to the difference found in the structural performance of the clamped section in both models. The study of this section is made comparing the results obtained in the top section (Ts) and the bottom section (Bs). The results corresponding to the top section are plotted with dashed lines and the results of the bottom section are plotted with continuous lines. This criterion is used in all graphs shown in this section.

In figure 4.70 are represented the longitudinal strains found in the top and bottom sections of the clamped edge as a function of the load applied to the structure. This graph shows how, in the Cant-FB model, the strains in the compressed section (Bs) start increasing before the beam failure while the strains in the tension section (Ts) maintain their linear behaviour. The strain increment obtained in the Bs section is produced by fiber micro-buckling. This effect is not reproduced by the Cant-noFB model, in which the compression and tension graphs present a nearly perfect symmetry. This symmetry proves that the structural behaviour of both sections is the same.

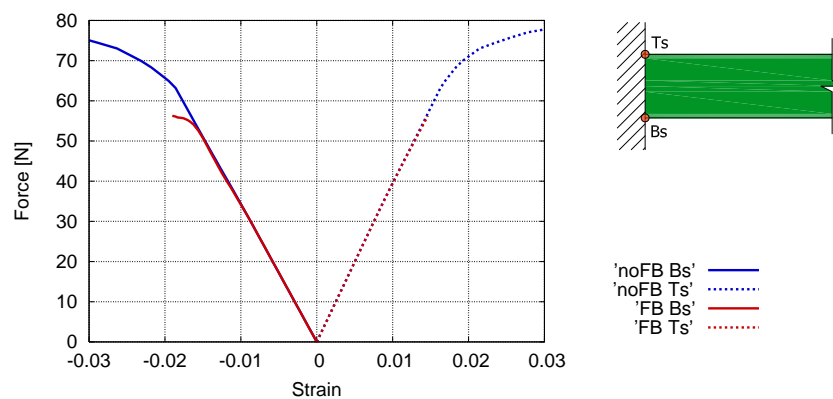


Figure 4.70: Force strain graphs obtained for the cantilever models

The difference found between the top and the bottom section of the cantilever, in its clamped edge, is found because the effect of fiber buckling. The maximum compression stress that can be applied to the composite is lower when the fiber buckling formulation is used to perform the numerical simulation. This stress reduction is only found in the compressed elements, therefore, the failure of these elements takes place for lower loads than for the elements under tensile stresses, which maintain their linear behaviour. This situation is perfectly shown when studying the stress-strain graphs obtained for the top section (Ts) and the bottom section (Bs) of the structure. These graphs are shown, for the composite material, in figure 4.71. In this figure, the strains are represented in its absolute value, so the tensile results are plotted in the same scale than the compression results, making easier the interpretation of the graph. This graph shows that the maximum compression strength obtained in the Cant-FB model is 24% smaller than the compression strength obtained when the fiber buckling formulation is not considered in the simulation; the compression stresses reached are 461.1MPa and 609.1MPa, respectively.

Fiber buckling phenomenon is produced by the interaction between matrix and fiber due to fiber initial misalignments. This interaction accelerates damage in matrix material which leads to a stiffness reduction of fiber material. Both effects can be clearly seen in the stress-

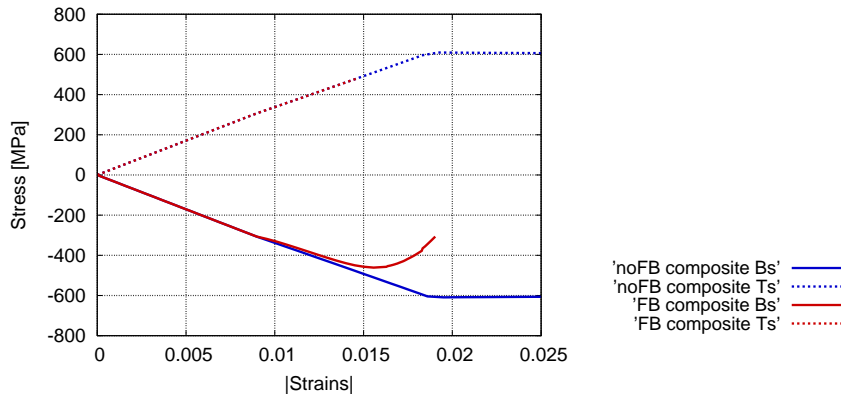


Figure 4.71: Composite longitudinal stress against longitudinal strain for the Cant-FB and the Cant-noFB models

strain graphs obtained for both materials. Again, it is interesting to see in these graphs that the tensile performance of the structure, in the model using the compression strength formulation, is the same that is obtained with the Cant-noFB model. This last model shows a symmetric behaviour for the compression and tensile cases. The stress-strain graph obtained for matrix material is shown in figure 4.72 and the graph obtained for fiber material is shown in figure 4.73.

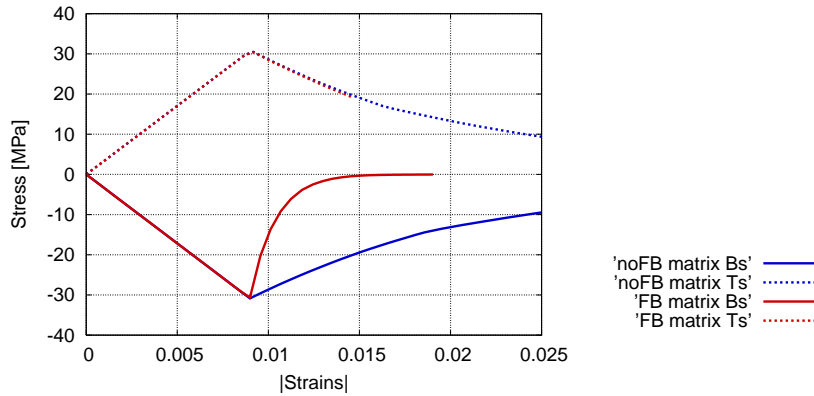


Figure 4.72: Matrix longitudinal stress against longitudinal strain for the Cant-FB and the Cant-noFB models

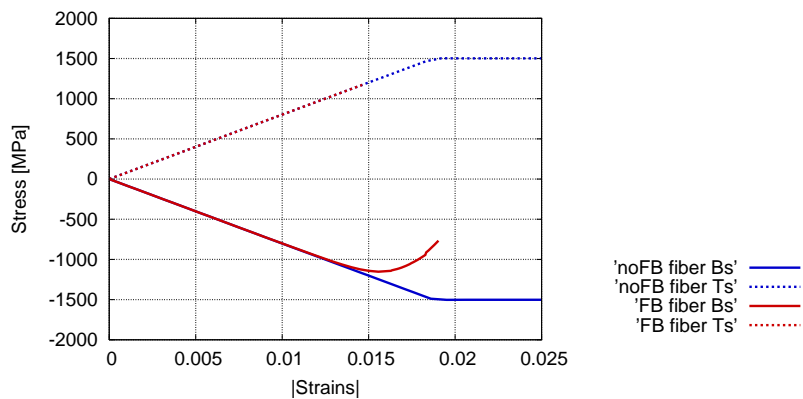


Figure 4.73: Fiber longitudinal stress against longitudinal strain for the Cant-FB and the Cant-noFB models

All results described above provide a detailed comprehension of the effects found in the clamped section of the cantilever. This section is the most relevant of the structure because beam failure occurs in it: the section cannot develop more compression forces being not possible to equilibrate the external load applied to the structure. However the fiber buckling formulation is applied to all the compressed elements of the structure, although its effect cannot be seen in the structural performance because the stresses in those elements are not large enough to reach the maximum compression load that can be applied to the composite.

In the following, the finite element maps containing the matrix and fiber structural damage parameter are included to prove that the fiber buckling formulation developed is applied to the whole structure. Matrix structural damage parameter is represented in figure 4.74. This figure shows that damage is larger in the compression region than in the tensile region. In fact, structural damage in the tensile area is zero because the fiber buckling formulation is not applied in this region (the values obtained in this region correspond to the constitutive damage in matrix material). Figure 4.74 shows that not only matrix structural damage is larger in the compression region but it increases towards the clamped edge of the structure, where compression stresses are larger. Thus, the performance of matrix material along the whole structure is proven to be as expected.

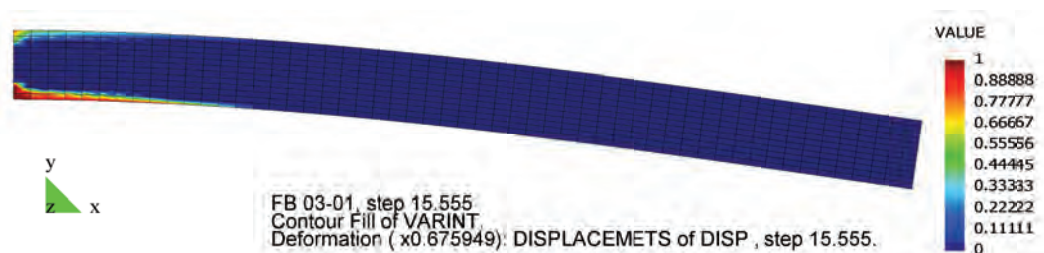


Figure 4.74: Matrix structural damage obtained at the last load step with the Cant-FB model

Fiber structural damage parameter (figure 4.75) provides the same information obtained with matrix damage parameter: Fiber structural damage only appears in the compressed area and it is larger as the section gets closer to the clamped end of the cantilever. The values of fiber structural damage shows that the element found in the clamped section has a damage value close to one, which implies that fiber buckling has occurred in that element. Otherwise, the rest of elements have a damage parameter lower than 0.004. This value corresponds to the damage in fiber due to its original misalignment and is small enough to be certain that fiber buckling has not yet occur in those elements.

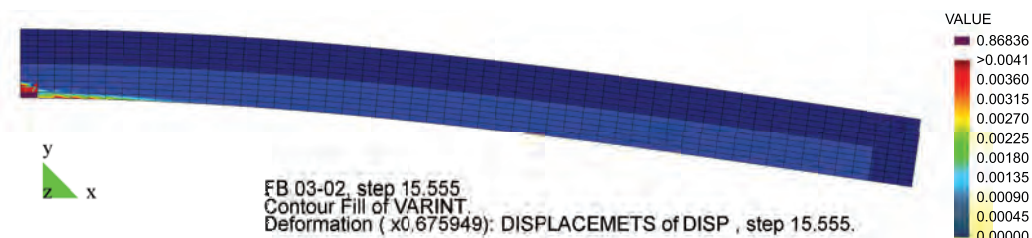


Figure 4.75: Fiber structural damage obtained at the last load step with the Cant-FB model

In this last figure it is also interesting to see that there are some elements in which damage is exactly equal to zero. Stresses in these elements are in tensile direction, so the fiber buckling formulation is not applied to them. Therefore this graph shows how the formulation developed is capable to differentiate between the finite elements in tension or in compression, and only apply the fiber buckling algorithm to those elements under compression stresses,

although the same material has been defined for all of them.

All results shown with the numerical example included in this section prove the ability of the formulation developed to perform more accurate and realistic numerical simulations of structural elements, as the real compression strength of the composite is taken into account. The results also show the necessity to reduce the compression strength of the composite due to fiber micro-buckling, as the failure cause of the structure is significantly different when this strength reduction is taken into account compared to the failure cause obtained when the compression strength is the same than the tensile strength. Moreover, in the case considered, if the compression strength of the composite due to fiber micro-buckling is not reduced, the beam increases its strength nearly a 40%. Results have also shown that the formulation developed is capable to differentiate between elements in tension or in compression, being applied only to the elements that require it.

4.7 Conclusions and further work

From the validation and the numerical performance obtained with the formulation developed to calculate the compression strength of long fiber composites, some conclusions are inferred in this section. This section also describes some improvements that can be done to the formulation and provides some guidelines of the further work that can be developed, following the path that has been started with the numerical procedure proposed.

4.7.1 Conclusions

In this chapter it has been described a new numerical procedure, which has been developed with the aim of obtaining the compression strength of long fiber composites due to the effect of fiber micro-buckling. The formulation provides the maximum compression stress that can be applied to the composite and it also provides the post-critical performance of the material once fiber buckling has occur. This last achievement is important because, when performing numerical simulations of structures, the failure of an element does not always imply the failure of the whole structure. Therefore, the post-critical strength of the element is required to continue the calculation.

The formulation presented has been developed taking into account that its implementation is made in a finite element code (PLCd) that deals with composite materials using the serial/parallel mixing theory. During the process of defining the formulation proposed, the characteristics of these two numerical methods have been always taken into consideration, in order to take advantage of all possibilities and information provided by them. Following this approach, the final formulation does not consist of an equation (or a set of equations) that provides the maximum stress that can be applied to the composite. Instead, it establish a relation between the mechanical performance of the composite components that leads, straightforward, to the result sought: the maximum compression that can be applied to the composite due to the fiber buckling phenomenon.

The compression strength formulation has been obtained defining an homogenization of the constitutive performance of fiber and matrix materials. This homogenization introduces the micro-structural interaction between these two composite components into their constitutive equations. This homogenization has been developed considering that both materials are simulated using a damage constitutive law. However, as has been said during the description of the homogenization process, the formulation can be easily modified to include in it any

other constitutive performance (such as plasticity). This is an important issue, as it gives a versatility to the procedure proposed not seen in any other model existing in literature. The homogenized constitutive equations have been introduced in an algorithm that interacts with the serial/parallel mixing theory taking into account all possible situations that can be found in a long fiber reinforced composite, from loading paths to level of initial misalignment in the fibers.

During the study of the numerical performance of the numerical procedure developed, it has been proved that the formulation has a strong dependence on the three parameters in which are based all formulations dealing with the problem (since the first approach proposed by Rosen, 1965): fiber initial misalignment, shear strength of matrix material and volumetric participation of fiber and matrix in the composite. The dependence on these three parameters is important because it proves that the formulation developed agrees with the existing knowledge on the field. Besides this agreement, the study of the formulation performance has also shown that the expected mechanical behavior of composites under compression forces is well represented by the numerical procedure proposed. In the following are described the most significant mechanical behaviors of compressed composites that are reproduced by the developed formulation.

- The damage obtained in the composite due to fiber buckling is partially recoverable. Damage found in fibers, as a result of buckling, can be recovered if the composite is unloaded because fibers recover their original alignment. However, the damage suffered by matrix as a result of the efforts applied to it, which are increased by the micro-structural interaction between fibers and matrix, is not recoverable. Therefore, although damage in fiber is recovered, damage in matrix not, so fiber buckling occurs for lower loads if the composite is loaded again.
- When fiber initial misalignments are too small or non-existent, the compression load that can be applied to the composite is substantially larger. However, in these cases, fiber buckling is followed by a sudden loss of strength in the composite, obtaining a brittle failure of the material. This performance agrees with the buckling performance obtained in any structural member, the new geometry adopted by the buckled structure produces a sudden reduction of the longitudinal length of the element, increases the second order effects and leads to a dramatic reduction of the structure stiffness.
- The brittle failure obtained in the case of having initially aligned fibers provides a lower post-critical strength in the composite than in the case of having initially misaligned fibers. In this last case, the post-critical path followed by the composite is smoother because the existing misalignment in fibers is smaller (the quotient between the amplitude and the wave-length is smaller). Having smaller misalignments provides stiffer fibers and reduces the structural damage in matrix due to the fiber-matrix interaction.
- The mechanical performance obtained in fibers with small misalignments, large wave-length with small amplitudes, is very similar to the mechanical performance obtained in fibers that are considered straight. The effects of fiber buckling are the same obtained for initially straight fibers: brittle failure and smaller post-critical strength (when compared with the post-critical strength obtained in fibers with larger misalignments).
- Matrix stiffness has an important role in fiber buckling phenomenon as it is confining fibers. If matrix stiffness is reduced, in example, because it is damaged due to tensile stresses applied before compressing the composite, its confinement capacity is also reduced and fiber buckling will occur for lower loads. This effect is obtained independently of the level of initial misalignment found in fibers.

The validation performed of the formulation developed, comparing numerical with experimental results, have proved the ability of the formulation to simulate real composites and to obtain their compression strength. This validation has also shown the necessity of taking into account the compression strength of the composite, as the maximum compression stress that can be applied to it is lower than a 30%, compared with the maximum compression applied if the algorithm developed is not used.

The necessity of using the formulation developed has also been proved in the numerical simulation performed of a cantilever beam. This simulation has shown that not only the load for which the beam failure occurs is lower (28% lower) when taking into account the compression strength reduction due to fiber buckling, but also the failure cause is different. When the compression strength is taken into account, the failure is produced because compression efforts cannot be developed in the clamped end of the cantilever while, if the formulation developed is not used, the failure occurs in the whole clamped section due to tensile and compression efforts.

Therefore, with the validations performed, it has been proved the ability of the procedure proposed to obtain the compression strength of long fiber composites due to fiber buckling, as well as its ability to perform numerical simulations of structural elements, taking into account the fiber buckling effects in the regions of the structure that require the use of the formulation.

Finally, it has to be said that one of the main achievements of the formulation proposed, as important as the results obtained with it, is the methodology developed to include micro-structural effects into the serial/parallel mixing theory. The homogenization method proposed takes the serial/parallel mixing theory one step beyond, as it allows introducing the interaction between composite components into the formulation. This new methodology, which validity has been proved with the implementation of a fiber buckling formulation, can be used to take into account many other micro-structural effects found in composites such as kink-band formation, fiber-matrix debonding, interaction between fibers and voids in the composite or the characterization of woven composites. With the new methodology developed, these micro-structural interactions are included in the formulation and are modifying the mechanical performance of the composite, without increasing significantly the computational cost of the numerical simulation, when compared with a simulation that uses an homogenization process, this last, nowadays, unaffordable. In section 4.4 has shown that neither the accuracy nor the amount of information obtained, is lost with this new procedure.

4.7.2 Further work

Improvements of the formulation developed

The conclusions inferred from the results obtained with the new procedure developed to obtain the compression strength of composite materials, have proved that the formulation has achieved its main objective. However, some improvements can be made to it that will provide a more powerful method to deal with composites under compression forces. Hereafter they are described.

- The curved bar with unilateral restriction problem, used to homogenize the constitutive equations of fiber and matrix material, is solved with an elastic formulation. Material and geometric non-linearities have been introduced in the solution using an incremental explicit method. Although the mechanical performance of the composite obtained with

this procedure provide good results, it would be interesting to replace the linear elastic formulation by a non-linear one, that will reduce the small errors obtained when using an explicit formulation.

- All formulations used to characterize the fiber buckling problem are based in a small displacement formulation. Their use has been considered valid to represent the phenomenology of the process and, the equations used, have also the advantage of their reduced computational cost. However, an accurate representation of any buckling problem requires solving it using a large displacement formulation. Therefore, to obtain a better representation of the phenomenon and more accurate results, some of the equations used in this work should be replaced by the equations obtained from a large displacement formulation.
- The homogenization method proposed to take into account the micro-structural interaction between fiber and matrix should be applied to other constitutive laws, such as plasticity. In this work, the constitutive equations used to simulate fiber and matrix are based on a damage formulation. However, the procedure developed can be implemented in any other constitutive law (it has been already defined how it should be done). This implementation would increase substantially the applications in which the formulation can be used.
- Include bending effects on fiber homogenized constitutive equation. These effects are not included in the formulation developed, which leads to an elastic performance of fiber material, as the only damage that appears in it is the structural damage produced by fiber buckling. However, the bending effects in fibers introduce some stresses in the material that will produce an unrecoverable damage in them. Or, in other words, fiber bending can break the fibers. This effect is not considered in the developed formulation and should be taken into account.
- Implement a large-displacement formulation in PLCd finite element code. This will be a large improvement which is required to perform accurate simulations of compressed composite structures. The buckling problem solved with the formulation proposed corresponds to a micro-buckling that leads to a material failure. This micro-buckling is usually followed by a macro-buckling of the structure that can be only simulated using a large displacement formulation, able to take into account the second order effects.

Further work

Having a compression strength formulation validated and implemented in a finite element code, the next step that should be followed is to use the formulation to perform numerical simulations of compressed structures made of composite materials. These simulations will be the real prove of the capabilities offered by the numerical procedure defined in this section. There are many engineering fields that deal with compressed composite structures and that can use the code developed, to name a few: In civil engineering it can be used to compute the critical strength of compressed columns, mainly in earthquake cases, where the concrete is damaged due to the the bending moments produced by the dynamic forces. In aeronautical engineering it can be used to simulate composite plane wings, in which the compression efforts are one of the main concerns. And, in mechanical engineering, it can be used to simulate compressed elements in fatigue conditions, where damage in matrix appears due to the periodic loads.

However, the most important research lines that can follow the work presented in this chapter would be based on using the homogenization procedure proposed, in which the micro-structural interaction of composite materials is included into the serial/parallel mixing theory formulation, to solve other micro-structural problems found in composite materials. It has been proved that the results obtained with this methodology are a good approach to reality and that the computational effort required does not make impossible to simulate real structures with the new algorithm developed. Applying this methodology to other micro-mechanical phenomenons such as kink-band formation, fiber debonding or to characterize woven composites can improve substantially the accuracy of the simulations performed with the serial/parallel mixing theory, making this formulation the most suitable to calculate composite structures with nowadays technology and computation capabilities.

References

- Akbarov, S. D. and Kosker, R. (2001). Fiber buckling in a viscoelastic matrix. *Mechanics of Composite Materials*, 37(4):299–306.
- Balacó de Morais, A. (1996). Modelling lamina longitudinal compression strength of carbon fibre composite laminates. *Journal of Composite Materials*, 30(10):1115–1131.
- Balacó de Morais, A. (2000). Prediction of the layer longitudinal compression strength. *Journal of Composite Materials*, 34(21):1808–1820.
- Balacó de Morais, A. and Torres Marques, A. (1997). A micromechanical model for the prediction of the lamina longitudinal compression strength of composite laminates. *Journal of Composite Materials*, 31(14):1397–1412.
- Barbat, A. H. and Cardona, O. D. (1999). Daños estructurales producidos por el terremoto de kocaeli, turquía, del 17 de agosto de 1999. *Hormigón y Acero*, 214:103–121.
- Barbat, A. H., Oller, S., Oñate, E., and Hanganu, A. (1997). Viscous damage model for timoshenko beam structures. *International Journal of Solids and Structures*, 34(30):3953–3976.
- Barbero, E. J. (1998). Prediction of compression strength of unidirectional polymer matrix composites. *Journal of Composite Materials*, 32(5):483–502.
- Barbero, E. J. and Tomblin, J. S. (1996). A damage mechanics model for compression strength of composites. *International Journal of Solids and Structures*, 33(29):4379–4393.
- Car, E., Zalamea, F., Oller, S., Miquel, J., and Oñate, E. (2002). Numerical simulation of fiber reinforced composites - two procedures. *International Journal of Solids and Structures*, 39(7):1967–1986.
- Cervera, M. and Blanco, E. (2004). *Mecánica de estructuras II. Métodos de análisis*. Edicions UPC, Barcelona, Spain.
- CIMNE (1991-2008). *PLCd Manual. Non-linear thermomechanic finite element code oriented to PhD student education*. Finite element code developed at CIMNE.
- Clarke, A. R., Archenhold, G., and Davidson, N. C. (1995). A novel technique for determining the 3d spatial distribution of glass fibers in polymer composites. *Composites and Science Technology*, 55(1):75–91.
- Drapier, S., Grandidier, J. C., and Potier-Ferry, M. (1999). Towards a numerical model of the compressive strength for long fibre composites. *European Journal of Mechanics A/Solids*, 18(1):69–92.
- Drapier, S., Grandidier, J. C., and Potier-Ferry, M. (2001). A structural approach of plastic microbuckling in long fibre composites: comparison with theoretical and experimental results. *International Journal of Solids and Structures*, 38(22-23):3877–3904.
- González, C. and Llorca, J. (2007). Mechanical behavior of unidirectional fiber-reinforced polymers under transverse compression: Microscopic mechanisms and modeling. *Composites and Science Technology*, 67(5):2795–2806.
- Guz, A. N. and Lapusta, Y. N. (1999). Three-dimensional problems of the near-surface instability of fiber composites in compression (model of a piecewise-uniform medium)(survey). 35(7):641–670.

- Hetényi, M. (1971). *Beams on elastic foundation. Theory with applications in the field of civil and mechanical engineering*. Ann Arbor: The University of Michigan Press, Michigan, USA.
- Hoffman, J. D. (2001). *Numerical methods for scientists and engineers*. Marcel Dekker, New York, USA.
- Jochum, C. and Grandidier, J.-C. (2004). Microbuckling elastic modelling approach of a single carbon fibre embedded in an epoxy matrix. *Composites and Science Technology*, 64(16):2441–2449.
- Jones, R. M. (1999). *Mechanics of composite materials*. Taylor & Francis, Philadelphia, USA, 2nd edition.
- Kachanov, L. M. (1986). *Introduction to continuum damage mechanics*. Mechanics of elastic stability. Martinus Nijhoff, Dordrecht, Netherlands.
- Kosker, R. and Akbarov, S. D. (2003). Influence of the interaction between two neighboring periodically curved fibres on the stress distribution in a composite material. *Mechanics of Composite Materials*, 39(2):165–176.
- Lo, K. H. and Chim, E. S. M. (1992). Compressive strength of unidirectional composites. *Journal of Reinforced Plastics and Composites*, 11(8):838–896.
- Lubliner, J., Oliver, J., Oller, S., and Oñate, E. (1989). A plastic–damage model for concrete. *International Journal of Solids and Structures*, 25(3):299–326.
- Malvern, L. E. (1968). *Introduction to the mechanics of a continuous medium*. Prentice-Hall, Englewood Cliffs, NJ, USA.
- Martínez, X., Oller, S., Barbat, A., and Rastellini, F. (2007). New procedure to calculate compression strength of FRP using the serial/parallel mixing theory. In *FRPRCS-8 – 8th International Symposium on Fiber Reinforced Polymer Reinforcement for Concrete Structures*, July, Patras, Greece.
- Mata, P., Oller, S., and Barbat, A. H. (2007). Static analysis of beam structures under nonlinear geometric and constitutive behaviour. *Computer Methods in Applied Mechanics and Engineering*, 196(45-48):4458–4478.
- Mata, P., Oller, S., and Barbat, A. H. (2008). Dynamic analysis of beam structures considering geometric and constitutive nonlinearity. *Computer Methods in Applied Mechanics and Engineering*, 197(6-8):857–878.
- Naik, N. K., Tiwari, S. I., and Kumar, R. S. (2003). An analytical model for compressive strength of plain wave fabric composites. *Composites and Science Technology*, 63(5):609–625.
- Oliver, J., Cervera, M., Oller, S., and Lubliner, J. (1990). Isotropic damage models and smeared crack analysis of concrete. In Mang, H. and Bicić, N., editors, *Second International Conference on Computer Aided Analysis and Design of Concrete Structures*, pages 945–958, April, Zell am See, Austria.
- Oller, S. (2001). *Fractura mecánica. Un enfoque global*. CIMNE (Centro Internacional de Métodos Numéricos en Ingeniería), Barcelona, Spain.
- Oller, S. (2002). *Dinámica no-lineal*. CIMNE (Centro Internacional de Métodos Numéricos en Ingeniería), Barcelona, Spain.

- Oller, S. (2003). *Simulación numérica del comportamiento mecánico de los materiales compuestos*. CIMNE (Centro Internacional de Métodos Numéricos en Ingeniería), Barcelona, Spain.
- Oller, S., Miquel, J., and Zalamea, F. (2005). Composite material behaviour using a homogenization double scale method. *Journal of Engineering Mechanics*, 131(1):65–79.
- Oller, S., Oñate, E., Oliver, J., and Lubliner, J. (1990). Finite element non-linear analysis of concrete structures using a plastic-damage model. *Engineering Fracture Mechanics*, 35(1–3):219–231.
- Paluch, B. (1996). Analysis of geometric imperfections affecting the fibers in unidirectional composites. *Journal of Composite Materials*, 30(4):454–485.
- Parnes, R. and Chiskis, A. (2002). Buckling of nano-fibre reinforced composites: a re-examination of elastic buckling. *Journal of the Mechanics and Physics of Solids*, 50(4):855–879.
- Puig, J. M. (2001). Resolución del problema de inestabilidad elástica por compresión en materiales compuestos con fibras largas. Master's thesis, Departament de Resistència de Materials i Estructures a l'Enginyeria (RMEE) – UPC. Directors: Sergio Oller.
- Puig, J. M., Car, E., and Oller, S. (2001). Solution for the inelastic buckling of long fibre reinforced composite materials. In Figueras, J., Juvanades, L., Farias, R., and Balkema, A., editors, *CCC 2001-Composites in Construction International Conference*, pages 119–124, October, Porto, Portugal.
- Puig, J. M., Car, E., and Oller, S. (2002). *Análisis y cálculo de estructuras de materiales compuestos*, chapter Solución numérica para el pandeo inelástico de materiales compuestos reforzados con fibras largas, pages 295–320. CIMNE (Centro Internacional de Métodos Numéricos en Ingeniería), Barcelona, Spain.
- Rastellini, F. (2006). *Modelización numérica de la no-linealidad constitutiva de laminados compuestos*. PhD thesis, Departament de Resistència de Materials i Estructures a l'Enginyeria (RMEE) – UPC. Directors: Sergio Oller and Eugenio Oñate.
- Rastellini, F., Oller, S., Salomon, O., and Oñate, E. (2007). Composite materials non-linear modelling for long fibre reinforced laminates: Continuum basis, computational aspects and validations. *Computers and Structures*, doi:10.1016/j.compstruc.2007.04.009.
- Rosen, B. (1965). *Fibre composite materials*, pages 37–45. ASM Metals Park, Ohio, USA.
- Sánchez-Palencia, E. (1987). *Homogenization techniques for composite media*, chapter Boundary layers and edge effects in composites, pages 121–192. Springer-Verlag, Berlin, Germany.
- Sonti, S. S. and Barbero, E. (1996). Material characterization of pultruded laminates and shapes. *Journal of Reinforced Plastics and Composites*, 15(7):701–717.
- Timoshenko, S. P. (1940a). *Strength of materials. Part I. Elementary theory and problems*. D. Van Nostrand Company, New York, USA.
- Timoshenko, S. P. (1940b). *Strength of materials. Part II. Advanced theory and problems*. D. Van Nostrand Company, New York, USA.
- Timoshenko, S. P. and Gere, J. M. (1961). *Theory of elastic stability*. McGraw-Hill Book Company, Tokyo, Japan, international student edition.

- Tomblin, J. S., Barbero, E. J., and Godoy, L. A. (1997). Imperfection sensitivity of fiber micro-buckling in elastic-nonlinear polymer-matrix composites. *International Journal of Solids and Structures*, 34(13):1667–1679.
- Wang, W. and Shenoi, R. A. (2004). Analytical solutions to predict flexural behaviour of curved sandwich beams. *Journal of Sandwich Structures and Materials*, 6:199–216.
- Welsh, J. S. and Adams, D. F. (1997). An experimental investigation of the mini-sandwich laminate as used to obtain unidirectional composite compression strengths. *Journal of Composite Materials*, 31(3):293–314.
- Xu, Y. L. and Reifsnider, K. L. (1993). Micromechanical modeling of composite compressive strength. *Journal of Composite Materials*, 27(6):558–572.
- Yurgartis, S. W. (1987). Measurement of small angle fiber misalignment in continuous fiber composites. *Composites and Science Technology*, 30(4):279–293.
- Zalamea, F. (2001). *Tratamiento numérico de materiales compuestos mediante la teoría de homogeneización*. PhD thesis, Departament de Resistència de Materials i Estructures a l'Enginyeria (RMEE) – UPC. Directors: Juan Miquel Canet and Sergio Oller.

Chapter 5
Final Remarks

5.1 Conclusions

The three topics discussed along this document,

1. Numerical simulation of composite materials using the serial/parallel mixing theory (SP RoM), and the finite element method.
2. Simulation of delamination using the SP RoM.
3. Development of a new procedure and formulation to predict the compression strength in composites, due to fiber buckling, using the SP RoM.

have provided a comprehensive description of the numerical procedure proposed in this work to perform large scale simulations of composite structures, taking into account their micro-mechanical failure modes.

This work has proved, in chapter 2, that the serial/parallel mixing theory is an adequate formulation to perform numerical simulations of composite materials. The scope used by the SP RoM to simulate advance composites has been proved capable to perform accurate simulations, taking into account the material non-linearities in the composite, with a reasonable computational cost. The serial/parallel mixing theory not only obtains the mechanical performance of the composite, coupling the constitutive behavior of fiber and matrix, but it also takes into account the directional behavior of fibers. This is done using an iso-strain condition in fiber direction (parallel direction) and an iso-stress condition in the remaining directions (serial directions). With these two closing equations, the contribution of fibers to the strength and stiffness of the composite is significantly larger in their longitudinal direction, than in the serial directions.

However, the most important achievement of this project is the development of a new numerical procedure capable to include the micro-structural interaction between fiber and matrix, into the serial/parallel mixing theory. The new methodology proposed takes the SP RoM a step beyond its actual performance. Now, the SP RoM, together with the new procedure developed, is capable to predict the mechanical behavior of the composite from the constitutive behavior of its components, and it is also capable to take into account the failure mechanisms found in the composite, consequence of the micro-structural interaction between its components.

The new procedure developed consist in modifying the constitutive equations of the composite components, according to the micro-structural interaction between them. The serial/parallel mixing theory provides, at each load step, the stress and strain fields for fiber and matrix materials. These two fields are used to establish the micro-structural interaction between the composite components and to modify their constitutive performance. This is done with an homogenization method. With this procedure, the interaction between fiber and matrix is actualized at each load step, using the current strain-stress state of each component material. Therefore, the procedure proposed modifies the constitutive performance of each composite component, taking into account the mechanical evolution of the other.

This new methodology has been applied to characterize the compression strength of fiber reinforced composites. This failure mechanism is produced by fiber micro-buckling. It has been proved, in chapter 4, that with the proposed procedure the fiber buckling phenomenon can be characterized. The homogenized constitutive equations are capable to predict the stress state for which fiber buckling occurs, this is, the maximum compression stress that can be applied to the composite, and they also provide the post-critical performance of the composite, once the maximum stress has been reached. Having a numerical procedure capable to obtain the post-critical performance of the material is important because the main aim

of this work is to obtain a code to perform numerical simulations of composite materials. This code must be capable to continue with the simulation although some elements have reached their maximum stress value and, to do so, it is necessary to know the post-critical performance of these elements.

The homogenized constitutive equations have been used to develop a compression strength algorithm. This algorithm interacts with the serial/parallel mixing theory to provide the compression strength of composites, taking into account all possible situations that can be found in long fiber reinforced composites under compression forces, from loading paths to the level of initial misalignments found in fibers.

The validation performed of the proposed compression strength formulation, has demonstrated the ability of this formulation to obtain, the maximum compression strength that can be applied to the composite, and its post-critical behavior. Moreover, this validation has also proved that the proposed methodology, developed to include the composite micro-structural effects into the serial/parallel mixing theory, is capable to do so. This is considered an important achievement, as this methodology can be used in further research to include other micro-mechanical effects that take place in fiber reinforced composites, such as kink-band formation, fiber-matrix debonding or to characterize woven composites.

The other micro-mechanical phenomenon studied in this work is delamination. This phenomenon consist in the lost of adherence between the different layers of the composite, which leads to a reduction of the section strength and stiffness, that can finish in a structural failure. It has been proved, in chapter 3, that this failure criteria can be simulated straightforward with the serial/parallel mixing theory, if the appropriate constitutive equations are chosen to predict the mechanical performance of the composite constituents.

Therefore, the serial/parallel mixing theory not only is capable to predict the material non-linear response of fiber reinforced composites, from the constitutive performance of their component materials, but along this work it has been proved that this theory is also capable to predict the failure of the composite due to micro-mechanical phenomenons. Although, to obtain this prediction capacity, it is necessary: either to implement an homogenization of the constitutive equations of the composite constituents, in order to take into account their micro-structural interaction; either to chose the appropriate constitutive equations, to simulate the composite constituents mechanical performance.

All numerical formulations and procedures presented along this work have been implemented in PLCd, an implicit finite element code developed by several researchers, professors and PhD candidates at CIMNE (International Center for Numerical Methods in Engineering) and RMEE (Department of Structures and Strength of Materials, UPC). Among the different features of PLCd, it should be remarked its ability to deal with material and geometric non-linearities, with an extensive database of constitutive equations and yield laws, and its capability to perform static or dynamic simulations. Before this work, PLCd dealt with composite materials using the classical lamination theory and simulations should be performed using two-dimensional solid elements.

During this project, in order to implement the different formulations and procedures developed, the mixing theory implemented in PLCd has been replaced for the serial/parallel mixing theory, and the solids elements have been upgraded to the three-dimensional case. It has been also modified the database system in order to improve the code computational performance. Therefore, the new version of PLCd has become a powerful numerical tool capable to perform 2D and 3D simulations of composite materials, using the SP RoM, and taking into account the composite micro-mechanical failures. Besides, its capacity to perform

dynamic calculations remains intact.

Also, in the frame of the FEMCOM project, some of the numerical procedures developed have been implemented in the ComPack-Aero code. This is an explicit finite element code that works with solid and shell elements. The numerical implementations performed in ComPack-Aero are co-authored with Fernando Flores and Fernando Rastellini. ComPack-Aero has been improved with a simplified version of the serial/parallel mixing theory and with the damage formulation presented in chapter 3. With these new implementations, the code has been used to propose a new procedure to take into account the delamination phenomenon in large scale simulations of laminated composites.

Besides the general achievements described previously, each topic discussed in this work (numerical simulation, delamination and compression strength of composites) has provided some important results that have been already described in the conclusions included in each chapter. These conclusions are summarized in the following,

Numerical simulation of composites

The numerical simulation of composite materials is performed using the serial/parallel mixing theory. This theory, as well as its numerical implementation in a finite element code, is described in detail in chapter 2 of the present document. The ability of the serial/parallel mixing theory to perform accurate simulations of composite structures has been proved using it to solve the problem of reinforcement and retrofitting, of reinforced concrete (RC) structures, using fiber reinforced polymers (FRP). The main conclusions obtained from the solution of this problem are described in the following:

- The first and main conclusion obtained from the simulations performed is that the serial/parallel mixing theory, implemented in a finite element code, is capable to predict the mechanical performance of structures made with composite materials. This assessment has been demonstrated comparing the experimental and numerical results obtained, in the case of a four node bending test of a RC beam, reinforced with FRP. The agreement between the numerical and the experimental simulations is found in the force-displacements graphs obtained for the structure and, also, in the failure mode observed.
- To solve the problem of structural retrofitting of RC structures with FRP, a new algorithm has been developed. This algorithm offers the possibility to add new elements to the calculation at a certain load step. So, the FRP reinforcement can be added to the simulation when the RC structure is already damaged. This new algorithm has shown that the stiffness of the retrofitted structure does not depend on the level of damage existing in the structure when the FRP is applied to it. However, the stresses and deformations reached by the structure are larger is the FRP is applied when the structure is already damaged, which can jeopardize the structure serviceability.
- Finally, regarding the effectiveness of the structural reinforcement with FRP, the simulations performed have proved the mechanical improvement of the structure when they are reinforced with FRP. This improvement can increase the strength capacity of the structure in, at least, a 20%. However, depending on the type of reinforcement applied to the structure, the finite element simulation can provide an overestimation of the effects of the FRP. This has been found in the simulation of the framed structure, when

applying lateral reinforcements. In this case, 2D simulations consider an even distribution of the reinforcement along the cross section of the structure, overestimating the contribution of the FRP.

Delamination using the SP RoM

Chapter 3 has proved the ability of the serial/parallel mixing theory to simulate the delamination phenomenon, if the appropriate constitutive equations are chosen to characterize the composite constituents. This chapter also contains the description of a new procedure to characterize delamination in large scale simulations of laminated composites. In the following are summarized the main conclusions obtained from the work performed.

- The main achievement of the work performed in this chapter has been to demonstrate that the serial/parallel mixing theory can simulate the delamination phenomenon straightforward. The damage obtained in the matrix material due to shear stresses reduces to zero the stiffness of the composite in its serial directions. This mechanical performance is exactly the same obtained in a delaminated composite. The main advantage of this procedure is that all elements in the simulation are computed with the same formulation, being unnecessary to define special elements where delamination takes place; which increases substantially the computational cost of the simulation if the delamination path is unknown and these elements have to be placed between all laminate layers. Also, the simulation of the delamination phenomenon using a constitutive approach makes unnecessary the addition of remeshing techniques or contact formulations, that also increase the computational cost of the simulation.
- This chapter also contains the description of a new procedure to deal with the delamination phenomenon in large scale simulations of composite laminated structures, using the classical lamination theory. This consist in localize the shell elements where delamination takes place, using the SP RoM and a damage formulation to characterize the composite. Afterwards, the damaged elements are replaced with solid elements, to obtain a better representation of the delamination phenomenon.
- This procedure has provided correct results in the simulation of the ply drop-off test. Taking into account the limitations of the shell formulation (it cannot propagate the delamination), the methodology is capable to localize the region of the structure where delamination takes place and to predict the load for which delamination occurs with a reasonable error. When the damaged shell elements are replaced with solid elements, the simulation of the delamination phenomenon is exactly the same obtained in a simulation performed with solid elements to define the whole structure. The advantage of the proposed procedure is found in the computational cost of the simulation, significantly lower than the computational cost required for three dimensional simulations, specially in the case of large structures.
- The damage constitutive equation used to simulate the delamination phenomenon has been improved with the addition of a friction parameter. The simulations performed with this new damage law have proved the importance of friction in delamination toughness, as friction is capable to stabilize the fracture propagation.

Compression strength of composites

Chapter 4 is dedicated to develop a new formulation to obtain the compression strength of composite materials and its post-critical performance. This formulation has been defined using a new methodology, consisting in the homogenization of the constitutive equations of the composite constituents, fiber and matrix, in order to include their micro-structural interaction in the serial/parallel mixing theory. The main conclusions obtained from the validation of the proposed methodology, as well as the validation of the formulation developed to obtain the compression strength of composites, are described in the following:

- This chapter contains what is considered the most important achievement of this work. The development of a numerical procedure capable to introduce the micro-structural effects, found in composite materials, into the serial/parallel mixing theory.
- The new formulation developed has been used to include the fiber micro-buckling phenomenon in the SP RoM. This formulation has been implemented in an algorithm capable to obtain the compression strength, and the post-critical response, of composite materials. The algorithm takes into account the loading-unloading conditions in the composite, as well as the fiber initial misalignments.
- The results obtained with the proposed formulation are in agreement with experimental values of compression strength of composite materials. This agreement is also found in the dependence, of the maximum stress that can be applied to the composite, in the parameters in which are based all other formulations found in literature: volumetric participation of fibers in the composite, shear strength of matrix material and fiber initial misalignments.
- The last numerical simulation performed has shown the effects of fiber buckling in real structural simulations. The maximum force that can be applied to a cantilever laminate, if the compression strength is limited due to fiber buckling, is a 28% lower than if this compression strength is limited by the material properties.
- Besides the previous conclusions, more have been obtained regarding the mechanics of the fiber buckling phenomenon, when studying the performance of the formulation developed. Some of them are outlined in the following,
 - The damage obtained due to the fiber buckling phenomenon is partially recoverable. If tensile stresses are applied to the composite after fiber buckling, fibers recover their original alignment, recovering also their strength properties.
 - Fibers with small initial misalignments behave like fibers without initial misalignments (straight fibers). In this case, fiber buckling is followed by a sudden lost of strength which reduces fiber post-critical performance to lower levels than the ones obtained in initially misaligned fibers.
 - Matrix stiffness plays an important role in the fiber buckling phenomenon, as it restrain fibers from buckling. If matrix material is damaged, due to a previous buckling of fibers, fatigue effects, etc. its confinement capacity is reduced and fiber buckling will occur for lower loads.

5.2 Further work

This work has presented different formulations and numerical procedures that have been developed to perform numerical simulations of composite structures, taking into account their micro-mechanical effects. Despite the good results obtained in the simulations performed, the different solutions provided to solve the problems treated are far from being perfect. Therefore, further work can be performed to improve their accuracy, their computational cost or to widen their application range. Also, the different topics discussed, and the solutions provided to the problems found, have opened new research paths that can be followed in further research studies.

Both issues, the improvements that can be made to the formulations and numerical procedures developed, and the research lines that can be followed from the path opened within this work, are described hereafter.

5.2.1 Improvements of the formulation developed

The serial/parallel mixing theory has proved, along this work, its capability to obtain the mechanical performance of composite materials, taking into account their material nonlinearities. However, the way in which this theory is implemented limits the number of constituent materials in the composite to only two of them: fiber and matrix. It could be interesting the development of an improved serial/parallel mixing theory, capable to include more than two constituents in the composite.

This new feature can be very useful to simulate the delamination phenomenon. Although the SP RoM has proved its ability to simulate delamination processes, with the actual formulation this failure effect relies in the constitutive performance of matrix material. If more materials are included in the SP RoM, the parameters defining delamination onset and propagation can be defined in a third material, which will increase the versatility of the simulation procedure.

But, regarding delamination, main improvements will come from a more detailed study of the friction developed between the fractured surfaces. The friction parameter included in the formulation has provided qualitative results of how friction affects the delamination toughness, and has shown the necessity to include this effect in the simulation. A better characterization of the friction effects and the implementation of those in the formulation will provide a better simulation and numerical prediction of the delamination phenomenon.

However, the formulation that can gain more of further work is the new procedure developed to obtain the compression strength of composites. This formulation is based in the homogenization of the constitutive equations of the composite components, to take into account their micro-structural interaction. In the development of this procedure, some assumptions have been made, and some effects have been omitted, which improvement will provide a better characterization of the fiber buckling phenomenon. In the following are described the main improvements proposed,

- Although the fiber buckling phenomenon is highly non-linear, the solution of a curved bar with unilateral restriction has been solved with a linear elastic formulation. To solve this drawback, an incremental explicit method has been applied to take into account the nonlinearities. The replacement of the formulation used for a non-linear formulation will provide a better characterization of fiber buckling, improving the accuracy of the simulation.

- The homogenization of the constitutive equations has been done, only, for the damage formulation. However, the methodology can be extended to other constitutive laws (such as plasticity). This extension will widen the applicability range of the formulation, as it will allow to consider other material performances.
- Bending effects in fibers, when they buckle, can lead to the fiber fracture. This phenomenon has not been considered and should be taken into account.
- The compression strength formulation developed should be integrated with a large displacement formulation. These two formulations, together, will provide a better characterization of the buckling phenomena that take place in laminated composites, as the simulation will be able to capture the mechanical coupling existing between the micro-buckling (defined by fiber buckling) and the structural macro-buckling (simulated with the large displacements formulation).

Finally, a detailed study of the numerical convergence obtained with all formulations developed can be performed in order to improve, when possible, the convergence obtained. Following the same purpose, the code algorithm and its databases can be optimized. These measures will improve the numerical performance of the code, reducing its computational cost, which will increase its capability to perform large scale simulations of composite structures. In addition to all these actions, the larger computational cost reduction will be obtained with the parallelization of the code.

5.2.2 New research lines

As important as the improvement of the formulation developed is to identify the research lines that can be followed from the path opened with this work.

Being, the main achievement of this work, the description of a new methodology to include micro-structural phenomena into the serial/parallel mixing theory; the main research lines that can follow this work are obtained from the application of the methodology proposed to other micro-mechanical effects found in composites. In the following are described some of them:

Kink-band formation: The kink band formation is also a compression failure mechanism, in which the loss of strength and stiffness of fibers is produced by the formation of a kink-band. As the strain-stress fields found in fiber and matrix due to this phenomenon are different from the ones obtained in case of fiber buckling, a new set of equations should be defined to characterize this effect and, these equations, should be introduced in the constitutive performance of fiber and matrix with an homogenization procedure similar to the one exposed in this work.

Fiber-matrix debonding: The phenomenon of fiber-matrix debonding is characterized by the lost of adherence between fiber and matrix materials. In this situation, matrix cannot transfer the efforts to fiber. With the new methodology developed, this effect can be characterized decoupling the stress and strain fields of both composite components.

Characterization of woven composites: In these composites, fibers in different directions are interweaved. The shape of fibers is curved, therefore, the curved bar under unilateral restriction equations can be also used to characterize these composites. However, in this case, it is necessary to establish an interaction among the different fibers interweaved and matrix material, and not only between fibers and matrix.

Further research lines are not only restricted to the development of new formulations but they also can be found in the application of the numerical procedures presented in this work. The codes developed, PLCd and ComPack-Aero, can be used to study the performance of composite materials, taking into account their micro mechanical effects in cases of fatigue, ageing, impact loads, etc.

But, the codes developed will provide their most if they are used to perform numerical simulations of composite structures. The purpose of these simulations can be to obtain the optimal composite configuration for the application developed or, simply, the study of the composite structure performance. All these simulations will increase the existing knowledge of the mechanical behavior of composite structures. More and better knowledge is translated in a more reliability on these materials, that will lead to an increase of the engineering applications in which they are used.

5.3 Original contributions of this work

The different procedures and formulations included in this document would not exist without the research and work performed by a large amount of research fellows, that have treated the different subjects contained in this dissertation previously. Along the whole document it has been tried to refer all these authors with honesty and excuses are asked for any possible omission.

Therefore, in order to do justice to all work performed by others, in this section are described what are considered to be the original contributions of this work.

Original formulation

In this group are included the different formulations developed and presented along this document, that are considered to be original contributions.

- The most important original formulation developed in this work corresponds to the new methodology proposed to take into account the micro-structural interaction between composite components into the serial/parallel mixing theory. This methodology is based in an homogenization of the constitutive equations of the composite components.
- The new methodology has been applied to obtain the compression strength of fiber reinforced composites. In this case, the homogenized constitutive equations take into account the interaction between fiber and matrix due to fiber initial misalignments and the level of damage in both materials.
- A new algorithm has been developed to obtain the compression strength of FRP, using the homogenized constitutive equations for fiber and matrix and the serial/parallel mixing theory. This algorithm takes into account the loading path in the composite, as well as the level of initial misalignments in fibers.
- A new friction damage law has been proposed, with the addition of a friction parameter into the damage formulation used to characterize delamination, in laminated composites.

- A construction stages algorithm has been formulated in order to be able to simulate FRP retrofitting of RC structures. This algorithm adds new elements to the simulation for the desired load case, when the rest of the structure has been already loaded.
- PLCd code has been improved with a numerical derivation, using a perturbation method, to obtain the tangent constitutive tensor. This procedure is capable to obtain an accurate approximation of the tangent constitutive tensor for any constitutive law.

Original applications and procedures

As important as the development of new formulations is the application of already existing formulations to solve engineering problems. In many occasions, to solve the targeted problem, is necessary to develop new numerical procedures and to adjust the existing formulation, in order to obtain an accurate simulation and characterization of the problem solved. In the following are described what are considered original contributions of this work in this field,

- Solution of the problem of reinforcement and retrofitting of RC structures using FRP. The solution of this problem has shown the capability of the SP RoM to perform simulations of composite structures and has also shown the mechanical performance of FRP when it is used to strengthen RC structures, as well as the mechanical performance of the RC structure once it has been reinforced.
- Solution of the delamination problem using the SP RoM. To solve this problem it has been necessary to find the constitutive equations that provide a better characterization of the delamination phenomenon.
- A new procedure has been proposed to characterize delamination in composite structures simulated using shell elements and the classical lamination theory. This new procedure is co-authored with all members working in the FEMCOM project, specially acknowledged is the contribution of F. Flores and F. Rastellini in this issue.
- The two procedures developed, to take into account the micro-mechanical effects in composite materials, are based in the constitutive performance of the composite constituents. Therefore, both phenomenons: delamination and fiber buckling, are coupled without requiring any other formulation. The result is a numerical procedure capable to simulate the delamination that takes place in compressed composites, consequence of the material strength reduction produced by the fiber buckling phenomenon.

List of Figures

1.1	Classification of FRP composites according to their fibre distribution	5
1.2	Main objectives of this work	13
2.1	Evolution of composite materials, from adobe to nano-technology	25
2.2	Discretization of a beam structure in tetrahedral elements	28
2.3	2D and 3D finite element simulations of composite structures	29
2.4	Laminated composite with layer orientation $+0/+45/-45/+0$	29
2.5	Homogenization method applied to a composite beam	34
2.6	Finite Element simulation of a thick composite cylinder with an internal compression using an homogenization method (Zalamea, 2001)	35
2.7	Anisotropy using a mapping space theory. Space transformations. Real and fictitious stress and strain spaces. (Car, 2000)	37
2.8	Implementation of the mixing theory in a finite element code (Car, 2000)	41
2.9	Serial-Parallel distribution of the components in a composite material	42
2.10	Flow chart of the serial/parallel rule of mixtures algorithm	47
2.11	Relative transversal stiffness of a carbon/epoxy composite. Comparison of different formulations with experimental results (Rastellini, 2006)	48
2.12	Flow chart of the perturbation method algorithm for obtaining the tangent constitutive tensor	50
2.13	Strains in a 3D finite element representing a laminate	51
2.14	Bending FRP reinforcement of the Pont del Dragó (Pedelta, 1996)	54
2.15	Retrofit process of a beam with a bending moment	56
2.16	Flow chart of the construction stages algorithm	58
2.17	Geometric definition of the studied beam	58
2.18	Strain-stress evolution of each constituent material considered in the analysis	60
2.19	Definition of the mesh and composite materials of the simulated beam. The model assumes symmetry at mid-span	60

2.20	Comparison between numerical and experimental capacity curves	61
2.21	Damage to the concrete at beam failure and detail of the most severely damaged cross-section. The numbers shown correspond to the damage parameter in each finite element. Sp3D-R0 model	62
2.22	Plastic damage to the steel at beam failure and detail of the most severely damaged cross-section. Sp3D-R0 model	62
2.23	Damage at the cross-section supporting heavier loads at beam failure. Sp3D-R1 model	62
2.24	Crack opening in the most severely damaged section	63
2.25	Stress state in CFRP reinforcement. Sp3D-R1 model	63
2.26	Transverse stresses in transverse steel stirrups. Sp3D-R0 model	64
2.27	Longitudinal stresses in concrete and in steel stirrups. Sp3D-R0 model	64
2.28	Comparison of CFRP reinforcements and retrofitting using capacity curves	65
2.29	Geometric definition of the frame	66
2.30	Reinforcements of the concrete frame	66
2.31	Capacity curves obtained with the 2D models	67
2.32	Plastic hinges in the concrete frame. 2D models	68
2.33	Capacity curves obtained with the 3D models	68
2.34	Crack evolution in the 3DF-noR model	69
2.35	Crack evolution in the 3DF-R model	69
2.36	Plastic hinge in 3DF-LR model. Lateral view	70
2.37	Elements with larger deformations in 3DF-LR model. Top view	70
3.1	Delamination due to compression in a carbon/epoxy composite (Paiva et al., 2005)	81
3.2	Crack modes defining the delamination growth	84
3.3	Most common tests used to obtain the delamination toughness of composites	85
3.4	Most common tests used to obtain the delamination toughness of composites	85
3.5	Fracture energy of the material	87
3.6	Displacements in the zero thickness decohesion element (Turon, 2006).	88
3.7	Simulation of a Skin-stiffener debonding (Turon, 2006).	89
3.8	Stress state of composite constituents with the serial/parallel mixing theory	91
3.9	Real damaged space and equivalent space (Oller, 2001)	93
3.10	Uniaxial stress-strain curve for a damage model (Oliver et al., 1990)	95

3.11	Stress–strain graph obtained with the damage formulation. (a) Linear softening (b) Exponential softening	95
3.12	Fracture in a real body and in its finite element discretization. Fracture length description	99
3.13	Damage simulation performed with two different mesh sizes: (a) Force-displacement plot, (b) stress-strain plot and (c) mesh discretization.	99
3.14	Structures that can be modeled with a damage constitutive law and which behavior when they are completely damaged is different	100
3.15	Comparison of the material performance when the the friction parameter is applied to it and when it is not	101
3.16	Sample geometry used for the ENF test	102
3.17	Three dimensional model developed. Mesh description	103
3.18	Force–displacement graph obtained for the different models.	104
3.19	Damage in matrix material when the maximum deflection has been reached .	105
3.20	Evolution of the damage parameter in the beam	106
3.21	Evolution of the horizontal gap in the beam along the loading-unloading process	106
3.22	Evolution of the horizontal gap (a) and the shear stresses (b) along the beam mid-width for different load steps	107
3.23	Longitudinal stresses in the composite for two different load steps	108
3.24	Finite elements and gauss points found around the gap opened by the insert in the beam	108
3.25	Force–displacement graph obtained for three different gap size models. General view and detail of the crack propagation zone	109
3.26	Resolution procedure to solve delamination problems with the code developed	112
3.27	Schematic representation the procedure that should be followed to solve large structural problems	112
3.28	Ply Drop-off model dimensions	113
3.29	Stacking sequence and thickness variation of the sample used in the Ply Drop-off test	113
3.30	Zones in which the model has been divided and number of finite elements defined in each zone	114
3.31	Materials defined in the numerical models	115
3.32	Mesh defined for the shell model. This figure also shows the different materials defined in the numerical model	116
3.33	Conversion of the eccentric forces to a pair of forces	117
3.34	Mesh defined for the solid-shell model. This figure also shows the different materials defined in the numerical model	118

3.35	Mesh defined for the solid model. This figure also shows the different materials defined in the numerical model	119
3.36	Deformation of the 3D-nF simulation when a displacement of 0.9 mm is applied to the right end of the structure	120
3.37	Shear stresses in the 3D-nF simulation	121
3.38	Force-displacement results for the solid models with and without friction . . .	122
3.39	Deformation of the Sh-nF simulation when a displacement of 0.9 mm is applied to the right end of the structure	122
3.40	Force-displacement results for the shell models with and without friction . . .	124
3.41	Deformation of the 3D-Sh-nF simulation when a displacement of 0.9 mm is applied to the right end of the structure	124
3.42	Force-displacement results for the solid-shell models with and without friction	125
3.43	Force-displacement graph comparing the results obtained for the non-friction models and the friction ones	126
3.44	Shear stresses and damage parameter in the 3D-nF model . This figure shows the evolution of both variables as the applied displacement increases	127
3.45	Shear stresses and damage parameter in the 3D-F model . This figure shows the evolution of both variables as the applied displacement increases	128
3.46	Damage parameter in the Sh-nF model . This figure shows the evolution of damage parameter as the applied displacement increases	129
3.47	Shear stresses and damage parameter in the solid elements of the 3D-Sh-nF model . This figure shows the evolution of both variables as the applied displacement increases	130
3.48	Damage parameter in the shell elements of the 3D-Sh-nF model . This figure shows the evolution of both variables as the applied displacement increases .	131
4.1	Initial fibre misalignments (Jochum and Grandidier, 2004)	141
4.2	Finite element model of a RVE that takes into account fibre initial misalignments	143
4.3	Problem of a curved bar under unilateral elastic restriction (CuBER problem)	143
4.4	Shear and extensional buckling modes defined by Rosen (1965)	144
4.5	Maximum compression stress that can be applied to an E-Glass composite using Rosen's formulation	145
4.6	Fibre-matrix system. Fibre behaviour when the composite is compressed . . .	151
4.7	Curved bar under unilateral elastic restrain problem	152
4.8	Geometry of the bar to be considered in the CuBER problem	152
4.9	Forces acting on an infinitesimal section of the curved bar	153
4.10	Boundary conditions to be applied to the CuBER problem	156

4.11	Transformation of a sinusoidal shape into a circumferential one	159
4.12	Evolution of fibre misalignments in the loading process	160
4.13	Serial coupling of the fibre structural and constitutive stiffness	160
4.14	Matrix structural stresses produced by fibre displacements	163
4.15	Stresses in a transversal section	164
4.16	Matrix volume affected by fibre buckling effects	167
4.17	Geometry of the Representative Volume Element simulated	169
4.18	micro-Bmod finite element model. Mesh and boundary conditions defined . .	171
4.19	RoM finite element models. Mesh and boundary conditions defined	171
4.20	Matrix stresses in micro-Bmod for a compression displacement of $5.0 \mu\text{m}$. . .	174
4.21	Matrix S_{xx} stresses in micro-Bmod for a compression displacement of $5.0 \mu\text{m}$	174
4.22	Matrix S_{yy} stresses in micro-Bmod for a compression displacement of $5.0 \mu\text{m}$	175
4.23	Matrix S_{xy} stresses in micro-Bmod for a compression displacement of $5.0 \mu\text{m}$	175
4.24	Stresses in matrix and evolution of the damage parameter in RoM-Bmod model	176
4.25	Nodes from which fibre misalignments are obtained	176
4.26	Evolution of fibre misalignments along the loading process in micro-Bmod and RoM-Bmod models	177
4.27	Force-displacement graph showing the global behavior of the Micro-Bmod and RoM-Bmod models	178
4.28	Stress-strain graphs obtained for the RVE with the serial/parallel mixing the- ory, with aligned and misaligned fibres	179
4.29	Fibre and matrix structural damage. RoM-Bmod model	179
4.30	Force-displacement graph showing the global behavior of the models in which the amplitude is modified	182
4.31	Force-displacement graph showing the global behavior of the models in which the wave length is modified	182
4.32	Force-displacement graph showing the global behavior of the models in which the fibre diameter is modified	183
4.33	Force-displacement graph showing the global behavior of the models in which the stiffness of the composite constituents is modified	183
4.34	Buckling of the steel reinforcement of a reinforced concrete column (Barbat and Cardona, 1999).	186
4.35	Geometry considered to obtain the buckling load of straight fibres	187
4.36	Fibre geometry before applying any load to the composite	190
4.37	Fibre geometry just before reaching the critical buckling load	190

4.38	Fibre geometry just after reaching the critical buckling load	191
4.39	Equilibrium defined between compression force in fibre and elastic restraint of matrix	192
4.40	Post critical performance of a composite with fibres with initial misalignments	194
4.41	Geometry of the curved bar problem when matrix is completely damaged . .	195
4.42	Second buckling mode of a curved beam in an elastic foundation	199
4.43	Flow chart with the implementation of the compression strength algorithm in the serial/parallel mixing theory	201
4.44	Fibre buckling algorithm included in the serial/parallel mixing theory	202
4.45	Flow-chart description of the numerical procedure used for misaligned fibres .	203
4.46	Geometry and mesh of the RVE used in the numerical simulations to study the procedure developed to obtain the composite compression strength	204
4.47	Comparison among the results obtained when fibres have original misalignments, when fibres are straight and when the fibre buckling problem is not considered	205
4.48	Evolution of matrix and fibre damage in the case of fibres with initial misalignments, straight fibres and when the fibre buckling problem is no considered	206
4.49	Evolution fibre misalignments in the case of fibres with initial misalignments, straight fibres and when the fibre buckling problem is no considered	206
4.50	Composite performance for different levels of fibre initial misalignments . . .	207
4.51	Fibre buckling load dependence on matrix confinement capacity in composites with initially aligned fibres	208
4.52	Finite element models used to prove the mesh independency of the new procedure developed	209
4.53	Force displacement graph for the different simulations performed	209
4.54	Load paths applied to the different RVE cell models	210
4.55	Composite with misaligned fibres under load path 1. Force-displacement graph	210
4.56	Composite with misaligned fibres under load path 1. Evolution of fibre initial misalignments	211
4.57	Composite with misaligned fibres under load path 1. Evolution of damage in matrix and fibre	211
4.58	Composite with misaligned fibres under load path 2. Force-displacement graph	212
4.59	Composite with misaligned fibres under load path 2. Evolution of damage in matrix and fibre	212
4.60	Composite with initially straight fibres under load path 1. Force-displacement graph	213

4.61	Composite with initially straight fibres under load path 1. Evolution of damage in fibre	213
4.62	Composite with initially straight fibres under load path 2. Force-displacement graph	214
4.63	Geometry and mesh defined for the simulation used to validate the formulation developed	217
4.64	Fiber misalignment and misalignment angle considered	218
4.65	Comparison among the experimental and the numerical compression stress obtained for each sample	219
4.66	Structural damage in fiber and matrix materials. ACA sample	220
4.67	Comparison of the results obtained when the fiber buckling formulation is or is not considered in the numerical simulation. ACA sample	220
4.68	Cantilever geometry and mesh used for the numerical simulation	221
4.69	Force displacement graph obtained for the Cant-FB and the Cant-noFB models	222
4.70	Force strain graphs obtained for the cantilever models	223
4.71	Composite longitudinal stress against longitudinal strain for the Cant-FB and the Cant-noFB models	224
4.72	Matrix longitudinal stress against longitudinal strain for the Cant-FB and the Cant-noFB models	224
4.73	Fiber longitudinal stress against longitudinal strain for the Cant-FB and the Cant-noFB models	224
4.74	Matrix structural damage obtained at the last load step with the Cant-FB model	225
4.75	Fiber structural damage obtained at the last load step with the Cant-FB model	225

List of Tables

1.1	Types of composite materials (Daniel and Ishai, 1994)	4
1.2	Mechanical properties of fiber materials	4
1.3	Mechanical properties of polymer matrix materials	5
1.4	Advantages and disadvantages of advanced composites (Peters, 1998)	6
2.1	Mechanical characteristics of the constituent materials defined in the beam models	59
2.2	Definition of composite materials. Volumetric participation of each constituent material in the composite	60
3.1	Composite components mechanical properties	103
3.2	Insert material mechanical properties	104
3.3	Mechanical properties of the UD prepeg IMS/977.2	113
3.4	Composite components mechanical properties. The value of the matrix tensile strength has been obtained from the brochure of CYCOM [®] 977-2 Toughened Epoxi Resin.	116
3.5	Number of layers and fibre orientation defined in the different materials of the shell model	117
3.6	Laminated solid materials defined in the solid-shell model	119
3.7	Notation used for each finite element simulation	120
3.8	Notation used for each finite element simulation	126
4.1	Composite components mechanical properties used to validate the homogenized constitutive equations	168
4.2	Misalignment properties and volumetric participations used to validate the homogenized constitutive equations	169
4.3	Parameters defining the different RVE models developed	170
4.4	Stress comparison between micro-Bmod and RoM-Bmod	176
4.5	Stress comparison between RVE simulations in which the amplitude is modified	180

4.6	Stress comparison between RVE simulations in which the wave length is modified	181
4.7	Stress comparison between RVE simulations in which the fibre diameter is modified	181
4.8	Stress comparison between RVE simulations in which the fibre and matrix stiffness are modified	181
4.9	Critical buckling load and length for different buckling modes	189
4.10	Parameters required by PLCd to obtain the compression strength of composites	199
4.11	Fibre and matrix mechanical properties used to study the performance of the numerical procedure developed to obtain the compression strength of composites	204
4.12	Compression strength of the samples that will be compared with the numerical results	215
4.13	Material components and volume fractions of the experimental samples used to validate the developed formulation	216
4.14	Matrix mechanical properties	216
4.15	Fiber mechanical properties	216
4.16	Misalignment values and number of measurements performed by Barbero and Tomblin	217
4.17	Misalignment parameters defined in the finite element models used to validate the developed formulation	218
4.18	Maximum compression load of the experimental and numerical samples and error obtained with the numerical simulations	219

In last decades, advanced composites have become a revolution in structural engineering. Their high strength/weight and stiffness/weight ratios, together with the possibility to tailor made the material for the specific loading environment in which it is used, make these new materials optimal for many structural applications. Despite all existing information and actual knowledge about these materials, their complex behavior, highly non-linear, anisotropic and with different failure causes not found in traditional materials, requires a greater effort in their study in order to improve their performance and take advantage of all possibilities offered by them.

Among all possible numerical procedures and formulation available to predict the mechanical performance of fiber reinforced composites, this work uses the serial/parallel mixing theory. This theory obtains the mechanical performance of the composite by coupling the constitutive performance of its constituents, fiber and matrix. This theory provides an accurate prediction of the mechanical performance of composites, taking into account their material non-linearities.

However, although it is necessary to consider material non-linearities for a correct characterization of fiber reinforced composites, it is not sufficient. The most common failure modes of advance composites, like delamination or fiber buckling, are produced by the interaction between the composite components, and not as a result of a material failure. Therefore, an accurate simulation of composites must take into account the micro-mechanical interaction between its components, in order to be able to characterize their failure modes.

This work studies and proposes different formulations and numerical procedures to simulate the micro-mechanical phenomenons that take place in composites, using the serial/parallel mixing theory. Two different failure modes are discussed: delamination and compression failure due to fiber buckling.

All formulations and procedures included in this work provide a new numerical approach to characterize composite materials, capable of considering both, the material non-linearities and the micro-mechanical phenomenons that take place in them. Simulations performed with this new formulation can contribute to increase the actual knowledge of advanced composites, improving their reliability and opening new application fields.

